

# **Nano-enabled disulfiram for cancer therapy**

Erazuliana Abd Kadir

A thesis submitted in partial fulfilment of the requirements for the degree of

**Doctor of Philosophy**

of

University College London

UCL School of Pharmacy

29-39 Brunswick Square

London, WC1N 1AX

February 2017

## **Declaration**

The thesis describes the research conducted in the UCL School of Pharmacy, University College London between 2012 and 2016 under the supervision of Professor Andreas Schätzlein. I, Erazuliana Abd Kadir, confirm that the work presented in this thesis is my own. Where information has been derived from other sources, I confirm that this has been indicated in the thesis.

Signature :

A handwritten signature in cursive script, appearing to read 'Erazuliana', written in black ink.

Date : 17<sup>th</sup> February 2017

# ABSTRACT

The hypothesis was that encapsulation of labile disulfiram (DS) in a high capacity nanoemulsion stabilized by quaternary ammonium palmitoyl glycol chitosan (GCPQ) could protect DS from degradation in the blood and increase its delivery to tumours. GCPQ was synthesized from glycol chitosan and characterized. GCP20Q11 polymer was chosen to be incorporated with DS in soybean oil into homogenous DS-GCP20Q11-E nanoemulsion. The nanoemulsions showed capability of oil-loading up to 50% v/v for a stable entrapment of high drug content. With increasing oil content (5 to 50%) the mean particle size increased, as did overall polydispersity (190 to 359 nm and 0.14 to 0.21, respectively). Transmission electron microscope (TEM) images showed existence of heterogeneous particles with a size below 100 nm. The drug load and colloidal stability were improved in lower oil-content formulations stored at low temperature. Formulations showed highly positive particle surface charge (51 mV at pH 4.50), proving the ionic stability of the individual particles. DS-GCP20Q11-E showed marked cytotoxicity effect against human pancreatic cancer cell line (MIAPaCa-2) with enhanced activity seen in the presence of copper ( $IC_{50}$  of 0.37  $\mu$ M compared to 34.17  $\mu$ M with the nanoemulsion treatment without copper). In vivo oral pharmacokinetic (PK) study of DS-GCP20Q11-E showed low DS level (low area under curve (AUC)) in the mouse plasma compared to control group whereas the intravenous (IV) PK showed an improved AUC value with DS half-life of 17 minutes. DS-GCP20Q11-E anticancer activity against development of human pancreatic cancer xenograft tumour in mice revealed significant prolonged survival in animals treated with IV DS-GCP20Q11-E or oral DS in soybean oil compared to control (no treatment). No toxicity or side effects were

seen from the multiple administration of the nanoemulsion. In conclusion, DS-GCP20Q11-E nanoemulsion has the potential to be used or developed further for cancer therapeutic purposes.

# ACKNOWLEDGEMENT

First and foremost, I would like to thank God for giving me the strength and dedication to finish this arduous journey.

My sincere acknowledgement to my supervisors, Andreas and Ijeoma for the guidance, encouragement and support throughout these years. It was an honour for me to have been given an opportunity to learn invaluable knowledge under your supervision.

A heartfelt gratitude to all of the group members in Lab 105 and 326 for all the help and care showered on me; Preethi for being there for me since day one, Sunish for the lab organisation and equipment technicalities, Ramesh and Uche for all types of help in the lab, Nick for the insightful chemistry-related guide, Funmi for the early introduction to animal work and Clemens for the companionship in the office. A big thank you also to Abdullah, Lisa, Antonio, Fionn, Ye, Lorenzo, Margarida, Xian and the rest of the people who have made the lab environment so inspiring to work in.

An enormous thanks to the staffs in the school especially to Steve Coppard and all the staffs in Animal Unit for the continuous help with the animals, David McCarthy for the help with TEM imaging, Colin James for the NMR and Rob, Renu and Chris for the tremendous service with the supplies. An extended gratitude to the mates in the school for sharing the ups and downs of working and living in London – Norkasihhan (KC), Atiqah, Yati, Raquel, Mina, Mandana, Mukhrish, Goh, Awis and Fauzi.

My utmost gratitude is to my mother, sister and family members. Thank you for your understanding and support although we are thousands of miles away. Last but not least, a huge appreciation to the sponsors, Ministry of Higher Education Malaysia and Universiti Sains Malaysia for the precious study opportunity and generous financial support.

## Table of Contents

<b>ABSTRACT.....</b>	<b>iii</b>
<b>List of Figures.....</b>	<b>xvi</b>
<b>List of Tables .....</b>	<b>xxi</b>
<b>List of Abbreviations .....</b>	<b>xxiii</b>
<b>Chapter 1 .....</b>	<b>1</b>
<b>Introduction.....</b>	<b>1</b>
1.1 Current cancer treatment .....	1
1.2 Issues with chemotherapeutic drug delivery .....	2
1.3 General issues with conventional drug delivery .....	3
1.4 Nanotechnology in cancer medicine .....	3
1.5 Strategies in cancer nanomedicine .....	5
1.6 Chitosan-based nanocarriers .....	7
1.6.1 Chitosan and chitosan-derived glycol chitosan.....	8
1.6.2 Quaternary ammonium palmitoyl glycol chitosan (GCPQ).....	11
1.7 Disulfiram as a potential chemotherapeutic drug.....	13
1.7.1 Anticancer properties of disulfiram .....	15
1.7.2 Disulfiram role against cancer stem cells.....	22
1.8 Formulation of disulfiram with GCPQ polymers.....	24
1.8.1 Polymeric micelles .....	27
1.8.2 Nanoemulsions.....	28

1.9	Objectives of the study .....	30
<b>Chapter 2 .....</b>		<b>31</b>
<b>Quaternary ammonium palmitoyl glycol chitosan (GCPQ) .....</b>		<b>31</b>
2.1	Overview .....	31
2.2	Synthesis of GCPQ .....	32
2.2.1	Materials.....	34
2.2.2	Degradation of glycol chitosan .....	35
2.2.3	Palmitoylation of degraded GC.....	36
2.2.4	Quaternisation of palmitoylated dGC (PGC).....	38
2.2.5	Removal of iodide .....	38
2.3	Characterization of GCPQ .....	39
2.3.1	NMR spectroscopy.....	39
2.3.2	Molecular weight of GCPQ .....	40
2.3.3	Materials.....	42
2.3.4	Methodology .....	42
2.3.4.1	Level of palmitoylation and quaternisation of GCPQ.....	42
2.3.4.2	Gel permeation chromatography .....	43
2.3.5	Results and discussion .....	44
2.3.5.1	Level of palmitoylation and quaternisation of GCPQ.....	44
2.3.5.2	Molecular weight of GCPQ.....	48
2.4	Conclusion.....	49
<b>Chapter 3 .....</b>		<b>50</b>

**Disulfiram nanoparticle formulations..... 50**

3.1	Overview .....	50
3.2	Nanoparticle characterization analysis.....	51
3.2.1	Principle of the methodologies used in nanoparticle characterization.....	51
3.2.1.1	HPLC.....	51
3.2.1.2	Particle size and particle size distribution with DLS analysis.....	53
3.2.1.3	Visual analysis of nanoparticles with TEM .....	54
3.2.1.4	Particle surface charge with DLS analysis .....	55
3.2.2	Ideal criteria of nanoparticle formulations.....	56
3.2.3	Materials.....	57
3.2.4	HPLC analysis.....	57
3.2.4.1	Instrumentation.....	57
3.2.4.2	HPLC method validation.....	57
3.2.4.2.1	Preparation of standards and quality control solutions for method validation	58
3.2.4.2.2	Selectivity .....	58
3.2.4.2.3	Linearity.....	59
3.2.4.2.4	Accuracy and precision.....	60
3.2.4.3	Drug encapsulation efficiency for nanoparticle formulation.....	61
3.2.5	Dynamic light scattering (DLS) analysis .....	61
3.2.6	Transmission electron microscopy (TEM) analysis.....	62
3.2.7	Statistical analysis .....	62

3.3	Formulation of DS into micellar nanoparticles .....	63
3.3.1	Formulation of DS with GCP10Q11 .....	63
3.3.1.1	No drug pre-dissolution step .....	63
3.3.1.1.1	Methodology .....	63
3.3.1.1.2	Results.....	64
3.3.1.2	Drug and polymer pre-dissolved in solvent .....	66
3.3.1.2.1	Methodology.....	66
3.3.1.2.2	Results.....	66
3.3.1.3	Conclusions for DS formulation with GCP10Q11 .....	67
3.3.2	Formulation of DS with GCP20Q11 .....	68
3.3.2.1	No drug pre-dissolution step .....	68
3.3.2.1.1	Results.....	68
3.3.2.2	Drug and polymer pre-dissolved in solvent .....	69
3.3.2.2.1	Results.....	69
3.3.3	Discussion for micellar formulations .....	70
3.3.4	Conclusions for micellar formulations.....	71
3.4	Formulation of DS and GCPQ into nanoemulsions .....	72
3.4.1	Solubility of DS in different types of oil.....	73
3.4.1.1	Methodology .....	74
3.4.1.2	Result.....	74
3.4.2	Stability of DS in soybean oil .....	75

3.4.3	Formulation of DS with GCP20Q11 at 5% oil .....	77
3.4.3.1	Drug content of DS-GCP20Q11-E.....	78
3.4.3.2	Particle size, polydispersity index and zeta potential of DS-GCP20Q11-E 80	
3.4.3.3	TEM images of DS-GCP20Q11-E .....	86
3.4.4	Formulation of DS with GCP20Q11 at different amount of oil.....	89
3.4.4.1	Determination of maximum oil content for DS-GCP20Q11-E.....	89
3.4.5	Characterization of DS-GCP20Q11-E at different amount of oil.....	93
3.4.6	Stability of DS-GCP20Q11-E upon storage .....	98
3.4.6.1	Changes in drug entrapment.....	98
3.4.6.2	Changes in particle size.....	100
3.4.6.3	Changes in PDI value .....	101
3.4.7	Stability of DS-GCP20Q11-E in acidic and basic pH .....	103
3.4.7.1	Overview .....	103
3.4.7.2	Materials .....	103
3.4.7.3	Methodology .....	103
3.4.7.4	Results .....	104
3.4.7.5	Discussion and conclusion .....	104
3.4.8	Stability of DS-GCP20Q11-E in buffers.....	106
3.4.8.1	Materials .....	106
3.4.8.2	Methodology .....	106
3.4.8.3	Results .....	107

3.4.8.4	Discussion and conclusion .....	107
3.4.9	Stability of DS-GCP20Q11-E in simulated biological samples .....	109
3.4.9.1	Overview .....	109
3.4.9.2	Materials .....	110
3.4.9.3	Methodology .....	110
3.4.9.3.1	Preparation of simulated gastric fluid.....	110
3.4.9.3.2	Preparation of simulated intestinal fluid.....	110
3.4.9.3.3	Experimental procedure.....	111
3.4.9.4	Results .....	111
3.4.9.5	Discussion and conclusion .....	112
3.4.10	Conclusions for nanoemulsion formulation.....	113
<b>Chapter 4</b>	.....	<b>114</b>
<b>Disulfiram nanoemulsion <i>in vitro</i> cytotoxicity</b>	.....	<b>114</b>
4.1	Overview .....	114
4.2	Materials.....	116
4.3	Methodology for MTT assay.....	117
4.3.1	Cell preparation in 96-well plate.....	117
4.3.2	Drug treatments .....	118
4.3.3	Addition of MTT reagent and formazan dissolution.....	120
4.3.4	Determination of cell viability and IC <sub>50</sub> of the treatments.....	120
4.3.5	Statistical analysis .....	121
4.4	Results and discussion.....	122

4.5	DS-GCP20Q11-E nanoemulsion-compatible vehicle for MTT assay .....	125
4.5.1	Results and discussion .....	126
4.6	Conclusions .....	128
<b>Chapter 5 .....</b>		<b>129</b>
<b>Pharmacokinetics of disulfiram nanoemulsion .....</b>		<b>129</b>
5.1	Pharmacokinetics in nanomedicine development .....	129
5.2	Principal of LC-MS/MS analysis .....	131
5.3	LC-MS/MS for DS and MeDDC analysis .....	134
5.3.1	Materials.....	134
5.3.2	Methodology .....	135
5.3.2.1	Instrumentation and analytical conditions.....	135
5.3.2.2	Preparation of cold stabilizing agent .....	136
5.3.2.3	Preparation of drug stock solution.....	136
5.3.2.4	Preparation of calibration standards and quality control (QC).....	136
5.3.2.5	Preparation of experimental samples for analysis .....	137
5.3.3	Statistical analysis .....	137
5.3.4	LC-MS/MS method validation.....	138
5.3.4.1	Validation procedures.....	138
5.3.4.2	Results .....	139
5.3.4.2.1	Optimization of mass spectrometry and chromatographic conditions	
	139	
5.3.4.2.2	Selectivity .....	142

5.3.4.2.3	Linearity.....	143
5.3.4.2.4	Accuracy and precision.....	144
5.3.4.2.5	Recovery and matrix effects .....	145
5.3.4.2.6	Post-extraction stability .....	146
5.3.4.3	Discussion and conclusion .....	148
5.4	Oral pharmacokinetic profile of DS-GCP20Q11-E .....	150
5.4.1	Methodology .....	150
5.4.1.1	Animals .....	150
5.4.1.2	Experimental procedure .....	150
5.4.1.3	Pharmacokinetic analysis .....	151
5.4.2	Results and discussion .....	151
5.4.3	Conclusions.....	157
5.5	DS-GCP20Q11-E stability in mouse plasma .....	158
5.5.1	Methodology .....	158
5.5.2	Results and discussion .....	159
5.6	Intravenous pharmacokinetic profile of DS-GCP20Q11-E .....	161
5.6.1	DS-GCPQ formulation evaluation for IV administration .....	161
5.6.1.1	Methodology .....	161
5.6.1.2	Results and discussion.....	162
5.6.2	Intravenous pharmacokinetic study of DS-GCP20Q11-E in mice .....	167
5.6.2.1	Methodology .....	167

5.6.2.2	Results and discussion.....	167
5.6.2.3	Conclusions .....	170
<b>Chapter 6</b>	.....	<b>171</b>
<b><i>In vivo</i> anticancer study of disulfiram nanoemulsion</b>	.....	<b>171</b>
6.1	Overview .....	171
6.2	Pancreatic cancer as the chosen type of malignancy.....	172
6.3	Xenograft tumour model for pancreatic tumour .....	173
6.4	Materials.....	175
6.5	Methodology .....	176
6.5.1	Animals .....	176
6.5.2	MIAPaCa-2 cells preparation and pancreatic xenograft implantation.....	176
6.5.3	Experimental design for DS-GCP20Q11-E and DS in SB oil treatments ...	177
6.5.4	Statistical analysis .....	179
6.6	Results.....	179
6.6.1	Bodyweight .....	179
6.6.2	Tumour incidence, volume and weight.....	181
6.6.3	Survival .....	184
6.7	Discussion .....	185
6.8	Conclusions.....	187
<b>Chapter 7</b>	.....	<b>189</b>
<b>Conclusion</b>	.....	<b>189</b>
<b>Future recommendations</b>	.....	<b>193</b>

**Bibliography ..... 194**

# List of Figures

Figure 1: Schematic diagrams of several nanotechnology-based nanocarriers representing nanoshells, polymeric micelles, liposomes and nanoemulsions.....	5
Figure 2: The flow of formation from chitin to chitosan and eventually into glycol chitosan. ....	10
Figure 3: Quaternary ammonium palmitoyl glycol chitosan (GCPQ). The w, x, y and z represent the different monomeric repeating unit in the structure of GCPQ polymer as a result of random palmitoylation and quaternization at the amine group of glycol chitosan. ....	11
Figure 4: Schematic diagram of proposed transport route for GCPQ nanoparticle formulation with peptide upon oral intake (reproduced from Lalatsa et al., 2012a with permission). .....	13
Figure 5: Chemical structure of disulfiram.....	14
Figure 6: Proposed structure of copper-disulfiram complex (CuDS) after reaction of copper with disulfiram in unbuffered aqueous solution (Cen et al., 2004)......	16
Figure 7: Disulfiram and its metabolic pathways in humans. DDC = Diethyldithiocarbamate; MeDDC = S-methyl-N,N-diethyldithiocarbamate; DTC = Diethylthiocarbamate; MeDTC = S-methyl-N,N-diethylthiocarbamate.....	17
Figure 8: Reaction scheme for the synthesis of GCPQ.....	33
Figure 9: Separation of the solution into three different layers was done in separating funnel to extract the aqueous and fatty layer from the solution. ....	37
Figure 10: <sup>1</sup> HNMR spectrum of GCP10Q11 in CD <sub>3</sub> OD. ....	46
Figure 11: <sup>1</sup> HNMR spectrum of GCP20Q11 in CD <sub>3</sub> OD .....	47
Figure 12: An example of chromatogram of light scattering (red line), quasi-elastic light scattering (pink line) and differential refractive index (blue line) detector signals used in ASTRA software in determination of GCPQ molecular weight.....	49
Figure 13: Schematic diagram of an HPLC system.....	52
Figure 14: Illustrations of hydrodynamic diameter for various size and shape of particles. ....	54
Figure 15: An illustration of the zeta potential at the surface of a negatively charged particle measured by DLS. ....	56

Figure 16: HPLC chromatogram shows disulfiram peak at LLOQ of 0.25 $\mu\text{g/ml}$ with retention time at 1.58 minutes. ....	59
Figure 17: The linear calibration curve of disulfiram obtained from the DS standards. ....	60
Figure 18: The TEM image (top) is the nanoparticles formed after the sonication of DS with GCP10Q11. The image (bottom) shows the example of DS crystals seen in the formulations. All images were captured before centrifugation. ....	65
Figure 19: Amount of DS detected in oil samples from DS in soybean oil stock made at 20 mg/ml at Day 0, 1, 3, 6 and 8. Data were presented as mean $\pm$ SD (n = 3). ....	76
Figure 20: GCP20Q11 micelles (a) appeared as a clear suspension, whereas 5% oil DS-GCP20Q11-E formulation (b) appeared as a milky-like emulsion. ....	78
Figure 21: Schematic diagram for the preparation of 1:10 drug to polymer ratio of DS-GCP20Q11-E at 5% oil v/v. ....	82
Figure 22: The distribution of particle size populations for 1:10 DS-GCP20Q11-E formulation, 5% oil sonicated for 15 minutes, based on the (a) intensity, (b) volume and (c) number weighted distributions. ....	84
Figure 23: GCP20Q11 at 10 mg/ml in MilliQ water. The size of GCPQ micelles shown here are between 12 to 23 nm in diameter. Left: 46,000x magnification, Right: 93,000x magnification. ....	87
Figure 24: GCP20Q11 at 10 mg/ml dissolved in MilliQ water and added with empty 5% v/v/ soybean oil. The size of particles is seen heterogeneous with size between 20 to 40 nm, whereas the bigger size was between 100 to 900 nm in diameter. Left: 135,000x magnification, Right: 65,000x magnification. ....	87
Figure 25: DS-GCP20Q11-E 1:10, 5% oil . The particle size was heterogeneous between 9 to 100 nm in diameter. Left: 46,000x magnification, Right: 93,000x magnification. ....	88
Figure 26: DS-GCP20Q11E formulations at different amount of oil in glass tubes for oil layer observation. The oil layer in the 55% oil content formulation is clearly visible in the picture after 24 hours at room temperature. ....	91
Figure 27: DS-GCP20Q11-E formulations at 50 and 55% oil content stained with Nile red before and after centrifugation. Three distinct layers can be seen in 55% oil formulation. ....	92

Figure 28: The milky-white appearance of freshly prepared DS-GCP20Q11-E formulations at (from left) 5, 10, 20, 30, 40 and 50% v/v oil content. The formulations appeared thicker and denser towards the higher amount of oil content.....	93
Figure 29: Drug content (left) and DE% (right) for the freshly prepared DS-GCP20Q11-E formulations at 5, 10, 20, 30, 40 and 50% oil content. The mean values for each type of formulations were labelled on top of the bars. Data were presented as mean $\pm$ SD (n = 3). .....	94
Figure 30: Particle size of freshly prepared DS-GCP20Q11-E formulations at 5, 10, 20, 30, 40 and 50% oil content. Data were presented as mean $\pm$ SD (n = 3). .....	94
Figure 31: PDI values of freshly prepared DS-GCP20Q11-E formulations at 5, 10, 20, 30, 40 and 50% oil content. Data were presented as mean $\pm$ SD (n = 3). .....	95
Figure 32: TEM images of DS-GCP20Q11-E at 40% (a), 50% (b) and 55% (c) oil content. ....	97
Figure 33: DE% of DS-GCP20Q11-E formulations at different oil content stored at 4°C (DE% 4°C, top) and RT (DE% RT, bottom) on Day 0, 1, 2 and 8. Data were presented as mean $\pm$ SD (n = 3). .....	99
Figure 34: Particle size of DS-GCP20Q11-E formulations at different oil content stored at 4°C (Particle size 4°C, top) and RT (Particle size RT, bottom) on Day 0, 1, 2 and 8. Data were presented as mean $\pm$ SD (n = 3). .....	100
Figure 35: PDI values of DS-GCP20Q11-E formulations at different oil content stored at 4°C (PDI 4°C, top) and RT (PDI RT, bottom) on Day 0, 1, 2 and 8. Data were presented as mean $\pm$ SD (n = 3). .....	102
Figure 36: DE% of DS-GCP20Q11-E in HCl and phosphate buffer at t = 0, 0.5, 1, 2 and 4 hours. Buffers were at room temperature at the time of measurement. Data were presented as mean $\pm$ SD (n = 3). .....	107
Figure 37: The stability of DS following incubation of the DS-GCP20Q11-E formulation or the drug alone (control) in SGF and SIF up to 4 hours at 37°C. The drug concentration in the graph was normalized by using percentages. Data were presented as mean $\pm$ SD (n = 3). .....	112
Figure 38: Conversion of MTT reagent into formazan by NADH coenzyme. ....	115
Figure 39: Sixty wells (highlighted in red box) from a 96-well plate used in the assay. ....	118

Figure 40: Drug dilutions (yellow box) was done in a new plate (drug plate, containing no cells). Lane 1 was added with the highest drug concentration and serially diluted towards Lane 10 (20 $\mu$ l from previous well into 180 $\mu$ l fresh medium in the next well ~ 10 times dilution) to get ten different concentrations of drug in one plate. Five wells (5 replicates) were allocated for each concentration. Red box was for positive control (total cell death) and green box for untreated cells. ....	119
Figure 41: Dose-response curve of MIAPaCa-2 cell viability after treatment with DS (a), DS- GCPQ nanoemulsions (b), DS with copper (c) and DS-GCPQ nanoemulsions with copper (d) for 4 hours. ....	122
Figure 42: Summary of IC <sub>50</sub> obtained from dose-response curves of all four treatments. ....	123
Figure 43: Cell viability (%) upon exposure to different DS-GCP20Q11-E-compatible vehicles for 4 hours. ....	126
Figure 44: Schematic diagram of electrospray ionization (ESI).....	132
Figure 45: MS/MS in a triple quadrupole mass spectrometer .....	133
Figure 46: MS/MS spectrum of disulfiram (A) and MeDDC (B) from the positive mode ESI.	141
Figure 47: Chromatograms of blank plasma for DS and MeDDC (A and B, respectively), zero plasma (C), and DS and MeDDC at LLOQ level of 10 ng/ml (D and E, respectively). .....	143
Figure 48: DS, IS and MeDDC stability in reconstitution solvent methanol on Day 0 and Day 3. Data were presented as mean $\pm$ SD (n = 3). ....	146
Figure 49: DS, MeDDC and IS stability in post-extraction methanol (Figure 49A, B and C, respectively) at room temperature (RT) and -79°C.....	147
Figure 50: Plasma concentration–time profile for DS in SB oil and DS-GCP20Q11-E oral treatment (a and b, respectively). Data were presented as mean $\pm$ SD (n = 4). ....	153
Figure 51: Stability of DS and DS-GCP20Q11-E 5% oil in diluted mouse plasma ( <i>in vitro</i> ). ..	159
Figure 52: Percentage of drug encapsulation of freshly prepared DS-GCP20Q11-E in 5% glucose formulations at 5, 10, 20, 30, 40 and 50% oil content. Data were presented as mean $\pm$ SD (n = 3). ....	162
Figure 53: Particle size of freshly prepared DS-GCP20Q11-E in 5% glucose formulations at 5, 10, 20, 30, 40 and 50% oil content. Data were presented as mean $\pm$ SD (n = 3). ....	163

Figure 54: PDI values of freshly prepared DS-GCP20Q11-E in 5% glucose formulations at 5, 10, 20, 30, 40 and 50% oil content. Data were presented as mean $\pm$ SD (n = 3). .....	164
Figure 55: Zeta potential (mean $\pm$ SD, n = 3) of freshly prepared DS-GCP20Q11-E in 5% glucose formulations at 5, 10, 20, 30, 40 and 50% oil content. ....	164
Figure 56: Apparent viscosity of DS-GCP20Q11-E nanoemulsion in 5% glucose at different oil content at shear rate 100s <sup>-1</sup> . ....	165
Figure 57: Rheological behaviour of DS-GCP20Q11-E nanoemulsion in 5% glucose at different oil content at shear rate between 0.01 to 100s <sup>-1</sup> . ....	165
Figure 58: Plasma concentration – time profile of DS-GCP20Q11-E in 5% glucose intravenous treatment. Data were presented as mean $\pm$ SD (n = 5). ....	168
Figure 59: Simplified diagram to summarize the flow of experiment for the pharmacodynamics study of DS-GCP20Q11-E using pancreatic xenograft tumour model. ....	178
Figure 60: Bodyweight changes in individual animal throughout the study (A, B and C) of control, IV DS-GCPQ + Oral Cu, and Oral DS + Oral Cu group, respectively.....	180
Figure 61: Mean tumour volume measured from Day 8 until end of study in all 3 groups. ....	181
Figure 62: Tumour volume progression in individual mouse for IV DS-GCPQ + Oral Cu (A), Oral DS + Oral DS (B), and control (C) group measured from Day 8 until end of study. ....	183
Figure 63: Kaplan-Meier survival curve of nude mice bearing pancreatic xenograft tumours..	184

# List of Tables

Table 1: Various properties of DS reported in the literature. ....	21
Table 2: DS-loaded nanocarriers and its brief formulation description.....	27
Table 3: Level of palmitoylation and quaternisation (P% and Q%, respectively) of GCP10Q11 and GCP20Q11 (GC source: Chitomerics and Sigma Aldrich, respectively).....	44
Table 4: Molecular weight of GCPQs based on weight average molecular weight ( $M_w$ ), number average molecular weight ( $M_n$ ) and polydispersity index ( $M_w/M_n$ ) of the polymer. ....	48
Table 5: Linearity of disulfiram standards by HPLC method. The linear regression equation was obtained from three calibration curves. ....	59
Table 6: Precision and accuracy of the HPLC assay method for disulfiram (DS). SD = standard deviation of the three replicates.....	60
Table 7: Drug content, DE%, particle size and PDI values for 1:5 and 1:10 DS-GCP10Q11 formulations prepared with no drug pre-dissolution step. Data were presented as mean $\pm$ SD (n = 3). ....	64
Table 8: Drug content, DE%, particle size and PDI values for 1:5 and 1:10 DS-GCP10Q11 formulations prepared whereby drug and polymer pre-dissolved in solvent. Data were presented as mean $\pm$ SD (n = 3).....	67
Table 9: Drug content, DE%, particle size and PDI values for 1:5 and 1:10 DS-GCP20Q11 formulations prepared with no drug-predissolution step. Data were presented as mean $\pm$ SD (n = 3). ....	69
Table 10: Drug content, DE%, particle size and PDI values for 1:5 and 1:10 DS-GCP20Q11 formulations prepared whereby drug and polymer pre-dissolved in solvent. Data were presented as mean $\pm$ SD (n = 3).....	70
Table 11: Solubility of DS in various types of oil. ....	75
Table 12: Table of ingredients for preparation of 5% oil v/v DS-GCP20Q11-E formulations....	77
Table 13: Drug content and DE% of the 1:5 and 1:10 DS-GCP20Q11-E formulations after 5 minutes' sonication. Data were presented as mean $\pm$ SD (n = 3). ....	79
Table 14: Drug content and DE% of the 1:5 and 1:10 DS-GCP20Q11-E formulations after 15 minutes' sonication. Data were presented as mean $\pm$ SD (n = 3). ....	79

Table 15: Average particle size, PDI value, zeta potential and pH of 5% oil DS-GCP20Q11-E formulations. Data were presented as mean $\pm$ SD (n = 3). N/A = data not available.....	81
Table 16: Table of ingredients for preparation of DS-GCP20Q11-E from 5 to 55% oil v/v formulations.....	90
Table 17: The particle size, PDI values of DS-GCP20Q11-E and GCP20Q11 suspensions in highly acidic and basic pH condition. Data were presented as mean $\pm$ SD (n = 3).....	104
Table 18: Four different groups of treatments for the MTT assay. ....	118
Table 19: LLOD and LLOQ of DS and MeDDC .....	144
Table 20: Intra-day and inter-day analysis of the QC samples for determination of precision and accuracy of the LC-MS/MS assay. Data were presented as mean $\pm$ SD (n = 5). ....	144
Table 21: Extraction recovery and matrix effects (ME%) of DS and MeDDC from plasma.....	145
Table 22: Pharmacokinetic parameters for single oral administration of DS-GCP20Q11-E and DS in SB oil. N/A = not available. ....	154
Table 23: Pharmacokinetic parameters for single IV administration of DS-GCP20Q11-E in 5% glucose. ....	169
Table 24: Mean tumour weight (g) in all three groups measured upon excision from the flank of the animals during post-mortem. ....	183

# List of Abbreviations

<b>%CV</b>	Percentage of coefficient of variation
<b>%ME</b>	Matrix effects
<b>%RE</b>	Percentage of relative error
<b>ALDH</b>	Aldehyde dehydrogenase
<b>API</b>	Atmospheric pressure ionization
<b>AUC</b>	Area under curve
<b>AUC<sub>0-t</sub></b>	Area under curve from zero (0) hours to time of last quantifiable concentration (t).
<b>BCSC</b>	Breast cancer stem-cell like
<b>C<sub>max</sub></b>	The maximum drug concentration in the plasma
<b>CMC</b>	Critical micellar concentration
<b>CO<sub>2</sub></b>	Carbon dioxide
<b>CSC</b>	Cancer stem cells
<b>CuCl<sub>2</sub></b>	Copper chloride
<b>CuDDC</b>	Copper-diethyldithiocarbamate
<b>CuDS</b>	Copper-disulfiram
<b>DAR</b>	Disulfiram-alcohol reaction
<b>DDC</b>	Diethyldithiocarbamate
<b>DDS</b>	Drug delivery systems
<b>DE%</b>	Drug entrapment
<b>dGC</b>	Degraded glycol chitosan

<b>DLS</b>	Dynamic light scattering
<b>DMEM</b>	Dulbecco's Modified Eagle's Medium
<b>dn/dc</b>	Refractive index increment
<b>DPH</b>	Diphenhydramine
<b>dRI</b>	Differential refractive index
<b>DS</b>	Disulfiram
<b>DS/Cu</b>	DS with copper
<b>EPR</b>	Enhanced permeation and retention
<b>ESI</b>	Electrospray ionization
<b>GC</b>	Glycol chitosan
<b>GCPQ</b>	Quaternary ammonium palmitoyl glycol chitosan
<b>GIT</b>	Gastrointestinal tract
<b>GPC</b>	Gel permeation chromatography
<b>HBBS</b>	Hanks' Balanced Salt Solution
<b>HCl</b>	Hydrochloric acid
<b>HPLC</b>	High-performance liquid chromatography
<b>IC<sub>50</sub></b>	Half-maximal inhibitory concentration
<b>IS</b>	Internal standard
<b>IV</b>	Intravenous
<b>LC-MS/MS</b>	Liquid chromatography with tandem mass spectrometry
<b>LLOD</b>	Lower limit of detection
<b>LLOQ</b>	Lower limit of quantification
<b>MeDDC</b>	S-methyl-N,N-diethyldithiocarbamate

<b>MeDTC</b>	S-methyl-N,N-diethylthiocarbamate
<b>MeDTC sulfone</b>	S-methyl-N,N-diethylthiocarbamate sulfone
<b>MeDTC sulfoxide</b>	S-methyl-N,N-diethylthiocarbamate sulfoxide
<b>M<sub>n</sub></b>	Number average molecular weight
<b>MPS</b>	Mononuclear phagocytic system
<b>MRM</b>	Multiple reaction monitoring
<b>MTT</b>	3-[4,5-dimethylthiazol-2-yl]-2,5 diphenyl tetrazolium bromide
<b>M<sub>w</sub></b>	Weight average molecular weight
<b>MWCO</b>	Molecular weight cut-off
<b>NaOH</b>	Sodium hydroxide
<b>NF-κB</b>	Nuclear-factor kappa B
<b>NMR</b>	Nuclear magnetic resonance
<b>O/W</b>	Oil-in-water
<b>PBS</b>	Phosphate buffered saline
<b>PDAC</b>	Pancreatic ductal adenocarcinoma
<b>PDI</b>	Polydispersity index
<b>PEG</b>	Poly(ethylene glycol)
<b>PES</b>	Polyethersulfone
<b>PGC</b>	Palmitoylated degraded glycol chitosan
<b>PLGA</b>	Poly (lactic-co-glycolic acid)
<b>PNS</b>	Palmitic acid N-hydroxysuccinimide ester
<b>QC</b>	Quality control
<b>RF</b>	Radio frequency

<b>ROS</b>	Reactive oxygen species
<b>RPC</b>	Reversed-phase chromatography
<b>RPMI</b>	Roswell Park Memorial Institute medium
<b>RT</b>	Room temperature
<b>SB</b>	Soybean oil
<b>SD</b>	Standard deviation
<b>SGF</b>	Simulated gastric fluid
<b>SIF</b>	Simulated intestinal fluid
<b><math>t_{1/2}</math></b>	Elimination half-life
<b>TEM</b>	Transmission electron microscope
<b><math>T_{max}</math></b>	The time at which the maximum drug concentration in the plasma is reached
<b>UV</b>	Ultraviolet
<b>W/O</b>	Water-in-oil

# Chapter 1

## Introduction

### 1.1 Current cancer treatment

Cancer is the leading cause of deaths worldwide with 8.2 million cancer-related death reported in 2012 (Forman and Ferlay, 2014). In the United Kingdom, 2.5 million people are estimated living with cancer and this number is predicted to increase up to 4 million by 2030 (Maddams et al., 2012). This staggering numbers of cancer-associated mortality could mean that the current cancer treatment regime is not sufficient enough to combat the rapid and aggressive progression of cancer, despite of the widely diverse of advanced chemotherapeutic drugs available in the market.

Patients who have early diagnosis of the tumours are usually subjected to localized treatment where surgery are performed to remove the malignant tissues. In the advanced stage of cancer where tumours have metastasized to other tissues, the common treatments after surgery is followed by the adjuvant therapy which involves chemotherapy, radiotherapy and immunotherapy. The goal of adjuvant therapy is to reduce recurrence of the disease locally and systemically thus improving the survival rate of the patients (Chu and Sartorelli, 2015).

## **1.2 Issues with chemotherapeutic drug delivery**

The oral use of many chemotherapeutic drugs is hindered by their low bioavailability which can be frequently attributed to the low aqueous solubility and low intestinal permeability of the drug; i.e. Class 4 category compounds according to the Biopharmaceutical Classification System (Calleja et al., 2011). These low water solubility drugs are usually being absorbed slowly in the gut leading to variable or inadequate therapeutic concentrations reaching the systemic circulations (Savjani et al., 2012).

Due to bioavailability and also potential toxicity, the chemotherapeutic drugs tend to be administered parenterally. Once the drug is administered intravenously, the drug directly circulates throughout the body thus in principle giving access to the whole body. However, the drug level in the system is likely to rapidly drop due to various reasons such as metabolism in the liver and glomerular excretion by the kidney. This potentially limits the portion of the drug reaching the target sites, therefore reducing its medicinal effect.

One of the major consequence in the use of chemotherapy drugs is the cytotoxic side effects resulting from the treatment. There is risk of side effects happening when part of the dose not reaching the target site thus toxic to the off-target tissues. Apart from killing the cancer cells, the drugs usually destroy surrounding healthy cells as well, especially the rapidly proliferating cells such in bone marrow, hair follicles, gonads and digestive tracts. This would later lead to occurrence of several adverse effects with symptoms such as fatigue, nausea, vomiting, loss of hair, impaired fertility, gastrointestinal disturbance and bone marrow suppression.

### **1.3 General issues with conventional drug delivery**

Suboptimal pharmacokinetics of conventional drugs is frequently related to the design and physicochemical property of the drugs, such as their chemical stability, dissolution rate, pKa and lipid solubility, all of which influence the drug's absorption across the gut membrane upon oral administration (Ashford, 2013).

Drug delivery systems (DDS) are commonly used to address the problems related to 1) poor solubility of the drug in aqueous solution causing the drugs to precipitate in aqueous medium; 2) rapid breakdown *in vivo*, causing loss of activity due to degradation upon contact with physiological pH or plasma proteins; 3) unfavourable pharmacokinetics, such as rapid drug clearance by the kidney and metabolic inactivation by the liver (Allen and Cullis, 2004). The problems with the conventional design of drugs have a major impact on the efficiency of chemotherapeutic drugs. In recent years, nanoparticulate delivery systems have created significant interest in the search of efficient way to improve the bioavailability of drugs.

### **1.4 Nanotechnology in cancer medicine**

The word "nanotechnology" was first introduced by Norio Taniguchi from Japan in 1974. The modern nanotechnology was initiated by the attention to colloid science and analytical tools such as the scanning tunnelling microscope in 1981 (Pathak, 2009). Application of nanotechnology in cancer medicine (cancer nanomedicine) is focusing more on creation of novel therapeutic and improving the state of current cancer treatment.

Nanomedicine is a broad area involving the use of nanotechnology in medical application specifically for the use in pharmaceuticals, imaging agents and theranostics (Duncan and Gaspar, 2011) for the improvement in diagnosis, imaging, treatment and

prevention of the disease (Farokhzad and Langer, 2009, Moghimi et al., 2005). Main attractive benefits of nanomedicine are basically related to the nanoscale size, high surface area and functionalized surface of the material which enable it to access target sites in the human body and interact with the local tissues in a specific manner (Sainz et al., 2015, Sahoo et al., 2007).

The involvement of nanomedicine in development of nanoscale drug delivery systems involves the use of nanoparticles. With size in range of one to several hundred nanometres, nanoparticles have been developed into various systems to create devices such as nanocarriers. Some of the well-known nanocarriers include polymeric nanoparticles, polymeric micelles, nanoemulsions, liposomes, and nanoshells (Ferrari, 2005, Shah et al., 2010) (Figure 1). Nanocarriers usually act as a vehicle by either physically entrapping the drugs in or covalently bound to it. Characteristics required for an optimal nanocarrier design include high binding affinity, long circulating half-life, easy intracellular penetration, biocompatibility and high drug protection (Pathak, 2009).

Application of nanomedicine in cancer therapies are directed to overcome issues such as nonspecific distribution of anticancer agents in the systemic circulation, unnecessary cytotoxicity to the non-cancerous cells and inadequate drug concentrations at the target tumour site (Misra et al., 2010). In recent years, nanocarriers have been utilized to improve the therapeutic efficacy of cancer treatment. Some examples of the chemotherapeutic drug-loaded nanocarriers available in the market include Abraxane® for paclitaxel, Caelyx®, Doxil®, Myocet® for liposomal doxorubicin (Green et al., 2006, Ellerhorst et al., 1999), Transdrug ® for doxorubicin nanoparticles and Daunoxome ® for liposomal daunorubicin (Fassas and Anagnostopoulos, 2005).

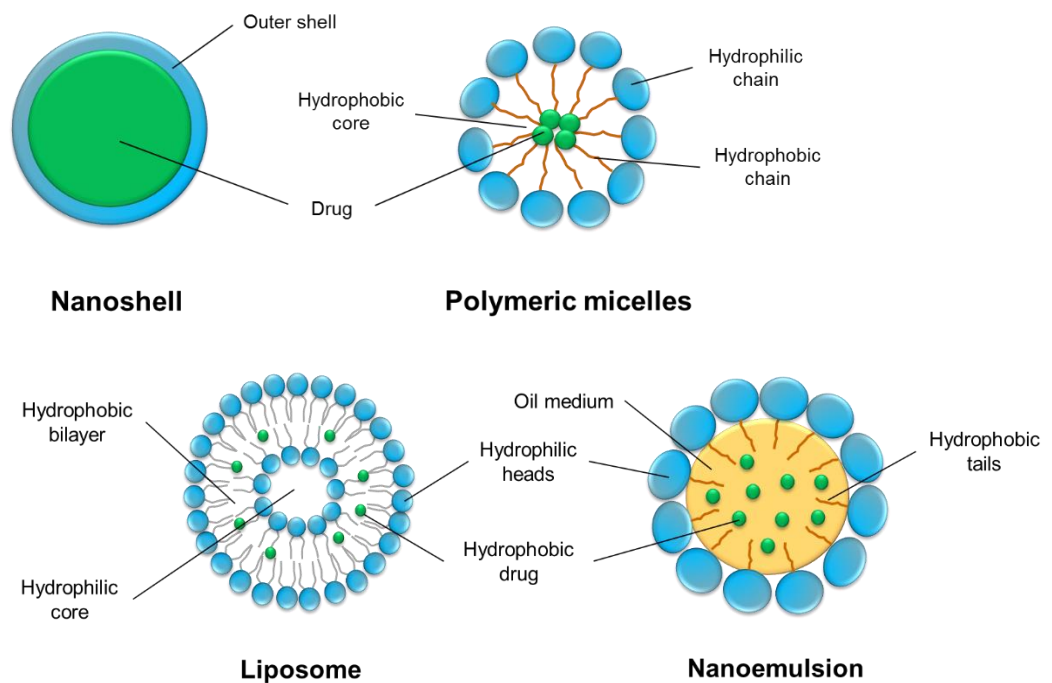


Figure 1: Schematic diagrams of several nanotechnology-based nanocarriers representing nanoshells, polymeric micelles, liposomes and nanoemulsions.

## 1.5 Strategies in cancer nanomedicine

Tumour physiology is different from the normal tissues. The vascularity of the tumours is highly heterogeneous. The tumours can be vascularized with blood vessels containing high proportions of endothelial cells, aberrant basement membrane and pericytes deficiency, while at the same time having open interendothelial junctions or transendothelial channels (size up to 400 nm in range) (Jain, 1997, Yuan et al., 1995). This would allow transport of macromolecules across the vasculature, including extravasation of nanometre-ranged particles from the main blood artery into the tumour microvasculatures. The lymphatic systems of the tumours are also abnormal, causing fluid retention and high interstitial pressure in the tumour as a consequence from the poor lymphatic drainage (Jain, 1987). The poor drainage system allows the particles that extravasate into the tumour to be retained in the malignant tissues. This combination of

leaky microvasculature and lack of intact lymphatic system contributes to the enhanced permeation and retention (EPR) effect, thus allow the strategy of passive targeting with the utilization of the nanoparticles (Arachchige et al., 2015, Maeda, 1992).

Mononuclear phagocytic system (MPS) or also known as reticuloendothelial system (RES) is a major factor in elimination of most nanoparticles. MPS composed of monoblasts, promonocytes and monocytes which originated from the bone marrow, transported into peripheral blood as monocytes, and as macrophages in the tissues (Lasser, 1983). Kupffer cells in the liver and dendritic cells in the lymph nodes and spleen are also part of MPS. MPS is part of immunological defence mechanism responsible for removal of foreign materials such as harmful microorganisms (Halma et al., 1992). This elimination mechanism involves series of steps which include opsonization on the surface of the particles and phagocytosis of the opsonized materials by the macrophages and other mononuclear phagocytes (Owens and Peppas, 2006).

Avoidance of MPS could be achieved by attaching shielding group on the particle surface to block electrostatic and hydrophobic attractions of opsonins from binding to the surface of the particles. Most widely used method is by covalently attaching poly(ethylene glycol) (PEG) chains to the particle surface, as the polymers are highly hydrophilic and typically neutral charge (Owens and Peppas, 2006). Hydrophilic particles are also more slowly opsonized compared to the hydrophobic ones (Carrstensen et al., 1992). This could lead to longer residence of the nanoparticles in the systemic circulation and improves the pharmacokinetic property of the drug.

Smaller size nanoparticles have more total surface area thus could allow more attachment to ligands such as peptides or monoclonal antibody for active targeting (Nie, 2010). The smallest capillaries in human body is around 4  $\mu\text{m}$ , therefore the particles are preferable to have sizes smaller than that in order to access locations by the intravenous, subcutaneous and intramuscular route. It was however reported that particles below the

size of 5 nm are rapidly cleared through renal clearance (Soo Choi et al., 2007) whereas particles of more than 1 $\mu$ m are prone to be trapped in the capillary beds of the liver and being taken up by the Kupffer cells (Illum et al., 1982, Caldorera-Moore et al., 2010). The size of spherical particles between 100-200 nm has the highest potential to stay longer in the circulation as they are small enough to avoid filtration in the spleen and large enough to avoid uptake by the liver (Petros and DeSimone, 2010), whereas particle size between 10-100 nm could utilize the EPR effect at the tumour site (Danhier et al., 2010). Polymer with molecular weight of around 15,000 Da is capable of stimulating the phagocytic activity whereas higher molecular weight polymer causes depression of the phagocytic activity of the MPS (Moghimi et al., 2001). Other benefits of small size particles include capability of cell membrane penetration and lysosomal escape after endocytosis (De Jong and Borm, 2008).

Therefore, in general, the DDS for anticancer drugs should be designed with the following criteria; 1) able to extravasate the target tissues, for instance, via the passive targeting through the EPR effect; 2) able to avoid the elimination by the MPS; 3) able to maintain drug concentration at effective dose at the target sites for certain period of time; and 4) minimal off-sites drug accumulation (drugs able to selectively destroy the malignant cells without affecting the normal ones).

## **1.6 Chitosan-based nanocarriers**

Nanoparticles made of biodegradable materials are more preferable as they are safer, low risk of toxicity and could be eliminated from the body through the natural process such as enzymatic degradation (Nair and Laurencin, 2007). In general, biodegradable polymers can be defined as the polymers that can be degraded and catabolized by microorganisms (bacteria, fungi, etc.) eventually into carbon dioxide and

water or other degradation products which are not harmful to the natural environment (Okada, 2002). Some of the presently available biodegradable polymers are made of polysaccharides (e.g. starch, chitosan, dextran and hyaluronic acid) and proteins (e.g. albumin, collagen and gelatine) (Piskin, 1995, Bohlmann, 2005, Chandra and Rustgi, 1998). These types of natural polymers are abundance in nature, making them cost-productive materials for the use as nanoparticles.

### **1.6.1 Chitosan and chitosan-derived glycol chitosan**

Chitosan is a type of natural aminopolysaccharide copolymer of glucosamine and N-acetylglucosamine units. Chitosan is a product of the alkaline deacetylation of chitin (Figure 2), a substance second most abundant in nature after cellulose (Rinaudo, 2006) which can be found in the shells of many crustaceans. Chitosan is favourable because of its biodegradability, biocompatibility, positively charged and low immunogenicity (Sonia and Sharma, 2011, Kumar et al., 2004).

The cationic property of chitosan is believed responsible for the mucoadhesive behaviour, as it is easily attracted to the negatively-charged mucin layer on the gut's epithelium, thus improving the residence time of the drug at the gut wall and consequently increase the chance of drug absorption (Lehr et al., 1992).

Since chitosan has a percentage of acetylation below 50%, it can only be dissolved in acidic solution with pH values below its pKa value of 6.5 by the protonation of the amine group on the C-2 position of the D-glucosamine unit (Rinaudo, 2006). This poor solubility of chitosan in neutral and basic aqueous solutions (around pH 7.5) is a restriction for absorption in the alkaline environment of the intestine. The chitosan structure however, contains many functional groups that can be chemically modified to

improve its solubility. The derivatization can utilize the primary amino group at the C-2 position, or the hydroxyl group at C-6 of the glucosamine unit (Zambito, 2013).

Glycol chitosan (GC) is one the derivatives of chitosan which is soluble in all pH values. GC is formed by reacting chitosan with ethylene glycol (Figure 2). The chemical modification of GC at the C-2 position, such as quaternisation and acylation, will improve properties of the polymer without changing the basic skeleton of chitosan.

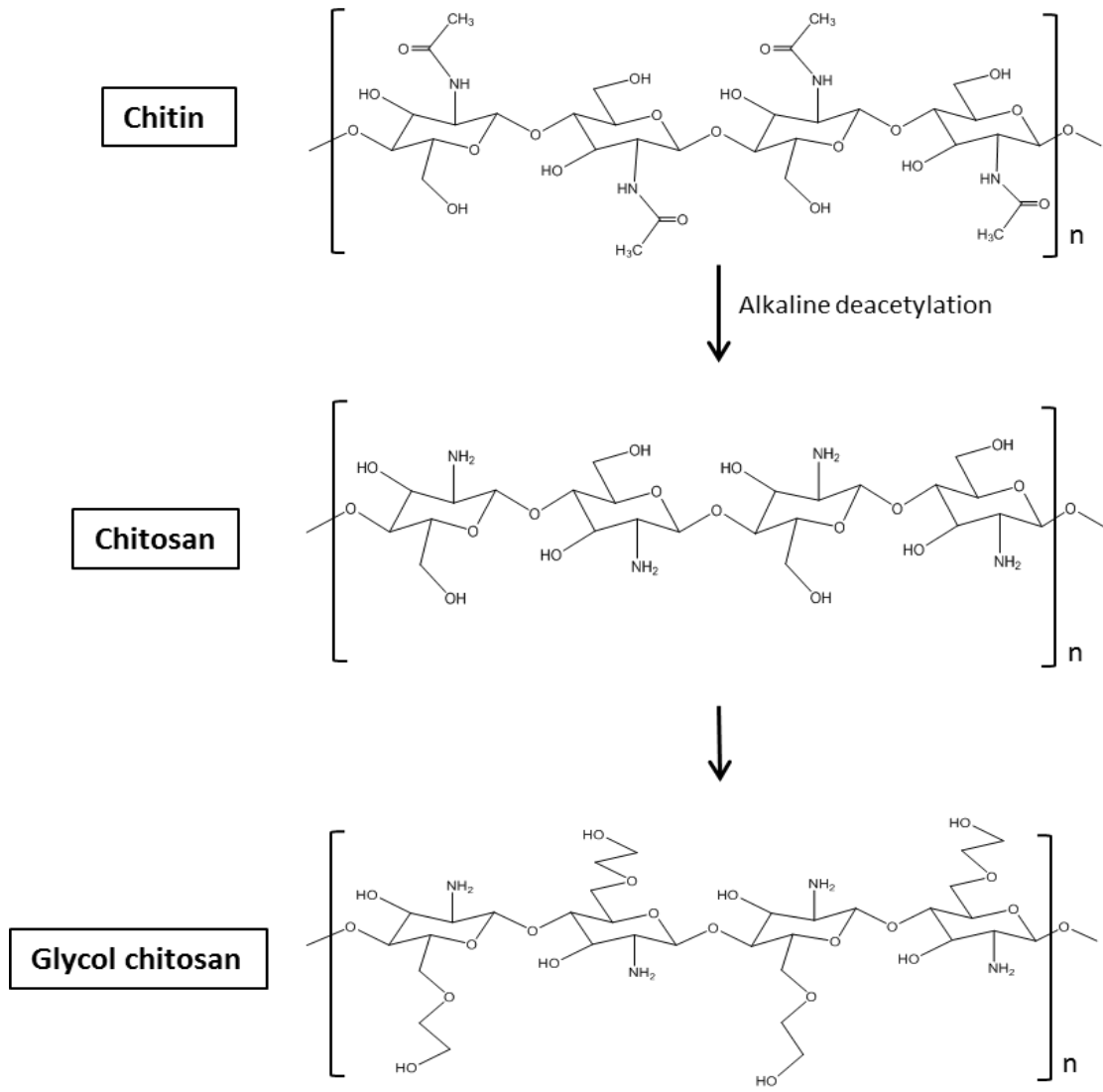


Figure 2: The flow of formation from chitin to chitosan and eventually into glycol chitosan.

### 1.6.2 Quaternary ammonium palmitoyl glycol chitosan (GCPQ)

Self-assembled polymeric micelles known as quaternary ammonium palmitoyl glycol chitosan (GCPQ) (Figure 3) are synthesized from glycol chitosan (Uchegbu et al., 2001). GCPQ is made into a polymer which spontaneously forms micelles in aqueous solution. Modification of glycol chitosan into amphiphilic GCPQ involves addition of hydrophobic pendant side chains and hydrophilic group connecting to the amine group of the GC backbone, causing the polymer to form spherical micelles in aqueous solution.

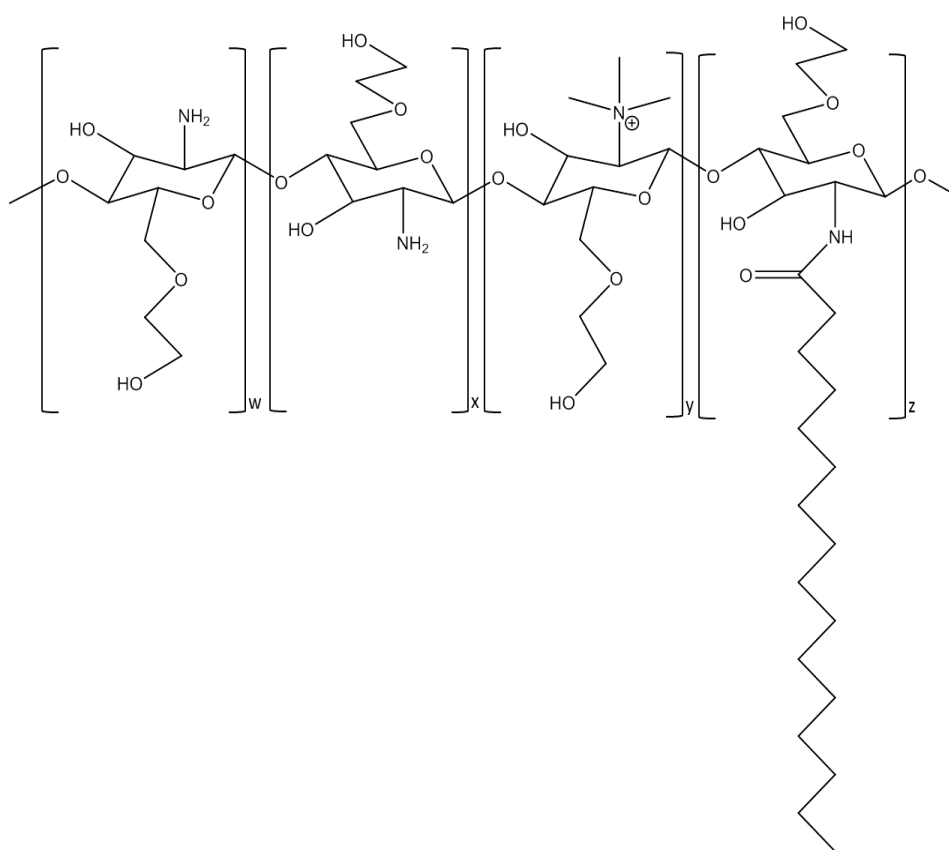


Figure 3: Quaternary ammonium palmitoyl glycol chitosan (GCPQ). The w, x, y and z represent the different monomeric repeating unit in the structure of GCPQ polymer as a result of random palmitoylation and quaternization at the amine group of glycol chitosan.

This polymer can be loaded with hydrophobic drugs such as griseofulvin, cyclosporine and propofol (Siew et al., 2012, Qu et al., 2006) in an aqueous media by using probe sonication method. The critical micellar concentration (CMC) is the concentration at which the micelles start to form (Fuguet et al., 2005). GCPQ has a low CMC value (Qu et al., 2006) which enables the nanoparticles to avoid premature disaggregation in the body fluid upon dilution and reach the target sites with full capacity of active drugs.

Encapsulation within GCPQ polymers could protect the drug from gastric and intestinal degradation and could improve absorption in the gut (Lalatsa et al., 2012b). Amphiphilic chitosan is bioadhesive (Martin et al., 2002) and this criterion will allow adherence of the chitosan-derived nanoparticles to the mucus membrane in the gut. The small size of GCPQ nanoparticles provides high surface area for faster drug dissolution (Lalatsa et al., 2012a).

Upon oral administration, GCPQ nanoparticles were able to promote drug transport by their adhesion to the mucus thus prolong the contact between loaded particles and absorptive enterocytes of the gastrointestinal tract (GIT) without disturbing intercellular tight junction permeability (Siew et al., 2012). In another study, GCPQ particles were proven to be absorbed in the GIT by the evidence of the particles being found within the villi of the ileum and duodenum which was presumably absorbed via the enterocytes. The particles had also been found in the intercellular spaces between hepatocytes in the liver, as well as in the gall bladder. Therefore, it was suggested that upon absorption via the enterocytes, GCPQ particles are transported to the liver via the venous blood in the villi or gut lymphatic vessels, later on to the gall bladder and presumably recirculated back to the GIT (Figure 4) (Lalatsa et al., 2012a).

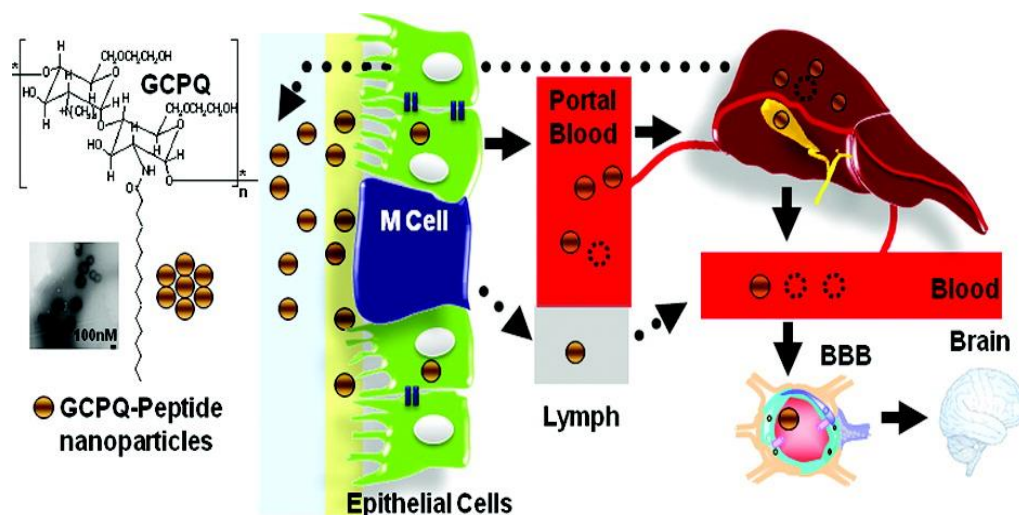


Figure 4: Schematic diagram of proposed transport route for GCPQ nanoparticle formulation with peptide upon oral intake (reproduced from Lalatsa et al., 2012a with permission).

Apart from enhancing oral drug absorption, GCPQ nanoparticles were also reported to promote brain delivery of neuropeptides known as leucine<sup>5</sup>-enkephalin (Lalatsa et al., 2012b). The same study also showed no accumulation of the particles in the lungs, suggesting GCPQ is capable to evade macrophage uptake by the reticuloendothelial system. Based on these properties, GCPQ should provide useful nanoparticles for delivery of drugs from the oral or intravenous route of administration into the tumours.

## 1.7 Disulfiram as a potential chemotherapeutic drug

The search continues for novel potent anticancer drugs capable of selectively killing cancer cells without harming the normal cells. In addition to looking at the development of novel chemical entities, there is also considerable interest in exploring the anticancer potential of existing drugs with known safety profile.

Disulfiram (DS) has been used for the treatment of alcoholism since the year of 1947 (Chick, 1999). The drug inhibits the activity of aldehyde dehydrogenase in the liver thus preventing the conversion of the highly reactive and toxic acetaldehyde into acetic acid. The serendipitous observation of the remission of breast cancer in a patient treated for alcoholism with disulfiram (Lewison, 1977) has led to an interest of DS as a candidate for the potential repurposing as an anticancer drug.

Disulfiram, chemically known as bis(diethylthiocarbamoyl)disulfide (Figure 5) is the first medication approved by U.S. Food and Drug Administration (FDA) for the treatment of chronic alcohol dependence. The treatment of alcoholism works when DS blocks the activity of aldehyde dehydrogenase (ALDH), an enzyme responsible for transforming acetaldehyde into acetate (Johansson, 1992). The inhibition of ALDH stops the oxidation of acetaldehyde, causing rapid formation of acetaldehyde in the blood resulting in the disulfiram-alcohol reaction (DAR). DAR is recognised by the moderate to severe side effects such as sweating and flushing on the upper chest and face (flush syndrome), nausea and vomiting, tachycardia, vertigo and blurred vision (Wright and Moore, 1990). The drug itself will not treat the addiction but the discomfort of DAR will encourage the abstinence towards drinking alcohol.

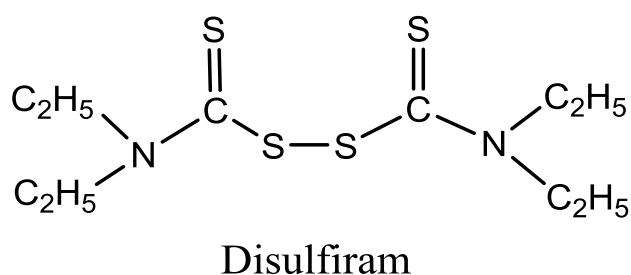


Figure 5: Chemical structure of disulfiram

### **1.7.1 Anticancer properties of disulfiram**

Years after the discovery of disulfiram, more scientific evidence of DS having anticancer properties has emerged. Studies have reported that DS has the cytotoxic effects against several types of cancer, such as pancreatic (Dalla Pozza et al., 2011, Kim et al., 2013), brain (Liu et al., 2012), prostate (Lin et al., 2011) and skin cancer (Cen et al., 2004). The anticancer property of metal-chelating DS is heightened when given to the patients in combination with metal, in particular, copper (Cvek, 2011). The cytotoxicity effect of DS given with copper appears to happen through inhibition of proteasome pathway leading to the induction of apoptosis activities in human cancer cell lines (Chen et al., 2006). There are other mechanisms of actions responsible for the anticancer effect of disulfiram which has been described later in this report in Table 1.

Copper ions are abundant in the human body and can be readily found in the stomach. The copper ions, Cu(II), could spontaneously combine with DS at its thiol groups, as well as with DS main metabolite, diethyldithiocarbamate (DDC), to form a much more stable compound known as copper-DDC (CuDDC) (Johansson and Stankiewicz, 1985). CuDDC is a neutral and hydrophobic metabolite of DS and is rapidly absorbed in the gut. Despite its stability, CuDDC is however rapidly degraded back into DDC and copper in the blood stream (Johansson, 1992). As proposed by Cen et al. (2004), the copper-disulfiram (CuDS) complex (Figure 6) can be synthesized by reacting DS and copper chloride (CuCl<sub>2</sub>) in unbuffered aqueous solution, followed by extraction in organic solvent such as anhydrous chloroform. The rapid reaction yields a dark brown precipitate which is hydrophobic and acidic with pH lower than 3. This stoichiometric product has been proven to have toxicity effect against melanoma cell line A375 as well as prostate cancer cell line DU145. Even though copper is known to be a cofactor in the tumour

angiogenesis (Duan et al., 2013), the role of Cu in promoting the toxicity effect of DS against cancer cells seems to outweigh the role of Cu in promoting the tumour growth.

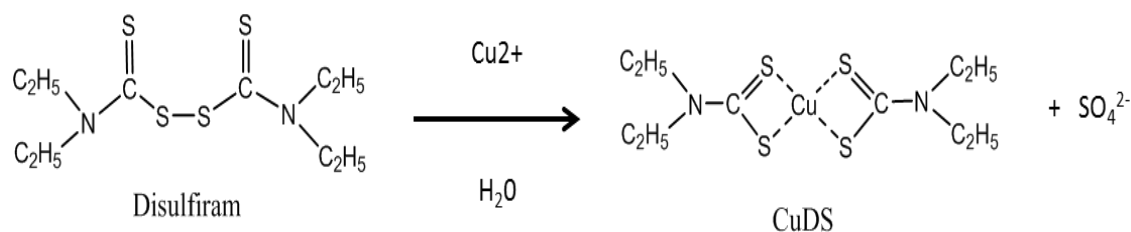


Figure 6: Proposed structure of copper-disulfiram complex (CuDS) after reaction of copper with disulfiram in unbuffered aqueous solution (Cen et al., 2004).

The metabolism of DS in humans is well-known (Figure 7) (Eneanya et al., 1981, Johansson, 1992) ensuring the safety of DS usage and this is a distinct advantage to repurpose of DS as a chemotherapy drug. About 80 to 95 percent of the orally ingested DS is absorbed in the GIT to be metabolized into DDC by the endogenous thiols and the glutathione reductase in the blood within four minutes (Cobby et al., 1977). The acidic condition in the stomach can also metabolize DS into the less stable DDC through the reduction process. DDC is polar, hydrophilic and decomposes rapidly into carbon disulfide and diethylamine (Eneanya et al., 1981). DDC in the bloodstream reaches the liver and undergoes methylation during the Phase II metabolism into S-methyl-N,N-diethyldithiocarbamate (MeDDC) by the action of S-methyl-transferase and later on into S-methyl-N,N-diethylthiocarbamate (MeDTC). Further oxidation process by the microsomal cytochrome-P450 produces S-methyl-N,N-diethylthiocarbamate sulfoxide (MeDTC sulfoxide) and S-methyl-N,N-diethylthiocarbamate sulfone (MeDTC sulfone). MeDTC sulfoxide and MeDTC sulfone are prone to carbamoylate the sulfhydryl of glutathione and produce S-(N, N-diethylcarbamoyl) glutathione or simply known as carbamathione (Faiman et al., 2013).

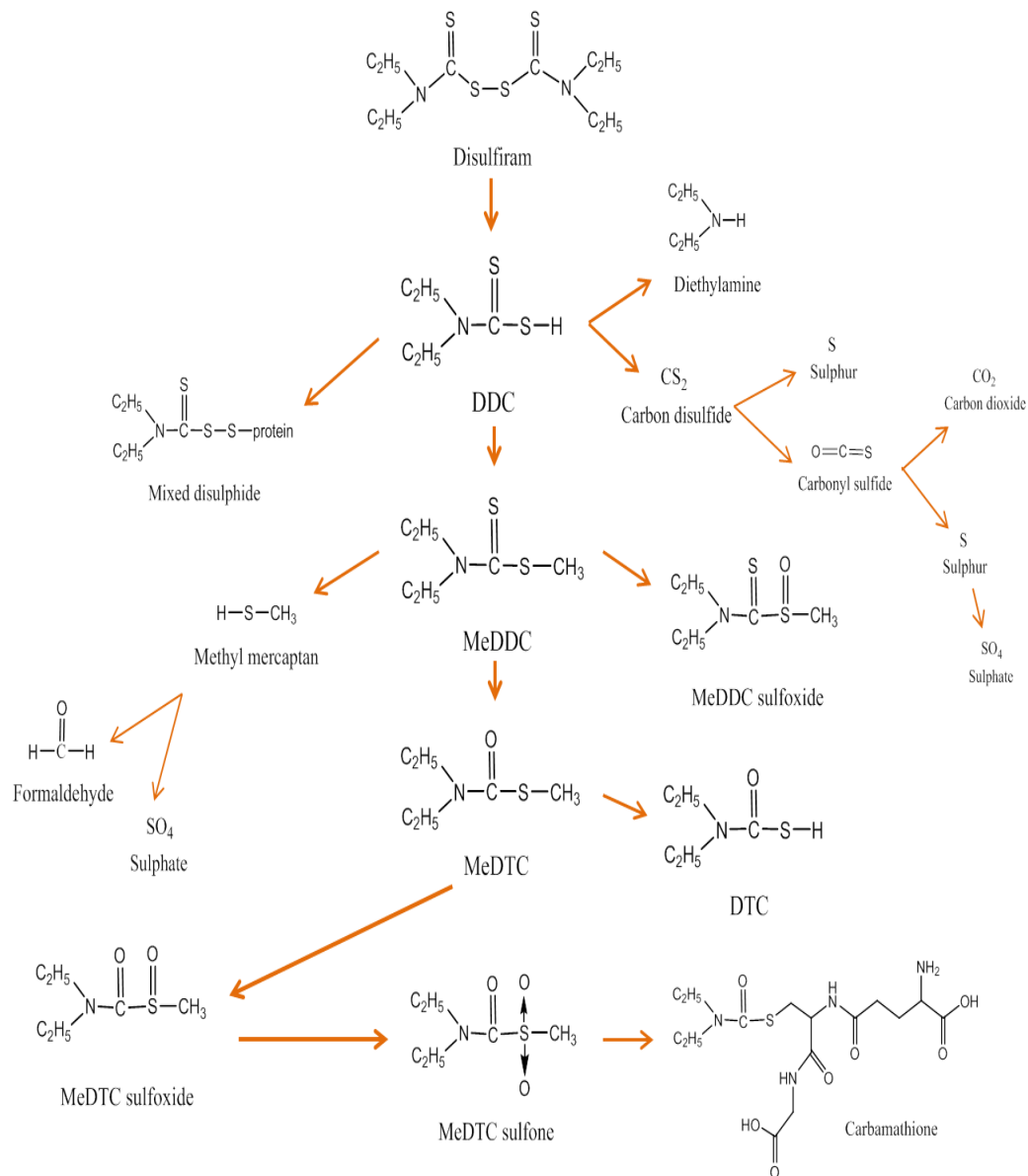


Figure 7: Disulfiram and its metabolic pathways in humans. DDC = Diethyldithiocarbamate; MeDDC = S-methyl-N,N-diethyldithiocarbamate; DTC = Diethylthiocarbamate; MeDTC = S-methyl-N,N-diethylthiocarbamate.

In the literature, DS has been reported to have various activities which have been studied thoroughly in both *in vitro* and *in vivo* models, as well as in human clinical trials. Table 1 summarizes some of the properties of disulfiram contributing to its anticancer activity.

Only DS, DDC and combination of copper with either DS or DDC possess the activity of anticancer effect against the tumour cells. Since the CuDDC is less stable than the CuDS, it is sensible to consider utilizing DS or combination of DS and copper to create nanoparticles that could enhance their delivery to the target sites in the tumours.

MECHANISM OF ACTION	ACTIVITY	EXPERIMENTAL MODEL	DRUG LEVEL	PUBLICATION
Induces reactive oxygen species (ROS), activates Jun N-terminal kinases (JNK) and p38 pathways	Cytotoxicity on glioblastoma multiforme stem-cell like	<i>In vitro</i>	10 $\mu$ M DS + 1 $\mu$ M Cu	Liu et al., 2012
Blocks the activity of P-glycoprotein membrane pump	Increased sensitivity of P-gp-transfected cells to vinblastine and colchicine and inhibited P-gp's verapamil-stimulated ATPase activity	<i>In vitro</i> ; <i>In vitro</i>	100 $\mu$ M DS; 0-200 $\mu$ M DS	Loo and Clarke, 2000; Loo et al., 2004
Potent inhibitor of nuclear-factor kappa B (NF- $\kappa$ B), a key pro-survival factor in cancer cells	Inhibition of NF- $\kappa$ B in Jurkat T cells; growth inhibition of colorectal and breast cancer cell line and breast cancer stem cells	<i>In vitro</i> ; <i>in vitro</i> ; <i>in vitro</i> ; <i>in vitro</i> ; <i>in vitro</i> , <i>in vivo</i> ,	100 $\mu$ M DS; 0-40 $\mu$ M DS; 10 $\mu$ M DS + 1 $\mu$ M Cu; 1 $\mu$ M DS + Cu; 1 $\mu$ M DS + 10 $\mu$ M Cu, 75 mg/kg DS + 8 mg/kg Cu	Schreck et al., 1992; Wang et al., 2003; Liu et al. 2012; Liu et al. 2013; Liu et al. 2014
	Synergistically enhances gemcitabine cytotoxicity, reverses gemcitabine resistance in colon and breast cancer cell lines	<i>In vitro</i>	0-6 $\mu$ M DS+Cu	Guo et al., 2010

	Inhibits breast cancer stem cells and enhances cytotoxicity of paclitaxel in breast cancer cell lines	<i>In vitro</i>	1µM DS and 1µM Cu	Yip et al., 2011
Induces apoptosis	Apoptosis in melanoma cells, multiple myeloma, acute myeloid and lymphoblastic leukaemia	<i>In vitro;</i> <i>in vitro;</i> <i>in vitro, in vivo;</i>  <i>in vitro</i>	25-50 ng/ml DS; 0.17 µm + 1 µm Cu; 5-20 µM DS+Cu, 50 mg/kg DS; 0.1-5 µM DS + 0.2-2 µM Cu	Cen et al., 2002; Cen et al., 2004; Chen et al., 2006;  Conticello et al., 2012
	Apoptosis in Jurkat cells by the caspase activity	<i>In vitro</i>	5-50 µM DS	Nobel et al., 1997
	Apoptosis in breast cancer cell line MDA-MB-231 by inhibition of proteasome activity	<i>In vitro</i>	5-20 µM DS+Cu	Chen et al., 2006
Reduces angiogenesis	Retards growth of C6 glioma and Lewis lung carcinoma in mice	<i>In vitro;</i> <i>in vivo</i>	1-10 µM DS; 13-30 ug/mouse DS	Shian et al., 2003; Marikovsky et al., 2002
Inhibits expression of matrix metalloproteinase 2 (MMP-2) and metalloproteinase 9 (MMP-9)	Invades human osteosarcoma cells	<i>In vitro;</i> <i>In vitro</i>	0-20 µM DS; 1-10 µM DS	Cho et al., 2007; Shian et al., 2003

Inhibits activating transcription factor/cyclic AMP-responsive element binding protein in metal dependent manner	Reduces hepatic metastases and ocular melanoma	<i>In vitro, in vivo</i>	0.15-5 $\mu$ M DS + 0.2-10 $\mu$ M Cu	Brar et al., 2004
Inhibits DNA methyltransferase by demethylating gene promoters and reactivating the expression of epigenetically silenced genes	Inhibits prostate cancer cell growth	<i>In vitro, in vivo</i>	100 nM DS, 10-40 mg/kg DS	Lin et al., 2011
Impairs the activity of endogenous arylamine N-acetyltransferase 1 (NAT-1)	Growth inhibition of human lung cancer cells	<i>In vitro</i>	8-30 $\mu$ M DS	Malka et al., 2009
Inhibits the expression of polo-like kinase 1 (PLK1) in glioblastoma multiforme (GBM) cells	Inhibits the growth of temozolomide resistant GBM cells without affecting normal human astrocytes, blocks self-renewal of the BT74 and GBM4 primary cell lines	<i>In vitro</i>	50-500 nM DS	Triscott et al., 2012

Table 1: Various properties of DS reported in the literature.

## **1.7.2 Disulfiram role against cancer stem cells**

Another DS feature that is gaining interest lately is its potential activity against the cancer stem cells. Cancer stem cells (CSC), similar to normal stem cells, have the capability of self-renewal (Lobo et al., 2007). Self-renewal enables the stem cell to divide and produce another stem cell that remains undifferentiated and possesses the same development and replication capabilities, while the other daughter cells undergoes proliferation and differentiation to tissue-specific cells. It was proposed that CSC can arise from either the normal stem cells (Fialkow, 1990, Lapidot et al., 1994) or from the progenitor cells that can give rise to self-renewing cancer stem cells (Reya et al., 2001, Clarke and Fuller, 2006). There is possibility that the tumour recurrence is caused by the treatment failure to eliminate the CSC and assumption is that the typical cancer treatments only shrink the bulk of the tumour cells without destroying the source of the cancer, i.e. the CSC.

ALDH activity has been recognized as a universal marker for the CSC. In particular, ALDH1A1 was the first one found among the 19 ALDH isoforms that is responsible for the CSC activity, while other isoforms (e.g. 1A2, 1A3, 1A7, 2\*2, 3A1, 4A1, 5A1, 6A1 and 9A1) was discovered later for their expression in CSC (Muzio et al., 2012). The detection of ALDH activity can be done using the aldefluor assay by measuring the fluorescent aldehyde substrate (Marcato et al., 2011, Ginestier et al., 2007, Storms et al., 1999). First ALDH-positive CSC isolation was the leukemia stem cells (Cheung et al., 2007) and later in the same year from breast cancers (Ginestier et al., 2007). This was later followed by the discovery in many types of cancer including pancreatic, prostate, brain, liver and lung (Jiang et al., 2009, Li et al., 2010, Ma et al., 2008, Rasheed et al., 2010, Rasper et al., 2010).

DS is known for blocking the activity of ALDH enzyme which prevents the transformation from acetaldehyde into acetate. This specific property of DS has made it a strong candidate for the activity inhibition or elimination of the CSC in the chemotherapeutic treatments. Several studies have been done to investigate the activity of DS against the CSC in different types of cancer. For glioblastoma multiforme (GBM), it was reported that DS with copper (DS/Cu) markedly inhibits the proliferation of glioma stem cells (GSC) (Hothi et al., 2012) with enhanced effect seen in combination with temozolomide (Lun et al., 2016). Liu et al. (2012) reported the GBM stem-like cell population was abolished by the cytotoxicity effect of DS and copper complex. Along with the complex enhancement on the activity of gemcitabine, the cytotoxicity was likely due to inhibition ALDH and NFkB pathway and the induction of reactive oxygen species (ROS).

DS was found cytotoxic against the breast cancer stem-cell like (BCSC) with and without presence of copper (Kim et al., 2016, Liu et al., 2013, Robinson et al., 2013, Yip et al., 2011). In another breast cancer study, the DS in liposome was able to block the hypoxia-induced NFkB activation of the BCSC and specifically targeted the BCSC population in both *in vitro* and *in vivo* (Liu et al., 2014). The DS anti-CSC activity was also seen against the ovarian cancer stem-like cells (Rezk et al., 2015).

The present study focused on the DS activity against pancreatic cancer. CSC was reported to cause the therapeutic resistance in pancreatic ductal adenocarcinoma (PDAC) (Hermann et al., 2007) and demonstrated resistance against gemcitabine and 5-fluorouracil (Hermann et al., 2007, Jimeno et al., 2009). Terminal ductal cells were reported as pancreatic/stem progenitor cells with ALDH1A1 expression in mice (Rovira et al., 2010, Strobel et al., 2007). Kim et al. (2013) reported DS to have significant cytotoxicity against the human PDAC-derived, MIAPaCa-2 and CFPAC-1 cell lines (high positive ALDH1A1 expression), without mortally affecting the normal pancreatic

epithelial cell line, hTERT-HPNE. The study also reported DS oral administration selectively eliminates ALDH1A1 cell in the xenograft tumours and inhibits the tumour growth upon combined treatment with low-dose gemcitabine.

Therefore, it is hypothesized that the DS formulation with GCPQ would curb the pancreatic CSC activity. Repurposing the use of DS as an adjuvant anticancer drug is worthwhile as it is inexpensive, easily available and has negligible adverse effects compared to the classical chemotherapeutic drugs. This can also avoid the expensive and time-consuming development process of new anticancer drugs that involves the costly pre-clinical and clinical testing (Chong and Sullivan, 2007).

## **1.8 Formulation of disulfiram with GCPQ polymers**

The oral administration of DS is preferable as patients can easily take the drug by mouth. The oral drug preparation is also at cheaper cost. The main issue in repurposing the use of DS as chemotherapeutic oral drug are the short half-life of the drug in the acidic gastric fluid and in the blood circulation (Johansson, 1992), while the highly hydrophobic property of the drug hinders its dissolution in aqueous bodily fluid which affects its absorption in the gut. Ultimately, to ensure the delivery of the drug molecules to reach the target tumours, the active form of DS must be able to pass the gut epithelium in intact form after an oral administration.

We hypothesized that GCPQ would encapsulate the hydrophobic DS within the interior part of the nanoparticles and form stable particles. The nanoparticles would allow more drug absorption in the gut by protecting the drug from degradation in the acidic condition of the stomach and from metabolism or degradation by the enzymes present in the liver and in the blood circulation, respectively. Hence the drug could be transported through blood or lymphatic circulation into the tumour site and released for the activity

against the malignant tissues. In order to produce a stable and robust formulation, fundamental approaches were taken such as thorough formulation characterization done both in *in vitro* and *in vivo* to ensure the optimum criteria of nanoparticles were achieved.

In literature, formulations of several types of DS-loaded nanocarriers have been published (Table 2) which include lipid emulsion, lipid nanocapsule, polymeric micelles, poly(lactic-co-glycolic acid) (PLGA) nanoparticle, liposome and mixed nanoparticle. Most of the formulations were made to improve DS stability in blood circulation and to improve the delivery of the drug to the tumour site by prolonging the DS-loaded nanoparticle's circulation and half-life, as well as developing the nanoparticle's controlled release. Almost all of the DS-loaded nanocarriers were reported to have encouraging effects on attenuating the cancerous progression in comparison to the free drug of which studies were done either *in vitro* or *in vivo*, or both.

NANOCARRIER	PUBLICATION	FORMULATION
Lipid emulsion	Chen et al., 2015	DS in oleic acid and soybean lecithin in medium chain triglycerides (MCT) as oil phase; glycerol, F68 and water as aqueous phase; both phases subjected for high-pressure homogenization
Lipid nanocapsule	Zhang et al., 2015	Phase-inversion method of DS with MCT, Kolliphor HS15, Lipoid S75 and sodium chloride
Polymeric micelles	Duan et al., 2013	Micelles and DS co-dissolved in dimethylformamide (DMF) followed by addition into water
	Löbner et al., 2009	PEG5000- <i>b</i> -PCL5000 dissolved in DS-DMF solution, then added dropwise into phosphate buffered saline
Poly(lactic-co-glycolic acid) (PLGA) nanoparticle	Fasehee et al., 2016b	DS in PLGA or PLGA-PEG-folate dissolved in dimethylsulfoxide followed by addition into water
	Hoda et al., 2015	Nanoprecipitation of DS with PLGA, 1% Pluronic 188, PS80 and Triton X-100
	Hoda et al., 2016	Addition of PLGA and DS in acetone into water containing 1% polysorbate 80, followed by evaporation and centrifugation
	Zembko et al., 2015	DS and PLGA mixture undergoes solving casting or heating compression method to produce DS-loaded wafers
	Wang et al., 2016	Emulsion-solvent evaporation method of PLGA and DS in dichloromethane and cyanomethyl diphenylcarbamide aqueous solution into oil-in-water emulsion, followed by evaporation and centrifugation to obtain purified nanoparticles
Liposome	Buckiova et al., 2012, Löbner et al., 2009	Reverse-phase evaporation method of DS with lipid stock (eggPC, DSPE-PEG-2000 and TRITC-DHPE)
Mixed nanoparticle	Song et al., 2016a, Song et al., 2016b	Nanoprecipitation method of methoxy poly(ethylene glycol)- <i>b</i> -poly(lactide-co-

		glycolide)/poly( $\epsilon$ -caprolactone (mPEG-PLGA/PCL) and DS mixture in DMF and water
--	--	---

Table 2: DS-loaded nanocarriers and its brief formulation description.

In order to find the most ideal and suitable type of DDS for utilization of DS and GCPQ in cancer therapy, two forms of nanoparticle formulations were investigated which were the polymeric micelles and nanoemulsion.

### 1.8.1 Polymeric micelles

Polymeric micelles are nanoparticles formed from amphiphilic copolymers that self-assembled in aqueous solution, forming inner hydrophobic core and outer hydrophilic layer based from the hydrophilic block of the copolymer (Sahoo and Labhassetwar, 2003). The inner micellar core is where the hydrophobic drug molecules are loaded. Application of polymeric micelles to be loaded with hydrophobic drugs and improve the drug delivery has been reported frequently in the literature (Lalatsa et al., 2012c). Generally, polymeric micelles improve dissolution of hydrophobic drugs by increasing their aqueous levels and the encapsulation is also increased with the increase of polymer hydrophobicity (Qu et al., 2006).

Several advantages of polymeric micelles are 1) better thermodynamic stability mostly from the intertwined polymer chains in the inner core (Xu et al., 2013), leading the low critical micellar concentration of the system thus rendering it more stable and able to avoid the rapid *in vivo* dissociation (Jones and Leroux, 1999, Rapoport, 2007); 2) narrow size distribution in nanometre range, owing to their unique core-shell structure which segregates the hydrophobic segments from the outer aqueous exterior. This makes them an ideal drug carrier system for the avoidance of the MPS and renal exclusion

following intravenous administration thus enhance the drug's bioavailability in the tumours (Gothwal et al., 2016).

Polymeric micelles have been used to improve drug delivery of sparingly soluble chemotherapeutic drugs (Wang et al., 2005). The micelles can be characterized based on their coatings which can be made of anticancer drugs, sugars or tumour-specific antibodies. The coatings enable the nanoparticles to target and bind the cancer cells, followed by the release of drug molecules (Gregoriadis and Florence, 1993, Miyata et al., 2011).

Some of the known biodegradable and biocompatible micelles for cytotoxic drug delivery are the utilization of non-toxic polymers such as PEG as the basic structure for the outer hydrophilic layer and PLGA as the base for the hydrophobic core (Gothwal et al., 2016). The polymeric micelles of PEG and PLGA conjugated with doxorubicin, paclitaxel or docetaxel have been reported (Yokoyama et al., 1990, Yoo and Park, 2001, Cheng et al., 2007).

## **1.8.2 Nanoemulsions**

By definition, an emulsion is a system consisting of two immiscible liquid phases, one of which is in the form of fine droplets (the dispersed phase) distributed uniformly throughout the other (continuous phase) (Eccleston, 2013). Emulsions are classified as oil-in-water (O/W) when oil droplets are dispersed in the aqueous medium, or water-in-oil (W/O) when the internal phase is formed by water. Emulsions are thermodynamically unstable. This is due to the high surface free energy which is caused by the high interfacial area between the dispersed phase and continuous phase droplets. Upon contact, the droplets coalesce to reduce the total interfacial area thus reducing the total surface energy. This leads to the phase separation (Attwood, 2013).

In order to kinetically stabilize the emulsions, emulsifying agents (emulsifiers) are added to help maintain the dispersion state after cessation of the agitation. The emulsifiers that are also known as surface active agents (surfactants), act by forming electrostatic or mechanical barrier at the droplet interface thus providing an interfacial film. The interfacial film increases droplet to droplet repulsions by introducing electrostatic or steric repulsive forces between the dispersed droplets (Eccleston, 2013, Attwood, 2013).

Emulsions, in particular the macroemulsions, have a wider range of droplet diameter with the range of 0.1 to 100  $\mu\text{m}$  (Attwood, 2013), whereas nanoemulsions are colloidal systems with droplets in nanometre range (10-300 nm). Nanoemulsions, which are also known as submicron emulsion or ultrafine emulsion, usually involve the use of oil, surfactant, co-surfactant and aqueous medium as the ingredients. The common O/W formulations involves the addition of surfactant to help lower the surface tension between oil and water and to prevent the coalescence during high-energy sonication procedure (Lovelyn and Attama, 2011).

A nanoemulsion drug delivery system is a promising way to enhance oral absorption of poorly soluble anticancer drugs such as paclitaxel, etoposide and doxorubicin (Tiwari and Amiji, 2006, Ganta and Amiji, 2009, Zhang et al., 2011, Mohan and Rapoport, 2010). For medicinal purposes, colloidal dispersion in nanometre range such as nanoemulsions is favourable for several reasons such as; 1) better stability to particle aggregation and gravitational separation thus prevents creaming and sedimentation during storage as well as avoidance of flocculation and creaming (Tadros et al., 2004); 2) large surface area of nanoparticles promotes rapid drug release thus increase the drug bioavailability. Nanoemulsions has the capacity to be loaded with large amount of hydrophobic drugs in the oil core (Lovelyn and Attama, 2011). This could avoid unnecessary toxicity from the use of high amount of surfactant needed to stabilize the higher amount of drug in the formulation.

## 1.9 Objectives of the study

The general objective of the study is to develop a DS nanoparticle formulation with ideal characteristics that could protect the drug, improve its delivery to the target sites and have a significant effect on the progression of the tumour. The specific objectives of the study are as follows:

- To synthesize glycol chitosan-based polymer GCPQ and to characterize the modification of the polymer based on the molecular weight, degree of palmitoylation and degree of quaternisation
- To develop DS nanoparticle formulation using GCPQ polymer that has the ideal characteristics such as high drug load, particle size at nano-range diameter and small particle size distribution
- To characterize the formulation based on the stability in various *in vitro* environments such as different temperatures, pH buffers and simulated biological fluids
- To determine the cytotoxicity effect of the DS nanoparticle formulation against human pancreatic cancer cell lines
- To determine the pharmacokinetic profile of the DS nanoparticle formulation in the mouse model
- To determine the anticancer property of the DS nanoparticle formulation against development of xenograft tumour of pancreatic cancer in mouse model.

## Chapter 2

# Quaternary ammonium palmitoyl glycol chitosan (GCPQ)

### 2.1 Overview

GC was modified into amphiphilic GCPQ polymer by conjugating hydrophobic palmitic chains and creating hydrophilic regions with quaternisation at the free amine group of the GC sugar backbones. This type of polymeric micelles has hydrophobic group with a chain length of 16 carbons that allows self-aggregation and behaves like a polysoap (soluble polymers bearing pendant amphiphilic or hydrophobic groups) (Uchegbu et al., 2001). Acid degradation of GC allows the control of molecular weight while preserving the primary amine group on the repeating sugar unit.

GCPQ is able to self-assemble at neutral pH because GC itself is soluble at neutral pH. GCPQ has the CMC in micromolar range (6-100  $\mu\text{M}$ ) (Qu et al., 2006) compared to other block copolymers, such as Pluronic block copolymer which has the CMC in millimolar range (Dwyer et al., 2005). The low CMC value helps to prevent premature disaggregation upon dilution in biological fluid, thus improving the micellar stability in the gastrointestinal fluid and blood circulation.

## 2.2 Synthesis of GCPQ

The synthesis of GCPQ involves four main stages (Figure 8); acid degradation of GC, palmitoylation (acylation) of degraded GC with palmitic acid ester, quaternisation of palmitoylated GC with methyl iodide at the primary amine and removal of iodide from the newly formed quaternary ammonium product (Uchegbu et al., 2001) to produce N-palmitoyl, N,N,N-trimethylamino, N,N-diethylamino, N-monomethylamino, 6-O-glycol chitosan (quaternary ammonium palmitoyl glycol chitosan, GCPQ).

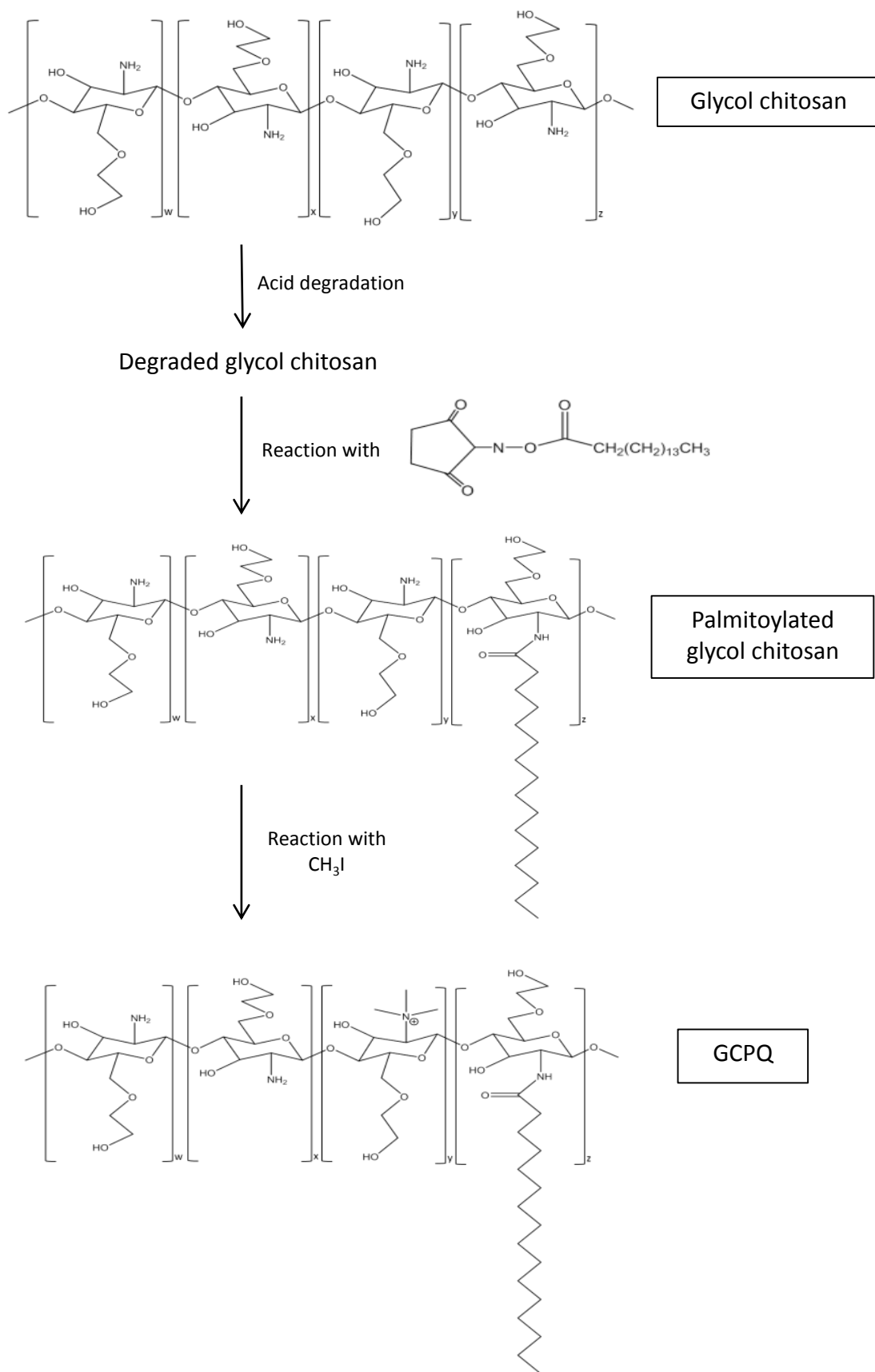


Figure 8: Reaction scheme for the synthesis of GCPQ.

## 2.2.1 Materials

Two batches of GCPQ were synthesized. The first batch (GCP10Q11) was synthesized using glycol chitosan (GC) supplied by Chitomerics whereas the second (GCP20Q11) batch was synthesized using GC from Sigma Aldrich.

Item	Supplier
Glycol chitosan Lot number: 120M1438V 081M1560V	Chitomerics Limited, Coventry, UK Sigma Aldrich, Missouri, USA
Palmitic acid N- hydroxysuccinimide ester	Sigma-Aldrich Company Limited, Dorset, UK
Sodium iodide	
Sodium bicarbonate	
Methyl iodide	
N-methyl-2-pyrrolidone	
Sodium hydroxide	
Resin (Amberlite IRA-96)	
Hydrochloric acid	
Absolute ethanol	
Diethyl ether	
Visking seamless cellulose dialysis membrane	Medicell International Limited, London, UK

## 2.2.2 Degradation of glycol chitosan

For acid degradation of GC, 2 g of GC was dissolved in 152 ml 4 M hydrochloric acid and incubated in 50<sup>0</sup>C water bath with shaking at 125 rpm for 24 hours. On the next day, the degraded GC (dGC) solution was cooled in a fridge for 10 minutes to bring it to room temperature before the exhaustive dialysis process against water. In the dialysis procedure, the dGC solution was transferred into seamless cellulose dialysis membranes with molecular weight cut-off (MWCO) 3500 Dalton. The tubes were then submerged in distilled water in 5 L conical flask and stirred. The water in the flask was changed 6 times in 24 hours, leaving at least 1 to 2 hours between changes. After 24 hours, the content of each membrane was emptied into a large beaker. Each membrane was rinsed with purified water to ensure no polymer was lost. The dialysed solution was poured into 60 ml freeze-drying bottles until 80 % full. Top of each bottle was covered with parafilm and small holes were pierced through the parafilm. The bottles containing dGC were placed in minus 20<sup>0</sup>C for at least an overnight to freeze the solution prior to the freeze drying process. The solution was freeze dried (ScanVac CoolSafe, LaboGene ApS, Lyngø, Denmark) until white, cotton-like solid was obtained.

### 2.2.3 Palmitoylation of degraded GC

After degradation, every 500 mg dGC was dissolved in 24 ml absolute ethanol and 76 ml Milli-Q water (MilliQ Integral Water Purification System, Millipore Corporation, Massachusetts, USA) added with 376 mg sodium bicarbonate. For every 500 mg dGC, 792 mg of palmitic acid N-hydroxysuccinimide ester (PNS) was dissolved in 150 ml absolute ethanol. The whole process involving PNS must be protected from light. The PNS solution was then transferred into a 1 L separating funnel wrapped with aluminium foil. The dGC solution was added with PNS solution in drop wise manner and with continuous stirring. The cloudy mixture produced was then left to stir for another 72 hours. The ethanol in the solution was removed by rotary evaporator at 50 to 52<sup>o</sup>C under reduced atmospheric pressure.

The remaining aqueous phase was extracted by adding diethyl ether three times the amount of the aqueous phase in a 1 L separating funnel (Figure 9). The solution was mixed by slow swirling movement of the funnel followed by intermittent release of pressure build-up from ether evaporation in the funnel. The funnel was left in upright position using a stand for at least 30 minutes to allow three distinct phases to separate. Among the three layers, only two bottom layers were collected (fatty and aqueous layers) while the top layer (organic ether layer) was discarded. The two layers collected was then added with new diethyl ether solution and extraction process was repeated twice more (three extractions in total).

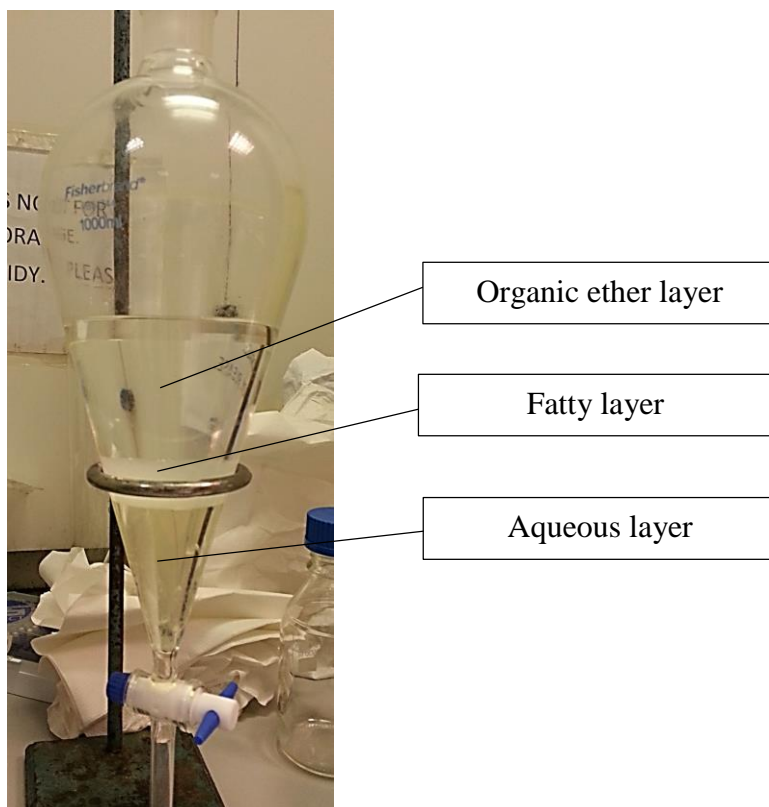


Figure 9: Separation of the solution into three different layers was done in separating funnel to extract the aqueous and fatty layer from the solution.

The cloudy aqueous solution was dialyzed exhaustively against water (as described previously in the dialysis process for degradation of GC) using dialysis membrane with MWCO 12,000 to 14,000 Dalton. After the 6 changes of water in 24 hours, the solutions were subjected for freeze-dry once again until cotton-like solid substance was obtained.

#### **2.2.4 Quaternisation of palmitoylated dGC (PGC)**

Each 300 mg PGC was dispersed in 25 ml N-methyl-2-pyrrolidone (NMP) in a conical flask capped with glass stopper and stirred vigorously overnight until a foamy dispersion was produced. In the next step, for each 300 mg PGC, 45 mg sodium iodide, 0.44 ml methyl iodide and 40 mg sodium hydroxide were dissolved in 4 ml absolute ethanol and added into the PGC dispersion. All of the ingredients were stirred in pre-heated oil bath at 36<sup>0</sup>C under a nitrogen atmosphere for 3 hours. The nitrogen atmosphere was obtained by filling a balloon with nitrogen gas and clamping it closed. Once the balloon was placed on top of the flask in the oil bath, the clamp was released and the balloon sealed in place with parafilm.

After 3 hours, the product was precipitated by adding diethyl ether into a conical flask and left for overnight. On the following day, a brown precipitate formed at the bottom of the flask. The diethyl ether was carefully decanted to avoid polymer loss. The precipitated product was washed with 300 ml diethyl ether twice more. The resultant solid was dissolved in 100 ml water (for every 400 mg PGC) and dialyzed exhaustively against water (the same dialysis method as before) using MWCO membrane 7,000 Dalton.

#### **2.2.5 Removal of iodide**

A column was prepared by packing 100 ml Amberlite IRA-96 in a 1 L separating funnel. The column was washed with 150 ml 1 M hydrochloric acid followed by 8 L of Milli-Q water or more until a neutral pH was obtained. The funnel was left wet overnight with the tap closed. On the following day, the column was washed with another 2 L of water. With the tap closed, the dialysate was added into the funnel and it was then allowed to pass the column slowly. Once it reached the end of the column by gravitational force,

the solution was collected directly into freeze dry bottles. The column was washed with water in amount equal to twice of the column volume plus the dialysate volume or until the brown solution was no longer seen collected into the bottles. The solution was let frozen in the  $-20^{\circ}\text{C}$  freezer and freeze-dried until white cotton-like product obtained.

## **2.3 Characterization of GCPQ**

### **2.3.1 NMR spectroscopy**

Nuclear magnetic resonance (NMR) spectroscopy is a method for identifying compound and determining structure of organic compounds. The NMR method is based on utilization of magnetic momentum produced by spinning of magnetic nuclei at its nuclear axis. The spinning motion is termed as spin quantum number ( $I$ ), of which is determined by the even or odd number of neutrons and positively charged protons in the nuclei. Only nuclei with half-integral  $I$  ( $I = 1/2$ ), such as in  $^1\text{H}$  and  $^{13}\text{C}$ , are suitable for NMR measurement as they have uniform charge distribution on the nuclear surface (Ning, 2005).

When a magnetic nucleus is placed in a large static magnetic field and subjected to pulses of electromagnetic radiation, such as radio frequency (RF), the energy absorbed by the nucleus causes transitions (flipping orientations) from lower to higher energy state, or the other way around. The frequency of absorbed energy is directly proportional to the magnetic field strength, thus allowing the modern Fourier transform spectrometer to be used for scanning the RF (Jones and Mulloy, 1993). This energy absorption induces a voltage detectable by tuned coil of wire which later translates into signals displayed as free induction decay. Relaxation happens when the spin system returns to thermal equilibrium where RF pulses are no longer present. The energy for flipping and thus

production of NMR signal is basically the energy difference between the two nuclear orientations which depends on the magnetic field strength (James, 1998).

Chemical shift ( $\delta$ ) shows the peak position for a particular functional group in parts per million (ppm) unit in the NMR spectrum. The chemical shift is the difference between position of the signal of interest and the reference standard at 0 ppm (James, 1998). Tetramethylsilane is commonly used as the standard for  $^1\text{H}$  measurement because it resonates at higher frequency than most other nuclei, having only single peak and can be removed easily from the sample (boiling point =  $27^\circ\text{C}$ ) (Ning, 2005). The area of the peak represents the number of nuclei contributing to the signal. Deuterium solvent (e.g. deuterated methanol) is usually used to dissolve the samples. Since deuterated solvent has the spin value of 1 ( $I = 1$ ), it has a completely different frequency from the  $^1\text{H}$  isotope thus avoiding solvent-sample signal interactions (Williams and Fleming, 1995).

### **2.3.2 Molecular weight of GCPQ**

The measurement of GCPQ's molecular weight was done using the gel permeation chromatography (GPC). GPC (Moore, 1964) is also known as size exclusion chromatography. It is a type of liquid chromatography in which the separation mechanism relies solely on size of the polymer molecules in solution rather than chemical interactions between the particles and the stationary phase.

The long chain polymers when dissolved in solvent would normally coil up to form coil formation that resemble a ball of strings and behave like tiny spheres. The hydrodynamic size of the spheres depends on the molecular weight of the polymers, with higher molecular weight polymers coil up to form larger spheres. These coiled polymers are then introduced into the mobile phase and flow through the pores of the GPC column. Large spheres that are unable to enter the pores are carried straight through the mobile

phase, whereas small spheres that fit the pores are retained in the stationary phase before eventually eluted out of the column at different rate depending on the size of the spheres (Agilent Technologies, 2015).

As a result, small coiled polymers that can enter many pores would take a long time to pass through the column, therefore exit the column slowly. Large coiled polymers that cannot enter the pores leave the column quickly, whereas the intermediate size coiled polymers leave the column in between these examples (Bly, 1970). This also means larger spheres (higher molecular weight polymers) eluting first, followed successively by smaller spheres (lower molecular weight polymers). As the spheres exit the column, elution behaviour of the samples is displayed in a chromatogram, which shows the volume of materials exited the column at any one time. The chromatogram data is then compared to a calibration that shows elution behaviour of polymer with known molecular weight.

Calculations of molecular weight in GPC are based on distribution. The amount of particles is counted at every weight in the distribution to calculate average value for the whole sample. This calculated average is known as number average molecular weight ( $M_n$ ) and the other molecular weight average used is known as weight average molecular weight ( $M_w$ ). It is common to see  $M_w$  value greater than  $M_n$  unless the polymer is completely monodisperse. The ratio of  $M_w$  to  $M_n$  is used to calculate polydispersity index ( $M_w/M_n$ ) as indication of the polymer's molecular mass range (Agilent Technologies, 2015).

Standard GPC detectors are not able to count number of molecules eluted from the column, meaning that the weight averages cannot be measured directly. Therefore, concentration of molecules on weight/volume basis is measured using concentration detector, which measures the differential refractive index (dRI). In combination with the refractive index detector, static light scattering detector can be used, such as multi-angle

laser light scattering (MALLS) detector (Trathnigg, 1995). MALLS detector works under the principle that scattering beam of light as it strikes a polymer molecule enables the instrument to directly measure the molar mass when the refractive index increment ( $dn/dc$ ) is known. This gives a response directly proportional to the molecular weight of the polymer molecules.

### 2.3.3 Materials

Item	Supplier
Deuterated methanol, CD <sub>3</sub> OD	Cambridge Isotope Laboratories, Inc, Massachusetts, USA
Sodium acetate anhydrous	Sigma-Aldrich Company Limited, Dorset, UK
Glacial acetic acid	Fisher Scientific Limited, Leicestershire, UK
Methanol	Fisher Scientific Limited, Leicestershire, UK
Polyethersulfone (PES) syringe filter	Merck Milipore Limited, Cork, Ireland

### 2.3.4 Methodology

#### 2.3.4.1 Level of palmitoylation and quaternisation of GCPQ

Nuclear magnetic resonance experiments (<sup>1</sup>H NMR) of GCPQ were performed using Bruker AMX 400 MHz spectrometer (Bruker Instruments, Coventry, UK). GCPQ solution was prepared by dissolving 3 mg GCPQ in 0.7 ml CD<sub>3</sub>OD. The level of palmitoylation (P%) and quaternisation (Q%) were determined by comparing the palmitoyl methyl protons ( $\delta = 0.89 - 0.90$  ppm) and the quaternary ammonium methyl

protons ( $\delta = 3.45$  ppm) respectively with the sugar methine/methylene protons ( $\delta = 3.50 - 4.40$  ppm) (Qu et al., 2006).

$$\text{Level of palmitoylation (P \%)} = \frac{\text{Area of CH}_3 \text{ signal / number of hydrogens in CH}_3}{\text{Area of sugar chain / number of hydrogens in the sugar chain}} \times 100$$

$$\text{Level of quaternization (Q \%)} = \frac{\text{Area of N(CH}_3)_3 \text{ signal / number of hydrogens in N(CH}_3)_3}{\text{Area of sugar chain / number of hydrogens in the sugar chain}} \times 100$$

#### 2.3.4.2 Gel permeation chromatography

The molecular weight of GCPQ was determined by gel permeation chromatography-multiangle laser light scattering (GPC-MALLS). The measurement was done using Dawn Heleos II MALLS detector ( $\lambda=658$  nm), Optilab rEX interferometric refractometer ( $\lambda=658$  nm) and quasielastic light scattering (QELS) detectors (Wyatt Technology Corporation, Santa Barbara, USA). The mobile phase used was a mixture of acetate buffer (0.5 M anhydrous sodium acetate, 0.2 M glacial acetic acid, pH 4.8) and methanol at ratio 35:65 v/v. The GCPQ samples prepared were filtered (0.2  $\mu\text{m}$  PES syringe filter) prior to injection into POLYSEP-GFC-P 4000 column (300 x 7.8 mm, Phenomenex, UK) coupled with POLYSEP-GFC-P guard column (35 x 7.8 mm, Phenomenex, UK) using Agilent 1200 series autosampler (Agilent Instruments, Stockport, UK) at loading concentration of 5 mg/ml and flow rate of 0.7 ml/min.  $Dn/dc$  was determined by preparing stock solutions of 0.1, 0.2, 0.3, 0.4, 0.5 and 0.6 mg/ml GCPQ in the mobile phase and injecting one stock solution at a time into the Optilab instrument. The data were analysed using ASTRA for Windows version 5.3.4.14 software (Wyatt Technology Corporation).

## 2.3.5 Results and discussion

### 2.3.5.1 Level of palmitoylation and quaternisation of GCPQ

Based on the calculation from the formula, the level of palmitoylation (P %) and quaternisation (Q %) for both batches of GCPQ are displayed in Table 3.

Polymer	P %	Q %
GCP10Q11	$P \% = \frac{1.18 / 3}{34.11/9} \times 100 = 10.38 \%$	$Q \% = \frac{3.89 / 9}{34.11/9} \times 100 = 11.40 \%$
GCP20Q11	$P \% = \frac{1.80 / 3}{27.22/9} \times 100 = 19.88 \%$	$Q \% = \frac{3.04 / 9}{27.22/9} \times 100 = 11.24 \%$

Table 3: Level of palmitoylation and quaternisation (P% and Q%, respectively) of GCP10Q11 and GCP20Q11 (GC source: Chitomerics and Sigma Aldrich, respectively).

These P% and Q% values were used in naming the GCPQ batches accordingly for easy reference in the upcoming experiments. Based on the results, both batches of which were synthesized using the same method but of different sources of GC had different level of palmitoylation. GCP20Q11 of GC from Sigma had twice the amount of P% of GCP10Q11 albeit same ratios of palmitic acid were used in both syntheses. This might due to the higher degree of N-acetylation of the GC from Chitomerics compared to the GC from Sigma, resulted in less primary amine group available for the conjugation with palmitic chain. Besides, the conjugation reactions occurred quite randomly in between batches of GCPQs and this had caused a difficulty to reproduce or replicate the exact same polymer configuration more than once.

Determination of palmitoylation and quaternisation degree enables the estimation of the hydrophobicity and hydrophilicity of the polymer. It is important as a way of

predicting the aggregation capability of the polymer and its stability upon micellization in aqueous media. The CMC value of GCPQ is highly influenced by the level of hydrophobic constituent of the polymer, with lower CMC values were observed with higher amount of hydrophobic molecules (Qu et al., 2006, Tanford, 1978). GCPQ polymer aggregation is influenced by the entropy gain from the interaction of water molecules with the hydrophobic C16 chains on the polymer, which at the same time also improves the stability of the micellar formation due to the high apolar surface area (Siew et al., 2012). The <sup>1</sup>HNMR spectra for the GCP10Q11 and GCP20Q11 which are shown in Figure 10 and Figure 11, respectively, confirmed the formation of GCPQ polymers. The chemical structure of the GCPQs are labelled with P% and Q% to show the random reactions of palmitoylation and quaternisation calculated per 100 glycol chitosan monomers into percentile unit. The presence of a distinct peak at 3.15 ppm means more free amine group in GCP10Q11, which further proved that there was less palmitoylation in this batch of polymer compared to GCP20Q11.

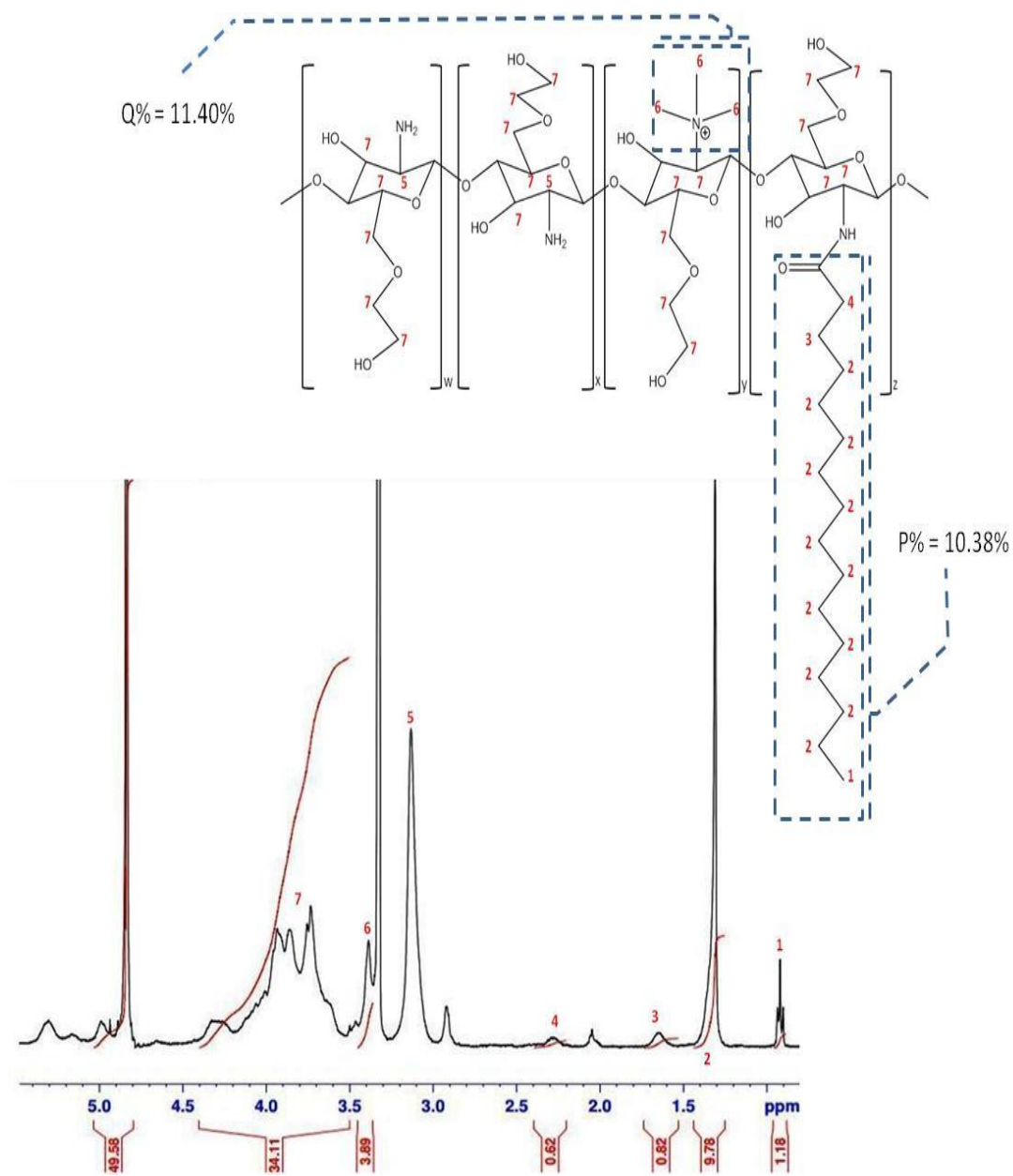


Figure 10:  $^1\text{H}$ NMR spectrum of GCP10Q11 in  $\text{CD}_3\text{OD}$ .

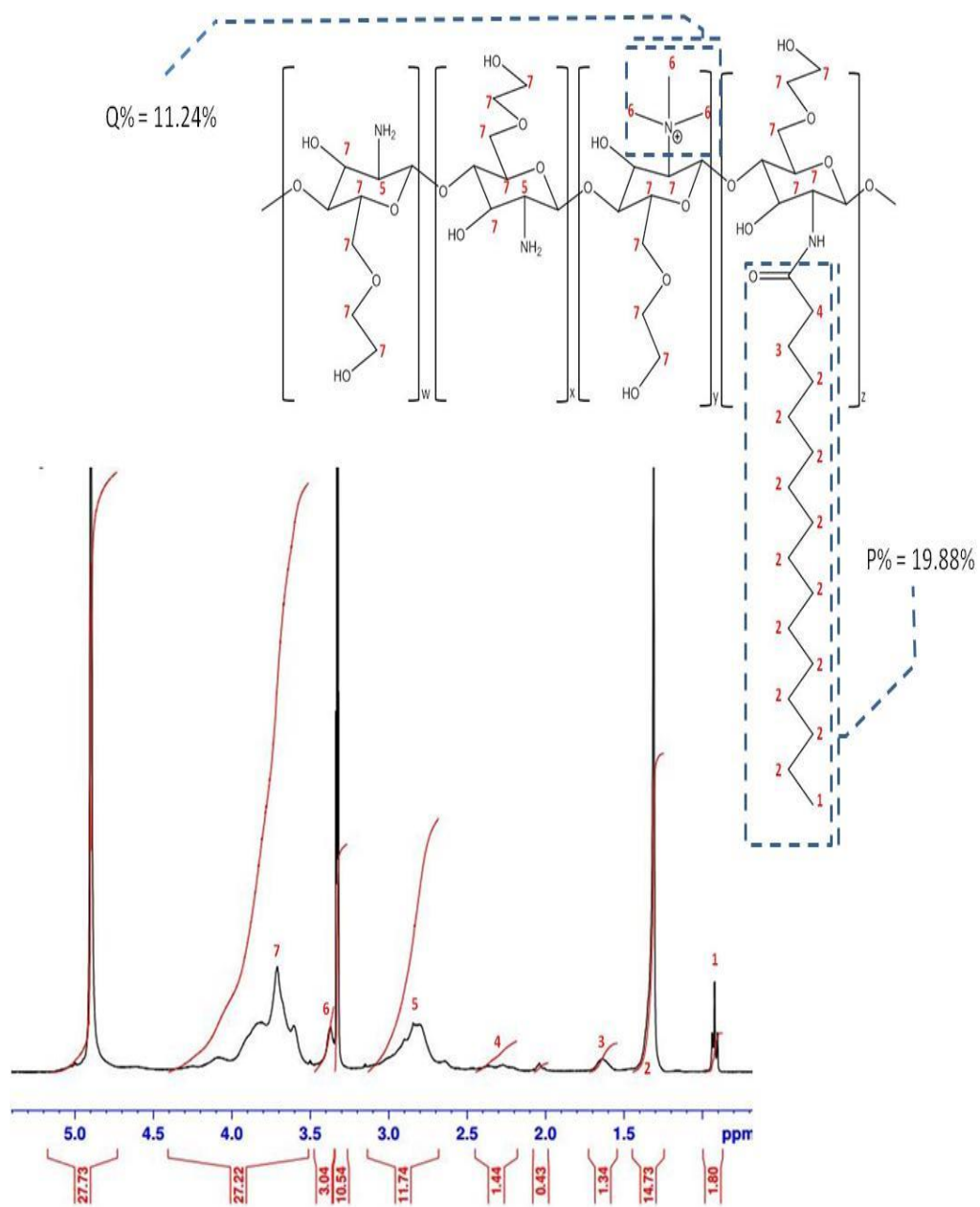


Figure 11:  $^1\text{H}$ NMR spectrum of GCP20Q11 in  $\text{CD}_3\text{OD}$

### 2.3.5.2 Molecular weight of GCPQ

The two batches of GCPQ showed two different values of average molecular weight with 15,100 Da for GCP10Q11 and 24,890 Da for GCP20Q11. Both  $M_w$  and  $M_n$  for GCP20Q11 showed higher values compared to the  $M_w$  and  $M_n$  of GCP10Q11 (Table 4). These higher values of molecular weight in GCP20Q11 could be related to its higher level of palmitoylation (P%), which remarks the higher acylation of the primary amine group with the palmitic acid chain thus adding more molecular weight or mass to every subunit of the GCPQ polymer in comparison to the lower palmitoylated GCP10Q11. The  $M_w / M_n$  polydispersity ratio for both batches at 1.18 and 1.24 for GCP10Q11 and GCP20Q11, respectively can be considered as in narrow distribution since the common values for synthetic polymer is between 1.2 and 3. The  $dn/dc$  for GCP10Q11 and GCP20Q11 was  $0.1763 \pm 0.0043$  ml/g and  $0.1399 \pm 0.0053$  ml/g, respectively.

Polymer	Molecular weight determination		
	$M_w$ (Da)	$M_n$ (Da)	$M_w/M_n$
GCP10Q11	15, 100	12, 790	1.180
GCP20Q11	24, 890	20, 110	1.238

Table 4: Molecular weight of GCPQs based on weight average molecular weight ( $M_w$ ), number average molecular weight ( $M_n$ ) and polydispersity index ( $M_w/M_n$ ) of the polymer.

Both GCPQ chromatograms showed good overlap of light scattering (red) and differential refractive index (blue) peaks. The additional peaks of dRI signals displayed after 15 minutes represent the exclusion limit of the column (Figure 12).

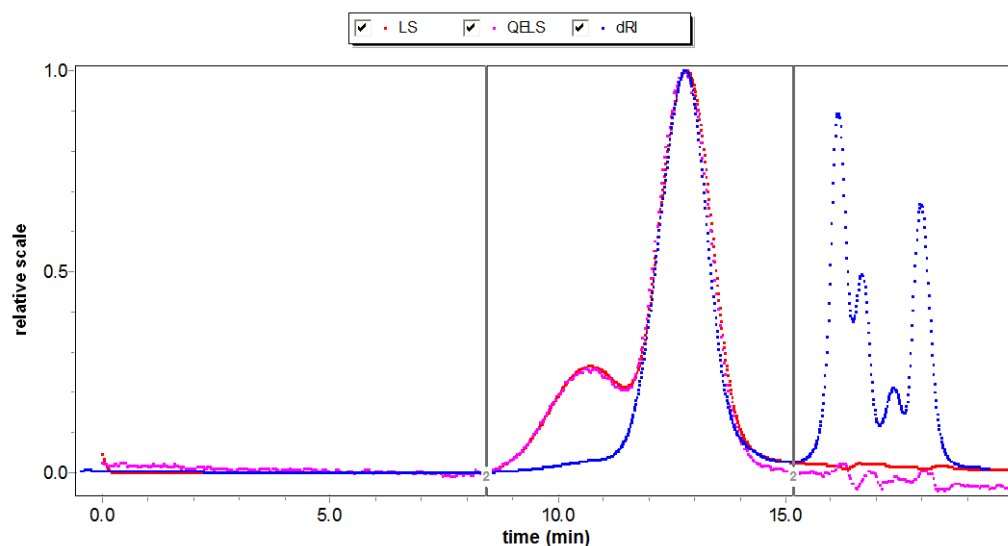


Figure 12: An example of chromatogram of light scattering (red line), quasi-elastic light scattering (pink line) and differential refractive index (blue line) detector signals used in ASTRA software in determination of GCPQ molecular weight.

## 2.4 Conclusion

The current synthesis methodology applied was successfully able to produce GCPQ polymers regardless of different sources of glycol chitosan used in the synthesis. Different level of palmitoylation polymers enabled more choices of GCPQ batches to be used for nanoparticle formulations.

## Chapter 3

# Disulfiram nanoparticle formulations

### 3.1 Overview

Two types of nanoparticle preparations have been attempted in the search of the most ideal type of nanoparticle formulation that can highly load the hydrophobic and labile disulfiram and remain stable upon exposure to various external factors. The first approach was to formulate DS with GCPQ into polymeric micellar nanoparticles. Application of polymeric micelles to be loaded with hydrophobic drugs and improve the drug delivery has been reported frequently in the literature (Lalatsa et al., 2012c).

Self-assembled GCPQ polymeric micelles had been used to be loaded with hydrophobic drugs such as griseofulvin and cyclosporine A (Siew et al., 2012), AZD6244 (selumetinib) (López-Dávila et al., 2016) and celecoxib (Mennini et al., 2014) in an aqueous media using probe sonication method. In order to improve solubility and permeability of amphotericin B for oral delivery, GCPQ was added into an alkaline solution of the drug to create the polymeric micellar nanoparticles (Serrano et al., 2015). Generally, polymeric micelles improve dissolution of hydrophobic drugs by increasing their aqueous levels and the encapsulation is also increased with the increase of polymer hydrophobicity (Qu et al., 2006).

The second approach was to create nanoemulsions with main ingredients DS-in-oil and GCPQ in aqueous medium. Unlike the polymeric micelles formulations, preparation of high capacity nanoemulsions using only GCPQ as the emulsifier has never been attempted in our laboratory. The surfactants are usually of amphiphilic structure with hydrophilic and hydrophobic moieties commonly called the heads and tails, respectively. This specification makes the GCPQ amphiphiles a possible polymeric surfactant for the formation of stable emulsions.

## **3.2 Nanoparticle characterization analysis**

### **3.2.1 Principle of the methodologies used in nanoparticle characterization**

#### **3.2.1.1 HPLC**

Physicochemical characterization is one of the fundamental aspects for determination of the safety, efficiency and biodistribution of the nanoparticle formulations. The most important criterion is the ability of nanoparticle to be able to encapsulate or attach maximum amount of drug. The content of the drug in the nanoparticle formulations is commonly measured using high-performance liquid chromatography (HPLC). HPLC is a rapid, simple and robust method especially for the analysis involving highly hydrophobic drugs.

HPLC is one of the chromatographic methods that can be used to provide quantitative and qualitative information of chemical substances based on the compound separations in a liquid medium under a set of conditions (Meyer, 2006). A common setup of a HPLC system consists of solvent reservoir, transfer line, high-pressure pump, sample

injection instrument, column and detector (Figure 13). The system is usually connected to a computer equipped with software to control the data acquisition and analysis.

A standard HPLC run is commonly initiated with the solvent (mobile phase) from the solvent reservoir continuously pumped throughout the system until all parts are equilibrated, followed by injection of the samples into the mobile phase at the injection valve. The separation of various compounds in the sample takes place within the column, and separated sample components leave (eluted) from the column at different times, which will be scanned by the ultraviolet (UV) detector (Snyder et al., 2010b). The detector signal is plotted against time which is interpreted by the software to produce a chromatogram.

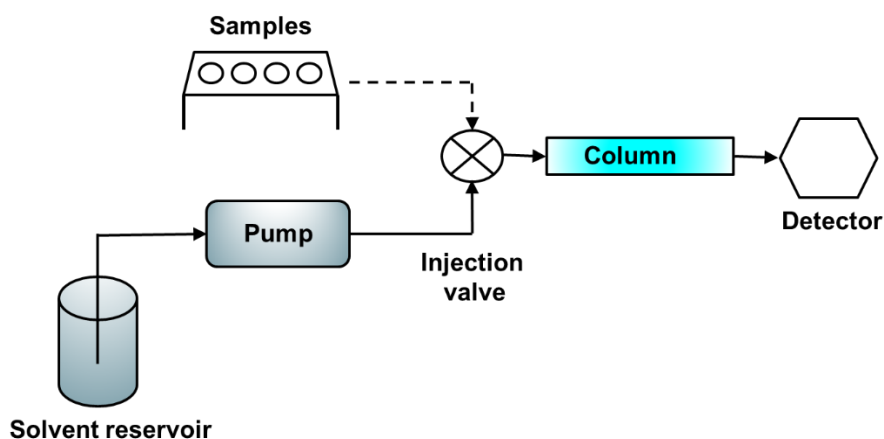


Figure 13: Schematic diagram of an HPLC system.

The choice of right column is fundamental for efficient separation of samples. Reversed-phase chromatography (RPC) is the most commonly used HPLC mode for analysing hydrophobic drugs. RPC features a nonpolar column in combination with polar mixture of water and organic solvent as the mobile phase. The column in RPC is usually consist of porous silica particles creating pores that are attached with C<sub>18</sub> groups as the stationary phase.

When the samples in the mobile phase flow through the column, the molecules of mobile phase are not retained thus leave the column the quickest. The differential migration (different speed at which the solute molecules migrate through the column) of the compounds in the sample forms the basis of the chromatographic separation. As the solute molecules move through the column, they occupy a volume which is called a band. The width of this solute-volume (band-width) is measured as it leaves the column and recorded in the chromatogram as a peak. Time of the band leaves the column is interpreted as the peak retention time for that particular solute, and concentration of the solute in the sample is proportional to the area or height of the peak (Snyder et al., 2010a).

### 3.2.1.2 Particle size and particle size distribution with DLS analysis

Another important criterion of nanoparticle formulations is to ensure the particle size is small and within the nanometre scale, as well as having narrow size distributions. This characterization can be done using dynamic light scattering (DLS) analysis or also known as photon correlation spectroscopy (PCS) (Hall et al., 2007). The principle of DLS measurement is based on the Brownian motion of particles in suspension that is caused by thermally induced collisions between suspended particles and solvent molecules. Once the particles illuminated with a laser, the intensity of the scattered light fluctuates depending on the size of the particles. Analysis of the intensity fluctuations determines the Brownian motion velocity which is defined by translational diffusion coefficient (D). D is converted into particle size using Stoke-Einstein equation:

$$d_H = \frac{kT}{3\eta\pi D}$$

where:

$d_H$  = hydrodynamic diameter

$k$  = Boltzmann's constant

$T$  = absolute temperature

$\eta$  = viscosity

$D$  = diffusion coefficient

The diameter measured using DLS is called hydrodynamic diameter, which refers to the diameter of the sphere that diffuses at the same speed as the particle being measured. Apart from the actual size of the particle, determination of hydrodynamic diameter also depends on the particle shape, particle surface structure and ionic strength in the medium.

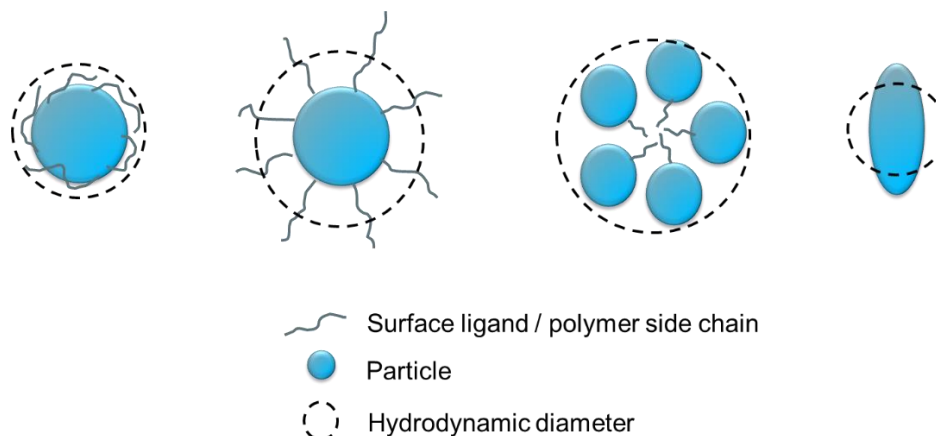


Figure 14: Illustrations of hydrodynamic diameter for various size and shape of particles.

Polydispersity index (PDI) is the measurement of heterogeneity of particle sizes in a mixture. Monodisperse or uniform particles have the same sizes, shapes and masses while a polydisperse or non-uniform collection of particles have inconsistent sizes, shapes and masses.

### 3.2.1.3 Visual analysis of nanoparticles with TEM

Transmission electron microscope (TEM) is able to provide a higher resolution and greater detail view of the nanoparticles shape and morphology at the nanometre scale. This imaging technique is usually used altogether with DLS for size measurement as DLS usually gives larger particle size compared to the values measured from TEM images (Hall et al., 2007). TEM works based on the principle of electron beam deflection and

diffraction from the particles where high-vacuum and thin sample sections are needed for the beam to penetrate.

#### **3.2.1.4 Particle surface charge with DLS analysis**

For optimal design of therapeutic nanoparticles, surface charge or known as zeta potential of a particle is also a fundamental parameter as it is known to affect dispersion stability. Zeta potential is a measure of charge repulsion or attraction between particles or electrostatic magnitude in a liquid suspension. For instance, in the development of nanoemulsions, information of the droplet charge is crucial as the negative ones are cleared more rapidly from the blood than neutral and positively charged (Eccleston, 2013).

When a charged particle is suspended in a liquid filled with cations and anions, the opposite charge will be attracted to the surface of the particle. A positively charged particle attracts negative ions in the liquid, and *vice versa*. Ions closest to the particle surface are strongly bound to the charged particle whereas ions further away are loosely bound forming a diffuse layer, forming two layers of ions which is known as electrical double layer. Ions in the diffuse layer will also move along with the particle when it moves in the liquid, but ions just outside the layer's boundary do not travel together. This boundary is called the slipping plane. The potential that exists between the particle surface and the dispersing liquid at the slipping plane is the zeta potential (Figure 15).

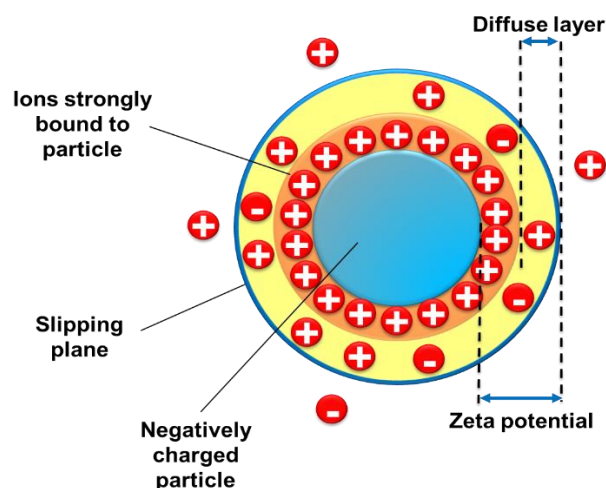


Figure 15: An illustration of the zeta potential at the surface of a negatively charged particle measured by DLS.

### 3.2.2 Ideal criteria of nanoparticle formulations

The aim of characterization is to ensure the obtained nanoparticle formulations have high amount of drug content inside or attached to the particles, nanometre range of particle size and narrow particle size distribution (preferably PDI value of less than 0.5). The formation of nanoparticles is further confirmed with visual examination of the TEM images for the particle size and shape distributions. The zeta potential is measured to determine the ionic strength of the particles formed whether the charge is weakly- or highly- positive, or weakly- or highly- negative. The stability of physicochemical properties of the nanoparticles were studied upon ingredient adjustments to the formulations, effect of storage and exposure to different pH environments and biological fluids.

### 3.2.3 Materials

Item	Supplier
Methanol, HPLC grade	Fisher Scientific Limited, Leicestershire, UK
Ethanol, HPLC grade	
Hexane, HPLC grade	Sigma-Aldrich Company Limited, Dorset, UK

### 3.2.4 HPLC analysis

#### 3.2.4.1 Instrumentation

One reverse phase Phenomenex Onyx Monolithic C<sub>18</sub> column (4.6 x 100 mm) connected with a guard column (4.6 x 5 mm) was used on Agilent 1200 series HPLC (Agilent Technologies, Wokingham, UK) equipped with a quaternary pump, degasser, autosampler and UV detector. The mobile phase used was a mixture of methanol and Milli-Q water at 80:20 v/v ratio. The flow rate was 1.0 ml/min with column temperature at 30°C and injection volume of 5 µl. The DS peak was measured at wavelength 275 nm. The software used for HPLC data analysis was Agilent Chemstation.

#### 3.2.4.2 HPLC method validation

Validation of bioanalytical methods is fundamental in order to ensure the reliability, quality and reproducibility of the data analysis and the findings that come out from it (Tiwari and Tiwari, 2010). The HPLC method was validated based on selectivity, linearity, accuracy and precision. The selectivity was determined by analysing samples of DS in ethanol at lower limit of quantification (LLOQ) level. The linearity was determined by plotting the calibration curve for disulfiram standards of the drug

concentration versus peak area response ( $y = ax + b$ ). The accuracy and precision of the assay method was determined for both intra-day and inter-day variations using the quality control (QC) samples. The precision of the assay was determined by analysing the repeatability and reproducibility of the assay. Repeatability refers to running the analyses on the same day in rapid succession (within-run precision or intra-day), whereas reproducibility is by running the assay on separate days when laboratory conditions may vary (between-run precision or inter-day) (Vogel, 1989). The accuracy was expressed as percentage of relative error (%RE), while precision as percentage of coefficient of variation (%CV).

$$\%RE = ((\text{Found DS} - \text{Added DS}) / \text{Added DS}) \times 100$$

$$\%CV = (\text{Standard deviation} / \text{Mean of found DS}) \times 100.$$

#### ***3.2.4.2.1 Preparation of standards and quality control solutions for method validation***

The stock standard solution was prepared by dissolving DS in methanol to create a stock solution of 100  $\mu\text{g/ml}$ . Six standard solutions at 7.5, 5.0, 2.5, 1.0, 0.5 and 0.25  $\mu\text{g/ml}$  of disulfiram in methanol were prepared by serial dilutions. Two QC solutions were also prepared at the concentrations of 0.75 and 6.0  $\mu\text{g/ml}$ . All samples were prepared in triplicate.

#### ***3.2.4.2.2 Selectivity***

The selectivity (specificity) of the method was proven by the chromatograms showing distinct peak of DS at retention time 1.58 minutes (Figure 16). The LLOQ was found to be at 0.25  $\mu\text{g/ml}$ .

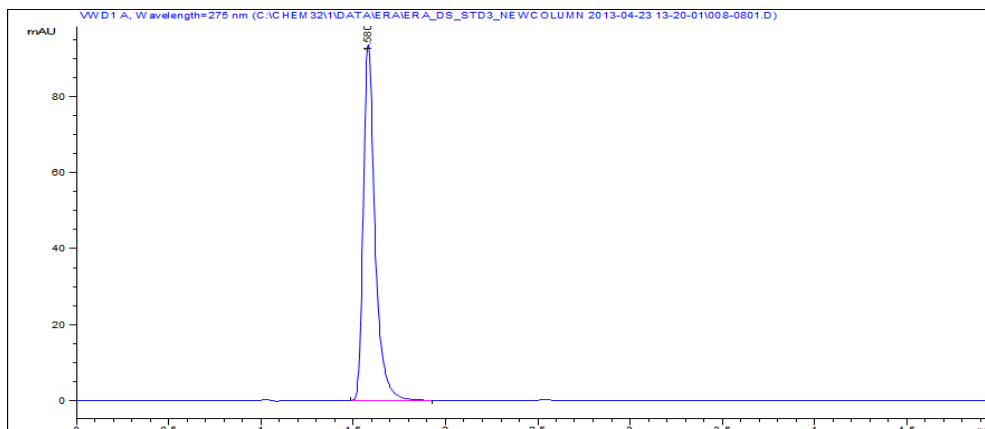


Figure 16: HPLC chromatogram shows disulfiram peak at LLOQ of 0.25 µg/ml with retention time at 1.58 minutes.

### 3.2.4.2.3 Linearity

The linearity of the calibration curve (Figure 17) was analysed using linear regression analysis from which the linear regression equation was obtained. The calibration curve was linear in the range concentration of 0.25 to 7.5 µg/ml with regression equation of  $y = 8.8749x - 0.6759$  with  $R^2$  value of 0.9989. The lower limit of detection (LLOD) was found to be at 0.15 µg/ml (Table 5).

DS concentration range	Linear regression	Coefficient of correlation ( $R^2$ )	LLOD (µg/ml)	LLOQ (µg/ml)
0.25 – 7.5 µg/ml	$y = 8.8749x - 0.6759$	0.9989	0.15	0.25

Table 5: Linearity of disulfiram standards by HPLC method. The linear regression equation was obtained from three calibration curves.

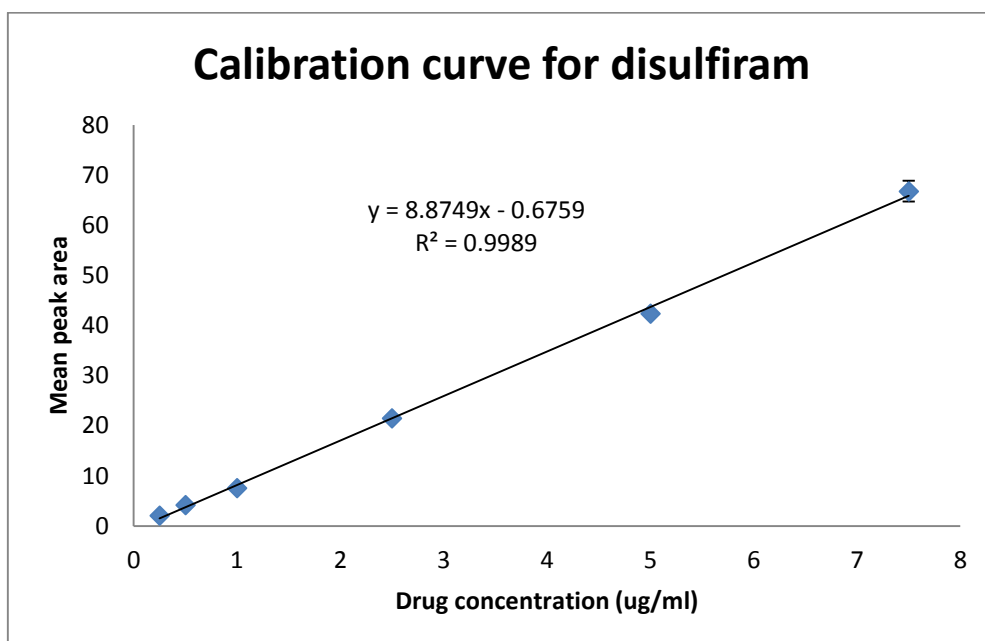


Figure 17: The linear calibration curve of disulfiram obtained from the DS standards.

#### 3.2.4.2.4 Accuracy and precision

The intra-day and inter-day for determination of accuracy and precision are displayed in Table 6. Both %RE and %CV showed values below 15%, which is acceptable by the Food and Drug Administration (FDA) (2001) guidance.

Added DS ( $\mu\text{g/ml}$ )	Intra-day			Inter-day		
	Found DS $\pm$ SD	%RE	%CV	Found DS $\pm$ SD	%RE	%CV
0.75	0.7522 $\pm$ 0.0113	0.2963	1.4979	0.7631 $\pm$ 0.0251	1.7467	3.2892
6.0	5.9316 $\pm$ 0.0815	-1.1396	1.3742	5.8911 $\pm$ 0.0124	-1.815	0.2105

Table 6: Precision and accuracy of the HPLC assay method for disulfiram (DS). SD = standard deviation of the three replicates.

### **3.2.4.3 Drug encapsulation efficiency for nanoparticle formulation**

The amount of DS encapsulated in the nanoparticles was determined as drug entrapment (DE%), which was the percentage amount of drug found (drug content) in proportion to amount of drug added in preparation of the formulation.

$$\text{Drug entrapment (\%)} = \frac{\text{Amount of drug detected}}{\text{Amount of drug added}} \times 100$$

The drug was measured using the same HPLC instrumentation as in the method validation. Sample for analysis was prepared by diluting 10  $\mu\text{l}$  formulation in 490  $\mu\text{l}$  of either absolute methanol (micellar formulation) or ethanol (nanoemulsions) to create 50 times dilution solution.

### **3.2.5 Dynamic light scattering (DLS) analysis**

Nanoparticle size (Z-average, Z<sub>Ave</sub>), polydispersity index and zeta potential of the nanoparticle formulations were measured using Malvern Zetasizer Nano ZS ZEN3600 (Malvern Instruments Ltd, Worcestershire, UK) fitted with 633 nm (red) laser. Samples were prepared by diluting 10  $\mu\text{l}$  formulation in 990  $\mu\text{l}$  Milli-Q water in order to meet the data quality criteria set by the DLS equipment.

### **3.2.6 Transmission electron microscopy (TEM) analysis**

Preparation of the samples for TEM imaging was performed by placing a small amount of the nanoparticle formulation ( $\pm 10 \mu\text{l}$ ) on a carbon coated grid and negatively stained with uranyl acetate (1% w/v). Images of the samples were then captured using FEI CM129 BioTwin transmission electron microscope (Philips, Eindhoven, The Netherlands) and advanced microscopy technique (AMT) digital camera.

### **3.2.7 Statistical analysis**

Statistical analysis was performed using IBM SPSS Statistics for Windows, Version 22.0 (IBM Corp, Armonk, New York, USA). Comparison of more than two groups was done using One-way ANOVA with Tukey's multiple comparison test for the post-hoc analysis, whereas comparison between two groups was done using Independent-samples t-test (Student's t-test). Data were presented as mean  $\pm$  standard deviation with significance value of  $p < 0.05$ .

### **3.3 Formulation of DS into micellar nanoparticles**

#### **3.3.1 Formulation of DS with GCP10Q11**

##### **3.3.1.1 No drug pre-dissolution step**

###### *3.3.1.1.1 Methodology*

In a brief experiment to determine solubility of DS in water, 5 mg of DS was added into 1 ml Milli-Q water and left to stir at room temperature for 24 hours. The solution was then centrifuged and the supernatant was sampled for HPLC measurement. The DS solubility in water was found to be  $4.34 \pm 0.01$   $\mu\text{g/ml}$ , slightly higher solubility than previously reported ( $4.09$   $\mu\text{g/ml}$  at  $25^\circ\text{C}$ ) (Yalkowsky and He, 2003).

The nanoparticle formulations were prepared based on the assumption that GCPQ would improve the solubility of highly hydrophobic DS in aqueous medium. The formulations were prepared by mixing DS crystals into pre-dissolved GCP10Q11 in Milli-Q water (pH 5.5) with drug to polymer ratio of 1 to 5 (1:5 w/w) and 1 to 10 (1:10 w/w) in 1 ml aqueous solution. The 1:5 and 1:10 formulations were prepared in 1 ml volume. Therefore, 5 mg or 10 mg GCPQ were dissolved in 1 ml deionized water respectively in glass vials, creating a transparent aqueous solution. One milligrams DS were then added into the vials containing GCPQ solution to create 1 mg/ml DS (DS-GCP10Q11) formulations. The formulations were sonicated using an ultrasonic disintegrator at amplitude 5 (Soniprep 150 Plus, MSE, U.K.) until the drug was dissolved or homogenization was achieved. The formulations were then centrifuged at 10,000 g for 10 minutes to separate the encapsulated drug from the non-encapsulated drug. The supernatant which contains the drug-loaded nanoparticles was measured for DE%, particle size and PDI. All measurements were done in triplicate and mean values were recorded.

### 3.3.1.1.2 Results

Table 7 shows the drug content, DE%, size of particles and PDI of the supernatant. Solid crystals of DS were seen in TEM images (Figure 18) and upon naked eye observation at the bottom of the vials after sonication, indicating the drug was not fully solubilized even after 1-hour sonication. This could explain the low drug content in the supernatant, which was 0.94 % and 2.26 % of the added drug for 1:5 and 1:10 formulations, respectively. The size of particles of the two formulations was considered small and closely similar to each other. The PDI values were also acceptable although 1:10 had higher value compared to the 1:5 formulations.

SAMPLES	DRUG CONTENT ( $\mu\text{g/ml}$ )	DE%	SIZE (nm)	PDI
1:5 DS-GCP10Q11	$9.35 \pm 0.05$	0.94	$168.3 \pm 2.5$	$0.29 \pm 0.01$
1:10 DS-GCP10Q11	$22.61 \pm 3.56$	2.26	$165.9 \pm 5.4$	$0.40 \pm 0.05$

Table 7: Drug content, DE%, particle size and PDI values for 1:5 and 1:10 DS-GCP10Q11 formulations prepared with no drug pre-dissolution step. Data were presented as mean  $\pm$  SD (n = 3).

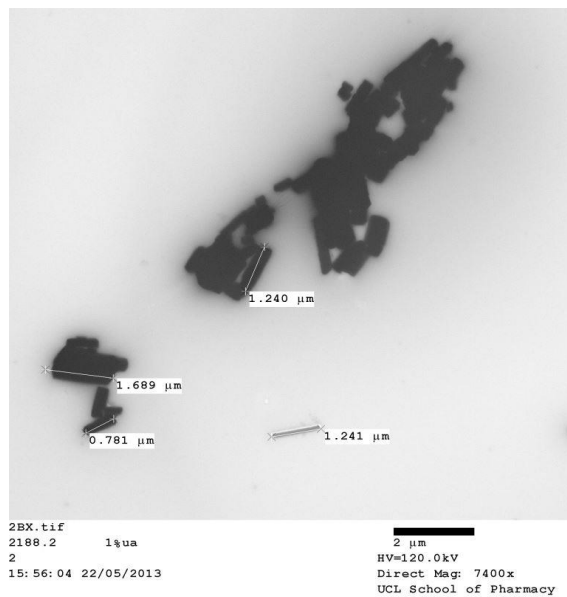
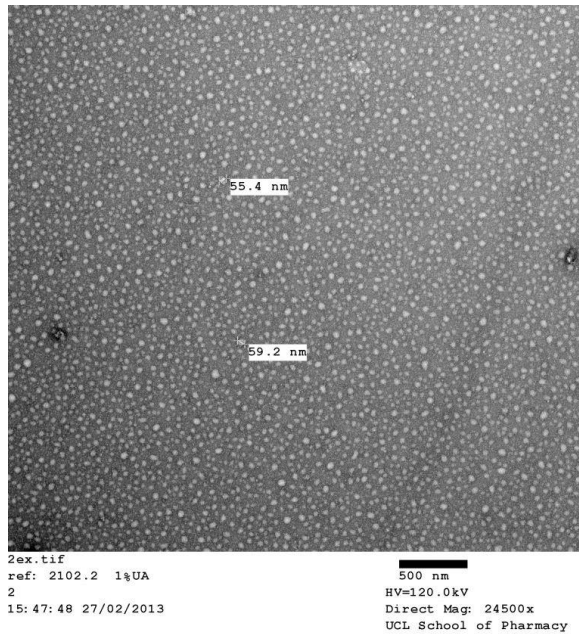


Figure 18: The TEM image (top) is the nanoparticles formed after the sonication of DS with GCP10Q11. The image (bottom) shows the example of DS crystals seen in the formulations. All images were captured before centrifugation.

### **3.3.1.2 Drug and polymer pre-dissolved in solvent**

The results from the previous attempt of DS-GCP10Q11 formulations suggest the low drug encapsulation was caused by the insolubility of the drug in solution therefore leads to low amount of free drug that can be encapsulated by the polymer. The next approach was to ensure the drug was completely dissolved prior to the addition into the GCPQ solution to increase the amount of free drug available in the aqueous solution. Methanol was chosen since both DS and GCPQ polymer can be solubilised in it.

#### **3.3.1.2.1 Methodology**

Two milligram DS were mixed with either 10 or 20 mg GCP10Q11 in a glass vial and dissolved in 2 ml methanol by vortex to create the 1 mg/ml of drug formulation. Once dissolved, the solvent was removed by evaporation using a vacuum concentrator (Savant SpeedVac, Asheville, USA) equipped with refrigerated vapour trap (Savant RVT400, Asheville, USA). The resultant paste-like substance after the evaporation was then reconstituted in 2 ml Milli-Q water and sonicated for 15 minutes to achieve homogenous dissolution and to create small size particles. The formulations were then centrifuged at 10,000 g for 10 minutes. As previously done, the supernatant which contains the drug-loaded nanoparticles was measured for drug content, particle size and PDI. All measurements were done in triplicate.

#### **3.3.1.2.2 Results**

Table 8 shows the drug content, DE%, size of particles and PDI of the formulations. After sonication, cloudy and homogenous dispersion was seen in the formulations without signs of drug crystal at the bottom of the glass vials. However, after settling the formulations in upright position for approximately 5 minutes, sedimentation

of large particles was formed and seen accumulated at the bottom of all formulations. This could indicate most of the drug and polymer aggregated together and formed large particles which later accumulated by the force of gravity. This could also explain the low level of encapsulated drug in the supernatant, which was 1.28 % and 2.21% of the added drug for 1:5 and 1:10 formulations, respectively. The size of particles was also considered small for both formulations. The PDI values were also acceptable for a homogenous distribution of particles.

SAMPLES	DRUG CONTENT (µg/ml)	DE%	SIZE (nm)	PDI
1:5 DS-GCP10Q11	12.78 ± 0.08	1.28	208.0 ± 6.8	0.30 ± 0.03
1:10 DS-GCP10Q11	22.15 ± 0.08	2.21	274.8 ± 14.2	0.33 ± 0.04

Table 8: Drug content, DE%, particle size and PDI values for 1:5 and 1:10 DS-GCP10Q11 formulations prepared whereby drug and polymer pre-dissolved in solvent. Data were presented as mean ± SD (n = 3).

### 3.3.1.3 Conclusions for DS formulation with GCP10Q11

The polymeric micellar formulations of DS with GCP10Q11 was unable to give a high drug load (less than 3% DE%) although the particle sizes (166 – 275 nm) and particle size distributions (PDI = 0.3-0.4) were within acceptable range. The next approach was then to formulate DS with higher palmitoylation GCP20Q11 for the attempt to increase the drug encapsulation.

### **3.3.2 Formulation of DS with GCP20Q11**

We hypothesized that the dissolution and encapsulation of hydrophobic DS could be elevated with the use of higher palmitoylation GCPQ. Therefore, formulations using GCPQ with higher palmitoylation level GCP20Q11 (P% = 19.88%, Q% = 11%) were made. The preparation steps and methods of analyses for the formulation of DS with GCP20Q11 were the same as have been done in the preparation of DS-GCP10Q11.

#### **3.3.2.1 No drug pre-dissolution step**

##### **3.3.2.1.1 Results**

Table 9 shows the mean drug content, size of particles and the PDI values of the DS-GCP20Q11 formulations. The added drug for each formulation was 1 mg/ml (1000 µg/ml). Similar to the DS-GCP10Q11, there were also solid crystals of DS seen at the bottom of the vials even after the 1 hour which explains the low amount of drug encapsulated by GCPQ (1.92% and 3.48% of the added drug for 1:5 and 1:10, respectively). The PDI values of 0.6 or more for both formulations were considered high for nanoparticle formulations. However, the particle sizes were acceptable for the optimum nanoparticle criteria.

SAMPLES	DRUG CONTENT ( $\mu\text{g/ml}$ )	DE%	SIZE (nm)	PDI
1:5 DS-GCP20Q11	$19.17 \pm 0.31$	1.92	$159.3 \pm 8.2$	$0.59 \pm 0.04$
1:10 DS-GCP20Q11	$34.76 \pm 0.27$	3.48	$112.4 \pm 1.1$	$0.68 \pm 0.01$

Table 9: Drug content, DE%, particle size and PDI values for 1:5 and 1:10 DS-GCP20Q11 formulations prepared with no drug-predissolution step. Data were presented as mean  $\pm$  SD (n = 3).

### 3.3.2.2 Drug and polymer pre-dissolved in solvent

#### 3.3.2.2.1 Results

Table 10 shows the mean drug content, DE%, size of particles and the PDI values of the DS-GCP20Q11 formulations. The added drug for each formulation was 1 mg/ml (1000  $\mu\text{g/ml}$ ). Similar to the DS-GCP10Q11 formulations (prepared with the same method as these ones), there were also sedimentation seen in the formulations shortly after the sonication and is also presumed to be the reason of the low level of encapsulated drug in the formulations (2.13% and 3.81% of the added drug for 1:5 and 1:10, respectively). The PDI values for the 1:10 formulations were found higher than 0.6. In fact, the overall PDI values for DS formulations with GCP20Q11 were higher than the ones with GCP10Q11 (approximately 0.3-0.4 vs. 0.5-0.6). This suggests the use of higher palmitoylation GCPQ in the formulations would produce higher polydispersity in nanoparticle size distributions.

SAMPLES	DRUG CONTENT ( $\mu\text{g/ml}$ )	DE%	SIZE (nm)	PDI
1:5 DS-GCP20Q11	$21.30 \pm 0.65$	2.13	$294.7 \pm 0.03$	$0.53 \pm 0.07$
1:10 DS-GCP20Q11	$38.09 \pm 0.18$	3.81	$143.9 \pm 6.01$	$0.62 \pm 0.04$

Table 10: Drug content, DE%, particle size and PDI values for 1:5 and 1:10 DS-GCP20Q11 formulations prepared whereby drug and polymer pre-dissolved in solvent. Data were presented as mean  $\pm$  SD (n = 3).

### 3.3.3 Discussion for micellar formulations

GCPQ which can act as a drug solubilizer (Uchegbu et al., 2001) was hypothesized to be able to dissolve the highly hydrophobic disulfiram in aqueous solution and form micellar nanoparticles. However, the results revealed that even after such a strong sonication power applied to break apart the disulfiram solid crystals into smaller sizes for easy dissolution, macroscopic form of disulfiram crystals were still detected indicating the incomplete dissolution of the drug even in the presence of GCPQ. The solvent evaporation method by which dissolving the drug in methanol to form free DS to enable encapsulation by the GCPQ micelles was also found failed to achieve high encapsulation of the drug within the particles.

At 1:10 ratio, the DS-GCP20Q11 formulations were found to have higher percentage of DE% compared to the DS-GCP10Q11 formulation at the same drug to polymer ratio. This shows the higher palmitoylation GCPQ is capable to entrap more drugs compared to the lower palmitoylation level. However, the PDI values of 0.6 or more

for DS-GCP20Q11 formulations were considered high compared to the DS-GCP10Q11 formulations (PDI range = 0.3 – 0.4). This shows the use of GCPQ polymers with higher palmitoylation level produces more polydisperse (heterogenous) size of nanoparticles.

The log P for disulfiram is 3.88 (Hansch et al., 1995) with molecular weight (MW) of 296.54. In literature, formulations of GCPQ with many hydrophobic drugs were reported to have higher drug encapsulation. GCPQ (P% = 21.6, Q% = 6.4, MW = 11,350 Da) formulations with celecoxib (Log P = 3.9, MW = 381.37) at 1:5 drug to polymer ratio was able to encapsulate between 14.8% and 15.8% w/w drugs, whereas at 1:10 ratio, the drug encapsulation was between 21.1% and 32.1% w/w depending on the sonication power during the preparation of the nanoparticles (Mennini et al., 2014). For comparison, the P% of the GCPQ used in the study was almost similar to GCP20Q11. In addition, the log P for celecoxib is also closely similar to the log P of disulfiram. Yet, the DE% of celecoxib by GCPQ was much higher compared to the formulation of DS with GCPQ. In another study, formulation of GCPQ (MW = 10, 159 Da) with cyclosporine A (log P = 4.3, MW = 1202.61) and griseofulvin (Log P = 2.18, MW = 352.77) had 15% and 3% drug entrapment, respectively (Siew et al., 2012).

### **3.3.4 Conclusions for micellar formulations**

The polymeric micelle formulations of DS with both GCP10Q11 and GCP20Q11 produced nanoparticles had low DE% value (< 4%), although formulation with the latter polymer produced higher than 3% DE% for the 1:10 ratio formulations. This showed a trend of higher drug load in formulation with higher palmitoylated GCPQ.

### 3.4 Formulation of DS and GCPQ into nanoemulsions

Based on the previous experiments, the polymeric micelle formulations were unable to give high encapsulation efficiency of DS. Nevertheless, one definite conclusion can be derived from those experiments is that the use of higher palmitoylated GCPQ gives a higher hydrophobic drug entrapment, as had been previously suggested in other GCPQ nanoparticle formulations (Qu et al., 2006). This also led to the hypothesis of using highly hydrophobic vehicle or excipient for the drug, such as oil, would give a possibility of high drug entrapment in the polymers. The combination of oil and water will produce a colloidal system known as emulsion, and with addition of surfactant and application of energy, nanoemulsion is formed.

Some of the O/W emulsions available commercially are for oral and intravenous routes. Medicinal oral O/W emulsions have been used for treatment of constipation (e.g. Emulsoil® and Neoloid® for castor oil) and as food supplement (e.g. Scott's® emulsion for fish liver oil). Intravenous O/W lipid emulsions such as Intralipid® is used in clinical practice to provide calories and essential fatty acids to the patients. Onxol™ is one example of paclitaxel intravenous emulsion used for treatment of cancer.

There are two common types of O/W colloidal dispersions; *microemulsions* and *nanoemulsions*. By definition, a microemulsion is a thermodynamically stable colloidal dispersion consisting of small particles dispersed homogeneously within an aqueous medium, which can be formed spontaneously when the components are mixed in appropriate ratios (McClements, 2012). Meanwhile, nanoemulsion is a thermodynamically unstable (but kinetically stable) colloidal dispersion consisting two immiscible liquids, with one of the liquids being dispersed as small spherical droplets in the other liquids. Nanoemulsion usually requires high energy methods for the formation of the particles by utilizing devices such as ultrasonic or high pressure homogenizers

(Anton and Vandamme, 2011). This means the major difference between these two types is mainly based on the thermodynamic stability. In terms of droplet size, both types are of particles within the nanometre range with microemulsion average droplet size is between 5 – 140 nm (Attwood, 2013).

Vegetable oil, which majorly consists of triacylglycerols (Ayorinde et al., 2000) has been used widely in preparation of nanoemulsions (Adamczak et al., 2013). It was reported DS can be solubilised in olive oil (Brar et al., 2004). The use of edible vegetable oil is a good candidate in oral drug formulation as it is safe to be administered via the enteric route (Chung et al., 2001). Soybean oil, for instance, is already one of the accepted excipient for oral drug formulation (Strickley, 2004). In the experiments ahead, preparation of the formulations involves dissolution of DS in soybean oil prior to the addition into GCPQ solution, followed by agitation by ultrasonic disintegrator to create homogenous distribution of nano-sized emulsions.

### **3.4.1 Solubility of DS in different types of oil**

It is crucial to choose the type of oil that can dissolve high amount of DS to minimize the use of oil as excipient in the formulation. Several types of edible oil that are listed as pharmaceutical excipients (Rowe et al., 2006) were chosen for determination of DS solubility.

### **3.4.1.1 Methodology**

An excess amount of DS (~ 100 mg) was added into 1 ml of oil of either cotton seed, olive, rapeseed, safflower, sesame, castor or soybean oil (Sigma Aldrich, Missouri, USA) and left to stir overnight at room temperature. Samples were prepared in triplicate for each type of oil. On the next day, the drug-in-oil dispersion was centrifuged at 10,000 g for 15 minutes to accumulate the large undissolved drug crystals at the bottom of the tubes. The clear supernatant was then collected and filtered with 0.45 µm PES syringe filter to remove any small undissolved drug crystals in the supernatant. The drug concentration was then measured using HPLC. For HPLC measurement, the oil samples were diluted (25 times dilution) in hexane followed by further dilution (50 times dilution) in ethanol to ensure the concentration of samples were within the concentration range of the calibration curve.

### **3.4.1.2 Result**

Table 11 shows concentration of DS measured in each type of oil. Soybean oil showed highest DS solubility (~ 21 mg/ml) whereas castor oil showed the lowest DS solubility. Therefore, soybean oil was chosen to be used in the formulation.

<b>OIL TYPE</b>	<b>DRUG CONTENT (mg/ml)</b>
Cotton seed	15.40 ± 0.92
Olive	12.58 ± 0.66
Rapeseed	11.63 ± 0.44
Safflower	14.54 ± 0.63
Sesame	13.87 ± 2.36
Castor	2.90 ± 0.64
Soybean	21.12 ± 1.04

Table 11: Solubility of DS in various types of oil.

### 3.4.2 Stability of DS in soybean oil

The stability of DS dissolved in soybean (SB) oil over a period of time was examined. The stock of DS in SB oil was prepared at 20 mg/ml. After the addition of 20 mg DS into 1 ml oil, the stock was heated at 50°C while stirring to speed up the solubilisation of DS crystals. The stock was then let to cool to room temperature and observed for signs of recrystallization. The stock was prepared in triplicate and kept at room temperature (22 to 24°C with 12-hour light and dark cycle). Samples of oil were taken at Day 0 (fresh preparation), 1, 3, 6 and 8 and analysed for drug content using HPLC. Oil samples were diluted in hexane (20 times dilutions) followed by ethanol (50 times dilution) prior to the HPLC measurements.

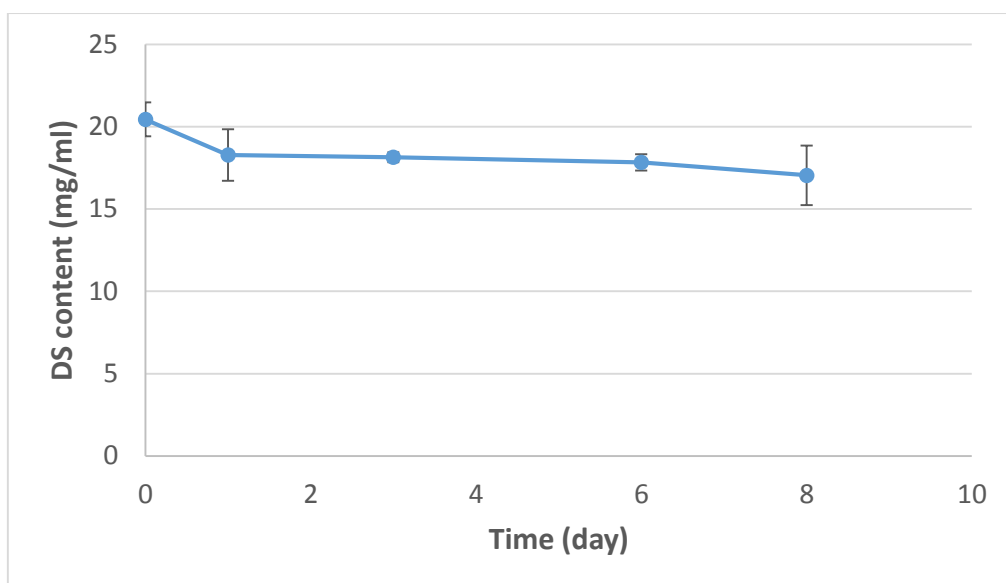


Figure 19: Amount of DS detected in oil samples from DS in soybean oil stock made at 20 mg/ml at Day 0, 1, 3, 6 and 8. Data were presented as mean  $\pm$  SD (n = 3).

No drug recrystallization was observed in all DS stocks after being cooled to room temperature. Statistical analysis showed no significant change in DS concentration in the SB oil medium over the period of 8 days in comparison with the amount of drug on Day 0 ( $p > 0.05$ ) (Figure 19).

### 3.4.3 Formulation of DS with GCP20Q11 at 5% oil

Based on assumption concluded from previous experiments using GCPQ polymer with higher palmitoylation, the attempt of DS formulation with GCPQ into nanoemulsions was made with GCP20Q11. The DS-GCP20Q11 nanoemulsions (DS-GCP20Q11-E) were made at 1 to 5 and 1 to 10 drug to polymer ratio (w/w) in 1 ml volume (Table 12). GCP20Q11 was dissolved in Milli-Q water prior to the addition of DS in SB oil. After the addition, the formulations were sonicated using ultrasonic disintegrator at amplitude 5 (Soniprep 150 Plus, MSE, U.K.) until homogenization was achieved which was 5 minutes. The resulting dispersion of 5% oil v/v DS-GCP20Q11-E was a uniform and milky white in colour (Figure 20). All formulations were prepared in triplicate. As GCPQ is able to act as surfactant or emulsifier itself, no additional surfactant was added to stabilize the formulations.

DS-GCP20Q11-E	Amount of DS (mg)	Amount of GCP20Q11 (mg)	20 mg/ml DS stock ( $\mu$ l)	GCP20Q11 in Milli-Q water ( $\mu$ l)	Final volume ( $\mu$ l)
1:5	1	5	50	950	1000
1:10	1	10	50	950	1000

Table 12: Table of ingredients for preparation of 5% oil v/v DS-GCP20Q11-E formulations.

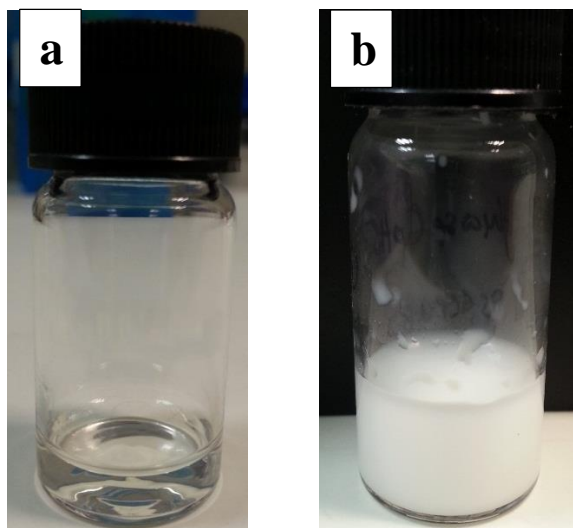


Figure 20: GCP20Q11 micelles (a) appeared as a clear suspension, whereas 5% oil DS-GCP20Q11-E formulation (b) appeared as a milky-like emulsion.

#### **3.4.3.1 Drug content of DS-GCP20Q11-E**

Table 13 shows the amount of drug detected in the DS-GCP20Q11-E formulations. The result shows higher DE% (87%) in the 1:10 formulations compared to only 30% DE% in 1:5 formulations after 5 minutes' sonication. This suggests the use of higher amount of GCPQ enables higher amount of particles (droplets) formed that are stabilized by the polymer. The low DE% in 1:5 formulations might be due to inadequate GCPQ to support formation of more stable particles. Although phase separation was not seen in the formulation, physical instability such as creaming might have occurred, where the less dense oil droplets rise to the surface to form a thin upper layer of cream, causing lesser amount of drug in the sampled emulsions.

DS-GCP20Q11-E	Amount of DS ( $\mu\text{g/ml}$ )	Drug content ( $\mu\text{g/ml}$ )	DE%
1:5	1000	$304.36 \pm 126.51$	30.4
1:10	1000	$868.25 \pm 27.01$	86.8

Table 13: Drug content and DE% of the 1:5 and 1:10 DS-GCP20Q11-E formulations after 5 minutes' sonication. Data were presented as mean  $\pm$  SD (n = 3).

In order to improve the encapsulation efficiency, the next attempt was to prolong the sonication time. Therefore, the newly prepared 1:5 and 1:10 DS-GCP20Q11-E formulations were sonicated for 15 minutes instead of 5 minutes. Table 14 shows the amount of drug detected in the DS-GCP20Q11-E formulations after 15 minutes' sonication.

DS-GCP20Q11-E	Amount of DS ( $\mu\text{g/ml}$ )	Drug content ( $\mu\text{g/ml}$ )	DE%
1:5	1000	$952.60 \pm 3.91$	95.2
1:10	1000	$1018.46 \pm 12.73$	101.8

Table 14: Drug content and DE% of the 1:5 and 1:10 DS-GCP20Q11-E formulations after 15 minutes' sonication. Data were presented as mean  $\pm$  SD (n = 3).

After a longer sonication time, the DE% for both 1:5 and 1:10 was seen to increase dramatically. The DE% for 1:5 formulations were increased 3 times the value of the formulations when sonicated for 5 minutes (from 30% to 95%). The excess of detected drug (slightly more than amount of added drug) in the 1:10 formulations might be due to the pipetting error during sampling.

#### **3.4.3.2 Particle size, polydispersity index and zeta potential of DS-GCP20Q11-E**

Table 15 shows the average particle size, PDI value, zeta potential and pH for the 1:5 and 1:10 DS-GCP20Q11-E formulations sonicated at both 5 and 15 minutes. Based on the results, longer sonication time produced smaller size nanoparticles and lower PDI values for both 1:5 and 1:10 formulations.

Sonication for a longer time at high power provided more agitation force to break the oil phase into more droplets at much smaller size. With the GCPQ acting as a cationic surfactant, the nanometre droplets (particles) formation was maintained due to the increase in interfacial area and decrease in interfacial tension (Solans et al., 2005).

The DS-GCP20Q11-E formulations at 1:10 drug to polymer ratio containing 5% oil content and sonicated for 15 minutes (Figure 21) was the formulation of choice for its high DE% and small particle size and PDI values.

DS-GCP20Q11-E	Sonication time (minutes)	Size (nm)	PDI	Zeta potential (mV)	pH
1:5	5	375.7 ± 5.5	0.29 ± 0.07	N/A	N/A
1:10	5	380.2 ± 3.0	0.49 ± 0.04	N/A	N/A
1:5	15	201.7 ± 0.4	0.13 ± 0.02	49.9 ± 3.0	4.96
1:10	15	183.2 ± 5.9	0.17 ± 0.01	50.9 ± 1.3	4.54

Table 15: Average particle size, PDI value, zeta potential and pH of 5% oil DS-GCP20Q11-E formulations. Data were presented as mean ± SD (n = 3). N/A = data not available.

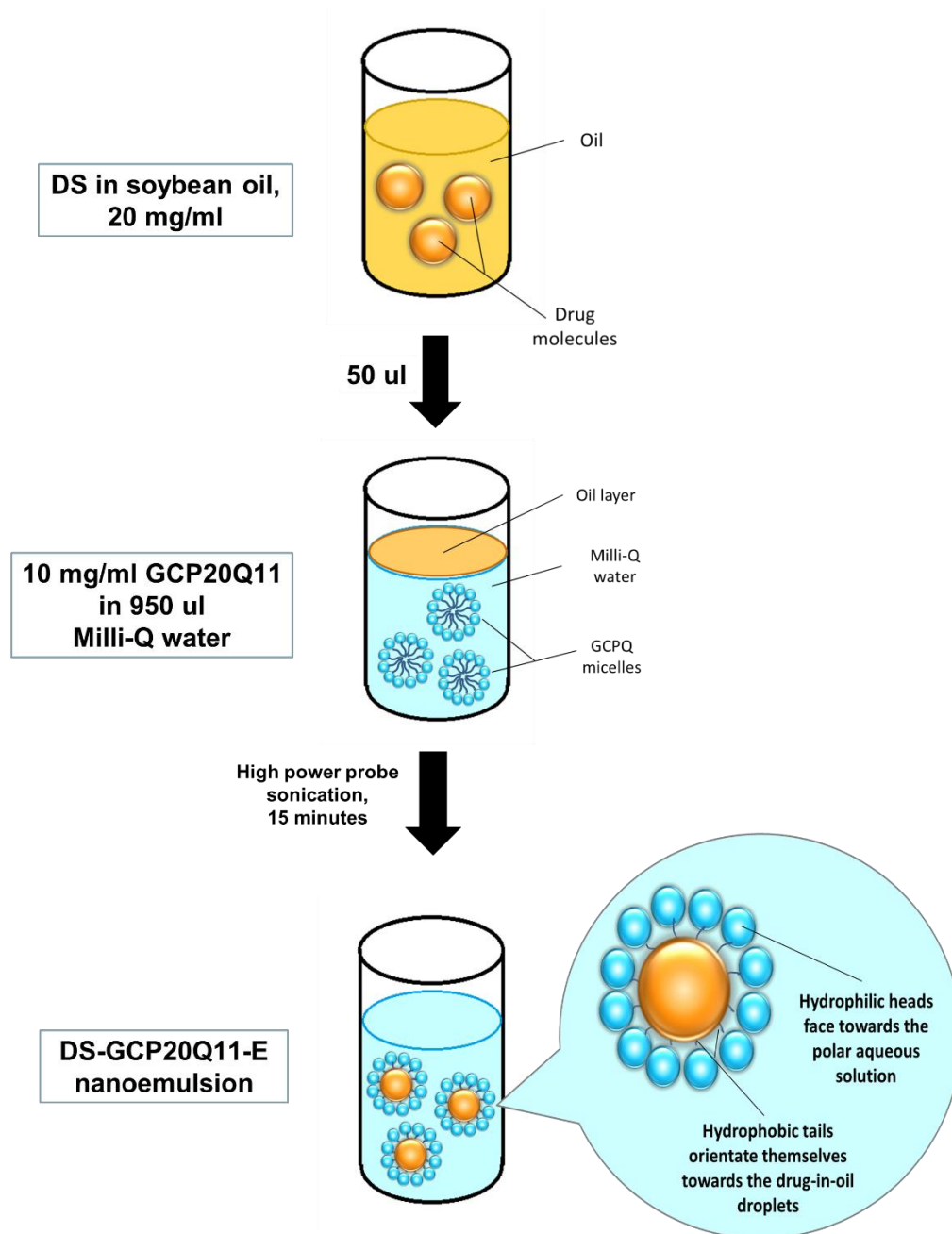
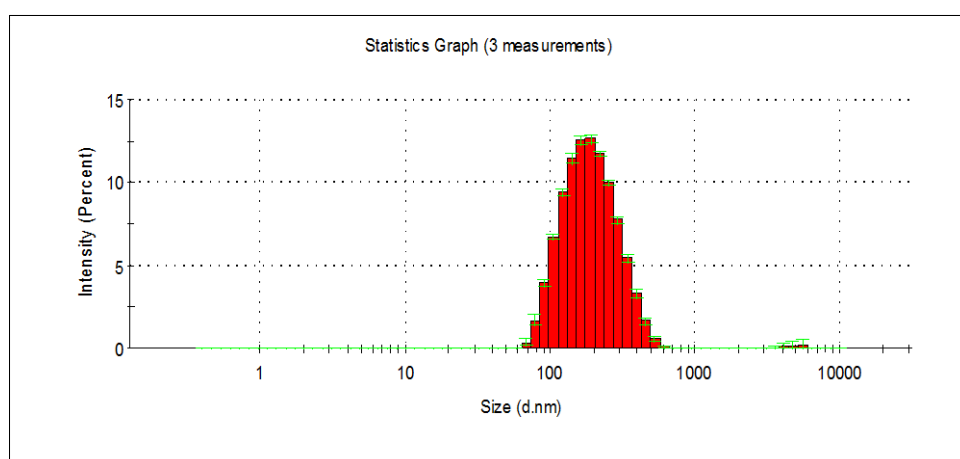


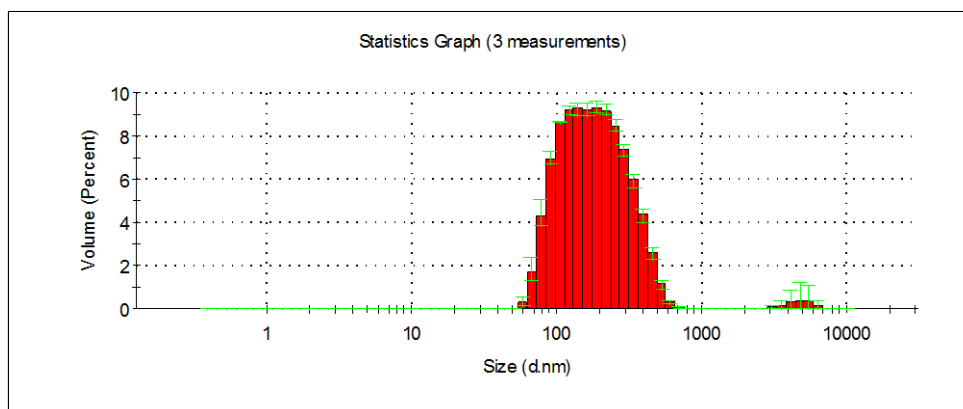
Figure 21: Schematic diagram for the preparation of 1:10 drug to polymer ratio of DS-GCP20Q11-E at 5% oil v/v.

For further confirmation of the particle size distributions for this formulation, the intensity, volume and number weighted distribution of the particle size were measured. Figure 22 shows the three types of particle size distribution graphs for triplicate measurements of the 1:10 formulations. The size distribution histograms are displayed as relative intensity of light scattered by particles (Y-axis) against the logarithmic size classes (X-axis).

(a)



(b)



(c)

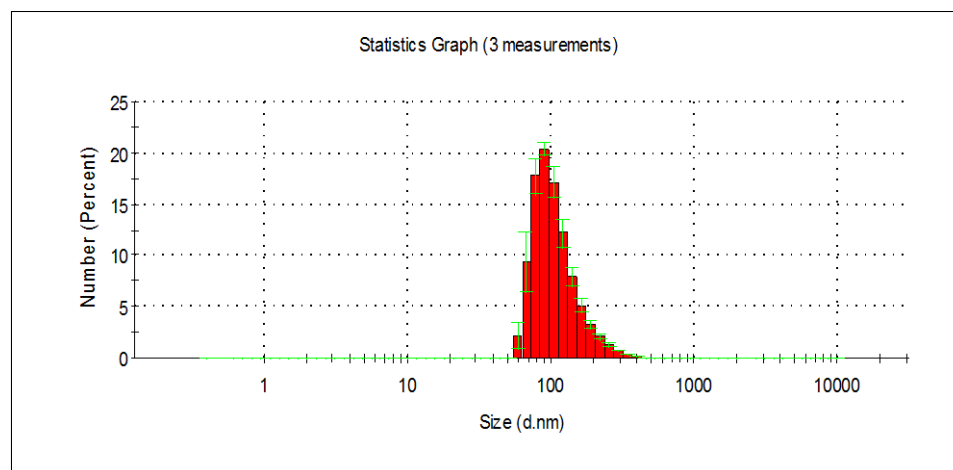


Figure 22: The distribution of particle size populations for 1:10 DS-GCP20Q11-E formulation, 5% oil sonicated for 15 minutes, based on the (a) intensity, (b) volume and (c) number weighted distributions.

The basic measurement for DLS is the intensity weighted distributions (including the Z-average), from which the number and volume weighted size distributions are calculated by default in the DLS instrument. The transformation from intensity into volume and number is based on assumptions: 1) all particles are spherical, homogenous and having equivalent density, 2) the optical properties are known, such as the refractive index of the sample dispersant. The graphs (Figure 22) show the intensity, number and volume weighted particle size distributions of DS-GCP20Q11-E at 5% oil having unimodal distribution of particle size. The volume and number distributions should only be used to estimate relative amount of particles in separate peaks. Since there were no distinct additional peaks in the aforementioned distribution graphs of this formulation, only the intensity weighted distribution is being considered for determination of the particle size. A small additional peak seen at 500 nm for the intensity weighted graph might due to the presence of large foreign particles (e.g. dust) in the cuvette or that entered during sample preparation.

From the zeta potential results, the DS-GCP20Q11-E at 5% oil showed highly positive charged formulations at an acidic pH of 5. This indicates stable formulations in which the particles repel each other because of the strong charges thus ensuring the dispersion stability by avoiding occurrence of aggregation or flocculation in the formulation. The positive surface charge of the nanoparticles was probably due to GCPQ hydrophilic substituent, where in this case owed to the presence of the trimethyl ammonium groups (Uchegbu et al., 2004).

### 3.4.3.3 TEM images of DS-GCP20Q11-E

TEM images showed formation of spherical particles in the formulations. The GCP20Q11 micelles (as control) were seen as a collection of very small particles with diameter of less than 30 nm (Figure 23). Another control formulation was made by vortexing together GCP20Q11 aqueous suspension and empty 5% v/v soybean oil (without drug) vigorously (no sonication). This particular control showed two populations of sizes; one with the smaller size ranged between 20 to 40 nm, and the other one was at bigger size in range of 100 to 900 nm (Figure 24). The DS-GCP20Q11-E particles at 1:10 ratio sonicated for 15 minutes were seen heterogeneous with size between 9 to 100 nm in diameter (Figure 25).

The overall size of the DS-GCP20Q11-E particles appeared bigger than the size of the GCP20Q11 micelles with no drug. This could indicate the encapsulation of the drug by the GCPQ polymer, positioning the oil droplets at the core and increasing the size of the DS-GCP20Q11-E particles. It was also noticed that the size of DS-GCP20Q11-E particles seen in the TEM images appeared smaller compared to the size detected using DLS. The smaller size in TEM images might be caused by the shrunken nanoparticles due to the drying process of the sample prior to the imaging. Apart from that, hydrodynamic size measured by DLS instrument is usually larger than the actual size of the particle itself since the particle surface structure and ionic strength could add extra nanometres into the hydrodynamic particle size.

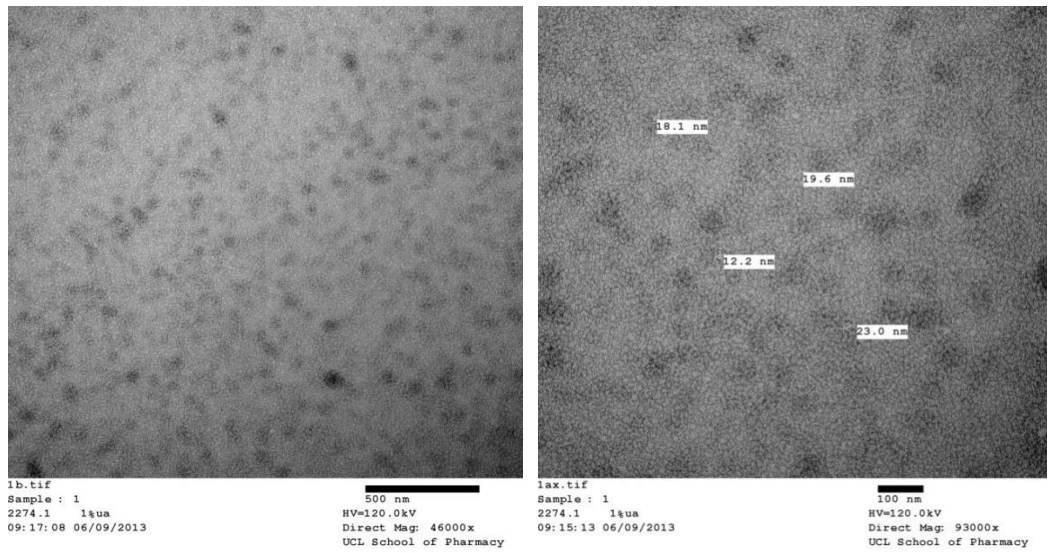


Figure 23: GCP20Q11 at 10 mg/ml in MilliQ water. The size of GCPQ micelles shown here are between 12 to 23 nm in diameter. Left: 46,000x magnification, Right: 93,000x magnification.

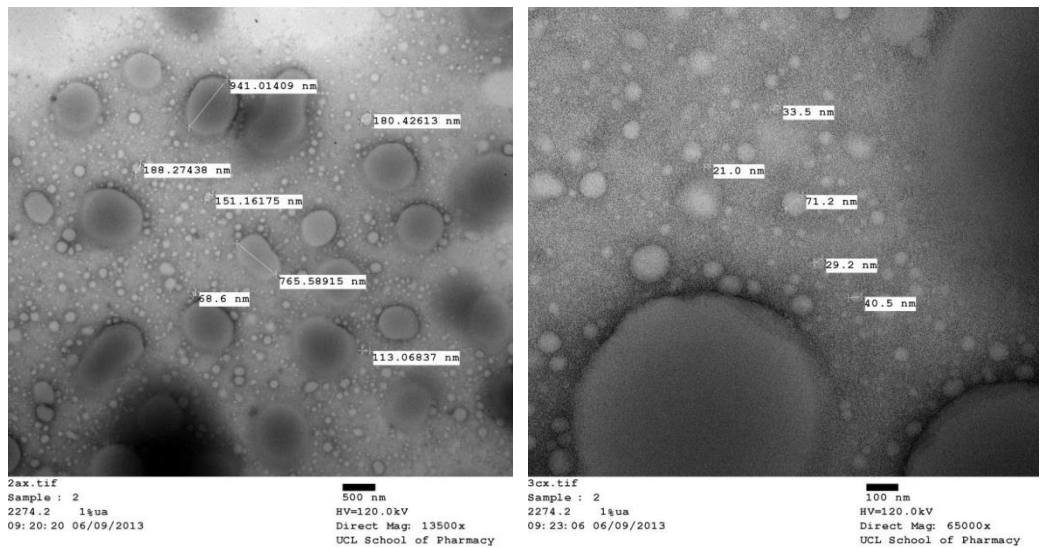


Figure 24: GCP20Q11 at 10 mg/ml dissolved in MilliQ water and added with empty 5% v/v/ soybean oil. The size of particles is seen heterogeneous with size between 20 to 40 nm, whereas the bigger size was between 100 to 900 nm in diameter. Left: 135,000x magnification, Right: 65,000x magnification.

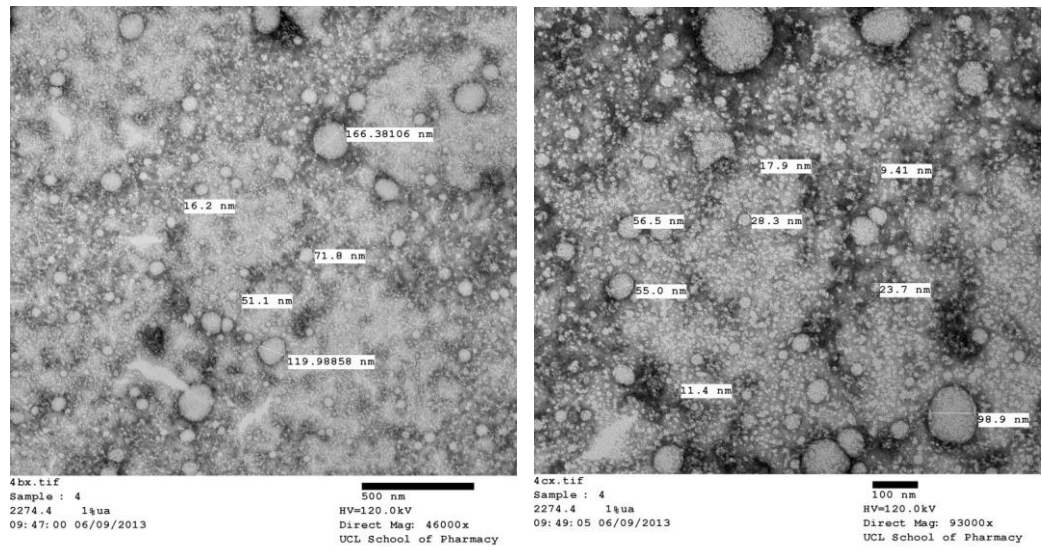


Figure 25: DS-GCP20Q11-E 1:10, 5% oil . The particle size was heterogeneous between 9 to 100 nm in diameter. Left: 46,000x magnification, Right: 93,000x magnification.

### **3.4.4 Formulation of DS with GCP20Q11 at different amount of oil**

The ability of GCPQ polymer to encapsulate high amount of drug is important to ensure the minimum use of polymer with the drug to reach the effective dose required for the administration in animal subjects later in the project. Therefore, the current experiment was to evaluate the maximal amount of drug/oil that can be stabilized by GCPQ at different ratios of oil/polymer in the formulation.

#### **3.4.4.1 Determination of maximum oil content for DS-GCP20Q11-E**

In the attempt to determine the maximum amount of oil the GCPQ is able to contain, separate DS-GCP20Q11-E formulations were made containing either 5, 10, 15, 20, 25, 30, 35, 40, 45, 50 or 55% oil v/v. Table 16 summarizes the preparation of DS-GCP20Q11-E formulations at different amount of oil. Amount of GCP20Q11 was fixed at 10 mg/ml in all formulations. The GCP20Q11 was dissolved in Milli-Q water prior to the addition of DS in SB oil. After the addition, the formulations were sonicated using ultrasonic disintegrator at amplitude 5 (Soniprep 150 Plus, MSE, U.K.) for 15 minutes. All formulations were prepared in triplicate.

Oil content v/v (%)	Amount of 20 mg/ml DS in SB oil (µl)	Amount of DS (mg)	Amount of GCP20Q11 (mg)	GCP20Q11 in Milli-Q water (µl)	Final volume (µl)
5	50	1	10	950	1000
10	100	2	10	900	1000
15	150	3	10	850	1000
20	200	4	10	800	1000
25	250	5	10	750	1000
30	300	6	10	700	1000
35	350	7	10	650	1000
40	400	8	10	600	1000
45	450	9	10	550	1000
50	500	10	10	500	1000
55	550	11	10	450	1000

Table 16: Table of ingredients for preparation of DS-GCP20Q11-E from 5 to 55% oil v/v formulations.

In this preliminary experiment, the freshly prepared formulations were placed in a long, thin and clear glass tubes (Figure 26) to allow better visibility of the oil layer forming at the top surface of the unstable colloidal dispersions. The oil layer formed from the excess of oil that cannot be contained by the polymer.

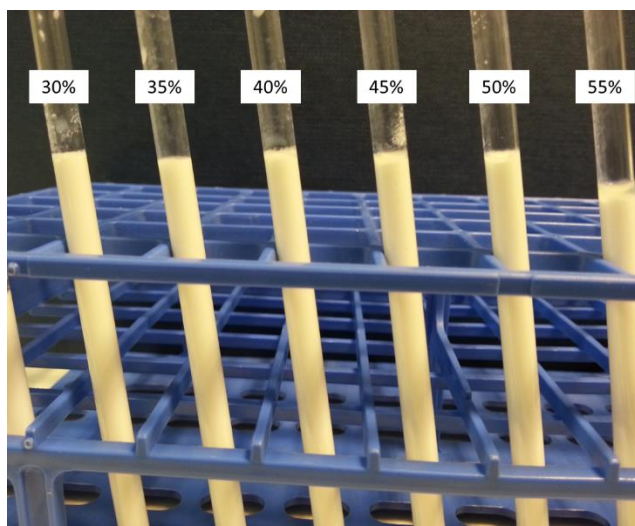


Figure 26: DS-GCP20Q11E formulations at different amount of oil in glass tubes for oil layer observation. The oil layer in the 55% oil content formulation is clearly visible in the picture after 24 hours at room temperature.

Based on the observation, only DS-GCP20Q11-E formulation at 55% oil content showed a clear visible layer of oil after the formulation left to stand at room temperature for 24 hours. There was no oil layer observed in other formulations. For further confirmation and better visibility of the excess oil layer formation in the high oil-content formulations, 20  $\mu$ l of 1 mg/ml Nile red dye solution (Sigma Aldrich, Missouri, USA) was added into 500  $\mu$ l of each formulation. The formulations were then mixed thoroughly by high speed vortex and centrifuged at 17,000 g for 45 minutes to induce phase separation.

Upon addition of the dye, the milky white colour of the formulations turned to pink. After the centrifugation, only 55% oil content formulation showed three distinct

layers while others showed only two layers' formation. The 3 layers in the 55% oil content were comprised of free oil layer (top layer), particle layer (middle layer) and water layer (bottom layer), whereas the 2 layers in other formulations were comprised of only particle and water layers (top and bottom layer, respectively) (Figure 27).

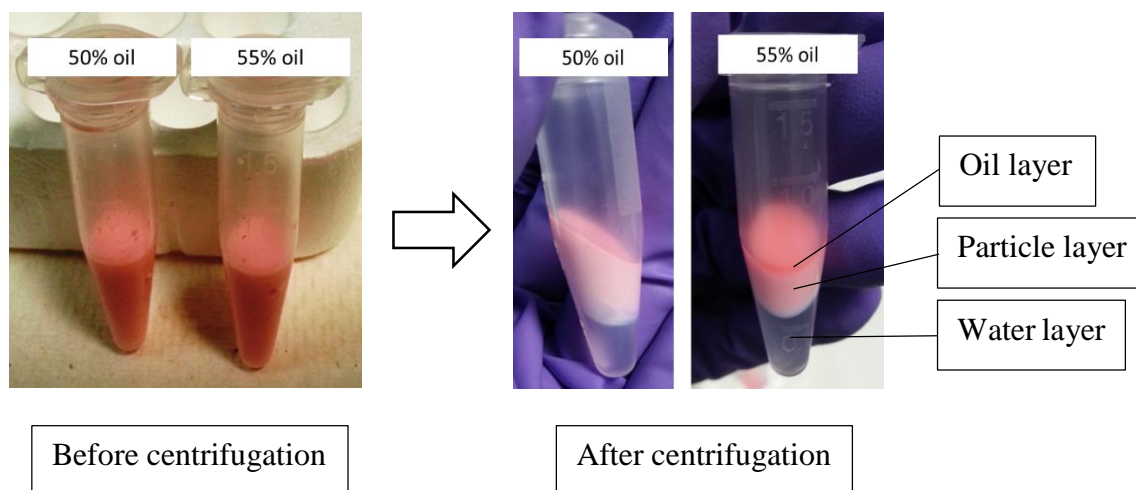


Figure 27: DS-GCP20Q11-E formulations at 50 and 55% oil content stained with Nile red before and after centrifugation. Three distinct layers can be seen in 55% oil formulation.

The Nile red is lipophilic and water insoluble, therefore it needs to be in lipophilic environment. This behaviour gave the oil and particle layers a translucent and opaque pink colouration, respectively, which in the latter was due to the scattered light by the particles giving it a turbid feature. The attraction of the dye to the particle layer was probably due to hydrophobic palmitic chain of the particles as well as to the oil content inside the particles. The clear and transparent hydrophilic water layer showed there was no presence of the dye.

As this preliminary result showed formulations at 55% oil content is incapable of encapsulating the whole amount of oil added, the endpoint amount of oil that can be added

into the formulation for a stable formulation was between 51 to 54% oil. At this point, the highest amount of oil that can be used to form a stable DS-GCP20Q11-E nanoemulsion is 50% v/v. In theory, the disperse phase in an emulsion can occupy up to 74% of the phase volume, but common pharmaceutical emulsion usually contain only between 10-30% disperse phase (Eccleston, 2013). This suggest GCP20Q11 is a good emulsifier for being able to stabilize up to 50% of the oil-loaded particles.

### 3.4.5 Characterization of DS-GCP20Q11-E at different amount of oil

DS-GCP20Q11-E formulations at 5, 10, 20, 30, 40 and 50% v/v oil content was prepared as described previously (Table 16) in triplicate. All freshly prepared formulations with different oil content (Figure 28) were characterized by measuring the mean drug content, DE%, particle size and PDI values.

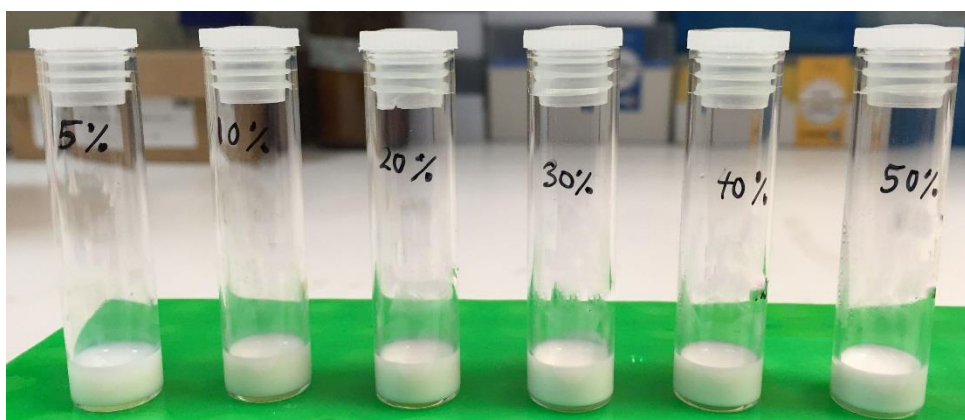


Figure 28: The milky-white appearance of freshly prepared DS-GCP20Q11-E formulations at (from left) 5, 10, 20, 30, 40 and 50% v/v oil content. The formulations appeared thicker and denser towards the higher amount of oil content.

The drug content graph shows the trend of increasing amount of DS detected towards the increasing amount of oil added into the formulations. This drug content was later interpreted into DE% to determine the encapsulation efficiency of GCPQ polymer on the different amount of oil. The result shows all formulations having almost 100% drug entrapment with no significant difference of entrapment percentage between the different oil content formulations ( $P > 0.05$ ) (Figure 29).

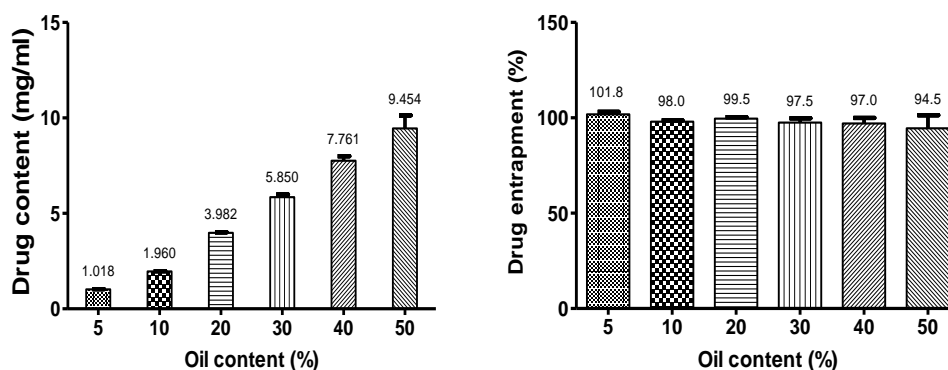
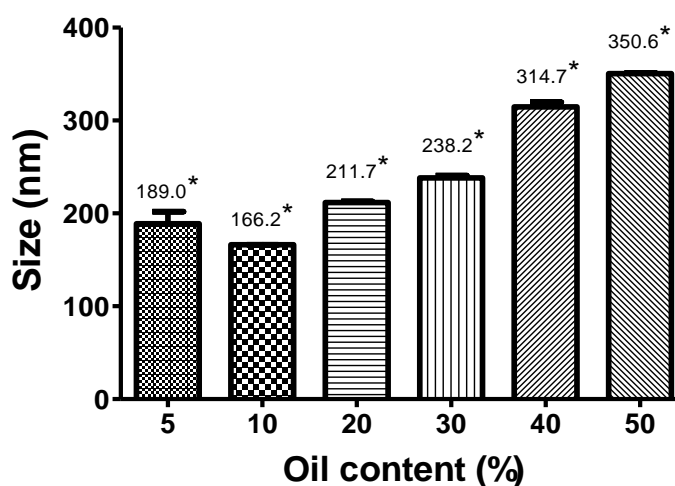


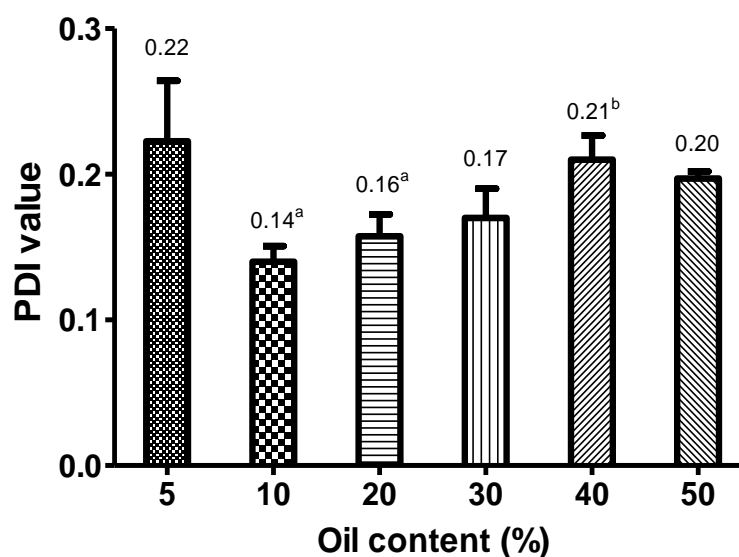
Figure 29: Drug content (left) and DE% (right) for the freshly prepared DS-GCP20Q11-E formulations at 5, 10, 20, 30, 40 and 50% oil content. The mean values for each type of formulations were labelled on top of the bars. Data were presented as mean  $\pm$  SD ( $n = 3$ ).



\* Significant compared to mean particle size of any other formulations with different oil content

Figure 30: Particle size of freshly prepared DS-GCP20Q11-E formulations at 5, 10, 20, 30, 40 and 50% oil content. Data were presented as mean  $\pm$  SD ( $n = 3$ ).

The particle size was in a range of 166 to 351 nm and was seen increased with higher amount of oil in the formulation (Figure 30). The mean particle size was found significantly different among the different oil content formulations ( $P < 0.05$ ). On the other hand, all formulations showed low PDI (less than 0.3), even though the values for 5% oil was significantly higher than 10 and 20% oil formulations and 40% oil significantly higher than 10% oil formulations (Figure 31).



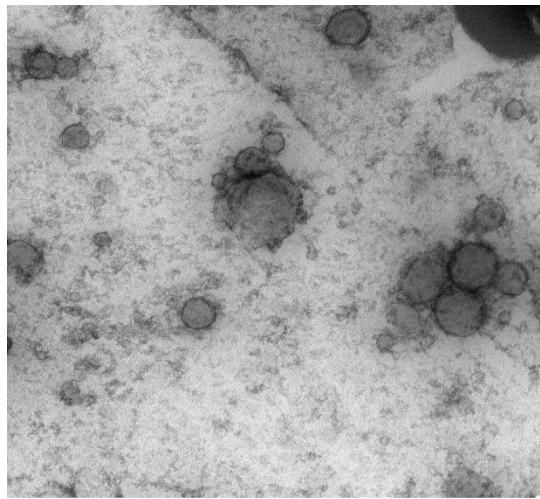
<sup>a</sup> Significant compared to mean PDI value of 5% oil content formulations

<sup>b</sup> Significant compared to mean PDI value of 10% oil content formulations

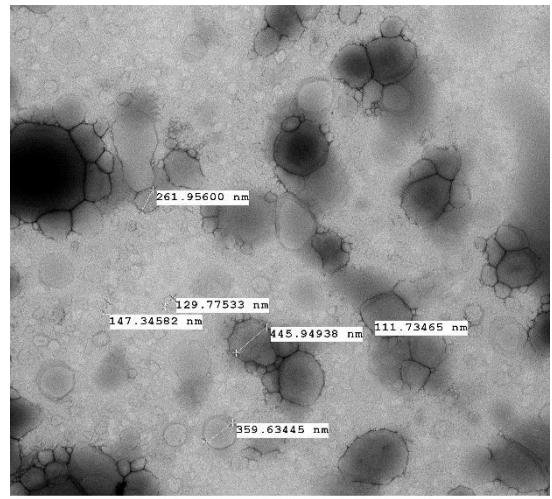
Figure 31: PDI values of freshly prepared DS-GCP20Q11-E formulations at 5, 10, 20, 30, 40 and 50% oil content. Data were presented as mean  $\pm$  SD ( $n = 3$ ).

TEM images of DS-GCP20Q11-E at 40% and 50% oil content showed formation of heterogenous particle size in the range of between 300 to 500 nm in diameter (Figure 32a and b, respectively). These values are almost similar as indicated by the DLS measurements (mean values of 314.7 and 350.6 nm for 40% and 50% oil content, respectively). The particles were also seen tightly packed together especially in the 50% oil formulation. The reason was probably that more amount of oil causing more particles to be formed by GCPQ up to a point where there was hardly free space for the particles to move around, which could explain the higher viscosity observed in higher oil content formulations.

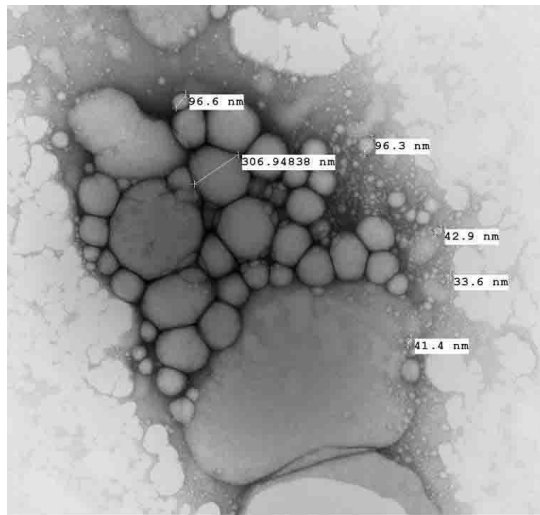
Formulations at 55% oil which exceeds the maximum amount of oil that can be added into the formulations, showed appearance of large droplets of oil (more than 1  $\mu\text{m}$ ) (Figure 32c). This was probably parts of the oil phase which were not encapsulated by the polymer merged together because of no free polymer left available for the formation of nanoparticles.



**a**  
 500 nm  
 HV=120.0kV  
 Direct Mag: 46000x  
 UCL School of Pharmacy



**b**  
 500 nm  
 HV=120.0kV  
 Direct Mag: 17500x  
 UCL School of Pharmacy



**c**  
 500 nm  
 HV=120.0kV  
 Direct Mag: 33000x  
 UCL School of Pharmacy

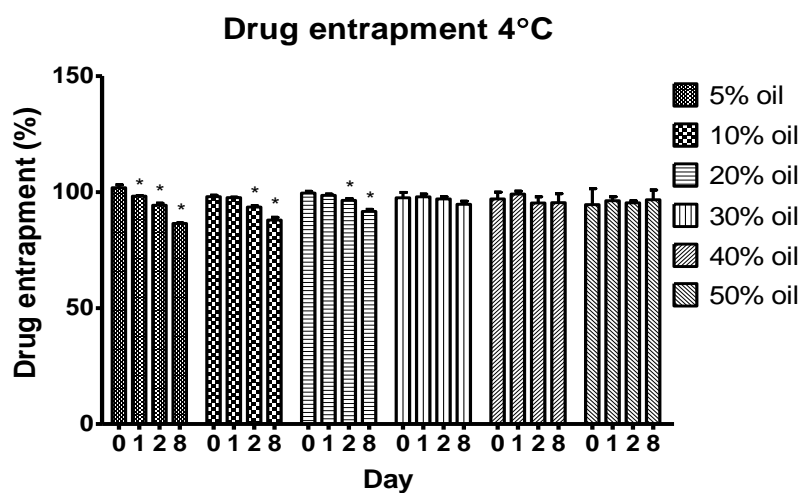
Figure 32: TEM images of DS-GCP20Q11-E at 40% (a), 50% (b) and 55% (c) oil content.

### **3.4.6 Stability of DS-GCP20Q11-E upon storage**

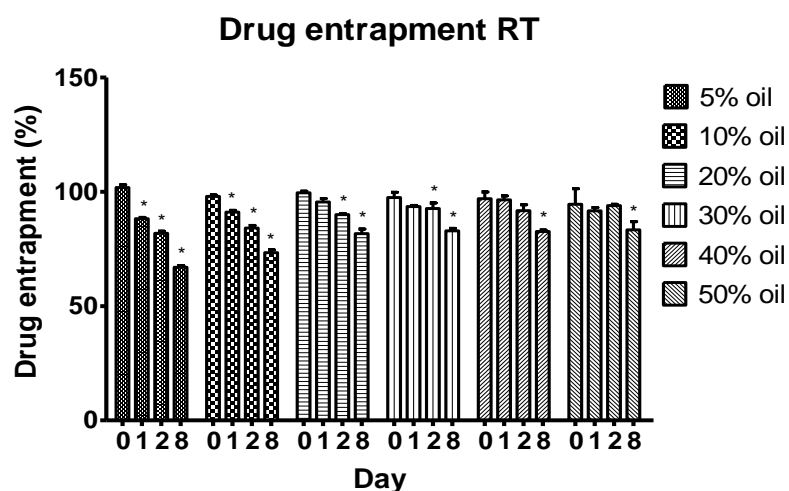
The stability of DS-GCP20Q11-E formulations at 5, 10, 20, 30, 40 and 50% oil content was tested upon storage at different temperatures by measuring the changes in drug entrapment, particle size and PDI value over a period of time. The formulations were kept at either room temperature (RT) by placing them on the bench in the lab, or at 4°C by placing them in the fridge. Samples were taken for analysis on Day 0 (day of preparation), 1, 2, and 8. The statistical analysis used to compare the values between days within a group was One-way ANOVA, followed by Tukey's HSD for the post-hoc analysis.

#### **3.4.6.1 Changes in drug entrapment**

Based on the result, the formulations were more stable when stored at 4°C as only 5, 10 and 20% oil formulations had significantly reduced DE% within the 8 days' period, compared to all formulations having significant DE% reduction at RT (Figure 33). At 4°C, formulations containing 30% oil and above showed no significant reductions in drug entrapment up until 8 days. This suggests such amount of oil in the formulations is optimum for the polymer to retain the DE% to a longer period of time. The lower temperature plays a role in giving more DE% stability by the GCPQ polymer. As explained in Section 3.4.3.1, there was possibility of unseen creaming or flocculation (clusters of particles behave as a single kinetic unit) occurring in the nanoemulsions over time, causing sampling of the area with less particles in the formulation thus decreased the DE% measurement.



\* Significant compared to mean DE% on Day 0 in its respective group

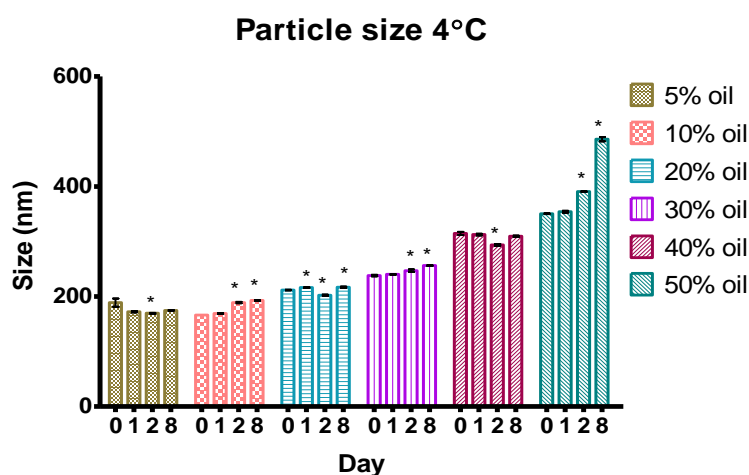


\* Significant compared to mean DE% on Day 0 in its respective group

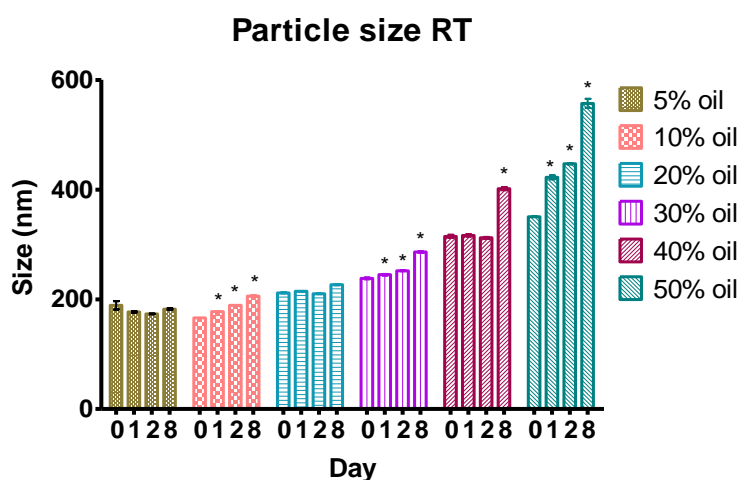
Figure 33: DE% of DS-GCP20Q11-E formulations at different oil content stored at 4°C (DE% 4°C, top) and RT (DE% RT, bottom) on Day 0, 1, 2 and 8. Data were presented as mean  $\pm$  SD (n = 3).

### 3.4.6.2 Changes in particle size

The pattern of the graphs (Figure 34) shows the more oil content in the formulation, the bigger the size of the particles. Despite the significant change in size, all formulations at both temperatures showed no large increase or decrease in values compared to the fresh preparation (change of size was observed less than half of the size on Day 0).



\* Significant compared to mean particle size on Day 0 in its respective group

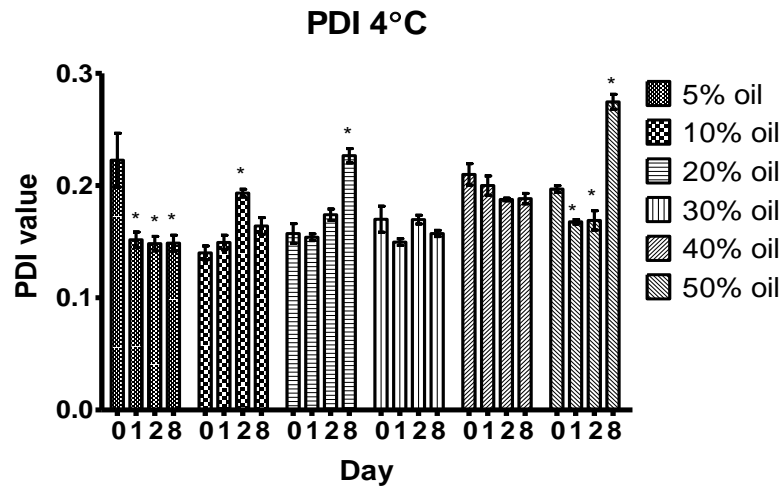


\* Significant compared to mean particle size on Day 0 in its respective group

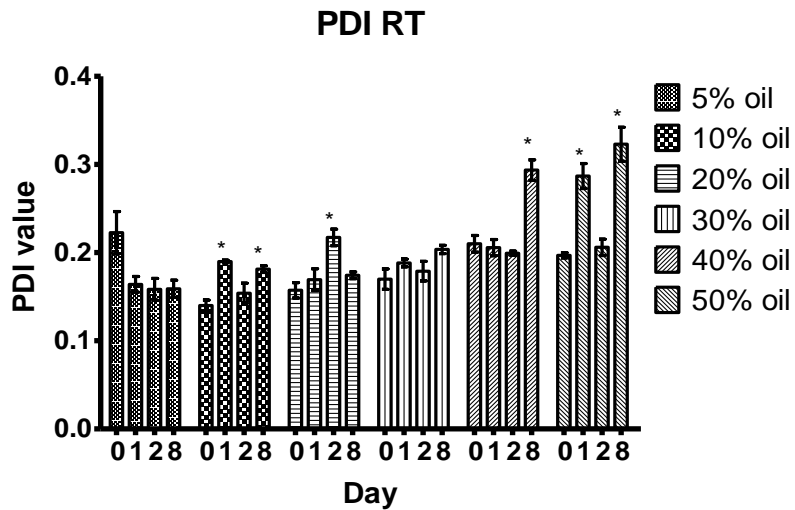
Figure 34: Particle size of DS-GCP20Q11-E formulations at different oil content stored at 4°C (Particle size 4°C, top) and RT (Particle size RT, bottom) on Day 0, 1, 2 and 8. Data were presented as mean  $\pm$  SD (n = 3).

### **3.4.6.3 Changes in PDI value**

In general, mean PDI values (Figure 35) for 5% oil content showed better stability at RT compared to 4°C. Significant increase in PDI was seen at earlier days for both 10% and 20% oil content formulations when stored at RT compared to storage at 4°C. There was no change observed in 30% oil content formulations at both temperatures throughout the study. Formulations of 40% oil content showed only significant increase in PDI on Day 8 at RT, whereas 50% oil content at both temperatures showed significant fluctuation on the PDI values until end of the study.



\* Significant compared to mean PDI on Day 0 in its respective group



\* Significant compared to mean PDI on Day 0 in its respective group

Figure 35: PDI values of DS-GCP20Q11-E formulations at different oil content stored at 4°C (PDI 4°C, top) and RT (PDI RT, bottom) on Day 0, 1, 2 and 8. Data were presented as mean  $\pm$  SD (n = 3).

### 3.4.7 Stability of DS-GCP20Q11-E in acidic and basic pH

#### 3.4.7.1 Overview

The experiment was done to analyse the influence of highly acidic or highly basic pH on the particle size and PDI value of the DS-GCP20Q11-E nanoparticles. Such changes in bulk pH conditions are typically encountered in the gastrointestinal tract, blood circulation and in the tumour where it could affect the morphology of the particles.

#### 3.4.7.2 Materials

Item	Supplier
Hydrochloric acid	Fisher Scientific Limited, Leicestershire, UK
Sodium hydroxide	Sigma-Aldrich Company Limited, Dorset, UK

#### 3.4.7.3 Methodology

One millilitre of DS-GCP20Q11-E at 5% oil content was prepared as described previously. As a control, 10 mg/ml of GCP20Q11 suspension was prepared by dissolving 10 mg of the polymer in 1 ml of MilliQ water. The formulations and GCP20Q11 suspensions (in triplicate) were titrated with either 0.1 M hydrochloric acid (HCl) or 0.1 M sodium hydroxide (NaOH) solution to create the highly acidic (pH 1.7) or highly basic (pH 11) condition, respectively. Both formulations and control were then sampled immediately for the DLS measurement, as described previously.

### 3.4.7.4 Results

	Particle size (nm) and pH		
	Fresh preparation	Acidic condition	Basic condition
DS-GCP20Q11-E	195.7 ± 2.3 pH 4.4	215.8 ± 0.7 pH 1.67	192.2 ± 1.4 pH 10.9
	PDI value and pH		
	Fresh preparation	Acidic condition	Basic condition
	0.24 ± 0.004 pH 4.4	0.33 ± 0.01 pH 1.67	0.24 ± 0.01 pH 10.9
GCP20Q11 (control)	Particle size (nm) and pH		
	Fresh preparation	Acidic condition	Basic condition
	156.0 ± 1.2 pH 4.53	152.6 ± 32.1 pH 1.73	125.7 ± 13.1 pH 11.1
	PDI value and pH		
	Fresh preparation	Acidic condition	Basic condition
	0.59 ± 0.15 pH 4.53	0.46 ± 0.07 pH 1.73	0.49 ± 0.06 pH 11.1

Table 17: The particle size, PDI values of DS-GCP20Q11-E and GCP20Q11 suspensions in highly acidic and basic pH condition. Data were presented as mean ± SD (n = 3).

### 3.4.7.5 Discussion and conclusion

Based on the result in Table 17, statistical analysis showed no significant changes in particle size and PDI value in both DS-GCP20Q11-E and GCP20Q11 suspensions when it is adjusted into highly acidic and basic environment when compared to the unaltered fresh preparation ( $p > 0.05$ ). It was noticed that the PDI values for GCP20Q11 suspension was large (0.50 – 0.60). This might due to the way the polymeric suspension was prepared of which the GCPQ suspension was not sonicated after completely

dissolved in Milli-Q water compared to the formulations where it was sonicated to reach homogeneity. There was no aggregation observed in all formulations that might have led to flocculation or cracking (phase separation) of the nanoemulsion, although it was expected to happen in the highly basic environment where the abundant presence of OH<sup>-</sup> ions might neutralize the positive charged particles, leading to instability of the particle structure. This perhaps attributed to the highly charged GCPQ particles outweighing the effect of the counter ions introduced into the formulations. In conclusion, both the DS-GCP20Q11-E and GCP20Q11 were stable in highly acidic and basic environment.

### 3.4.8 Stability of DS-GCP20Q11-E in buffers

The next experiment carried out was to determine the stability of DE% of the DS-GCP20Q11-E in HCl (pH 1.2) and phosphate (pH 6.8) buffers.

#### Materials

Item	Supplier
Potassium chloride	Sigma-Aldrich Company Limited, Dorset, UK
Monobasic potassium phosphate	
Sodium hydroxide	
Hydrochloric acid	Fisher Scientific Limited, Leicestershire, UK

#### 3.4.8.2 Methodology

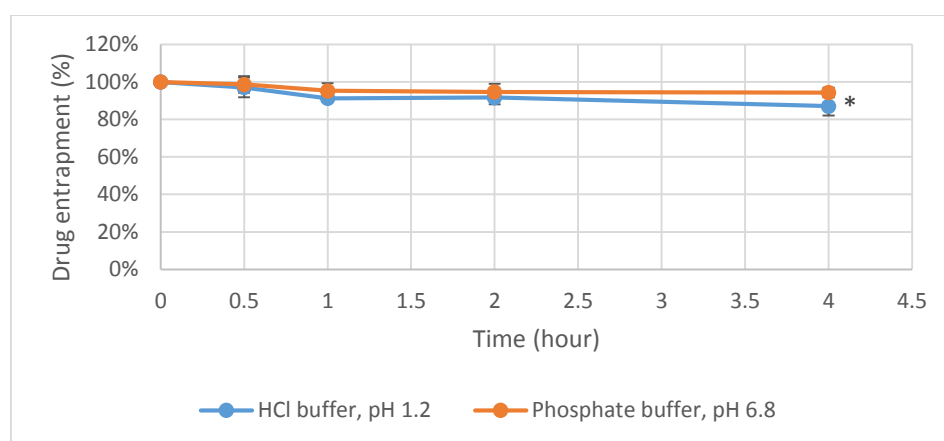
HCl buffer was prepared by mixing together 50 ml of 0.2 M potassium chloride and 85 ml of 0.2 M HCl solution in a 200 ml volumetric flask. Milli-Q water was then added into the volumetric flask to prepare 200 ml HCl buffer at pH 1.2. Phosphate buffer was prepared by mixing 50 ml of 0.2 M monobasic potassium phosphate with 22.4 ml of 0.2 M NaOH solution in a 200 ml volumetric flask. Milli-Q water was then added into the flask to create 200 ml phosphate buffer at pH 6.8.

The stability of DS-GCP20Q11-E in the buffer was determined by assessing the DE% of the formulation in the buffer over a period of time. DS-GCP20Q11-E at 5% oil content (DS concentration = 1 mg/ml) was freshly prepared and 400  $\mu$ l of this formulation was added into 3600  $\mu$ l of either the HCl or phosphate buffer (DS concentration = 100  $\mu$ g/ml) with solutions at room temperature (22-24°C). Samples were taken (50  $\mu$ l) at 0 minutes (right after addition), 30 minutes, 1, 2 and 4 hours after the addition (t = 0, 0.5, 1, 2 and 4, respectively) and diluted with 950  $\mu$ l ethanol (20 times dilution). The samples

were then centrifuged at 1,000 g for 10 minutes to sediment any large particles such as salt present in the samples. Without any further sample dilution, the drug content in the supernatant was then measured with HPLC.

### 3.4.8.3 Results

The results showed no significant decrease of DE% for formulation incubated in phosphate buffer (pH 6.8) up to 4 hours, whereas the significant decrease was seen in HCl buffer (pH 1.2) only at t = 4 hour (Figure 36).



\* Significant compared to mean DE% at t = 0 hour

Figure 36: DE% of DS-GCP20Q11-E in HCl and phosphate buffer at t = 0, 0.5, 1, 2 and 4 hours. Buffers were at room temperature at the time of measurement. Data were presented as mean  $\pm$  SD (n = 3).

### 3.4.8.4 Discussion and conclusion

Colloidal stability depends on the balance of attractive and repulsion interactions between particles. The repulsion of particles might be attributed to the electrical charge around the particles and/or attached polymer layers on the particle surface which causes electrostatic and/or steric stability, respectively. Presence of salts could increase the electrolyte concentration in the particles' environment which leads to compression of the

electrical double layer. This causes the energy barrier to decrease or disappear, leading the Van der Waals attraction to induce aggregation of the particles (Schramm, 2006). HCl buffer could imitate the highly acidic environment in the stomach where chloride was found as the dominating ion at concentration range between 48 to 173 mM in the fasted state (Lindahl et al., 1997).

Despite the presence of salts, the formulation was able to maintain its colloidal stability. In conclusion, it could be summarized that with the presence of 0.2 M salt in the acidic and neutral buffer, DS-GCP20Q11-E is stable and able to withhold the drug loading for as long as 2 and 4 hours, respectively.

### **3.4.9 Stability of DS-GCP20Q11-E in simulated biological samples**

#### **3.4.9.1 Overview**

The crucial point of an oral drug formulation is the ability to withstand the variation in pH level and exposure to various enzymes and bile salts in the GIT. This experiment was conducted as an *in vitro* test to study the effect of the physicochemical environment of the GIT on the digestive stability of the formulations. In other words, it was also to study the GIT fluid effect on the stability of the polymer structure that encapsulates the drug to protect it from degradation.

The simulated gastric fluid (SGF) and simulated intestinal fluid (SIF) were used as an imitation to the human GIT fluids. These two fluids are more commonly used to study the drug dissolution in the gut (Marques et al., 2011). SGF represents the acidic environment in the stomach which is more adequately reflects the physiological conditions of the fasted-state fluid (Vertzoni et al., 2005), whereas the SIF represents the conditions in the small intestine. Pepsin enzyme, a digestive protease simulates closely the fasting conditions in the stomach (Vertzoni et al., 2005). On the other hand, pancreatin enzyme that is added into the SIF contains many enzymes such as amylase, trypsin, lipase, ribonuclease and protease to imitate more of the activities happening in the small intestine (Das and Lin, 2005).

### 3.4.9.2 Materials

Item	Supplier
Sodium chloride	Sigma-Aldrich Company Limited, Dorset, UK
Potassium dihydrogen phosphate	
Sodium hydroxide	
Pepsin powder from porcine gastric mucosa	
Pancreas powder from pancreatin of porcine pancreas	
Dimethyl sulfoxide	
Hydrochloric acid	Fisher Scientific Limited, Leicestershire, UK

### 3.4.9.3 Methodology

#### 3.4.9.3.1 Preparation of simulated gastric fluid

SGF was prepared as described in British Pharmacopoeia (2013) and consist of 2 g sodium chloride, 3.2 g pepsin powder and later on added with 80 ml 1M hydrochloric acid to make 1 L of SGF solution, pH 1.2.

#### 3.4.9.3.2 Preparation of simulated intestinal fluid

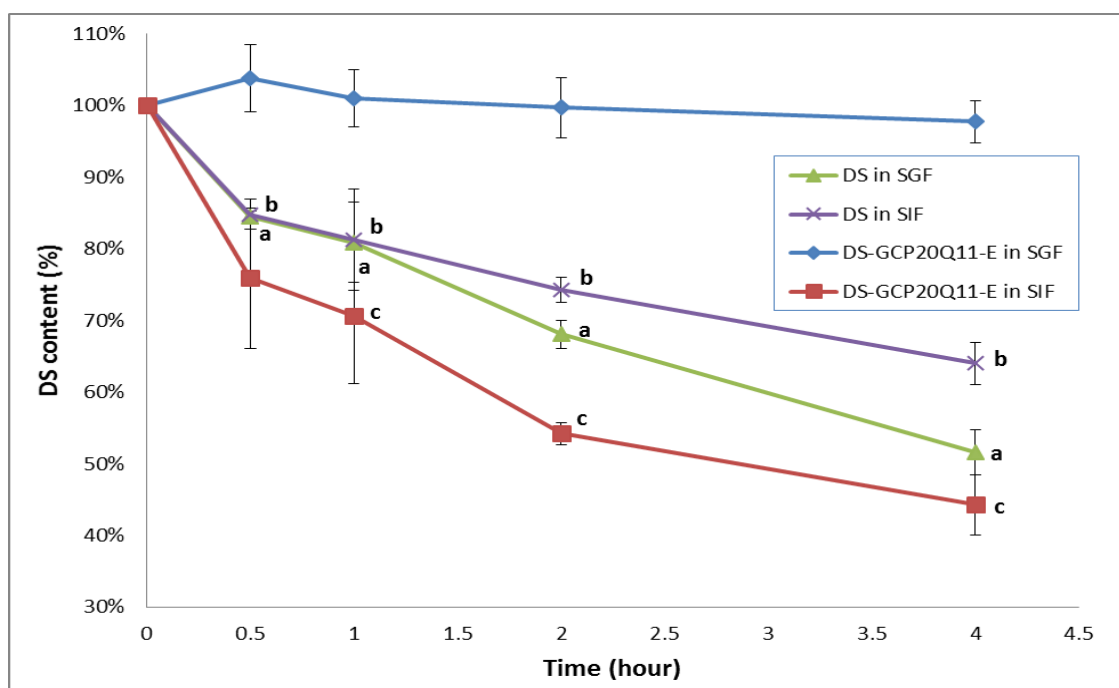
SIF was prepared as described in British Pharmacopoeia (2013) by mixing 77 ml of 0.2 M sodium hydroxide, 250 ml of 6.8 g potassium dihydrogen phosphate and 10 g pancreas powder to make 1 L of SIF solution at pH 6.8.

#### **3.4.9.3.3 Experimental procedure**

DS-GCP20Q11-E formulations containing 5% oil and 1 mg/ml DS were prepared. As for control, 1 mg/ml of DS was prepared in 2% dimethyl sulfoxide (DMSO). An amount of 400  $\mu$ l of the formulations or control was added into 3.6 ml of either SGF or SIF to make ratio of 1 to 10 (drug to SGF or SIF) and maintained in 37°C water bath. The drug content was assessed at several time points after the addition into the SGF or SIF; right after the addition ( $t = 0$ ) and at 30 minutes, 1 hour, 2 hours and 4 hours post-addition ( $t = 0.5, 1, 2$  and 4, respectively). At each time point, 50  $\mu$ l of the SGF or SIF solutions were taken and diluted in 950  $\mu$ l ethanol (added drug concentration = 5  $\mu$ g/ml). The samples were then centrifuged at 1,000 g for 10 minutes. The supernatant was collected and subjected for HPLC analysis and the pellet was discarded. All samples were prepared in triplicate.

#### **3.4.9.4 Results**

As shown in Figure 37, the stability of DS in SGF was improved greatly when it is incorporated with GCP20Q11 with no significant degradation throughout the 4 hours' period whereas DS in DMSO (control) was significantly degraded over time. Meanwhile in SIF, the DS content was seen decreasing gradually over time in both control and DS-GCP20Q11-E samples.



<sup>a, b, c</sup> Significant compared to drug content at t = 0 for DS in SGF, DS in SIF and DS-GCP20Q11-E in SIF, respectively.

Figure 37: The stability of DS following incubation of the DS-GCP20Q11-E formulation or the drug alone (control) in SGF and SIF up to 4 hours at 37°C. The drug concentration in the graph was normalized by using percentages. Data were presented as mean  $\pm$  SD (n = 3).

### 3.4.9.5 Discussion and conclusion

The SGF solution did not seem to affect the drug content of DS-GCP20Q11-E up to 4 hours' incubation, indicating the GCPQ polymer is capable of protecting the drug from digesting activity of the pepsin enzyme and the low pH environment in the SGF. The DS-GCP20Q11-E formulation is however unstable in SIF as the drug concentration was seen to decrease over time. The loss of the drug content could indicate that the multiple enzymes affect the structure of the GCPQ polymers causing the release of the encapsulated drug into the SIF thus degraded upon contact with the pancreatin enzyme or

the high pH. As a conclusion, the DS-GCP20Q11-E formulation is suitable to be used for protection of DS against degradation in the stomach.

### **3.4.10 Conclusions for nanoemulsion formulation**

The encouraging criteria of the nanoemulsion formulations (e.g. high drug load) and its stability in the low pH environment provide enough reasons for the nanoemulsion to be chosen for further studies in the *in vitro* and *in vivo* model. Apart from giving an insight of the possible protection of the drug content when the formulations are given to the animal subjects later in the project, the information on the stability of the formulations in different environments also allows us to set the right condition for the preparation of the formulation prior to the dosing process for the *in vivo* experiments.

## Chapter 4

# Disulfiram nanoemulsion *in vitro* cytotoxicity

### 4.1 Overview

*In vitro* cell-based cytotoxicity assays are employed to allow quick compound screening to determine effects on cell proliferation and toxicity. One of the ways to assess cell survival upon exposure to test compounds is by measuring the general metabolism or the enzymatic activity of the cells. There are handful of tetrazolium compounds that have been used for detection of viable cells. One tetrazolium compound known as MTT (3-[4,5-dimethylthiazol-2-yl]-2,5 diphenyl tetrazolium bromide) has been used widely in laboratory as a homogenous cell viability assay developed for 96-well plate format.

The MTT reduction assay is based on conversion of MTT reagent by mitochondrial activity of living cells into formazan crystals, thus the level of product is proportional to the relative number of viable cells (Mosmann, 1983). The tetrazolium salt MTT is positively charged and can penetrate eukaryotic cells by cellular uptake via plasma membrane potential (Berridge et al., 2005). After the incubation of yellow MTT reagent with the cells for 1 to 4 hours, the amount of purple coloured formazan crystals formed is

later measured with plate reader spectrophotometer to record the changes in absorbance at 570 nm.

The principal of this colorimetric assay is that mitochondrial activity of most viable cells are usually constant, therefore higher mitochondrial activity linearly related to higher number of viable cells (van Meerloo et al., 2011, Denizot and Lang, 1986). The precise cellular mechanism of MTT reduction into formazan is still unknown, but it is likely by mitochondrial succinate dehydrogenase (Slater et al., 1963), or involving the transfer of electrons to MTT from nicotinamide adenine dinucleotide (NADH) coenzyme generated in the mitochondria (Stockert et al., 2012, Berridge et al., 1996) (Figure 38).

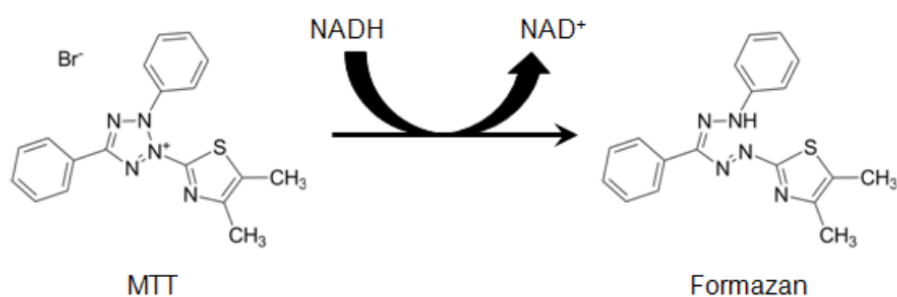


Figure 38: Conversion of MTT reagent into formazan by NADH coenzyme.

## 4.2 Materials

Item	Supplier / Manufacturer
MIAPaCa-2	American Type Culture Collection, Rockville, Maryland, USA.
Dimethyl sulfoxide	Sigma-Aldrich Company Limited, Dorset, UK
Copper (II) chloride	
Dulbecco's Modified Eagle's Medium (DMEM), high glucose with L-glutamine and sodium bicarbonate (D5796)	
Fetal bovine serum	
Dulbecco's Phosphate Buffered Saline	
Thiazolyl blue tetrazolium bromide	
Triton X-100	
Hanks' Balanced Salt Solution, 10X	
Sodium pyruvate, 100 mM	
Trypsin-ethylenediaminetetraacetic acid (EDTA), 0.25%, phenol red	
Glucose intravenous infusion 50% w/v	Hameln Pharmaceuticals Limited, Gloucester, UK

### **4.3 Methodology for MTT assay**

The cytotoxic effect of DS and DS-GCP20Q11-E, with and without the presence of copper was determined in the human pancreatic cancer cell line MIAPaCa-2.

#### **4.3.1 Cell preparation in 96-well plate**

Freshly thawed MIAPaCa-2 cells from cryopreservation were grown for at least 2 weeks prior to the experiment. The complete growth medium used for the cells was sterile-filtered DMEM added with 10% v/v fetal bovine serum and 1 mM sodium pyruvate. The cells were maintained in carbon dioxide (CO<sub>2</sub>) incubator with environment set at 5% CO<sub>2</sub> and temperature at 37°C.

For propagation, cells that were grown in 75 cm<sup>2</sup> cell culture flask were detached from the bottom of the flask by rinsing the cells first with phosphate buffered saline (PBS) followed by adding 3 ml of trypsin-EDTA for detachment and incubation in CO<sub>2</sub> incubator for 3 minutes. The flask was then shaken to completely detach the cells. After confirmation of full detachment by examination under the light microscope, the cells were immediately added with 7 ml complete growth medium to neutralize the activity of trypsin-EDTA. The cell suspension was then mixed thoroughly with serological pipette to break the clumps of cells into individual cells. The number of cells was then counted by measuring 200 µl cell suspension with a flow cytometer (MACSQuant®, Miltenyi Biotec GmbH, Bergisch Gladbach, Germany) or haemocytometer.

The cells were seeded at 500 cells in 200 µl volume per well (2,500 cells/ml) into sterile flat bottom 96-well plate using multichannel pipette. For each plate, only the inner 60 wells were used (Figure 39) for the assay, avoiding the outer wells that are prone to evaporation and contamination from the outside air. The cells were then kept in the CO<sub>2</sub>

incubator for 3 days to allow the cells to be in log phase growth by the time the treatment was applied.

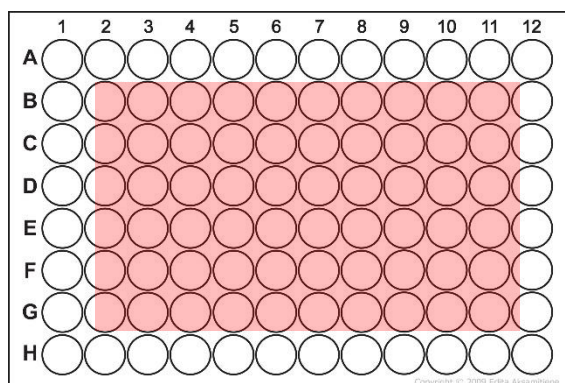


Figure 39: Sixty wells (highlighted in red box) from a 96-well plate used in the assay.

### 4.3.2 Drug treatments

Four different types of treatments were tested against the MIAPaCa-2 cells, as summarized in Table 18.

GROUP	TREATMENT
DS	DS in 2% DMSO
DS-GCPQ	DS-GCP20Q11-E, 5% oil content
DS + Cu	DS in 2% DMSO with copper chloride ( $\text{CuCl}_2$ )
DS-GCPQ + Cu	DS-GCP20Q11-E, 5% oil content with $\text{CuCl}_2$

Table 18: Four different groups of treatments for the MTT assay.

$\text{CuCl}_2$  solution was prepared in PBS at a concentration equimolar to the DS molarity ( $1 \text{ mg DS} = 3.37 \times 10^{-6} \text{ moles} = 0.45 \text{ mg CuCl}_2$ ). Prior to the drug addition, the medium in the plate (cell plate) was replaced with fresh  $100 \mu\text{l/well}$  growth medium. Ten

different concentrations for each type of treatment were achieved by serial dilution from 500 µg/ml (highest concentration) to  $5 \times 10^7$  µg/ml (lowest concentration). The drug dilutions for each treatment type were prepared in a new sterile plate (drug plate, containing no cells) (Figure 40) at double the final concentration of the intended drug concentration for incubation with the cells (200 µl/well). After the dilutions, only 100 µl of the drug solution in medium from each well in the drug plate was added into the cell plate (already containing 100 µl fresh medium) to achieve the intended drug concentration.

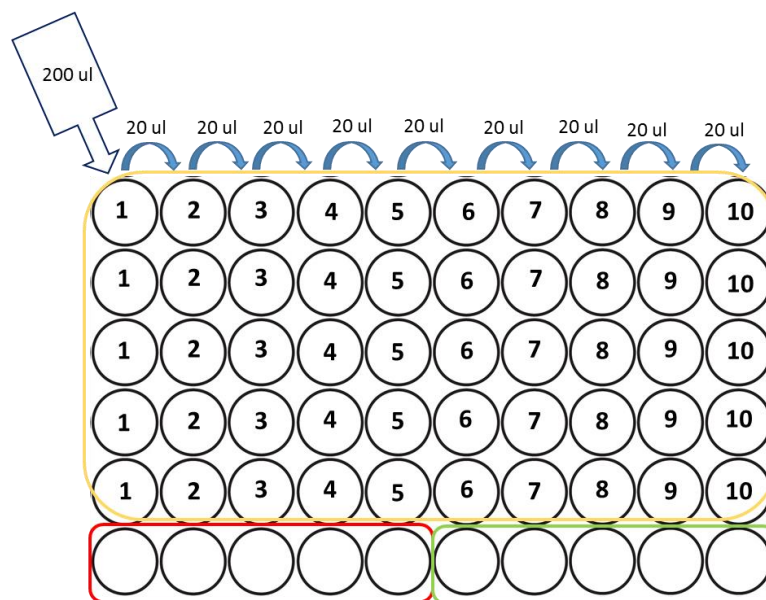


Figure 40: Drug dilutions (yellow box) was done in a new plate (drug plate, containing no cells). Lane 1 was added with the highest drug concentration and serially diluted towards Lane 10 (20 µl from previous well into 180 µl fresh medium in the next well ~ 10 times dilution) to get ten different concentrations of drug in one plate. Five wells (5 replicates) were allocated for each concentration. Red box was for positive control (total cell death) and green box for untreated cells.

Three plates were prepared for each type of treatment. The cells were incubated with the treatment for 4 hours in the CO<sub>2</sub> incubator. After the incubation, drug solutions were removed and cells were washed three times with PBS. Cells were then added with 200 µl/well fresh growth medium and left in the CO<sub>2</sub> incubator overnight.

### **4.3.3 Addition of MTT reagent and formazan dissolution**

MTT solution was prepared by dissolving 5 mg/ml of thiazolyl blue tetrazolium bromide powder in PBS protected from light, followed by filtration with 0.22 µm syringe filter to remove dust and foreign particles. The MTT solution was then further diluted with growth medium to create 0.5 mg/ml MTT solution. For positive control, growth medium in allocated 5 wells (Figure 40) were replaced with 200 µl of 1% Triton-X solution and incubated for 10 minutes or until all cells were dead. After the removal of the Triton-X, the rest of the medium in all wells were removed and replaced with the 0.5 mg/ml MTT solution. The plates were then incubated for 2 hours in the dark inside the CO<sub>2</sub> incubator.

After 2 hours, formation of purple formazan crystals in the wells was confirmed with examination under an inverted light microscope. The MTT solution in the wells was then removed and replaced with 100 µl DMSO per well to dissolve the crystals. The plate was placed on the shaker for 10 to 15 minutes to completely dissolve the crystals. The absorbance of each well was then measured using ELX808™ Absorbance Microplate Reader (Bio-TEK Instruments Inc., Winooski, Vermont, USA) at wavelength 570 nm.

### **4.3.4 Determination of cell viability and IC<sub>50</sub> of the treatments**

Percentage of cell survival upon each treatment was calculated as below:

- a) Mean absorbance calculation of 5 wells in positive control (p)
- b) Subtraction of p value from the absorbance of each treated well (t)
- c) Mean absorbance calculation of 5 wells in untreated group (u)
- d) Transformation of absorbance value into viability figure for each well:

$$\text{Viability of cells (V\%)} = [(t - p) / u] \times 100$$

- e) Calculation of V% mean and SD values of 5 wells for each drug concentration

The mean and SD values of V% for each concentration was then used in scatter plot graph to create a dose-response curve for determination of half-maximal inhibitory concentration (IC<sub>50</sub>) for each type of treatment.

#### **4.3.5 Statistical analysis**

Statistical analysis was performed using IBM SPSS Statistics for Windows, Version 22.0 (IBM Corp, Armonk, New York, USA). Data was analysed using One-way ANOVA, with Tukey's multiple comparison test for the post-hoc analysis. Data was presented as mean  $\pm$  standard deviation with significance value of  $p < 0.05$ .

## 4.4 Results and discussion

Dose-response curve plotting the cell viability (Figure 41) of MIAPaCa-2 cell lines after exposure to DS, DS-GCPQ, Cu + DS and Cu + DS-GCPQ and determination of the  $IC_{50}$  for each treatment were done using OriginPro 2016 software (OriginLab Corporation, Massachusetts, USA).

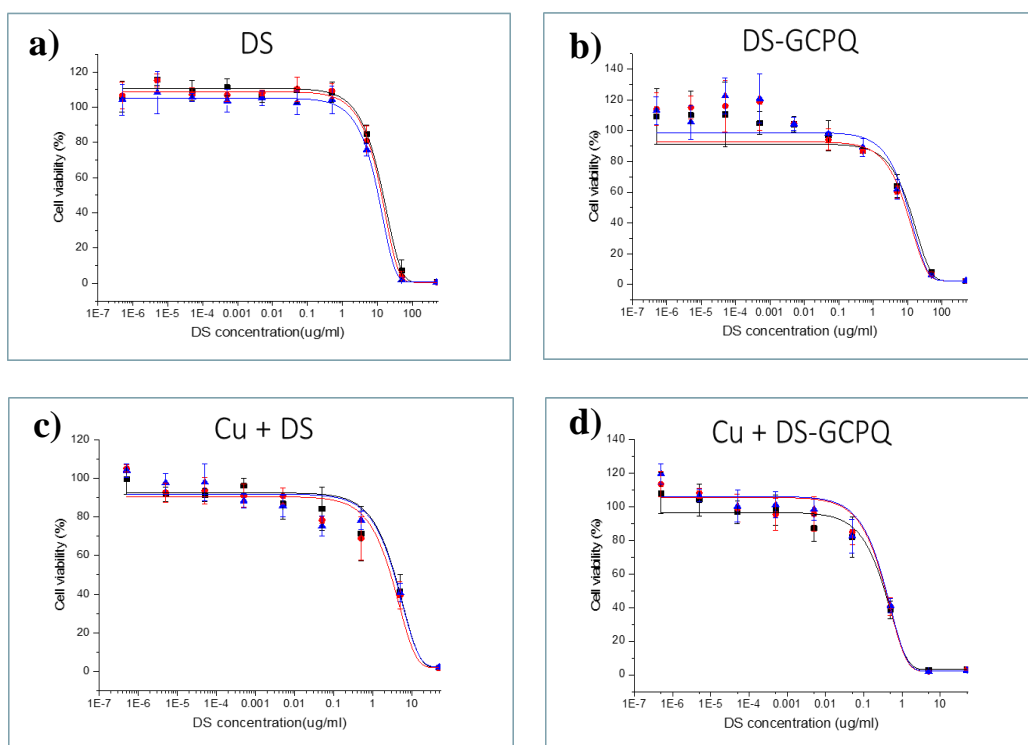
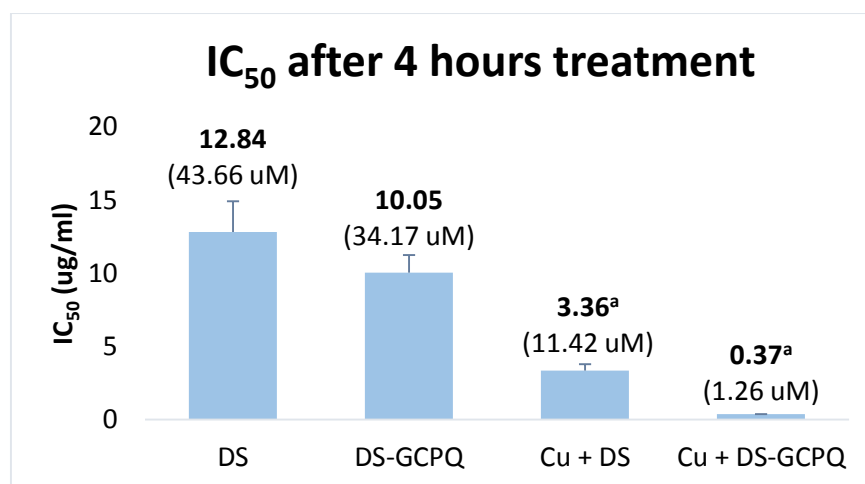


Figure 41: Dose-response curve of MIAPaCa-2 cell viability after treatment with DS (a), DS-GCPQ nanoemulsions (b), DS with copper (c) and DS-GCPQ nanoemulsions with copper (d) for 4 hours.



<sup>a</sup>Significant compared to IC<sub>50</sub> of DS and DS-GCPQ

Figure 42: Summary of IC<sub>50</sub> obtained from dose-response curves of all four treatments.

The results showed that IC<sub>50</sub> for MIAPaCa-2 cells treated with DS in the presence of copper ion with or without GCPQ encapsulation were significantly lower than groups treated without copper (Figure 42). This showed that copper highly enhanced the potency of the DS in the cytotoxic activity against the cancer cell lines. This effect of copper on DS activity has been reported previously against melanoma, myeloma, and breast cancer cell lines (Chen et al., 2006, Chen and Dou, 2008, Conticello et al., 2012, Yip et al., 2011). A pattern of lower IC<sub>50</sub> was also seen in groups with drug + GCPQ when comparing it to the group treated with the same drug but without GCPQ, although none of the difference was statistically significant. Cells that are treated with DS-GCPQ nanoemulsion and copper showed a remarkably low IC<sub>50</sub> value which was almost 10 times the effect seen in cells treated with Cu + DS.

Kim and his colleagues (2013) explored in detail the effects of DS on ALDH positive human pancreatic ductal adenocarcinoma cell lines. One of the findings was MIAPaCa-2 cell lines to have the highest expression of ALDH compared to several other human pancreatic cancer cell lines such as CFPAC-1, PANC-1 and AsPc-1. Since DS can irreversibly block the activity of ALDH, this supports the choice to use MIAPaCa-2 in

the present study as it is the most suitable pancreatic cell line to be used for determination of DS nanoemulsion activity on ALDH-expressed cells. Kim et al. however reported a much lower  $IC_{50}$  (0.77  $\mu$ M) for treatment of DS alone against MIAPaCa-2 cell lines compared to our study (43.66  $\mu$ M). This could have attributed to the 12 hours' drug incubation with the cells in his study in comparison to only 4 hours in our study. Besides, Kim et al. performed the viability assay using water-soluble tetrazolium salt dye (EZ-Cytox Enhanced cell viability assay kit). This type of assay was claimed to be more sensitive and precise than MTT-based assay since the step of MTT reagent removal prior to addition of DMSO is omitted therefore avoids the risk of accidentally removing the formazan-contained cells from the wells.

## **4.5 DS-GCP20Q11-E nanoemulsion-compatible vehicle for MTT assay**

The DS-GCP20Q11-E nanoemulsion was considered stable when there was no phase separation or aggregation seen upon addition into the medium. The formulation stability in various mediums was found different. Formulations in complete DMEM growth medium at 1:9 v/v ratio were stable up to 4 hours after which time creaming layer was observed on the surface, whereas in PBS 1X, Hanks' Balanced Salt Solution (HBBS) 1X, and 5% glucose (dextrose), the nanoemulsions were stable for more than 4 hours when added into the medium at the same 1:9 ratios.

At this point, it appeared the best vehicle to use was either the PBS, HBBS 1X and 5% glucose since the formulations were stable in those media for longer time than in DMEM. Therefore, prior to the MTT assay for determination of cell cytotoxicity of the drug treatments against the MIAPaCa-2 cell lines, effects of the various medium on its own on the cells viability was determined from the MTT assay using the method described in the previous sections. This was done to select the most suitable medium or vehicle which was not compromising the viability of the cells on its own and compatible with the drug formulation for the treatment. The cells grown in 96-well, flat bottom plates were incubated with either DMEM (control), HBBS 1X, HBBS 0.1X, HBBS 0.01X, PBS 1X, PBS 0.1X, PBS 0.01X, or 5% glucose for 4 hours. The procedure of adding MTT reagent into the plate up until measuring the absorbance and determination of the cell viability were done as described previously (Section 4.3.3 and 4.3.4).

## 4.5.1 Results and discussion

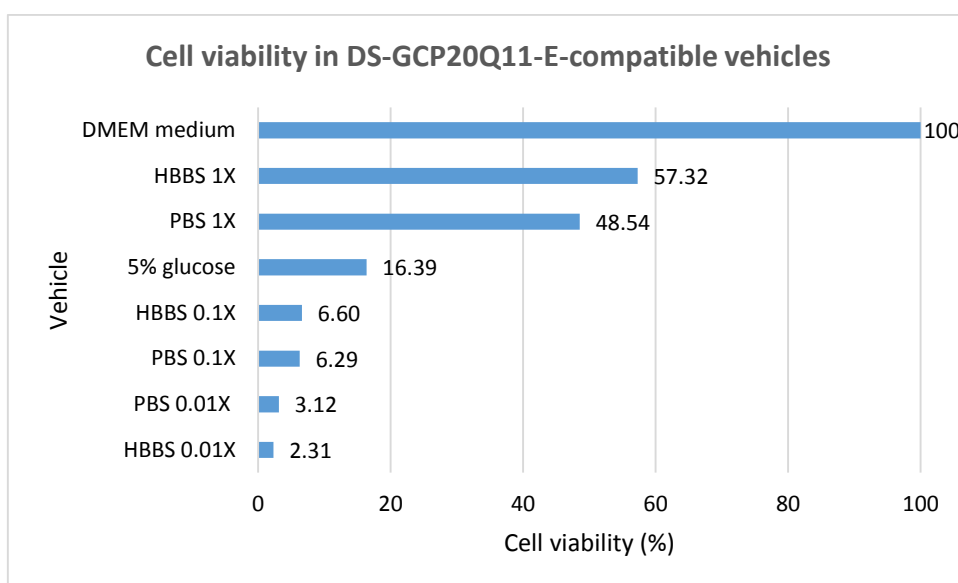


Figure 43: Cell viability (%) upon exposure to different DS-GCP20Q11-E-compatible vehicles for 4 hours.

Cell viability in DMEM growth medium was made as reference in which all cells would survive throughout the incubation period (100% cell viability). The results (Figure 43) showed only half of cell population survived in the HBBS 1X (57.3%) and PBS 1X (48.54%) after incubation for 4 hours. The viability was even lower in 5% glucose (16.4%). Lower concentrations of HBBS and PBS were also tested in order to see if their cell viability would be the same as 1X concentration cell viability. It was found that the viability was however further decreased with incubation in lower concentration buffers. This might be due to the higher amount of Milli-Q water content used in more diluted buffers which increases the osmolarity difference between the cells and the vehicle, leading to more cell burst caused by osmosis. These results had led to the use of DMEM medium as the vehicle for all treatments used in the MTT cell cytotoxicity assay as it had no effect on the cell viability on its own. The incubation period of the cells with the treatments

could only be done for 4 hours as the nanoemulsion was only stable up until such period before phase separation occur in the DMEM medium.

The instability of the formulation in DMEM after 4 hours might due to the activity of proteins in the cell culture medium against the nanoparticle physicochemistry. Nanoparticles tend to be covered with protein corona upon contact with biological medium. In blood, different biological molecules compete to adsorb on the surface of nanoparticles with majority of them are the proteins and small portions of lipids. Over time, the corona will be replaced by the higher affinity proteins (Vroman et al., 1980). This activity is driven by protein-nanoparticle binding affinities and protein-protein interactions. The protein corona alters size and surface composition of the nanoparticles, giving a new biological identity that could trigger physiological response such as agglomeration, transport, circulation lifetime and toxicity thus affecting the particle stability. Structure and composition of corona depends on physicochemical property of nanomaterials (e.g. size, shape, surface charge and duration of exposure) (Rahman et al., 2013).

Drop in surface charge and increase in hydrodynamic size has been reported in nanoparticles exposed to cell culture media containing 10% FBS (Casals et al., 2010). In a nano-biointeraction study of gold nanoparticles with commonly used cell culture media DMEM and Roswell Park Memorial Institute medium (RPMI) supplemented with FBS, it was found that DMEM caused formation of time-dependent larger, more abundant and stable protein corona compared to RPMI medium (Casals et al., 2010). This shows that protein-nanoparticle interaction also depends on the different cellular media components.

## 4.6 Conclusions

Presence of copper in the treatment of DS whether with or without encapsulation with GCPQ had a significant effect on reducing the cell viability of the human pancreatic cancer MIAPaCa-2 cell lines after only 4 hours' incubation period with the treatment. However, in comparison to the non-encapsulated DS, the encapsulation of DS with GCPQ with the presence of copper ions produced more significant cytotoxicity effect against the cancer cells. This gave an insight and better understanding of the possible effect that could be observed if the DS-GCP20Q11-E nanoemulsions reach the cancerous target site in the *in vivo* model.

## **Chapter 5**

# **Pharmacokinetics of disulfiram nanoemulsion**

### **5.1 Pharmacokinetics in nanomedicine development**

By definition, the pharmacokinetics of a drug is the study of the drug's absorption, distribution, metabolism and elimination in human, as well as in animals over a period of time (Benet and Zia-Amirhosseini, 1995). Absorption and distribution involves the process of the drug molecules entering the blood stream from the administration site and when the drug molecules are disseminated throughout the fluid and tissues in the body, respectively. Metabolism is when the drug is transformed into parent-derived metabolites, whereas elimination is the process of drug excretion from the body (Yáñez et al., 2011).

Determination of pharmacokinetic profile is a crucial part in understanding the fate of a newly developed or modified drug formulation. This will determine if the new formulation is either the same efficacy, improved, or downgraded in comparison to the original formulation. Apart from that, pharmacokinetics is also important (1) to support the preclinical toxicology in animals as the drug level in plasma or tissues are usually more reliable and predictive to extrapolate the toxicity data in human; (2) for correct use

of the drug formulations in therapy by knowing the best route of administration and dose regimen to exert the maximum effect from the drug (Urso et al., 2002).

Assessment of bioavailability by measuring the amounts or concentrations of the drug in blood, tissues, urine or other fluids at different times after the administration gives information on the release of drug in the physiological fluid, its permeability and possible pre-systemic metabolism (Aulton and Taylor, 2013). This is possible by constructing the concentration-time profile of the drug. After single dose of the drug is administered orally or parenterally, serial blood samples are withdrawn at specific time points and plasma samples are assayed for construction of the plasma concentration-time curve.

The most important part of a pharmacokinetic study is to be able to use a proper technique for selective and efficient detection of the drug and its associated metabolites in biological samples. The bioanalytical methods must be fully validated, standardized and characterized to yield reliable results. The application of mass spectrometry alongside with liquid chromatography is common in pharmacokinetic analysis because of the complex nature of the sample matrix and the need for high sensitivity to be able to detect low concentration of analyte.

The hypothesis was that the DS-GCP20Q11-E nanoemulsions would increase the bioavailability of DS in the blood circulation by improving the drug absorption in the gut whilst protecting the drug against degradation. This study was hence conducted to compare the plasma drug level in mice administered with either free DS or the DS-GCP20Q11-E nanoemulsions by application of the sensitive and robust liquid chromatography with tandem mass spectrometry (LC-MS/MS) technique for detection of the analytes.

## 5.2 Principal of LC-MS/MS analysis

LC-MS/MS has been used widely for quantification of small molecule drugs in biological samples. The coupling of LC unit with mass spectrometry (MS) improves the sensitivity, specificity and accuracy of compound detection in samples with many interferences such as blood and plasma. The advantages of using MS as the detector compared to other LC detectors such as ultraviolet-visible (UV-Vis), fluorescence or refractive index detectors is that the MS capable of not only giving signal strength data but also spectral data as a function of time. The ability of the method to precisely isolate and distinguish the analyte spectra of choice from the background components improves the specificity of the analysis and increases the sensitivity of the analyte detection.

In general, the principles of MS involve molecule ionizations at the ion source chambers, followed by sorting and identifying the generated ions according to the mass-to-charge ( $m/z$ ) ratios. The analyte molecules are usually ionized by a technique called atmospheric pressure ionization (API) where analytes are ionized at atmospheric pressure before analyte ions are mechanically and electrostatically separated from neutral molecules. The most commonly used API is the electrospray ionization (ESI) where analytes in solution are sprayed (nebulized) into a chamber at atmospheric pressure in presence of heated drying nitrogen gas and strong electrostatic field (Figure 44). The heated drying gas evaporates the solvent in the droplets causing an increase in the charge concentration in the droplets, whereas the electrostatic field causes dissociation of analyte molecules as the repulsive force between same charge ions increases thus ejecting (desorbed) the ions into gas phase (Kang, 2012). The 'soft' ionization by API mainly creates molecular ions ( $M^+$  or  $M^-$ ), protonated molecules  $[M + H]^+$  and simple adduct ions such as  $[M + Na]^+$ . The ions then pass through capillary into the mass analyser.

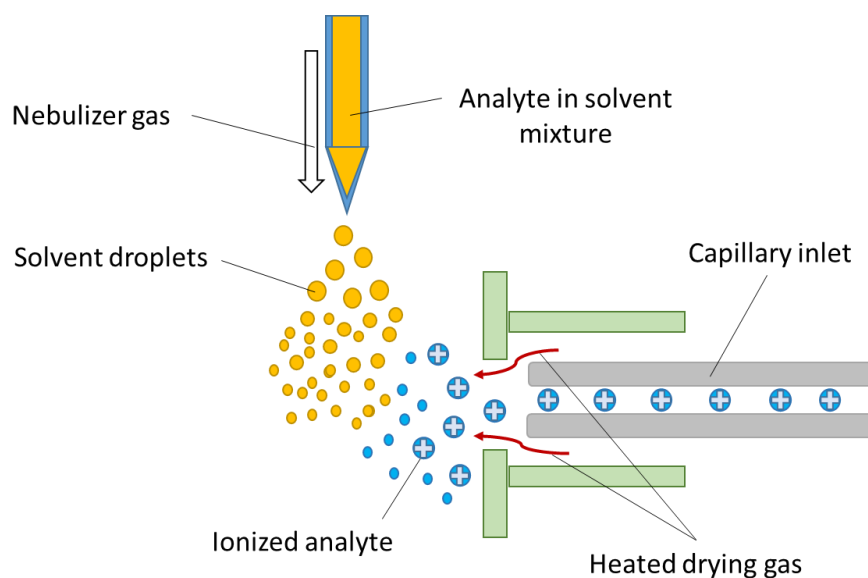


Figure 44: Schematic diagram of electrospray ionization (ESI)

The use of quadrupole type of mass analyser allows scanning of  $m/z$  values across a range of mass spectrum. A quadrupole consists of a set of four parallel metal rods arranged in a square. Voltages are applied to the rods in varying frequencies to allow generation of electromagnetic fields which later on determines  $m/z$  ratios of ions that can pass through the filter. One example of widely used tandem mass spectrometry is the triple quadrupole mass spectrometer which allows monitoring of specific  $m/z$  values only rather than scanning the whole ions that are unrelated to the analysis.

In triple quadrupole (also known as quadrupole/quadrupole/time-of-flight) (Figure 45), the first quadrupole (Q1) selects the precursor ion, followed by the second quadrupole (Q2) where collision-induced dissociation (CID) of the precursor ion occurs in the collision cell. This to allow the fragmentation of the analyte ions by collision with inert gas such as nitrogen. The dissociated and fragmented ions are then transmitted to the third quadrupole (Q3) to generate spectrum of resulting product ions with respect to the precursor ions (Madeira and Florêncio, 2012).

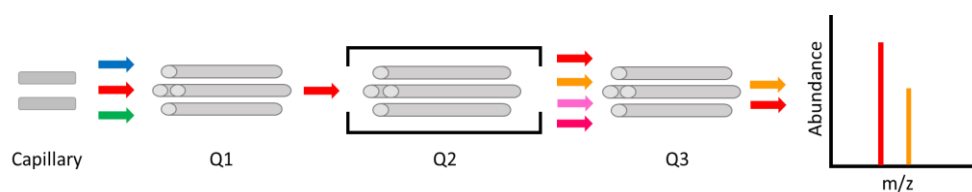


Figure 45: MS/MS in a triple quadrupole mass spectrometer

When the first and third quadrupoles are set to monitor specific  $m/z$  values simultaneously in which panels of precursor/product ion pairs are set, the process is called selected reaction monitoring (SRM). Multiple reaction monitoring (MRM) happens when the triple quadrupole MS instrument running multiple SRMs for the same precursor ions. Several advantages of multiple-stage MS are 1) specificity of the analysis is greatly enhanced as the first stage of MS (first quadrupole) discards nonanalyte ions, 2) chemical background is mostly removed at the second stage MS (third quadrupole) hence avoiding the isobaric interference of the same exact mass as the fragmented ions of the analytes (Watson and Sparkman, 2008).

### 5.3 LC-MS/MS for DS and MeDDC analysis

Determination of DS bioavailability upon administration of the nanoemulsions to the animal subjects was done by the application LC-MS/MS analysis. Optimization of the analysis method from mouse plasma samples was carried out for detection of two main analytes; the parent drug disulfiram and its major metabolite, S-methyl-N,N-diethyldithiocarbamate (MeDDC), along with the internal standard, diphenhydramine (DPH).

#### 5.3.1 Materials

Item	Supplier / Manufacturer
Sodium chloride	Sigma-Aldrich Company Limited, Dorset, UK
Sodium acetate	
Diethylene triamine	
pentaacetic acid	
Methanol	
Absolute ethanol	
Diphenhydramine hydrochloride	
Acetonitrile (LCMS grade)	
Water (LCMS grade)	
Methyl diethyldithiocarbamate	
Formic acid	Fisher Scientific Limited, Leicestershire, UK

## 5.3.2 Methodology

### 5.3.2.1 Instrumentation and analytical conditions

The LC-MS/MS experiments were conducted using Agilent 1260 Infinity LC (Agilent Technologies, California, USA) connected to Agilent 6460 Triple Quadrupole LC/MS system with ESI source equipped with Agilent Jet Stream technology. The data acquisition, quantitative and qualitative analysis for both liquid chromatography (LC) and mass spectrometry units were performed using Agilent MassHunter Workstation software.

The chromatographic separations were performed using Phenomenex Onyx™ Monolithic C18 analytical column (50 x 2 mm, 130Å) connected to Phenomenex Onyx™ Monolithic C18 guard column (5 x 2 mm, 130Å) (Phenomenex, Torrance, California, USA). The column temperature was maintained at 30°C. The LC run was carried out by injecting 5 µl of sample into the mobile phase of water added with 0.1% formic acid (A) and acetonitrile (B) under gradient elution of 5 minutes' runtime. The gradient conditions were as follows: B was increased from 5 to 95% at 1 minute and stayed at the same value for 1.5 minutes. At 2.5 minutes, B was decreased back to 5% to be at the original ratio for re-equilibration of the column until stop time at 5 minutes. The flow was kept constant at 0.4 ml/min.

The tandem mass spectrometry was done under positive ion mode (positive ESI). The source parameters used were as follows: nitrogen as collision gas, gas temperature at 300°C, gas flow at 5 l/min, nebulizer at 45 psi, sheath gas heater and gas flow at 250°C and 11 l/min, respectively and capillary voltage at 3.5 kV. Detection of the analytes was done using MRM scan type to monitor transitions of precursor-product ion of DS at  $m/z$  297.1>116.1, MeDDC at  $m/z$  164.06>116, and DPH as the internal standard (IS) at  $m/z$

256>167 with fragmentor voltage at 73 V for both DS and DPH and 45 V for MeDDC, collision energy 9 V for all analytes.

### **5.3.2.2 Preparation of cold stabilizing agent**

For 10 ml of stabilizing agent, 90 mg of sodium chloride, 64 mg of sodium acetate, and 80 mg of diethylene triamine pentaacetic acid (DTPA) were mix altogether in 10 ml of Milli-Q water and stirred until all substances were dissolved. The pH was measured to ensure it was at pH 4.5. The solution was kept at 4<sup>0</sup>C until use.

### **5.3.2.3 Preparation of drug stock solution**

DS and MeDDC stock solutions were prepared in absolute ethanol at 100 µg/ml. The stocks were then diluted further for preparation of calibration curve to have final concentrations of 10, 20, 40, 60, 80, 100, 200, 400, 600, 800 ng/ml upon addition into mouse plasma. DPH was added into methanol (extraction solvent) to have final concentration of 1.0 ng/ml in the plasma samples.

### **5.3.2.4 Preparation of calibration standards and quality control (QC)**

Blood from animal subjects was collected in K<sub>2</sub>EDTA blood tubes. The blood was then transferred into 1.5 ml microcentrifuge tube, added with equal volume of cold stabilizing agent and centrifuged for 5 minutes at 10,000 g to obtain the stabilized plasma which was later kept at -80<sup>0</sup>C until use.

An amount of 50 µl stabilized plasma was put into 1.5 ml microcentrifuge tubes and kept on ice at all times. Drug stock solutions (5 µl) containing different concentrations of both DS and MeDDC was added into the plasma samples to have final

concentration of 10, 20, 40, 60, 80, 100, 200, 400, 600, 800 ng/ml for the calibration standards and 15, 75 and 750 ng/ml for the QC samples. The samples were vortexed for 10 seconds. The samples were then added with 150  $\mu$ l of methanol (3x the volume of plasma) containing the IS and vortexed vigorously for 10 minutes for drug extraction, followed by centrifugation at 10,000 g for 5 minutes to precipitate the protein. The methanol supernatant (100  $\mu$ l) was collected carefully without disturbing the pellet and placed into a new tube. Tubes were then immediately placed on dry ice to avoid unnecessary drug degradation. The samples were analysed with LC-MS/MS as soon as possible. The samples were brought to room temperature 5 minutes before sampling.

#### **5.3.2.5 Preparation of experimental samples for analysis**

For experimental samples, fresh blood samples from animals were immediately processed for drug extraction upon collection. The drug extraction process involved was the same as described before (Section 5.3.2.4) except for the addition of drug stock solutions which was omitted in this procedure.

#### **5.3.3 Statistical analysis**

All statistical analyses in this chapter were performed using IBM SPSS Statistics for Windows, Version 22.0 (IBM Corp, Armonk, New York, USA). Comparison of more than two groups was done using One-way ANOVA with Tukey's multiple comparison test for the post-hoc analysis, whereas comparison between two groups was done using Independent-samples t-test (Student's t-test). Data was presented as mean  $\pm$  standard deviation with significance value of  $p < 0.05$ .

### 5.3.4 LC-MS/MS method validation

#### 5.3.4.1 Validation procedures

The LC-MS/MS method was validated based on selectivity, linearity, accuracy, precision, recovery, and stability (Tiwari and Tiwari, 2010).

Selectivity analysis was done to ensure no interference to the analyte peak from other components in the samples at its retention time which enables differentiation and quantification of the analyte. The selectivity of the method was validated by analysing samples of blank stabilized plasma spiked with either IS (1 ng/ml), DS or MeDDC, where the concentration of DS and MeDDC was at the lower limit of quantification (LLOQ) level.

The samples for calibration standards were prepared in triplicate. The calibration curves ( $y = ax + b$ ) were constructed by plotting peak area ratios of the drug to the IS ( $y$ ) versus the drugs concentration ( $x$ ). The linearity of the plots was assessed in the range of eleven concentrations levels from 5 to 800 ng/ml altogether with blank plasma spiked with only the IS (zero plasma). The percentage of coefficient of variation (CV%) for every drug concentration was calculated for determination of the LLOQ. LLOQ was determined as the lowest concentration of calibration standard at which precision was less than 20% and accuracy within 20% of the added drug concentration.

Precision and accuracy of the method was determined by analysing QC samples at low, medium and high concentrations of the drug (15, 75 and 750 ng/ml of either DS or MeDDC, respectively). The QC samples were prepared in 5 replicates and measured intra-day (within the same day) and inter-day (on different days for three consecutive days). The accuracy was expressed as percentage of relative error (%RE), while precision as percentage of coefficient of variation (%CV). The precision at each concentration should not exceed 15%. Calculations were performed as in the formulas below:

$$\%RE = ([\text{Found drug} - \text{added drug}] / \text{added drug}) \times 100$$

$$\%CV = (\text{Standard deviation} / \text{Mean}) \times 100$$

Recovery of DS and MeDDC from the extraction method was determined by comparing analyte mean peak area of extracted QC samples (pre-extraction spike) to the samples of extracted blank plasma spiked with drugs at the same concentration as the QC samples (post-extraction spike). Matrix effects (%ME) were determined by comparing the mean peak area of post-extraction spike samples to the ones also containing equivalent drug concentrations as the QC but prepared in ethanol (no extraction). %ME less than 100% could represent ionization suppression, whereas %ME at or more than 100% could represent no ionization suppression or ionization enhancement occurred. Samples per concentration were also prepared in 5 replicates (n=5).

Stability of processed samples (post-extraction) in methanol was assessed by measuring DS and MeDDC level 1) before (Day 0) and after storage at -80°C for three days (Day 3) and 2) at room temperature (in the autosampler) and in the dry ice (-79°) for up to two and a half hours prior to the injection into the LC-MS/MS instrument. QC samples at 750 ng/ml were prepared in 5 replicates (n=5).

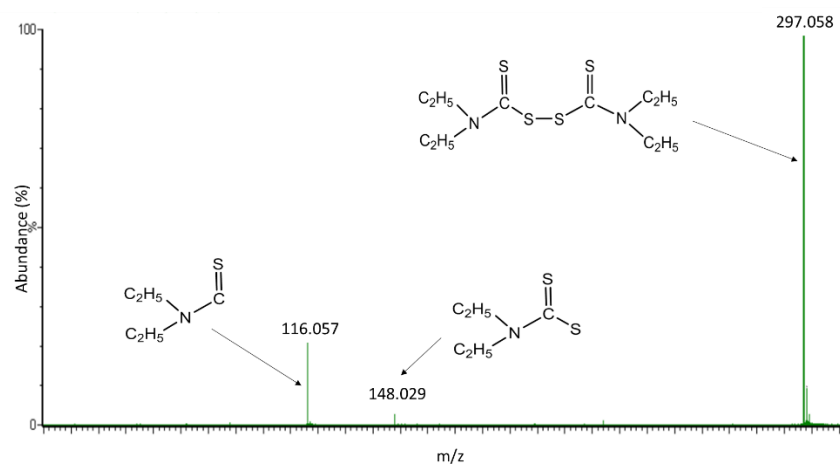
#### **5.3.4.2 Results**

##### ***5.3.4.2.1 Optimization of mass spectrometry and chromatographic conditions***

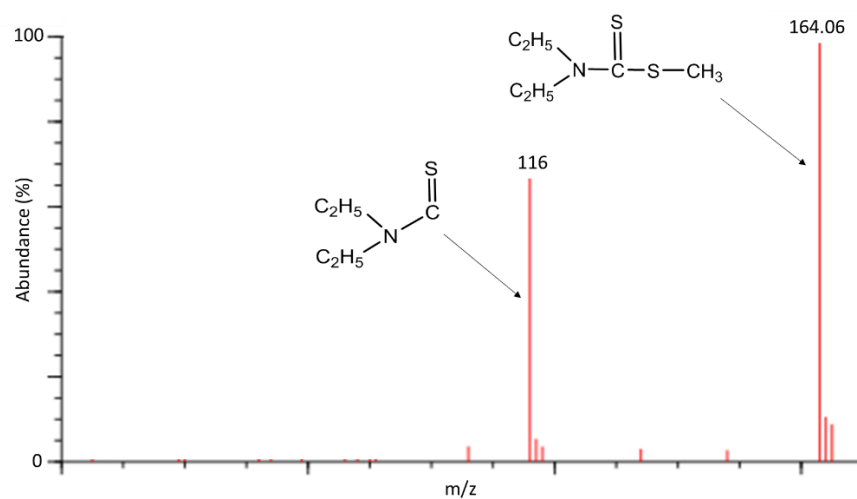
The initial optimization of DS and MeDDC with the MS was to find the optimum precursor and product ion for DS and MeDDC. Standard solution of DS or MeDDC was injected into the MS unit without the LC column and Agilent MassHunter Optimizer software was used to rapidly determine the precursor and product ion (m/z values) with the most abundance at both positive and negative ion mode. Later on, the software

automatically optimized the fragmentor voltage and collision energy for each of the m/z values provided. Here it was found that precursor ion 297.1 and product ion 116.1 was the most abundant for DS (Figure 46A) whereas precursor ion 164.06 and product ion 116 was for the MeDDC (Figure 46B). The rest of the MS parameters including for the source was optimized manually later on to maximize the signal response of the analytes.

The liquid chromatography condition was set to have good separation and distinct peaks of all three DS, MeDDC and IS analytes within reasonable run time per analysis. It was found that acetonitrile was better in providing sharper peaks of the analytes compared to other organic phase such as methanol. Addition of 0.1% formic acid into the water phase enhanced the ionization of the analytes. Gradient elution was also used instead of isocratic for better separation of the hydrophobic analytes from the endogenous substances present in the samples. The selection of diphenhydramine as the internal standard was based on the work done by Zhang et al. (2013) and was chosen for its stability in plasma and peak is detectable within the set run time of 5 minutes with no interference with DS and MeDDC peaks.



(A)

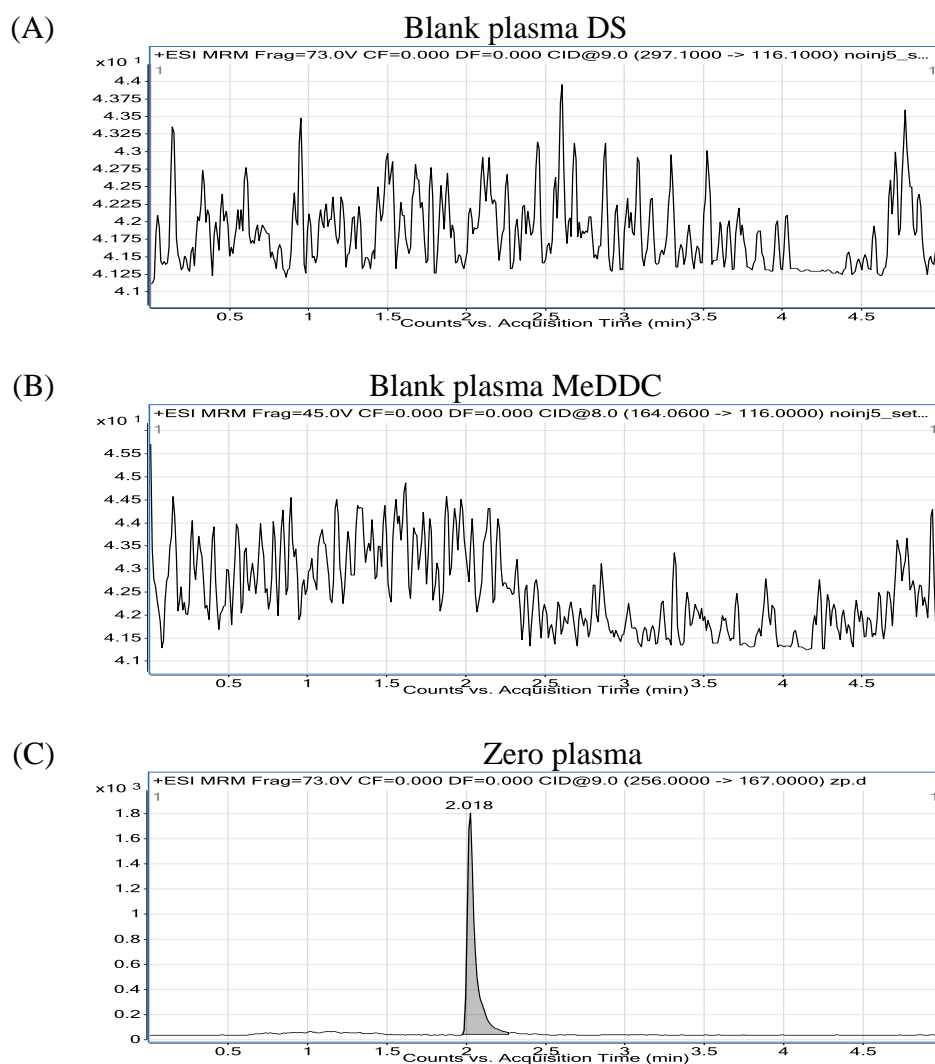


(B)

Figure 46: MS/MS spectrum of disulfiram (A) and MeDDC (B) from the positive mode ESI.

### 5.3.4.2.2 Selectivity

The selectivity (specificity) of the method was proven by the chromatograms showing distinct peaks of DS and MeDDC at retention time 2.6 minutes (Figure 47D) and 2.4 minutes (Figure 47E), respectively. Zero plasma (blank plasma spiked with only IS) showed a peak representing DPH analyte at retention time 2.0 minutes (Figure 47C). Blank plasma samples also showed no prominent peak at the DS and MeDDC retention times (Figure 47A and B, respectively). The results prove that the processing method prevented the interference from possible endogenous components and impurities present in the samples to the analyte peaks.



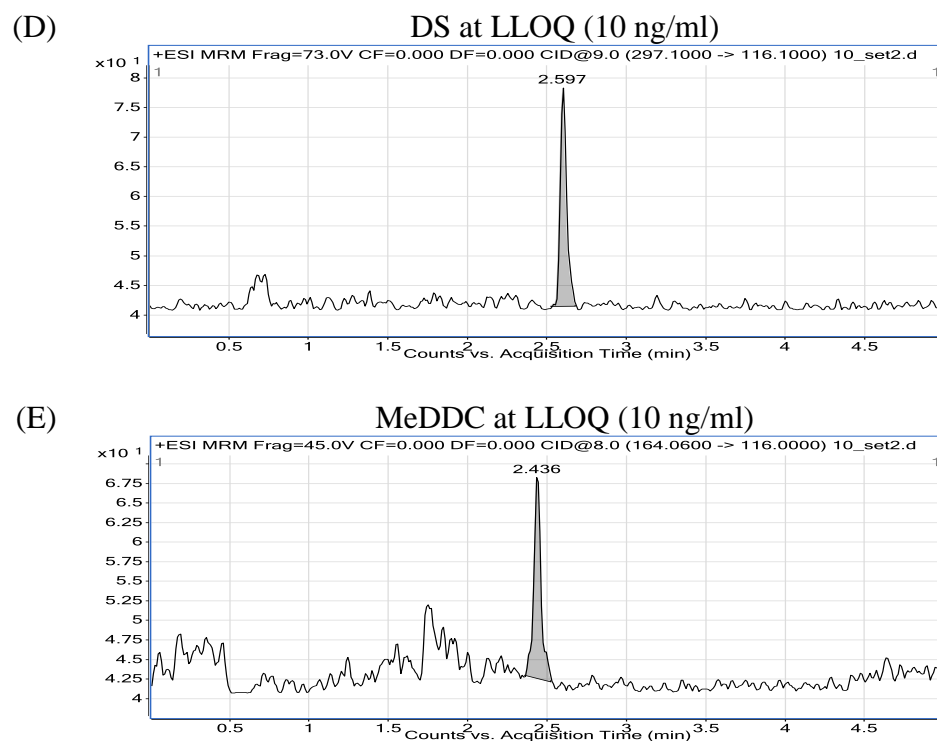


Figure 47: Chromatograms of blank plasma for DS and MeDDC (A and B, respectively), zero plasma (C), and DS and MeDDC at LLOQ level of 10 ng/ml (D and E, respectively).

### 5.3.4.2.3 Linearity

The calibration curve was linear in the range concentration of 5 to 800 ng/ml for both DS and MeDDC with regression equation of  $y = 0.0017x + 0.0221$  and  $y = 0.0009x + 0.0089$ , respectively. The curves also showed good linearity with  $R^2$  values of 0.9887 and 0.9960 for DS and MeDDC, respectively. The lower limit of detection (LLOD) for both drugs was found to be at 5 ng/ml, whereas the LLOQ was determined to be at 10 ng/ml since the %CV at 5 ng/ml for both DS and MeDDC were more than acceptable value of 20% (67% and 56%, respectively) (Table 19).

	Drug concentration (ng/ml)	%CV	
		DS	MeDDC
LLOD	5	67	56
LLOQ	10	10	3

Table 19: LLOD and LLOQ of DS and MeDDC

#### 5.3.4.2.4 Accuracy and precision

The intra-day and inter-day results for determination of accuracy and precision of the method is displayed in Table 20. Both %RE and %CV were not more than 15%, which is the value recommended by the Food and Drug Administration (FDA) (2001) guidance.

Drug	Added drug (ng/ml)	Intra-day			Inter-day		
		Found drug (ng/ml)	%RE	%CV	Found drug (ng/ml)	%RE	%CV
DS	15	15.77 ± 1.26	5.16	7.99	14.31 ± 1.56	-4.60	10.90
	75	73.55 ± 6.61	-1.93	8.98	72.05 ± 4.72	-3.94	6.56
	750	743.76 ± 23.41	-0.83	3.15	732.87 ± 17.89	-2.28	2.44
MeDDC	15	14.69 ± 1.39	-2.06	9.44	15.55 ± 0.74	3.66	4.76
	75	743.76 ± 23.41	0.41	3.16	73.50 ± 2.92	-1.99	3.98
	750	756.12 ± 16.32	0.82	2.16	749.31 ± 19.50	-0.09	2.60

Table 20: Intra-day and inter-day analysis of the QC samples for determination of precision and accuracy of the LC-MS/MS assay. Data were presented as mean ± SD (n = 5).

#### 5.3.4.2.5 Recovery and matrix effects

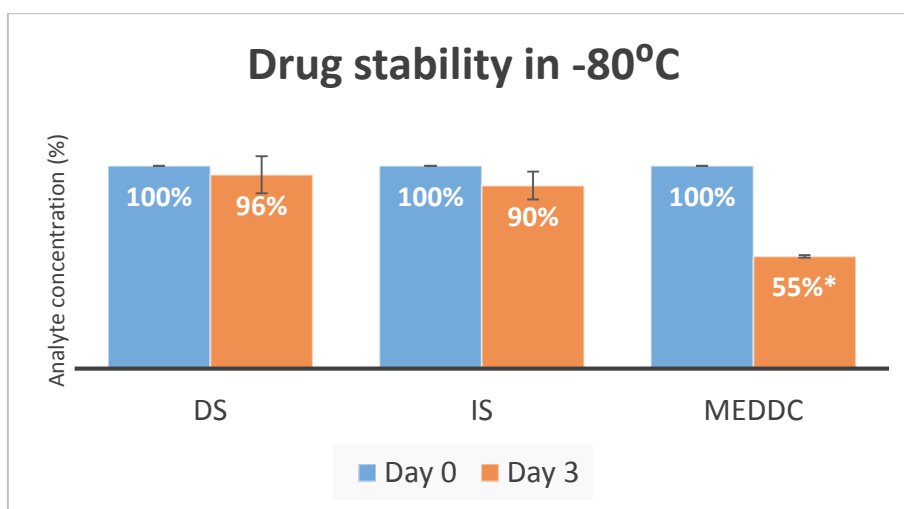
Table 21 summarizes the extraction recovery of DS and MeDDC from plasma samples and the matrix effects on both drugs following the processing method of the samples. The mean recovery of the IS at single concentration (1 ng/ml) was 108%. The recovery results of both drugs suggest the extraction method for DS and MeDDC is acceptable to be used in preparing plasma samples for analysis. The high recovery values for MeDDC (> 100%) at all concentrations might be attributed to the pipetting error during preparation of post-extraction spike samples. The high %ME values at 15 ng/ml DS and MeDDC (123% and 118%, respectively) indicates the biological matrix causes no ion suppression at such concentration. The effect was however increased at higher concentration of drugs.

Drug concentration (ng/ml)	Recovery (%)		%ME	
	DS	MeDDC	DS	MeDDC
15	70	147	123	118
75	65	139	42	89
750	75	154	12	49

Table 21: Extraction recovery and matrix effects (ME%) of DS and MeDDC from plasma.

#### 5.3.4.2.6 Post-extraction stability

Storage of processed samples at  $-80^{\circ}\text{C}$  for 3 days caused reduction of all DS, IS (DPH) and MeDDC concentrations (Figure 48). However, only MeDDC level was significantly reduced to nearly half of the Day 0 concentration.



\* Significant compared to MeDDC on Day 0.

Figure 48: DS, IS and MeDDC stability in reconstitution solvent methanol on Day 0 and Day 3. Data were presented as mean  $\pm$  SD (n = 3).

Post-extraction samples kept at room temperature were found to be unstable as both DS and MeDDC showed gradual decrease in drug concentration over time. The labile DS showed sharper drop in drug level than MeDDC (Figure 49B) with more than half the original drug content lost within an hour (Figure 49A). The IS concentration also dropped to 84% over duration of 2.5 hours at RT (Figure 49C). Meanwhile, at freezing temperature of  $-79^{\circ}\text{C}$  on dry ice, drug level of DS, MeDCC and IS was found consistent throughout the experiment period. This indicates the activity of the endogenous substance in the samples that causes the drug instability can be blocked in the subfreezing condition. The results also proved the integrity of DPH as IS since it was very stable with no sudden

drug degradation at different temperatures and also not affected by the presence of biological matrices.

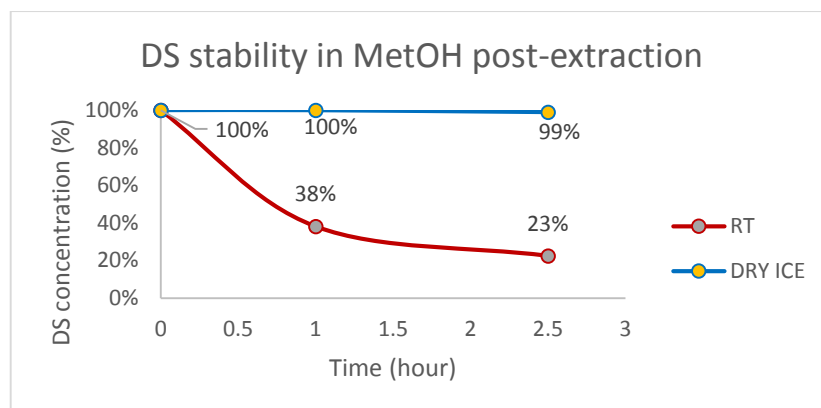


Figure 49A

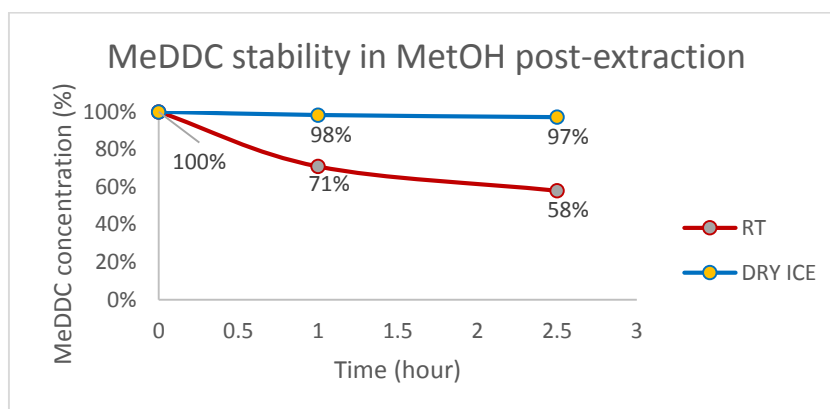


Figure 49B

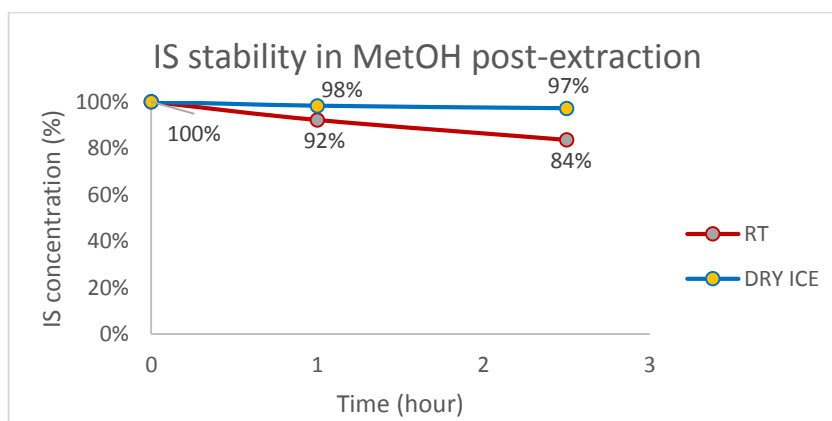


Figure 49C

Figure 49: DS, MeDDC and IS stability in post-extraction methanol (Figure 49A, B and C, respectively) at room temperature (RT) and  $-79^{\circ}\text{C}$ .

### 5.3.4.3 Discussion and conclusion

Zhang et al. (2013) were the first and the only one to publish detail LC-MS/MS methodology for the detection of DS in the plasma. The methodology uses the tedious, slower and high in cost solid phase extraction (SPE) method for the extraction of the drug, rather than the simpler and effective protein precipitation (PP) technique used in the present study. The LLOQ for DS in Zhang's method was however reported lower (0.6 ng/ml) than the LLOQ found in the present study (10 ng/ml). This perhaps due to the more efficient SPE method in extracting the drug as other DS LLOQ value from PP technique applied in the extraction method was also higher (15 ng/ml) (Spivak et al., 2014). It is therefore down to the preference of the analyst on whether to have a robust and simple technique of sample preparation but modest limit detection of the drug, or costlier and laborious preparation for more sensitive detection of the lower drug amount.

DS is known as a very labile drug and prone to degradation in the smallest amount of protein present in the samples (Cobby et al., 1977, Agarwal et al., 1986). The use of stabilized plasma to minimize the rapid degradation of DS in plasma samples for analytical measurement was first attempted by Johansson (1988) and later on by Zhang et al. (2013) with modifications to the former method stabilizing agents for more practical approach of the sample preparation. The stabilizing agent was composed of DTPA as chelating agent (chelates plasma protein bound cupric ion) and prepared in acidic condition to acidify the plasma in order to stop the interference of various thiols in the blood.

Despite the addition of stabilizing agent to reduce DS degradation rate by the activity of the proteins and protein removal during the PP technique, drug degradation was still observed in the processed samples with marked activity seen at room temperature. The drug degradation process however was found halted when the processed samples stored at sub-zero temperature. This drug degradative prevention step was

therefore applied in the present study by keeping the processed samples on dry ice the whole time prior to the LCMS analysis apart from the immediate blood sample processing upon collection from the animals.

MeDDC is one of the major metabolites produced from the metabolism of DS. Unlike the polar DDC, MeDDC is highly hydrophobic (Faiman et al., 1983) and therefore easier to be measured simultaneously alongside with DS using the hydrophobic-based C<sub>18</sub> column during the liquid chromatography run. MeDDC is also rapidly metabolized from DDC (Faiman et al., 1980, Faiman et al., 1978) thus making it a suitable choice of DS metabolite to be measured.

In conclusion, a validated LC-MS/MS method was successfully developed and optimized for simultaneous detection of DS and MeDDC analytes in mouse plasma samples. This method was later on used in the analysis for determination of pharmacokinetic profile of the DS-GCP20Q11-E nanoemulsion in animal model.

## **5.4 Oral pharmacokinetic profile of DS-GCP20Q11-E**

The objective of the study was to determine the pharmacokinetic profile of DS and MeDDC following oral administration of either DS-GCP20Q11-E nanoemulsions (encapsulated DS) or DS in soybean oil (free DS) in the mouse model.

### **5.4.1 Methodology**

#### **5.4.1.1 Animals**

The animal experiments were carried out under license from the Home Office and by the policies and regulations stated in Animals and Scientific Acts 1986 UK. All animals were housed at UCL School of Pharmacy Biological Service Unit (BSU) and the animal handling and care for scientific research was implemented as recommended by the BSU guidelines.

Female CD-1 mouse (Charles River, Kent, UK), 17-21 g were maintained in controlled room conditions with ambient temperature at 22-25°C, relative humidity at 55-60% and 12-hour light and dark cycles. Food and water were given *ad libitum* to the animals. All animals were acclimatized for a week prior to the start of experiments.

#### **5.4.1.2 Experimental procedure**

Animals were randomly divided into two groups of 28 based on the type of treatment given: 1) DS-GCP20Q11-E with 40% oil content, 2) DS in soybean oil (20 mg/ml). The single oral administration of the treatment was given at a dosage of 70 mg/kg using oral gavage needle. Animals were then euthanized at 7 different time points (n = 4 per time point) of 15 minutes, 30 minutes, 60 minutes, 90 minutes, 2 hours, 4 hours and 8 hours by CO<sub>2</sub> asphyxiation. The blood was then immediately taken by cardiac puncture

and collected into K<sub>2</sub>EDTA blood tubes. The blood samples were processed immediately upon collection as described previously in Section 5.3.2.5 for LC-MS/MS analysis.

#### 5.4.1.3 Pharmacokinetic analysis

Pharmacokinetic parameters were determined using PK solver software (Zhang et al., 2010) with implementation of noncompartmental analysis. The following parameters were used to evaluate the treatments: (1) elimination half-life ( $t_{1/2}$ ) is the time for the concentration of the drug to reach half of its initial amount; (2)  $T_{max}$  is the time at which the maximum drug concentration in the plasma is reached; (3)  $C_{max}$  is the maximum drug concentration in the plasma; (4) Area under curve (AUC) is the total area under the plasma drug concentration–time curve and  $AUC_{0-t}$  is the AUC from zero (0) hour to time of last quantifiable concentration (t).

### 5.4.2 Results and discussion

The developed and validated LC-MS/MS method was applied to analyse the pharmacokinetic profile of both treatments in mouse plasma. The graph of plasma concentration-time profile for oral administration of DS in SB oil and DS-GCP20Q11-E are displayed in Figure 50a and Figure 50b respectively.

Based on the qualitative visual examination of the data, there was presence of double peaks in the plasma concentration-time profile for DS analyte in both DS in SB oil and DS-GCP20Q11-E treatments, whereas for MeDDC metabolite, it only occurred in the DS-GCP20Q11-E treatment. The quantitative analysis of DS and MeDDC plasma concentration data (Table 22) was conducted to determine the location ( $T1_{max}$  and  $T2_{max}$ ) and magnitude ( $C1_{max}$  and  $C2_{max}$ ) of the two peaks (Table 22). The  $T1_{max}$  for DS and

MeDDC appeared to happen earlier (15 minutes) in group treated with free DS (DS in SB oil) compared to the encapsulated DS (DS-GCP20Q11-E) group (30 minutes). The situation was also the same for the  $T_{2_{max}}$  of DS with 90 minutes for the free DS compared 120 minutes for the encapsulated DS group. The delayed  $T_{max}$  in encapsulated DS group could be related to the fact that DS in the formulation is encapsulated and it takes time to be released into the blood. The two peaks phenomenon of MeDDC was however seen only with the DS-GCP20Q11-E treatment, with  $C1_{max}$  was found significantly higher than  $C2_{max}$ , whereas for the DS in SB oil treatment, only one peak was seen of which gradually decline over time.

Nevertheless, the AUC value measured from  $t = 0$  hour to  $t = 8$  hours ( $AUC_{0-8hr}$ ) which represents an index of overall drug exposure in the blood circulation were found significantly higher in free DS group for both analytes (almost 60 times higher for DS level) compared to the encapsulated DS group. The very low DS detection level throughout the study could have contributed to the inability to calculate the  $t_{1/2}$  for DS in the DS-GCP20Q11-E group.

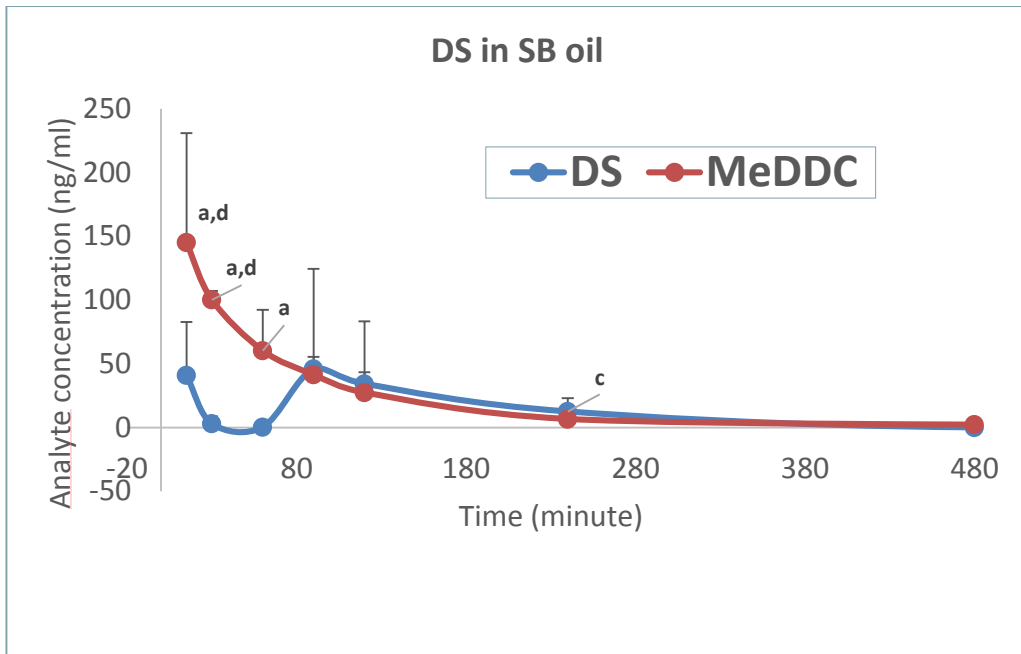


Figure 50a

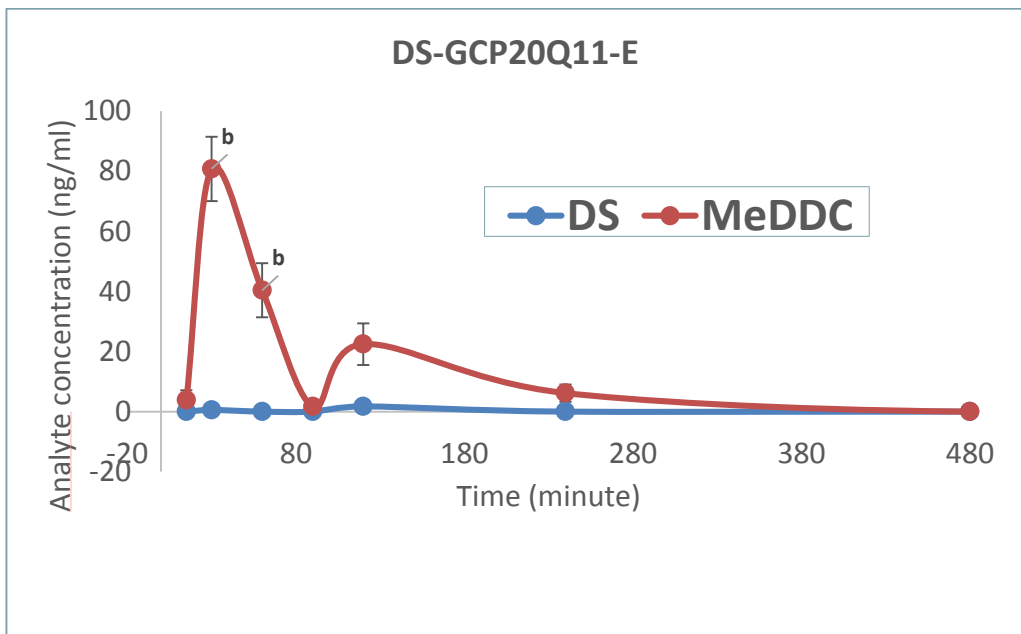


Figure 50b

- <sup>a</sup> MeDDC was significantly higher compared to DS level in DS in SB oil group
- <sup>b</sup> MeDDC was significantly higher compared to DS level in DS-GCP20Q11-E group
- <sup>c</sup> DS was significantly higher compared to DS level in DS-GCP20Q11-E group
- <sup>d</sup> MeDDC was significantly higher compared to MeDDC level in DS-GCP20Q11-E group

Figure 50: Plasma concentration–time profile for DS in SB oil and DS-GCP20Q11-E oral treatment (a and b, respectively). Data were presented as mean  $\pm$  SD (n = 4).

Parameter	Unit	DS-GCP20Q11-E		DS in SB oil	
		DS	MeDDC	DS	MeDDC
$t_{1/2}$	min	N/A	72	44	83
$T1_{max}$	min	30	30	15	15
$C1_{max}$	ng/ml	0.538	80.772	40.937	144.993
$T2_{max}$	min	120	120	90	N/A
$C2_{max}$	ng/ml	1.694	22.481	45.908	N/A
$AUC_{0-8hr}$	ng/ml.min	104.428	5193.796	6909.827	11000.036

Table 22: Pharmacokinetic parameters for single oral administration of DS-GCP20Q11-E and DS in SB oil. N/A = not available.

The multi-peaks phenomenon in plasma concentration-time profile of drugs following oral administration has been reported previously for several types of oral drug that shares no common structure similarities such as alprazolam, cimetidine and talinolol (Wang et al., 1999, Oberle and Amidon, 1987, Weitschies et al., 2005). Some common factors speculated for this occurrence are: 1) variability in gastric emptying and intestinal flow rates (Oberle and Amidon, 1987); 2) enterohepatic recycling (Roberts et al., 2002); and 3) presence of absorption sites along the gastrointestinal tract (Gramatte et al., 1994).

The first DS peak in the free DS treatment profile could be caused by the rapid absorption of the drug due to its high hydrophobicity along the gastrointestinal tract especially in the stomach where tissue absorption of the drug is the highest within 30 minutes post-administration (Faiman et al., 1980). Faiman and colleagues (1980) also reported the plasma  $T_{max}$  for both DS and MeDDC was 5 hours following oral 7 mg/kg DS administration to the rats, which was later than the  $T1_{max}$  found in the present study. Perhaps the use of oil as the DS solvent promoted the earlier rapid DS absorption into the blood circulation. The oral PK study of DS in the human male volunteers following 500 mg DS dosage reported a plasma  $T_{max}$  at 5 hours for DS and 8 hours for MeDDC (Jensen

and Faiman, 1980). The following absorption in the intestinal tract could have caused the second peak. Despite the two distinct phases of DS absorption, the MeDDC level was seen highest only at the first peak which later on steadily decreased due to being metabolized into other forms of metabolite (e.g. MeDTC) or due to elimination.

The occurrence of two peaks for DS analyte in DS-GCP20Q11-E group can be rendered negligible as the values were lower than the LLOQ. This low DS level detection in the plasma could be attributed to the fast absorption of the formulation in the gastrointestinal wall, even faster than the rate of absorption when the drug is in SB oil free form due to the highly positive charge of GCPQ encapsulating the drug (Ensign et al., 2012), causing faster transportation of the nanoemulsion to the liver. This could explain the high  $C_{1_{max}}$  value of MeDDC first peak with the formulation treatment as it was highly formed from the parent drug during the time course of the first peak. The conversion of DDC metabolite into MeDDC is rapid in the liver and kidney. The two peaks scenario of DDC pharmacokinetic profile following oral administration has been reported previously (Faiman et al., 1984). Enterohepatic recycling was believed to play a role based on the evidence of subsequent hydrolysis of DDC-glucuronide found in the gastrointestinal tract that led to the second peak formation.

The bigger values of MeDDC found in the plasma compared to DS is likely due to MeDDC considerably more stable than DS (Scappaticci et al., 1990). MeDDC does not go through covalent disulphide interchange like DS does to inhibit ALDH activity (Kitson, 1976). DS was also found able to stop the activity of microsomal esterases enzyme (Zemaitis and Greene, 1976) which responsible for metabolising MeDDC into methyl mercaptan and thiocarboxylic acid (Eneanya et al., 1981). This blockage of enzyme by DS could lead to the rise of the MeDDC level in the plasma, represented by the high MeDDC AUC value compared to DS AUC for both treatments.

Lower AUC of DS in animals given with the DS-GCP20Q11-E compared to the DS in SB oil could be caused by the properties of GCPQ. Following oral administration of deuterated GCPQ in mice, the GCPQ was found only localised at the enzyme-rich mucus lining in the gut instead of in the villi of the jejunum (Garrett et al., 2012). This gives an opportunity for the nanoparticles to release the drug at the gut wall and drug being absorbed through the epithelial cells into the villi thus into the blood circulation. In the case of disulfiram, the drug should be absorbed in the gut encapsulated by the GCPQ polymer in the nanoparticle form and not as free drug in order for its protection against blood proteins. If the drug is released from the nanoparticles at the mucus layer, even if the drug is highly penetrating the epithelial wall into the villi, the drug would be degraded as soon as it is in contact with the blood.

In another finding (Serrano et al., 2015) based on a different technique applied that detects individual polymer molecules of GCPQ instead of detecting signals from self-assembled nanoparticle (Garrett et al., 2012), GCPQ nanoparticles were found absorbed via enterocytes into the intestinal villi. The nanoparticles were also found in the liver and lungs. This has also been observed in formulation of GCPQ with peptides (Lalatsa et al., 2012a). If the same situation happens to DS-GCPQ, the low DS detection in the plasma could only happen because of the DS-GCP20Q11-E nanoemulsion was rapidly absorbed by tissue upon reaching the systemic circulation.

Meanwhile, higher DS detection in the plasma when the drug is given in SB oil medium could be related to increased absorption of the highly lipophilic drug-oil combination into the lymphatic system in the gut. Lymphatic circulation is known for transportation of dietary lipids such as triglycerides and many lipophilic substances such as chylomicrons (Dixon, 2010), the lipoprotein that carries dietary lipid before eventually released into the blood circulation at the thoracic duct (Trevaskis et al., 2015). Soybean oil is composed of long-chain triglycerides (Goulet et al., 2010) and various components

of fatty acids such as palmitic acid, oleic acids, linoleic acid and linolenic acid (Baughman and Jamieson, 1922). DS in SB oil could have accessed the lymphatic circulation via association with lipid absorption and lipoprotein assembly pathways across the intestinal enterocytes. Drug administration with long-chain lipids has been reported effective in promoting lymphatic transportation (Caliph et al., 2000). One major advantage of intestinal lymphatic transport is that it circumvents hepatic first-pass metabolism (Trevaskis et al., 2015). This would have substantially improved oral bioavailability of DS as less amount of the drug is metabolized in the liver.

### **5.4.3 Conclusions**

The administration of DS-GCP20Q11-E via oral route was found as not the ideal route of administration in the attempt to elevate DS level in the blood circulation of the animals. It is uncertain whether the cause of the low level of DS in the plasma is due to the lack of absorption in the GIT, degradation upon contact with the GIT fluid and blood components, or the nanoemulsion was rapidly absorbed by the surrounding tissue in the body. Another solution in the attempt to elevate the DS level in plasma is to study the drug bioavailability upon administration of the formulation via the intravenous route.

## 5.5 DS-GCP20Q11-E stability in mouse plasma

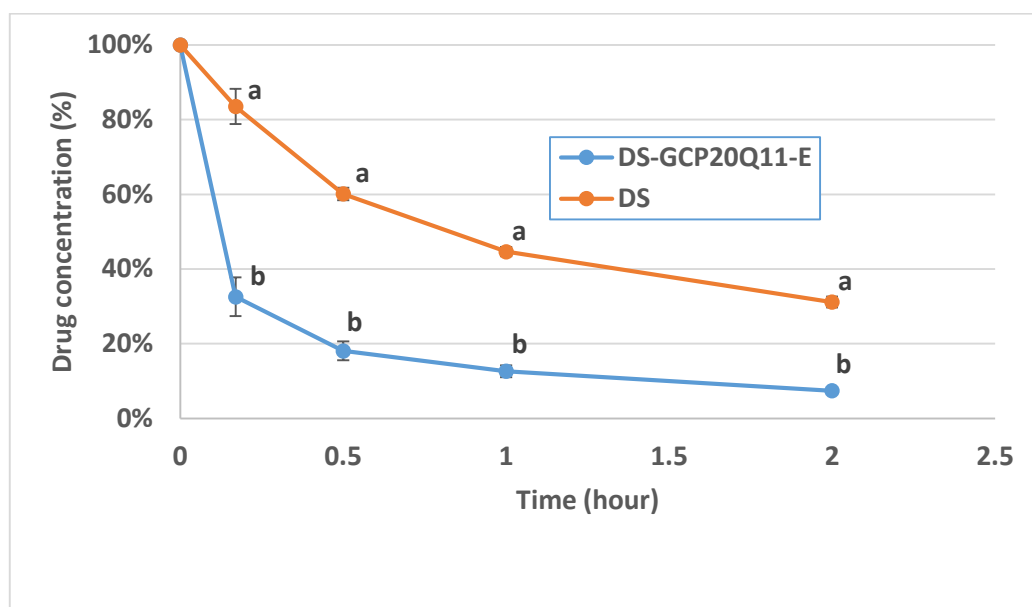
Prior to the intravenous pharmacokinetic study of DS-GCP20Q11-E in animal model, stability of the nanoemulsion formulations in plasma was tested *in vitro* by comparing it to the stability of the non-encapsulated DS in the same environment.

### 5.5.1 Methodology

DS-GCP20Q11-E formulations at 5% oil was used in the experiment, whereas for DS solution (without polymer), it was prepared at 1mg/ml in 0.5% DMSO. Mouse plasma diluted to 50% of initial concentration using 0.9% w/v sodium chloride solution was prepared in bulk (approximately 8 ml) prior to the experiment. An amount of 995  $\mu$ l of the diluted plasma was placed in a 1.5 ml microcentrifuge tube and placed in 37°C water bath for at least 30 minutes. As soon as the temperature of plasma stabilized, 5  $\mu$ l of either DS-GCP20Q11-E 5% oil or 1 mg/ml DS solution in DMSO was added into the plasma. Samples were prepared in triplicate for each treatment. Plasma samples added with the test substances were placed in the temperature-controlled water bath (37°C) at all times. A small sample of plasma (50  $\mu$ l) was taken from each tube at time point 0, 10, 30, 60 and 120 minutes and immediately processed according to the drug extraction method described previously for LC-MS/MS analysis.

## 5.5.2 Results and discussion

Figure 51 shows the percentage of DS drug entrapment derived from analysis of DS drug level from plasma samples added with either DS solution in 0.5% DMSO or DS-GCP20Q11-E at 5% oil for 2-hours period. The result showed significant decline in DS level in plasma with both treatments, with sharper drop seen in plasma with the nanoemulsions compared to plasma added with the naked DS. The  $t_{1/2}$  for DS-GCP20Q11-E formulation and DS in DMSO was 7 minutes and 49 minutes, respectively.



<sup>a,b</sup> Significant compared to drug entrapment at 0 hour for DS and DS-GCP20Q11-E 5%, respectively.

Figure 51: Stability of DS and DS-GCP20Q11-E 5% oil in diluted mouse plasma (*in vitro*).

The plasma was diluted to reduce the activity of protein and other endogenous components against the drug in order to see the rate of possible degradation of the drug upon contact with the plasma (Lalatsa et al., 2012a). The rapid decrease of DS level in the plasma added with DS-GCP20Q11-E formulation suggests the instability of the nanoparticle upon exposure to the components in the plasma. This instability had been observed previously when the formulations were incubated in the SIF, in which medium DS concentration was also decreased over time. The presence of multiple endogenous enzymes in both SIF and plasma was believed to be the cause of the lack of stability of the nanoparticles.

The instability of the particles might be due to the formation of protein corona around the surface of the particle, as discussed previously in Section 4.5.1 regarding the probable cause of nanoparticle instability in DMEM medium. There are over several thousand different types of protein in the blood that compete for the limited attachment space on the nanoparticle surface (Monopoli et al., 2011). This increases the chance of protein adsorption to the nanoparticles thus promotes more configuration change to the particle's surface morphology. Albumin, fibrinogen, apolipoprotein and immunoglobulin G (IgG) are the proteins most commonly present in the corona (Aggarwal et al., 2009) as there are high abundance of these proteins in the blood plasma. The protein corona formation is however not permanently fixed and composition is due to change depending on the kinetic rate of the adsorption and desorption of the protein, as well as upon movement of particle from one site to the other such as from the blood circulation into the tissue. This is due to the different relative abundance for different types of protein. This suggests that the nanoparticle behaviour from *in vitro* data does not necessarily predict the exact same activity happening *in vivo* for the same nanoparticles (Rahman et al., 2013).

## **5.6 Intravenous pharmacokinetic profile of DS-GCP20Q11-E**

Pharmacokinetic profile of a drug formulation via intravenous (IV) administration is commonly used as a reference to compare with the pharmacokinetic profile of other routes of administrations such as oral and subcutaneous administration. This is due to the absence of barrier via the IV route that could limit the absorption and distribution of the drug as the drug is directly introduced into the systemic system. The IV route could also provide an enhanced level of drug that could be of therapeutic benefit. The objective of this study was to determine if the DS level in plasma is improved and maintained at acceptable level upon administration of the DS-GCP20Q11-E nanoemulsions through the IV route.

### **5.6.1 DS-GCPQ formulation evaluation for IV administration**

#### **5.6.1.1 Methodology**

The DS-GCP20Q11-E formulation was modified to suit the requirement for the IV administration by preparing it in 5% w/v glucose instead of Milli-Q water. The preparation of DS-GCP20Q11-E formulations at different oil content (5, 10, 20, 30, 40 and 50% oil) was the same as described previously (Section 3.4.4.1) except for using the sterile 5% w/v glucose (Hameln Pharmaceuticals Limited, Gloucester, UK) as the aqueous phase to replace Milli-Q water (Table 16). Freshly prepared formulations at each oil content were prepared in triplicate for the characterization. All formulations were characterized by analysing the mean drug entrapment (%), particle size and PDI, as well as the zeta potential, as described previously.

Another characterization of the DS-GCP20Q11-E in 5% w/v glucose at different oil content was the measurement of viscosity as this could affect administration with small

bore needles. Viscosity was measured using Bohlin Gemini Rheometer (Malvern Instruments, Malvern, UK). A stainless-steel cone and plate at 4° angle and 40 mm diameter (CP 4/40) was used for the measurement at 25°C over the shear rate range of 0.01 to 100 s<sup>-1</sup>. Apparent viscosity was measured under the shear rate of 100 s<sup>-1</sup>.

### 5.6.1.2 Results and discussion

The purpose of preparing the formulation in 5% glucose is to avoid the osmolarity difference between formulations and blood constituents upon its administration into the blood circulations that could lead to cell rupture or haemolysis. The formulations were also prepared and kept in sterile condition at all times to avoid any exposure of the bacteria or harmful foreign particles into the formulations that could be transferred to the test subjects.

The resulting dispersion of DS-GCP20Q11-E in 5% glucose at all oil content appeared uniform, milky white in colour and more viscous towards higher amount of oil content. The result shows all formulations at different oil content having 100% drug entrapment (Figure 52).

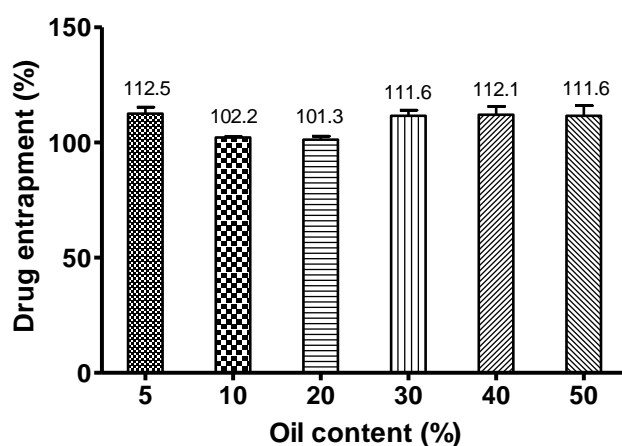
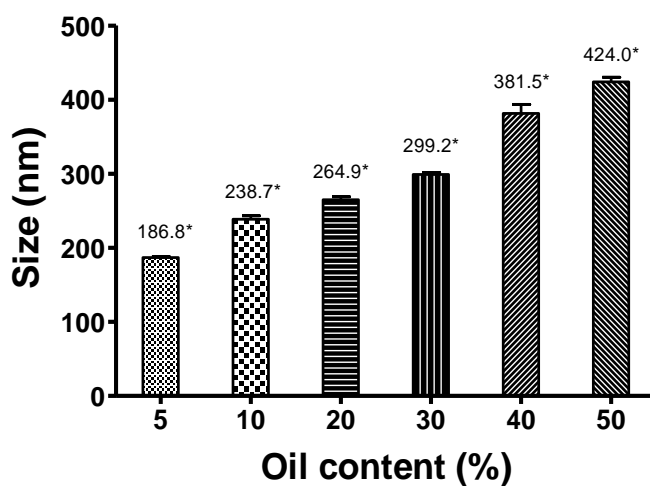


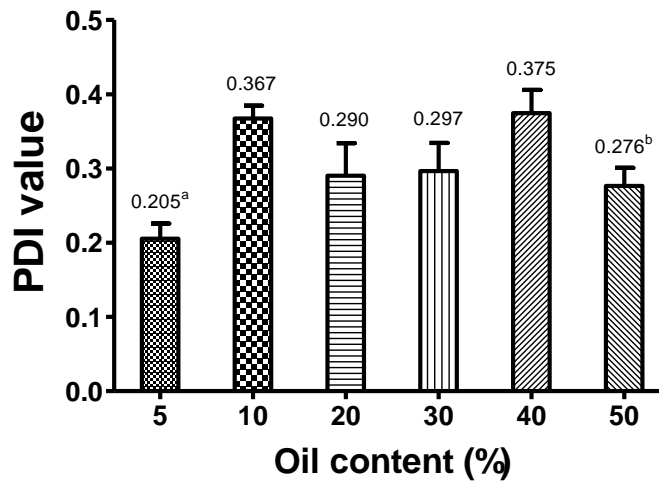
Figure 52: Percentage of drug encapsulation of freshly prepared DS-GCP20Q11-E in 5% glucose formulations at 5, 10, 20, 30, 40 and 50% oil content. Data were presented as mean ± SD (n = 3).

The mean particle size of the formulations (Figure 53) showed an increasing pattern of size towards higher amount oil content, similar to the pattern seen in DS-GCP20Q11-E nanoemulsion prepared in Milli-Q water. Both the size and PDI values were also found significantly different among different oil content formulations ( $P < 0.05$ ).



\* Significant compared to mean particle size of any other formulations with different oil content

Figure 53: Particle size of freshly prepared DS-GCP20Q11-E in 5% glucose formulations at 5, 10, 20, 30, 40 and 50% oil content. Data were presented as mean  $\pm$  SD ( $n = 3$ ).

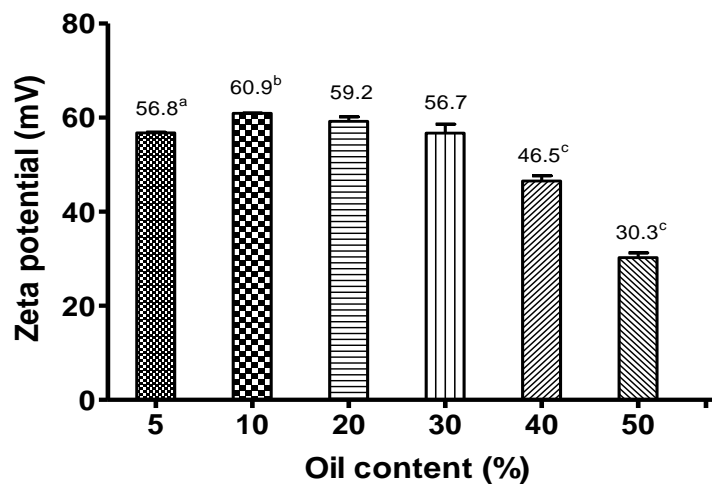


<sup>a</sup> Significant compared to mean PDI value of 10, 30 and 40% oil content formulations

<sup>b</sup> Significant compared to mean PDI value of 10 and 40% oil content formulations

Figure 54: PDI values of freshly prepared DS-GCP20Q11-E in 5% glucose formulations at 5, 10, 20, 30, 40 and 50% oil content. Data were presented as mean  $\pm$  SD (n = 3).

The zeta potential measurements showed highly positive surface charge in all formulations (pH 4 to 5). It appeared however that the charge was decreasing in formulations having higher amount of oil (Figure 55).



<sup>a</sup> Significant compared to mean zeta potential of 10% oil content formulations

<sup>b</sup> Significant compared to mean zeta potential of 30% oil content formulations

<sup>c</sup> Significant compared to mean zeta potential of any other formulations with different oil content

Figure 55: Zeta potential (mean  $\pm$  SD, n = 3) of freshly prepared DS-GCP20Q11-E in 5% glucose formulations at 5, 10, 20, 30, 40 and 50% oil content.

Apparent viscosity is defined by the shear stress applied to the fluid divided by the shear rate. The apparent viscosity at highest shear rate of  $100\text{s}^{-1}$  was chosen to compare formulations with different oil content because of measurement at maximum torque by the rheometer gives high accuracy of the reading (Ngan et al., 2014). Based on the graph in Figure 56, the apparent viscosity was increased towards higher content of oil in the DS-GCP20Q11-E nanoemulsion.

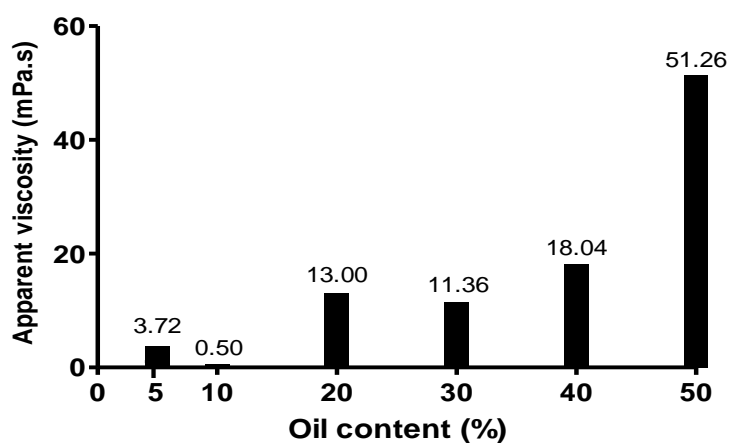


Figure 56: Apparent viscosity of DS-GCP20Q11-E nanoemulsion in 5% glucose at different oil content at shear rate  $100\text{s}^{-1}$ .

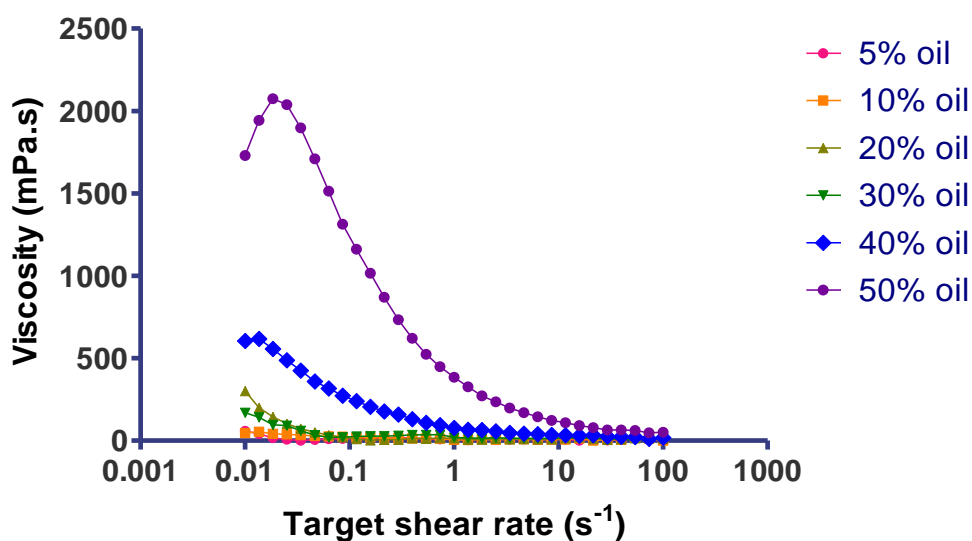


Figure 57: Rheological behaviour of DS-GCP20Q11-E nanoemulsion in 5% glucose at different oil content at shear rate between  $0.01$  to  $100\text{s}^{-1}$ .

Figure 57 shows the DS-GCP20Q11-E nanoemulsions having the flow behaviour of shear thinning (pseudoplastic) at higher shear rate. This means more occurrence of fluid system when subjected to external pressure, which is a desirable character for easier administration from the syringe during the intravenous bolus injection. During the shear thinning, as the shear rate increases, the polymer chains are more uniformly aligned, causing the viscosity to decrease accordingly (Likavčan et al., 2014). It could also mean that the polymeric nanoparticles network of GCPQ is broken at high shear rates, as reported previously in our group (Chooi et al., 2014). In comparison to other formulations, only formulation at 50% oil showed a distinct yield stress (amount of stress needed for the dispersion to flow) peak at shear rate  $0.018 \text{ s}^{-1}$ . This is a common situation in highly concentrated nanoemulsions when subjected to small shear deformation as they exhibit strong elastic response (Pal, 1999). The absence of yield stress peak means no force needed for the dispersion to flow.

In summary, it can be concluded that the drug entrapment, particle size and particle size distribution of DS-GCP20Q11-E in 5% glucose showed no distinct differences compared to the ones prepared in Milli-Q water. This formulation was therefore used for the IV pharmacokinetic study in mouse model.

## **5.6.2 Intravenous pharmacokinetic study of DS-GCP20Q11-E in mice**

### **5.6.2.1 Methodology**

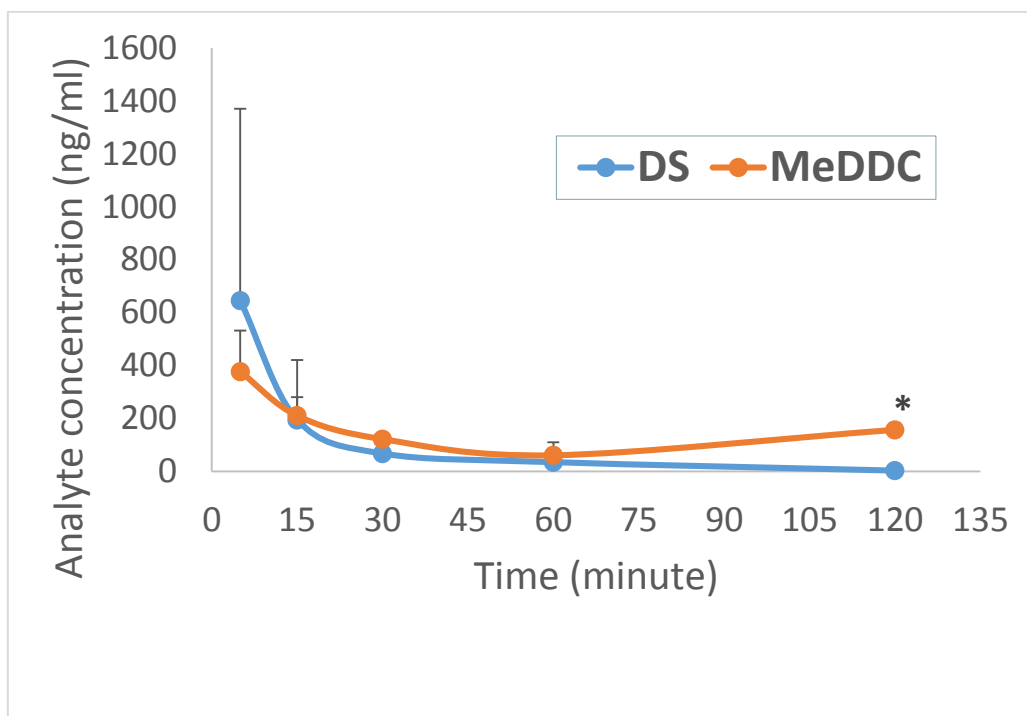
The animals condition used was as described previously in Section 5.4.1.1. Animals were given with single IV administration of DS-GCP20Q11-E in 5% glucose with 20% oil content (4 mg/ml DS) at 20 mg/kg dose via the tail vein injection. Animals were then euthanized at 5 different time points (n = 5 per time point) of 5 minutes, 15 minutes, 30 minutes, 1 hour and 2 hours by the CO<sub>2</sub> asphyxiation. The blood was then immediately taken by cardiac puncture and collected into K<sub>2</sub>EDTA blood tubes. The blood samples were processed immediately upon collection as described previously in Section 5.3.2.5 for LC-MS/MS analysis. The pharmacokinetic analysis done was as described in Section 5.4.1.3.

### **5.6.2.2 Results and discussion**

The developed and validated LC-MS/MS method was used to determine the pharmacokinetic profile of DS in mouse plasma from the IV administration of DS-GCP20Q11-E in 5% glucose. In this study, there was no DS control group (non-encapsulated) to be used as a comparison to the formulation group since DS is routinely given to the subjects through oral routes only. As the DS-GCP20Q11-E at 40% oil was too viscous and difficult to be administered IV through the mouse tail vein because of high backpressure, DS-GCP20Q11-E in 5% glucose at 20% oil (4 mg/ml DS) was used in the dosing regimen.

The plasma concentration-time profile of the single IV administration of the formulation is shown in Figure 58. Qualitative visual examination of the graph showed a gradual decline of both analytes concentration within one-hour post-injection with plasma DS level continuously decreased until end of observation period of t = 2 hours. MeDDC

level was however seen increased starting from  $t = 1$  hour onwards. The decrease in DS level might be attributed to the action of MPS mechanism eliminating the nanoparticles as positively-charged nanoparticles was reported having higher rate of opsonisation compared to ones with neutral charge (Roser et al., 1998). It could also mean that the nanoparticles are rapidly absorbed into the tissues.



\* MeDDC was significantly higher compared to DS level at  $t = 2$  hours

Figure 58: Plasma concentration – time profile of DS-GCP20Q11-E in 5% glucose intravenous treatment. Data were presented as mean  $\pm$  SD ( $n = 5$ ).

Parameter	Unit	DS-GCP20Q11-E	
		DS	MeDDC
$t_{1/2}$	min	17	110
$T_{max}$	min	5	5
$C_{max}$	ng/ml	645.593	376.573
$AUC_{0-2hr}$	ng/ml.min	13348.471	16883.166

Table 23: Pharmacokinetic parameters for single IV administration of DS-GCP20Q11-E in 5% glucose.

The pharmacokinetic parameters for IV administration of DS-GCP20Q11-E are shown in Table 23. Despite the gradual decline of the drug level, DS  $t_{1/2}$  at 17 mins was longer than previously reported (6 mins) for IV administration (Liu et al., 2014). The improved AUC value of DS from IV administration (13348.471 ng/ml.min) compared to oral administration (104.428 ng/ml.min) could be due to the avoidance of the first-pass metabolism through the IV route. This was supported by findings from Serrano et al. (2015) in which very low levels of GCPQ nanoparticles have been found in the liver and none in the spleen following an IV administration. There was also a slight elevation of MeDDC level, higher than the DS level at time point 120 minutes. The elevation of MeDDC level might be due to the late release of DS from some of the nanoparticles, causing parts of the administered DS to be converted into MeDDC in the liver at a later time than the rest of the drug.

For the DS anticancer study, the DS-GCP20Q11-E nanoemulsion was one of the few DS nanoparticle formulations made for IV administration route. Two of the reported studies investigated the effects of DS nanoparticles from the IV administration against breast cancer xenograft development in mice. A liposome-encapsulated disulfiram formulation was developed by Liu and colleagues (2014) while in the other study, a folate-receptor-targeted PLGA-PEG nanoparticle for encapsulation of DS was developed

by Fasehee and colleagues (2016a) for the passive (EPR effect) and active (folate receptor) tumour targeting. A DS-loaded lipid emulsion was formulated by Chen and colleagues (2015) aiming for an IV route delivery. The lipid emulsion made of mixture of medium chain triglycerides, glycerine, oleic acid, soybean lecithin and non-ionic surfactant Poloxamer 188 was yet to be tested for the *in vivo* stability. Unfortunately, no PK data of the nanoparticle formulations were disclosed in any of the studies.

### **5.6.2.3 Conclusions**

The IV route of administration of DS-GCP20Q11-E was able to improve the DS bioavailability in the blood circulation of the test animals by prolonging the half-life and increasing the AUC level of the drug. At the present moment, IV administration was seen as the better choice of route of administration for the nanoemulsion formulation to be given to the animals in the pharmacodynamics study, which will be covered in the next chapter.

## Chapter 6

# *In vivo* anticancer study of disulfiram nanoemulsion

### 6.1 Overview

In the previous chapter, the pharmacokinetic aspect of the DS-GCP20Q11-E formulations following both oral and intravenous administration to the mice were determined with the conclusion that these nanoparticles could be administered intravenously. The drug dose and percentage of oil content of the nanoemulsions that could be used were also determined. This chapter evaluates the pharmacodynamic aspect of DS-GCP20Q11-E nanoemulsions on the development of xenograft tumour of pancreatic cancer in mouse model using the dose regimens pre-determined in the pharmacokinetic study.

Pharmacodynamic studies explore the relationship between concentration of the drug at the site of action and the observed resulting effect in a set time course (Meibohm and Derendorf, 1997, Derendorf and Meibohm, 1999). In a simpler way, pharmacokinetics explores what the body does to the drug, while pharmacodynamics is about what the drug does to the body to produce the pharmacological effect (Yáñez et al., 2011).

## **6.2 Pancreatic cancer as the chosen type of malignancy**

Pancreatic cancer is one of the high mortality-type of cancer with five-year survival rate of less than 5% and the median survival measured in months (Bailey et al., 2016, Guerra and Barbacid, 2013). The most common factor contributing to the poor prognosis is the late diagnosis of the disease, at an advanced state of the tumour development with metastasis outside of the pancreas (Hidalgo, 2010, Vincent et al., 2011).

Patients at an early (local) stage of cancer usually have surgery to remove the resectable tumours. Nevertheless, even after the tumour removal, the patients frequently still need to have postoperative administration chemotherapy to minimize the risk of systemic spread. Drugs of choice include fluorouracil and leucovorin or gemcitabine (Burriss et al., 1997). These are also commonly used to treat advanced pancreatic cancer to improve overall survival (Hidalgo, 2010) but with limited benefit. This is why the development of more effective, safer anticancer drugs important in the treatment of pancreatic cancer so that the adverse effects of anticancer drug treatments do not outweigh the effects coming from the disease itself, especially during the treatment of early stage tumours.

### 6.3 Xenograft tumour model for pancreatic tumour

Murine tumour xenograft model has been used widely as a cancer model in preclinical studies to provide significant advances in the understanding of this family of diseases (Huynh et al., 2011). Rodent models are used to recapitulate the human disease for evaluation of chemopreventive and therapeutic measures. The most common xenograft models use cultured pancreatic cancer cells, which are available in more than 25 types of cultured cell lines. Some of the regularly used parental cell lines include MIAPaCa-2, Panc-1, AsPC-1, Capan-2 and BxPC-3 (Ding et al., 2010).

The subcutaneous xenograft models using cultured cells involve implanting cells or tissues in the subcutaneous pocket under the skin, usually at the flank area on either side of the animals near the hind legs or along the animal's back. For this cell implantation to grow and not undergoing rejection from the host, athymic nude mice are commonly used as these animals have defective development of the thymus and hair follicles, thus lack of T-lymphocytes and hair (Fidler, 1986). In other words, the immunocompromised nude mice will not be able to reject foreign cells and tissues because of absence of these immune cells.

There are several advantages of this subcutaneous xenograft *in vivo* system. Since the implanted cells under the skin develop into palpable solid tumours, this enables the tumour size and volume to be estimated by direct measurement of the tumour dimensions (Dai et al., 2015). The tumour mass and its general morphology can also be assessed at the end of the experiment after the tumours are resected from the host. The histopathology of the tumours also maintains the morphological phenotype of the primary tumour from human despite being grown in rodents. The simple implantation technique into the mice at the heterotopic sites reduces cost, lowers the incidence of complications from the procedure and provides convenience for cell manipulation by limited skill personnel to achieve successful engraftments (Kim et al., 2009).

Nevertheless, there are also limitations for this approach. There is probable risk of genetic instability to the cancer cell lines after several multiples passages. This adaptation of neoplastic cells to the *in vitro* conditions with long periods of successive passages may resulted in gain or loss of genetic alterations, which might be different form the parental tumours (Ding et al., 2010). The systemic environment of the immunocompromised mouse also does not allow evaluation of the host's immune system contribution to the growth modulation of the tumours. Subcutaneous xenograft tumours also rarely metastasize and usually show local growth only (Fidler, 1986), therefore they fail to truly imitate the invasive nature of pancreatic cancer in human.

Despite of all the weaknesses surrounding this approach of *in vivo* model, it is still commonly used for studies involving evaluations of drug formulation effect and determination of tumour growth and invasion. It is undoubtedly a simple, fast, reliable and inexpensive method compared to others such as orthotopic xenograft implantation and genetically engineered models as a way to reach defined end point evaluation of an experiment.

## 6.4 Materials

Item	Supplier / Manufacturer
MIAPaCa-2 (CRL-1420)	American Type Culture Collection, Rockville, Maryland, USA.
Copper gluconate	Sigma-Aldrich Company Limited, Dorset, UK
Dulbecco's Modified Eagle's Medium (DMEM), high glucose with L-glutamine	
Dulbecco's Phosphate Buffered Saline	
Fetal bovine serum	
Sodium pyruvate, 100 mM	Gibco Life Technologies, Bleiswijk, Netherlands
Trypsin-ethylenediaminetetraacetic acid (EDTA), 0.25%, phenol red	Gibco Life Technologies, Paisley, Scotland
Corning® Matrigel® Matrix	Corning, New York, USA
Glucose intravenous infusion 50% w/v	Hameln Pharmaceuticals Limited, Gloucester, UK

## **6.5 Methodology**

### **6.5.1 Animals**

The animal experiments were carried out under ethical approval from the Home Office, as described previously in Chapter 5, Section 5.4.1.1. Fifteen female CD-1 nude mice (Charles River, Kent, UK) of 17-21 g were kept in the individually ventilated cages (IVCs) with constant temperature and humidity monitoring according to the UCL School of Pharmacy BSU guidelines. Food and water were given *ad libitum* to the animals. All animals were acclimatized for a week prior to the start of experiment.

### **6.5.2 MIAPaCa-2 cells preparation and pancreatic xenograft implantation**

Similar to the cell conditions described previously in Chapter 4, Section 4.3.1, the MIAPaCa-2 cancer cells were grown for at least 2 weeks prior to the use for implantation in the complete DMEM growth medium (DMEM added with 10% v/v fetal bovine serum and 1 mM sodium pyruvate), maintained in CO<sub>2</sub> incubator with 5% CO<sub>2</sub> at 37°C. Cells that were grown in 175 cm<sup>2</sup> cell culture flask and reached 90% confluency were used after the amount of cells was determined with the flow cytometer.

Cells for the implantation were prepared in a combination of blank growth medium (DMEM medium without FBS and sodium pyruvate) and Matrigel at 1:1 ratio, containing  $2 \times 10^6$  cells in 100  $\mu$ l suspension ( $2 \times 10^7$  cells per ml). Cells were first removed from complete growth medium by centrifuging the cell suspension at 1000-2000 g for 3 minutes at 4°C, removing the supernatant (complete growth medium) and adding the blank growth medium into the cells. The centrifugation and replacement with blank

growth medium was repeated twice. Prior to the mix, frozen Matrigel from -50°C freezer was thawed into liquid form and then kept on ice (Matrigel solidifies into gel above 10°C). After mixing the cell suspension in blank growth medium with the Matrigel, the cell mixture was kept on ice at all times prior to the injection.

The freshly prepared MIAPaCa-2 cell mixture was injected subcutaneously into the right flank of the mouse at the volume of 100 µl per flank using 25G needle and 1 ml syringe. The day of implantation was determined as Day 0. The animals were monitored daily for the first tumour appearance, bodyweight change and health condition. Once tumours were detected in all mice, animals were randomly divided into 3 groups (n = 5).

### **6.5.3 Experimental design for DS-GCP20Q11-E and DS in SB oil treatments**

Treatment was started when the tumour reached a palpable size of approximately 6-7 mm in diameter. The tumour diameter was measured using a vernier calliper. For the treatments, Group 1 was the control group (no treatment); Group 2 for the treatment of intravenous 20 mg/kg DS-GCP20Q11-E at 20% oil content in 5% glucose (IV DS-GCPQ) with oral 11.4 mg/kg copper gluconate (Oral Cu); and Group 3 for the treatment of oral 20 mg/kg DS in SB oil (Oral DS) with Oral Cu. Treatments were given once every two days, along with the subsequent monitoring of tumour growth and bodyweight of the animals. Treatments were terminated in all groups after the total amount 10 intravenous injections were given to the mice in Group 2. Afterwards, the tumour growth was continuously measured until it reached maximum diameter of 13 mm, at which point the study was terminated (Figure 59). Mice were euthanized with CO<sub>2</sub> asphyxiation. The tumours were then excised, measured for tumour volume and weight and fixed in 10% formalin. The tumour volume (mm<sup>3</sup>) was calculated as (width<sup>2</sup> x length)/2.

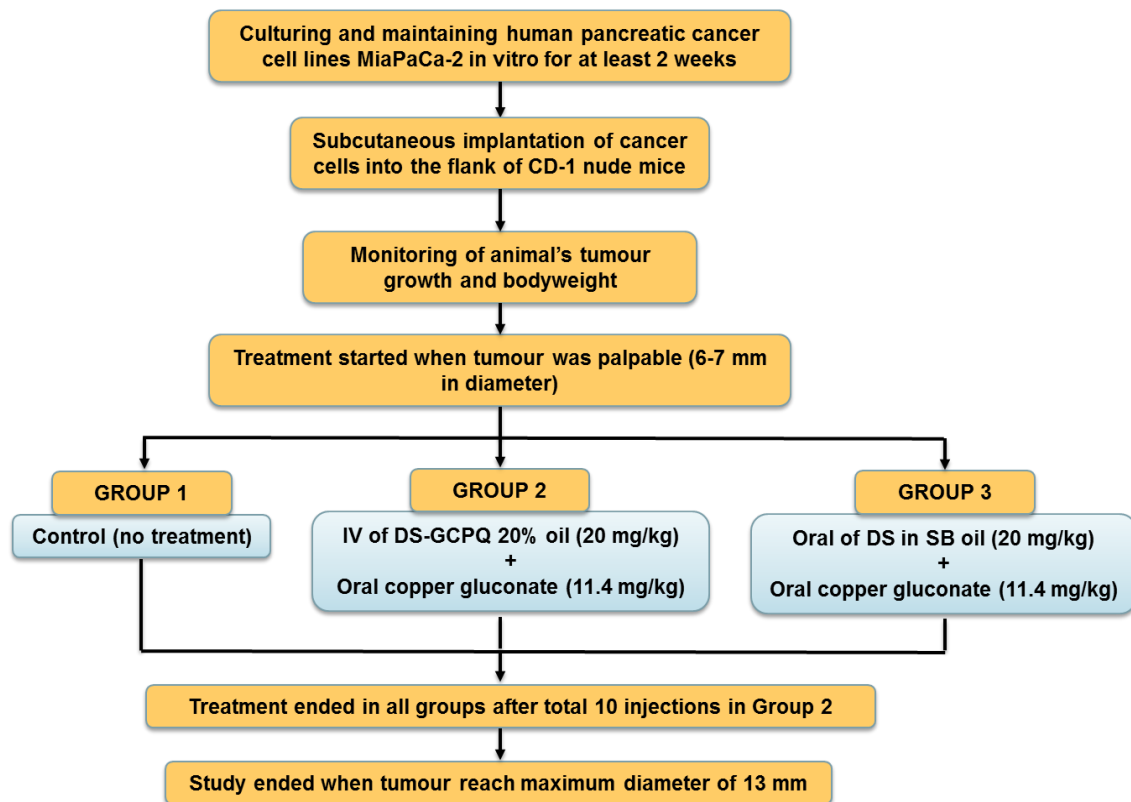


Figure 59: Simplified diagram to summarize the flow of experiment for the pharmacodynamics study of DS-GCP20Q11-E using pancreatic xenograft tumour model.

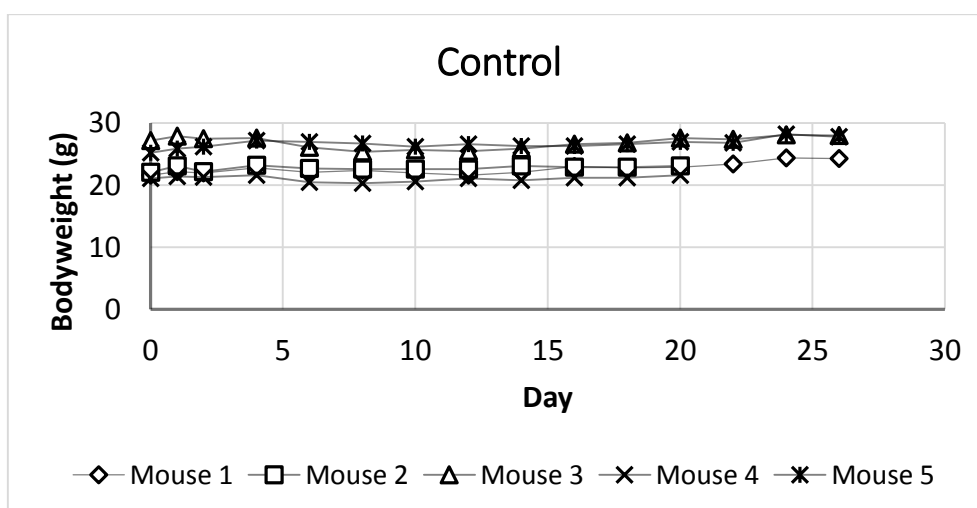
## 6.5.4 Statistical analysis

Data presented as mean  $\pm$  standard deviation was analysed using One-way ANOVA with Tukey's multiple comparison test for the post-hoc analysis, using IBM SPSS Statistics for Windows, Version 22.0 (IBM Corp, Armonk, New York, USA). Analysis of survival data was performed using GraphPad Prism version 5.00 for Windows (GraphPad Software, San Diego, California, USA). The survival of animals was determined using Kaplan-Meier analysis with Log rank (Mantel-Cox) test for comparison of two survival curves. The differences were considered significant when value of  $p < 0.05$ .

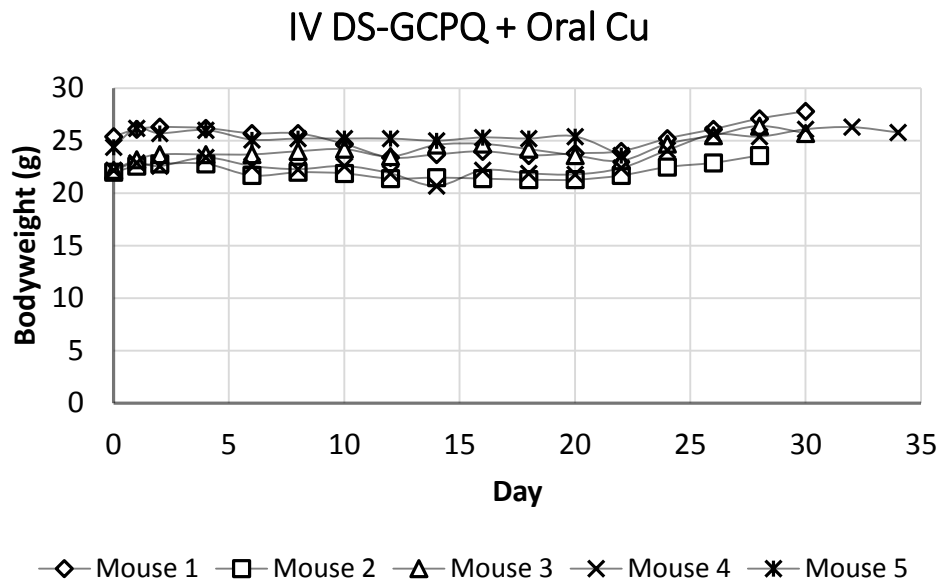
## 6.6 Results

### 6.6.1 Bodyweight

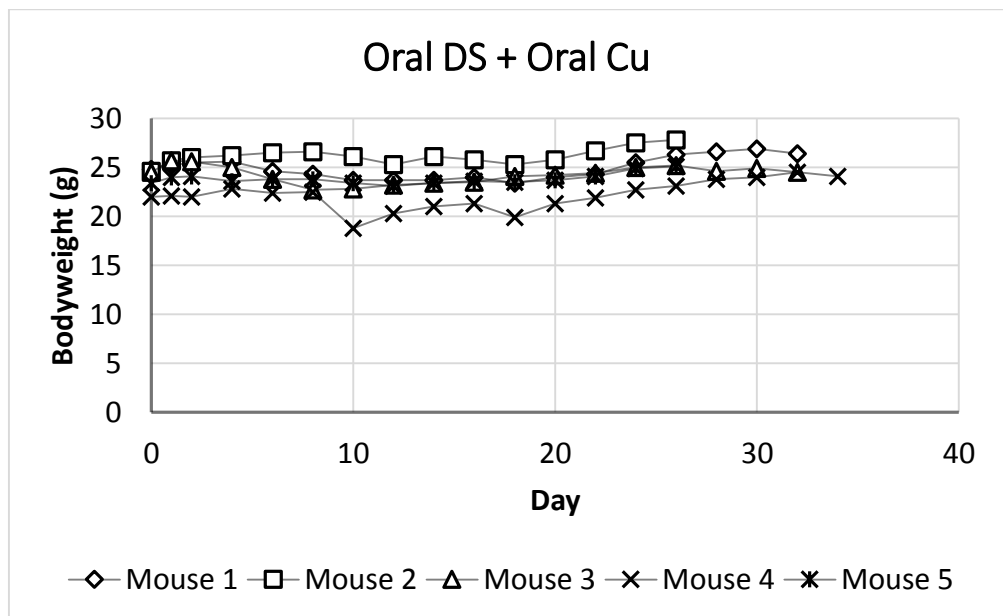
Figure 60 shows the bodyweight of all animals in all groups throughout the period of experiment. There was no significant difference in bodyweight change for each individual animal in all groups upon tumour implantation and administration of the treatments.



(A)



(B)



(C)

Figure 60: Bodyweight changes in individual animal throughout the study (A, B and C) of control, IV DS-GCPQ + Oral Cu, and Oral DS + Oral Cu group, respectively.

## 6.6.2 Tumour incidence, volume and weight

Treatments were started on Day 8 when the palpable tumour in mice reached approximately between 6 to 7 mm in diameter. The data (Figure 61) displays the mean tumour volume in each group vs. day of post-tumour implantation, with a few exceptions; Day 32 and 34 for IV DS-GCPQ + Oral Cu and Day 34 for Oral DS + Oral Cu group displayed volume from one animal only. All tumours, with or without treatments, showed a gradual increase in tumour volume over time (Figure 62 A, B, and C). Despite lower mean tumour weight seen in IV DS-GCPQ + Oral Cu group (Table 24), the weights were not significantly different among the treatment groups ( $p>0.05$ ).

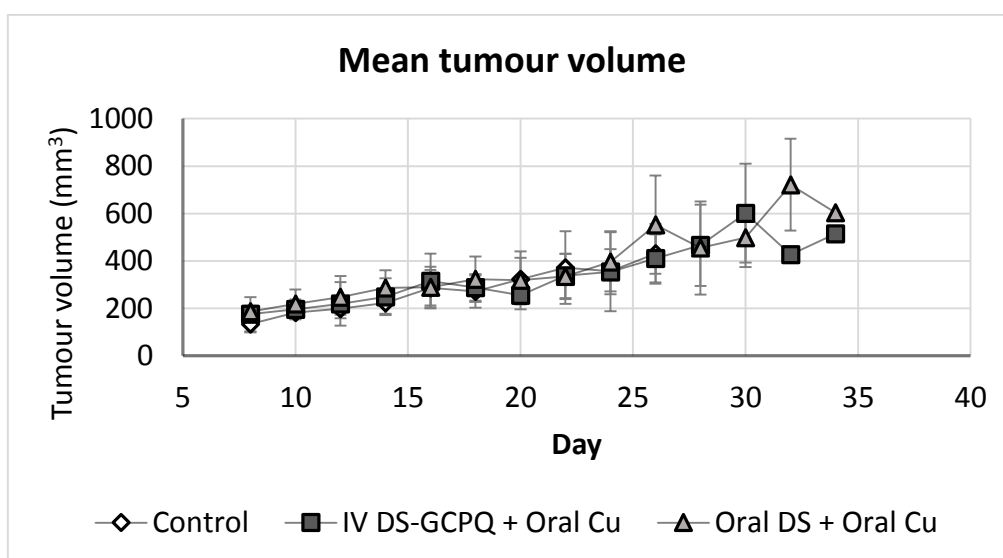
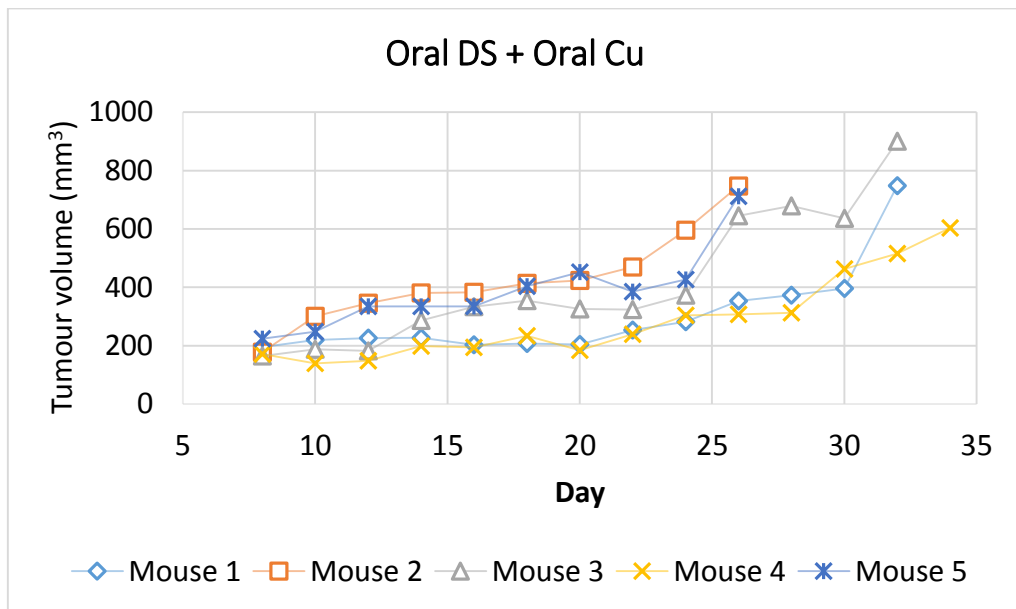
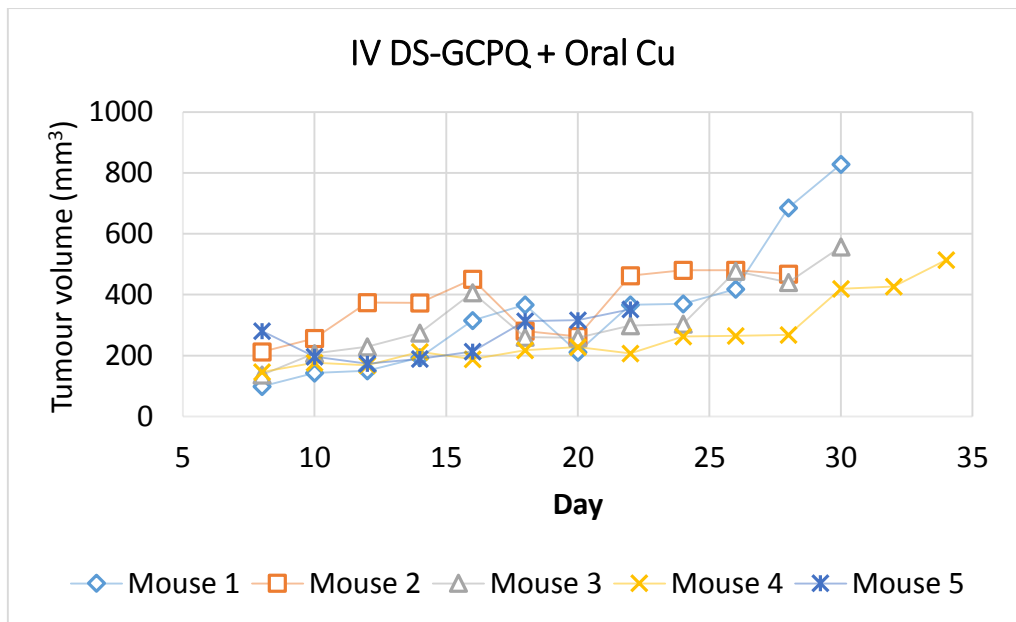
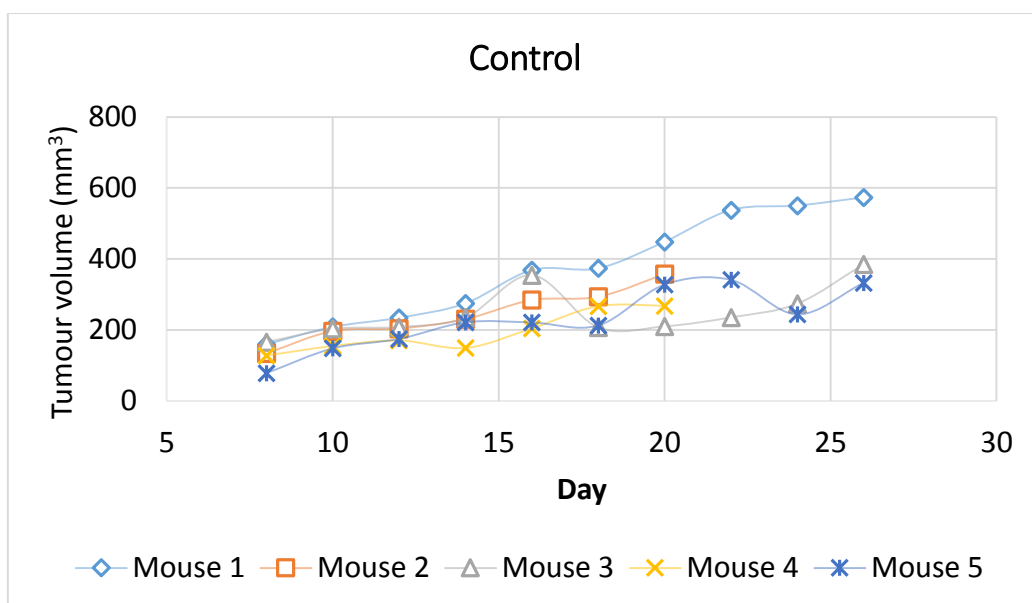


Figure 61: Mean tumour volume measured from Day 8 until end of study in all 3 groups.





(C)

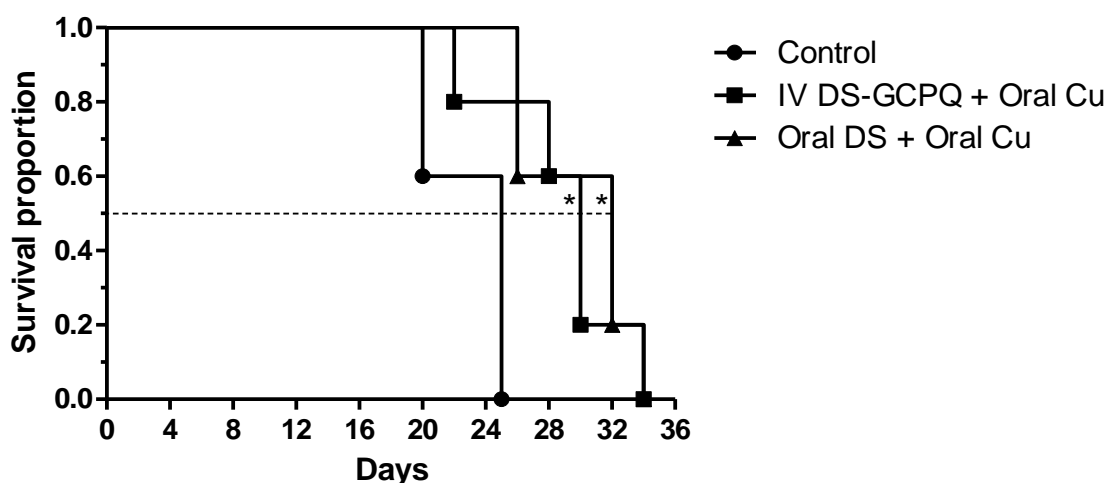
Figure 62: Tumour volume progression in individual mouse for IV DS-GCPQ + Oral Cu (A), Oral DS + Oral DS (B), and control (C) group measured from Day 8 until end of study.

Group	Tumour weight (g)	
	Mean	SD
Control	260.2	48.8
IV DS-GCPQ + Oral Cu	183.4	52.1
Oral DS + Oral DS	204.2	59.0

Table 24: Mean tumour weight (g) in all three groups measured upon excision from the flank of the animals during post-mortem.

### 6.6.3 Survival

Treatments were started on Day 8 and ended on Day 26 which was equivalent to the total amount of 10 IV injections given to the animals in IV DS-GCPQ + Oral Cu group. The median survival time for animals received IV DS-GCPQ + Oral Cu, Oral DS + Oral Cu and control group was 30, 32 and 25 days, respectively (Figure 63). Statistically, the median survival time in animals received no treatment (control) was significantly shorter compared to the values in both IV DS-GCPQ + Oral Cu and Oral DS + Oral Cu treatment groups ( $p = 0.0305$ ,  $p = 0.0031$ , respectively). There was no significant difference in the survival time values between the two treatment groups.



\*Median survival for IV DS-GCPQ + Oral Cu and Oral DS + Oral Cu group was significantly different compared to control

Figure 63: Kaplan-Meier survival curve of nude mice bearing pancreatic xenograft tumours.

## 6.7 Discussion

The analysis of animal survival is commonly used to measure clinical outcomes. Since the humane practice of the experiment only allows the animals to bear single tumour up to certain size only (maximum of 13 mm in diameter for the present case), this was used as a surrogate marker and endpoint to study the anticancer effects of DS-GCP20Q11-E nanoemulsion treatments.

Based on this modified survival study, the treatment of DS with copper supplementation showed significant effect in increasing the survival of the animals bearing MIAPaCa-2 xenograft pancreatic tumour. It has been shown that both oral and IV treatment of DS produced the effect of tumour growth suppression, rendering IV route as the less preferable choice for route of administration of the drug. The method of administering DS in soybean oil is however only feasible in this experiment for easy oral administration of DS via oral gavage to the mice. This approach is less desirable in human as the drug is more conveniently and commonly taken in solid form of capsules or tablets.

Since the oral pharmacokinetic of DS-GCP20Q11-E revealed very low DS level in the mouse plasma, study of the anticancer effect following oral route of DS-GCP20Q11-E administration was omitted. Perhaps with better understanding of DS-GCP20Q11-E fate in the body following oral administration, such as investigating the DS level or nanoparticle deposition in the main organs and other tissues, oral DS-GCP20Q11-E administration to study its effect on tumour progression can be taken into consideration in the future studies. No significant bodyweight change in control and treated animals means the tumour burden did not induce health deterioration effect and the treatments not producing toxicity or any adverse side effects, respectively, to the animals.

The effectiveness of DS in suppressing the progression and growth of pancreatic cancer xenografts has been reported by many for the past several years. DS with copper has been made into a complex for the intraperitoneal (i.p.) treatment against SW1990

cells subcutaneous pancreatic tumour xenograft in nude mice (Han et al., 2013). The treatment was able to inhibit 62.8% of the tumour growth when compared to control. The positive effect was also achieved when disulfiram administered in combination with other active ingredients. Combined treatments of gemcitabine and disulfiram with zinc sulphate via intraperitoneal administration were able to reduce mean tumour mass of PaCa44 cells subcutaneous pancreatic xenograft in nude mice to 40-fold compared to control after 4 weeks of treatments (Dalla Pozza et al., 2011). In another study involving treatments with oral DS and intraperitoneal of low-dose gemcitabine, the growth of the CFPAC-1 xenograft tumour was significantly suppressed which was comparable to the effects of 10-times higher dose of gemcitabine treatment (Kim et al., 2013). Another combined treatment of disulfiram was with arsenic trioxide and ascorbic acid (AAA), where the intraperitoneal injection of the combination had caused 61% reduction in mean tumour size and eliminated tumours in 30% of nude mice with PANC-1 xenografts (Dinnen et al., 2013). Intraperitoneal treatment of DDC, the reduced metabolite of disulfiram with 12-O-tetradecanoylphorbol-13-acetate was also found strongly inhibited the growth of PANC-1 xenograft tumours (Huang et al., 2015).

Copper is an essential ingredient in elevating the anticancer property of DS. It would be practical to administer copper intravenously along with the DS-GCP20Q11-E formulation. Since there was lack of information on the possible interactions between the copper ions and the particles of the nanoemulsions in the blood environment, the copper was administered orally in the form of copper gluconate. Copper (cupric) gluconate is a widely available salt as a dietary supplement and is one of the Generally Regarded as Safe (GRAS) substance (FDA, 2015). In fact, it has also been used in the Phase 1 clinical trials for the study of DS against hepatic metastases from solid tumours (ClinicalTrials.gov Identifier NCT00742911). As the copper is capable of forming complex with DS *in vivo* (Johansson, 1992), it is possible to have the copper and DS complex formed in the tissues

such as in the liver or to a greater extent in the tumour. Accumulation of copper in cancer cells is high (Gupte and Mumper, 2009). The supplementation of copper gluconate was therefore assumed helping to increase the bioavailability of copper in the blood circulation and in the tumour microenvironment thus aid the anticancer activity of the DS-GCP20Q11-E without causing unnecessary toxicity from the copper overdose.

The DS-GCP20Q11-E formulation was able to show positive effects against the development of the pancreatic tumour xenograft. Nevertheless, there are still a lot of improvement that could be made to fully utilize the benefits of the nanoemulsion. To take advantage of the high drug loading that can be put into the nanoemulsion, it is worthwhile to attempt for combination of DS with other potent hydrophobic anticancer drugs such as gemcitabine into the formulation for a more potent anticancer activity. For a more precise imitation of the actual pancreatic cancer environment and its metastatic nature, the anticancer activity of the formulation could also be tested using the murine orthotopic model of the pancreatic cancer by direct injection of the pancreatic cancer cells into the proximal portion of the pancreas (Alves et al., 2001) or into the common bile duct (Tsuji et al., 2006). It is no doubt that the orthotopic method requires expertise and more challenging to be executed, but the significance of the outcome from such study is invaluable for better mimics of the pancreatic cancer in human.

## **6.8 Conclusions**

The treatment of DS-GCP20Q11-E with copper was able to produce a significant inhibition effect against the progression of MIAPaCa-2 cells subcutaneous xenograft tumour growth when the nanoemulsion is given intravenously to the nude mice. The treatment was also found not causing any toxicological effects to the animals even after it was given over the period of 23 days. This showed that the DS-GCP20Q11-E has the

ability to alleviate the rapid progression of pancreatic cancer without causing harmful side effects from its continuous use in a set period of time. This therefore suggests that the DS-GCP20Q11-E nanoemulsion has the potential to be studied further as a safe adjuvant for chemotherapeutic treatment.

## Chapter 7

# Conclusion

In order to improve the delivery system of DS, the aim was to develop a nanoparticle formulation by incorporating the drug with chitosan-derived GCPQ polymer. Two batches of GCPQ had been synthesized from two different sources of glycol chitosan via step-by-step process of acid degradation, palmitoylation and quaternisation. Despite the same synthesis procedure applied, the NMR spectroscopy showed different P% but same Q% between the GCP10Q11 and GCP20Q11 polymers, which led to two different molecular weights of 15,100 and 24,890 kDa respectively, based on the GCP-MALLS analysis. There was possibility that the lower P% and molecular weight of GCP10Q11 was caused by the GC used had less primary amine group available (higher N-acetylation degree) for the conjugation with palmitic acid chain synthesis to happen in comparison to the GC for GCP20Q11. Apart from that, the influence of random conjugation reactions is also a factor that cannot be ruled out.

The polymeric micelles formulation approach was unable to give high DE% for both DS-GCP10Q11 and DS-GCP20Q11 formulations (3-4% DE% only), despite the attempt to use different drug-to-polymer ratio of 1:5 and 1:10 w/w, higher palmitoylated GCPQ and high-powered probe sonication procedure. The range of particle size (166-275 and 112-295 nm) and particle size distribution (0.3-0.4 and 0.53-0.68) of DS-GCP10Q11

and DS-GCP20Q11 respectively, were however within the acceptable criteria for a nanoparticle formulation. The presence of undissolved DS crystals in the formulation upon naked eye observation and TEM imaging proved the incomplete solubilisation of DS by the polymer and explained the low drug encapsulation into the nanoparticles.

In the attempt to increase the DS encapsulation while maintaining other optimum nanoparticle criteria, the formulation of DS with higher palmitoylation GCP20Q11 into nanoemulsions showed promising results. Incorporation of soybean oil into the DS-GCP20Q11-E formulation produced a milky white and homogenous nanoemulsion with DE% as high as 100% at 1:10 drug to polymer ratio after a 15-minutes probe sonication. At 5% oil content, the nanoparticle criteria were found ideal with particle size of  $183.2 \pm 5.9$  nm, PDI of  $0.17 \pm 0.01$  and zeta potential of  $50.9 \pm 1.3$  at pH 4.54. Despite the low PDI, TEM images however revealed heterogeneous particle size distribution between 9 to 100 nm.

DS-GCP20Q11-E at higher content of oil (10, 20, 30, 40 and 50% oil) was investigated to determine the maximum limits of oil-drug loading of the nanoemulsions. Results showed high DE% in all formulations (95-100%). It was found that with increasing oil content (5-50%) the mean particle increased, as did overall polydispersity (190 to 359 nm and 0.14 to 0.21, respectively). The colloidal and drug load stability of formulations at all oil content were seen improved when stored at 4°C compared to room temperature. DS-GCP20Q11-E at 5% oil showed no significant change in 1) particle size and PDI values upon exposure to acidic and basic pH solution; 2) DE% in phosphate and HCl buffer up to 4 hours, and; 3) DE% upon incubation in simulated gastric fluid for 4 hours.

The potential of the nanoemulsions formulation to be developed for oral delivery was studied by conducting the *in vivo* oral pharmacokinetic study of DS-GCP20Q11-E in a mouse model. The oral administration of DS-GCP20Q11-E at 40% oil, 70 mg/kg dose

was however showed low DS level in the mouse plasma compared to control group (DS in soybean oil) with AUC of 104.428 compared to 6909.827 ng/ml.min, respectively. The change of route of administration to intravenous was able to improve the pharmacokinetic profile of DS-GCP20Q11-E even upon administration of lower oil content formulations and lower dosage (20% oil and 20 mg/kg DS, respectively). This was proved by the increased IV's AUC value (13348.471 ng/ml.min) ~ over 100-fold of the oral AUC value, as well as better DS  $t_{1/2}$  compared to the other previously reported DS IV nanoparticle formulation.

Presence of copper in the treatment increases the potency of DS-GCP20Q11-E nanoemulsions, as shown by the significant low  $IC_{50}$  values of the treatment compared to the ones without copper in the *in vitro* cellular toxicity experiment against MIAPaCa-2 cancer cell lines. This finding was later implemented in the treatment regime to investigate DS-GCP20Q11-E anticancer activity against the development of pancreatic cancer xenograft tumour. Improved survival days of the tumour-bearing animals was seen in groups treated with continuous IV treatment of DS-GCP20Q11-E, as well as oral DS in soybean oil. Treated animals also showed no significant changes in bodyweight throughout the study, suggesting no toxicity or side effects from the prolonged administration of the DS formulations.

In conclusion, the DS-GCP20Q11-E nanoemulsion was found capable of protecting the drug in the blood circulation to some extent and delivered the drug load to the tumour site. Additional feature of the nanoemulsions was the ability to be loaded with high amount of oil thus high amount of drug without compromising the colloidal stability of the nanoparticle formulation. This could help reaching the therapeutic dose needed for the treatment without the risk of toxicity from the use of high surfactant/emulsifier amount to stabilize the drug formulation. This proves the potential of the newly found

DS-GCP20Q11-E nanoemulsions to be used or developed further for cancer therapeutic purposes.

## Future recommendations

Polymeric micelles formulation of DS and GCPQ could probably be improved by adding cosurfactant into the formulation such as the biodegradable PEG for avoidance of the MPS elimination, or by adding ligands for tumour site active targeting. For drug release study, the ultracentrifugation method is not suitable for nanoemulsions. Therefore, the release study could be done using the dialysis tube method. The low level of DS found in the mouse plasma following the oral administration of the formulation would be better understood by analysing the DS level in the main organs such as the liver, kidney, lung and brain, as well as fat tissues since DS is known to deposit more in the fatty deposits in the body. For the investigation of DS-GCP20Q11-E anticancer activity, it would be useful to add treatment group of oral DS-GCP20Q11-E administration for the equal comparison with the effects seen in the oral DS in soybean oil group. The anticancer study of the nanoemulsions could also be attempted on other types of cancer such as the brain cancer, where the transport of the nanoemulsion through the blood brain barrier could be investigated.

# Bibliography

- ADAMCZAK, M., PARA, G., SIMON, C. & WARSZYNSKI, P. 2013. Natural oil nanoemulsions as cores for layer-by-layer encapsulation. *J Microencapsul*, 30, 479-89.
- AGARWAL, R. P., PHILLIPS, M., MCPHERSON, R. A. & HENSLEY, P. 1986. Serum albumin and the metabolism of disulfiram. *Biochemical Pharmacology*, 35, 3341-3347.
- AGGARWAL, P., HALL, J. B., MCLELAND, C. B., DOBROVOLSKAIA, M. A. & MCNEIL, S. E. 2009. Nanoparticle interaction with plasma proteins as it relates to particle biodistribution, biocompatibility and therapeutic efficacy. *Adv Drug Deliv Rev*, 61, 428-37.
- AGILENT TECHNOLOGIES, I. 2015. An introduction to gel permeation chromatography and size exclusion chromatography Available: <https://www.agilent.com/cs/library/primers/Public/5990-6969EN%20GPC%20SEC%20Chrom%20Guide.pdf>.
- ALLEN, T. M. & CULLIS, P. R. 2004. Drug delivery systems: entering the mainstream. *Science*, 303, 1818-22.
- ALVES, F., CONTAG, S., MISSBACH, M., KASPAREIT, J., NEBENDAHL, K., BORCHERS, U., HEIDRICH, B., STREICH, R. & HIDDEMANN, W. 2001. An Orthotopic Model of Ductal Adenocarcinoma of the Pancreas in Severe Combined Immunodeficient Mice Representing All Steps of the Metastatic Cascade. *Pancreas*, 23, 227-235.
- ANTON, N. & VANDAMME, T. F. 2011. Nano-emulsions and Micro-emulsions: Clarifications of the Critical Differences. *Pharm Res*, 28, 978-985.
- ARACHCHIGE, M. C. M., RESHETNYAK, Y. K. & ANDREEV, O. A. 2015. Advanced targeted nanomedicine. *Journal of Biotechnology*, 202, 88-97.
- ASHFORD, M. 2013. Bioavailability - Physicochemical and Dosage Form Factors. *Aulton's Pharmaceutics: The Design and Manufacture of Medicines*. Fourth ed.: Elsevier Ltd.
- ATTWOOD, D. 2013. Disperse systems. In: AULTON, M. E. & TAYLOR, K. M. G. (eds.) *Aulton's Pharmaceutics; The Design and Manufacture of Medicines* Fourth ed.: Churchill Livingstone
- AULTON, M. E. & TAYLOR, K. 2013. *Aulton's Pharmaceutics: The Design and Manufacture of Medicines*, Churchill Livingstone.
- AYORINDE, F. O., GARVIN, K. & SAEED, K. 2000. Determination of the fatty acid composition of saponified vegetable oils using matrix-assisted laser desorption/ionization time-of-flight mass spectrometry. *Rapid Commun Mass Spectrom*, 14, 608-15.
- BAILEY, P., CHANG, D. K., NONES, K., JOHNS, A. L., PATCH, A.-M., GINGRAS, M.-C., MILLER, D. K., CHRIST, A. N., BRUXNER, T. J. C., QUINN, M. C., NOURSE, C., MURTAUGH, L. C., HARLIWONG, I., IDRISOGLU, S., MANNING, S., NOURBAKHSH, E., WANI, S., FINK, L., HOLMES, O., CHIN, V., ANDERSON, M. J., KAZAKOFF, S., LEONARD, C., NEWELL, F., WADDELL, N., WOOD, S., XU, Q., WILSON, P. J., CLOONAN, N., KASSAHN, K. S., TAYLOR, D., QUEK, K., ROBERTSON, A., PANTANO, L., MINCARELLI, L., SANCHEZ, L. N., EVERS, L., WU, J., PINESE, M., COWLEY, M. J., JONES, M. D., COLVIN, E. K., NAGRIAL, A. M., HUMPHREY, E. S., CHANTRILL, L. A., MAWSON, A., HUMPHRIS, J., CHOU, A., PAJIC, M., SCARLETT, C. J., PINHO, A. V., GIRY-LATERRIERE, M., ROOMAN, I., SAMRA, J. S., KENCH, J. G., LOVELL, J. A., MERRETT, N. D., TOON, C. W., EPARI, K., NGUYEN, N. Q., BARBOUR, A., ZEPS, N., MORAN-JONES, K., JAMIESON, N. B., GRAHAM, J. S., DUTHIE, F., OIEN, K., HAIR, J., GRÜTZMANN, R., MAITRA, A., IACOBUZIO-DONAHUE, C. A., WOLFGANG, C. L., MORGAN, R. A., LAWLOR, R. T., CORBO, V., BASSI, C., RUSEV, B., CAPELLI, P., SALVIA, R., TORTORA, G., MUKHOPADHYAY, D., PETERSEN, G. M., AUSTRALIAN PANCREATIC CANCER GENOME, I., MUNZY, D. M., FISHER, W. E., KARIM, S. A., ESHLEMAN, J. R., HRUBAN, R. H., PILARSKY, C., MORTON, J. P., SANSOM, O. J., SCARPA, A., MUSGROVE, E. A., BAILEY, U.-M. H., HOFMANN, O., SUTHERLAND, R. L., WHEELER, D. A., GILL, A. J., GIBBS, R. A., PEARSON, J.

- V., et al. 2016. Genomic analyses identify molecular subtypes of pancreatic cancer. *Nature*, 531, 47-52.
- BAKER, J. R., JATLOW, P. & MCCANCE-KATZ, E. F. 2007. Disulfiram effects on responses to intravenous cocaine administration. *Drug and Alcohol Dependence*, 87, 202-209.
- BAUGHMAN, W. F. & JAMIESON, G. S. 1922. THE CHEMICAL COMPOSITION OF SOYA BEAN OIL. *Journal of the American Chemical Society*, 44, 2947-2952.
- BENET, L. Z. & ZIA-AMIRHOSSEINI, P. 1995. Basic Principles of Pharmacokinetics. *Toxicologic Pathology*, 23, 115-123.
- BERRIDGE, M. V., HERST, P. M. & TAN, A. S. 2005. Tetrazolium dyes as tools in cell biology: New insights into their cellular reduction. *Biotechnology Annual Review*. Elsevier.
- BERRIDGE, M. V., TAN, A. S., MCCOY, K. D. & WANG, R. 1996. The biochemical and cellular basis of cell proliferation assays that use tetrazolium salts. *Biochemica*, 4, 14-19.
- BHADHPRASIT, W., KODAMA, H., FUJISAWA, C., HIROKI, T. & OGAWA, E. 2012. Effect of copper and disulfiram combination therapy on the macular mouse, a model of Menkes disease. *J Trace Elem Med Biol*, 26, 105-8.
- BLY, D. D. 1970. Gel Permeation Chromatography. *Science*, 168, 527-533.
- BODENNER, D. L., DEDON, P. C., KENG, P. C., KATZ, J. C. & BORCH, R. F. 1986. Selective protection against cis-diamminedichloroplatinum(II)-induced toxicity in kidney, gut, and bone marrow by diethyldithiocarbamate. *Cancer Res*, 46, 2751-5.
- BOHLMANN, G. M. 2005. 6. General Characteristics, Processability, Industrial Applications and Market Evolution of Biodegradable Polymers. In: BASTIOLI, C. (ed.) *Handbook of Biodegradable Polymers*. UK: Smithers Rapra Technology.
- BRAR, S. S., GRIGG, C., WILSON, K. S., HOLDER, W. D., JR., DREAU, D., AUSTIN, C., FOSTER, M., GHIO, A. J., WHORTON, A. R., STOWELL, G. W., WHITTALL, L. B., WHITTLE, R. R., WHITE, D. P. & KENNEDY, T. P. 2004. Disulfiram inhibits activating transcription factor/cyclic AMP-responsive element binding protein and human melanoma growth in a metal-dependent manner in vitro, in mice and in a patient with metastatic disease. *Mol Cancer Ther*, 3, 1049-60.
- BUCKIOVA, D., RANJAN, S., NEWMAN, T. A., JOHNSTON, A. H., SOOD, R., KINNUNEN, P. K., POPELAR, J., CHUMAK, T. & SYKA, J. 2012. Minimally invasive drug delivery to the cochlea through application of nanoparticles to the round window membrane. *Nanomedicine (Lond)*, 7, 1339-54.
- BURRIS, H. A., 3RD, MOORE, M. J., ANDERSEN, J., GREEN, M. R., ROTHENBERG, M. L., MODIANO, M. R., CRIPPS, M. C., PORTENOY, R. K., STORNILO, A. M., TARASSOFF, P., NELSON, R., DORR, F. A., STEPHENS, C. D. & VON HOFF, D. D. 1997. Improvements in survival and clinical benefit with gemcitabine as first-line therapy for patients with advanced pancreas cancer: a randomized trial. *J Clin Oncol*, 15, 2403-13.
- CALDORERA-MOORE, M., GUIMARD, N., SHI, L. & ROY, K. 2010. Designer nanoparticles: incorporating size, shape and triggered release into nanoscale drug carriers. *Expert Opin Drug Deliv*, 7, 479-495.
- CALIPH, S. M., CHARMAN, W. N. & PORTER, C. J. H. 2000. Effect of Short-, Medium-, and Long-Chain Fatty Acid-Based Vehicles on the Absolute Oral Bioavailability and Intestinal Lymphatic Transport of Halofantrine and Assessment of Mass Balance in Lymph-Cannulated and Non-cannulated Rats. *Journal of Pharmaceutical Sciences*, 89, 1073-1084.
- CALLEJA, P., HUARTE, J., AGÜEROS, M., RUIZ-GATÓN, L., ESPUELAS, S. & IRACHE, J. M. 2011. Molecular buckets: cyclodextrins for oral cancer therapy. *Therapeutic Delivery*, 3, 43-57.
- CARROLL, K. M., FENTON, L. R., BALL, S. A., NICH, C., FRANKFORTER, T. L., SHI, J. & ROUNSAVILLE, B. J. 2004. Efficacy of disulfiram and cognitive behavior therapy in cocaine-dependent outpatients: a randomized placebo-controlled trial. *Arch Gen Psychiatry*, 61, 264-72.
- CARROLL, K. M., NICH, C., BALL, S. A., MCCANCE, E., FRANKFORTER, T. L. & ROUNSAVILLE, B. J. 2000. One-year follow-up of disulfiram and psychotherapy for cocaine-alcohol users: sustained effects of treatment. *Addiction*, 95, 1335-49.

- CARROLL, K. M., NICH, C., BALL, S. A., MCCANCE, E. & ROUNSAVILE, B. J. 1998. Treatment of cocaine and alcohol dependence with psychotherapy and disulfiram. *Addiction*, 93, 713-27.
- CARRSTENSEN, H., MULLER, R. H. & MULLER, B. W. 1992. Particle size, surface hydrophobicity and interaction with serum of parenteral fat emulsions and model drug carriers as parameters related to RES uptake. *Clin Nutr*, 11, 289-97.
- CASALS, E., PFALLER, T., DUSCHL, A., OOSTINGH, G. J. & PUNTES, V. 2010. Time evolution of the nanoparticle protein corona. *ACS Nano*, 4, 3623-32.
- CEN, D., BRAYTON, D., SHAHANDEH, B., MEYSKENS, F. L., JR. & FARMER, P. J. 2004. Disulfiram facilitates intracellular Cu uptake and induces apoptosis in human melanoma cells. *J Med Chem*, 47, 6914-20.
- CEN, D., GONZALEZ, R. I., BUCKMEIER, J. A., KAHLON, R. S., TOHIDIAN, N. B. & MEYSKENS, F. L., JR. 2002. Disulfiram induces apoptosis in human melanoma cells: a redox-related process. *Mol Cancer Ther*, 1, 197-204.
- CHANDRA, R. & RUSTGI, R. 1998. Biodegradable polymers. *Progress in Polymer Science*, 23, 1273-1335.
- CHEN, D., CUI, Q. C., YANG, H. & DOU, Q. P. 2006. Disulfiram, a clinically used anti-alcoholism drug and copper-binding agent, induces apoptotic cell death in breast cancer cultures and xenografts via inhibition of the proteasome activity. *Cancer Res*, 66, 10425-33.
- CHEN, D. & DOU, Q. P. 2008. New uses for old copper-binding drugs: converting the pro-angiogenic copper to a specific cancer cell death inducer. *Expert Opin Ther Targets*, 12, 739-48.
- CHEN, X., ZHANG, L., HU, X., LIN, X., ZHANG, Y. & TANG, X. 2015. Formulation and preparation of a stable intravenous disulfiram-loaded lipid emulsion. *European Journal of Lipid Science and Technology*, 117, 869-878.
- CHENG, J., TEPLY, B. A., SHERIFI, I., SUNG, J., LUTHER, G., GU, F. X., LEVY-NISSENBAUM, E., RADOVIC-MORENO, A. F., LANGER, R. & FAROKHZAD, O. C. 2007. Formulation of Functionalized PLGA-PEG Nanoparticles for In Vivo Targeted Drug Delivery. *Biomaterials*, 28, 869-876.
- CHEUNG, A. M., WAN, T. S., LEUNG, J. C., CHAN, L. Y., HUANG, H., KWONG, Y. L., LIANG, R. & LEUNG, A. Y. 2007. Aldehyde dehydrogenase activity in leukemic blasts defines a subgroup of acute myeloid leukemia with adverse prognosis and superior NOD/SCID engrafting potential. *Leukemia*, 21, 1423-30.
- CHICK, J. 1999. Safety issues concerning the use of disulfiram in treating alcohol dependence. *Drug Saf*, 20, 427-35.
- CHO, H. J., LEE, T. S., PARK, J. B., PARK, K. K., CHOE, J. Y., SIN, D. I., PARK, Y. Y., MOON, Y. S., LEE, K. G., YEO, J. H., HAN, S. M., CHO, Y. S., CHOI, M. R., PARK, N. G., LEE, Y. S. & CHANG, Y. C. 2007. Disulfiram suppresses invasive ability of osteosarcoma cells via the inhibition of MMP-2 and MMP-9 expression. *J Biochem Mol Biol*, 40, 1069-76.
- CHONG, C. R. & SULLIVAN, D. J. 2007. New uses for old drugs. *Nature*, 448, 645-646.
- CHOOI, K. W., SIMAO CARLOS, M. I., SOUNDARARAJAN, R., GAISFORD, S., ARIFIN, N., SCHATZLEIN, A. G. & UCHEGBU, I. F. 2014. Physical characterisation and long-term stability studies on quaternary ammonium palmitoyl glycol chitosan (GCPQ)--a new drug delivery polymer. *J Pharm Sci*, 103, 2296-306.
- CHU, E. & SARTORELLI, A. C. 2015. Cancer chemotherapy. In: KATZUNG, B. G. & TREVOR, A. J. (eds.) *Basic & Clinical Pharmacology*. Thirteenth ed. United States of America: McGraw-Hill Education.
- CHUNG, H., KIM, T. W., KWON, M., KWON, I. C. & JEONG, S. Y. 2001. Oil components modulate physical characteristics and function of the natural oil emulsions as drug or gene delivery system. *Journal of Controlled Release*, 71, 339-350.
- CLARKE, M. F. & FULLER, M. 2006. Stem cells and cancer: two faces of eve. *Cell*, 124, 1111-5.
- COBBY, J., MAYERSOHN, M. & SELLIAH, S. 1977. The rapid reduction of disulfiram in blood and plasma. *J Pharmacol Exp Ther*, 202, 724-31.

- CONTICELLO, C., MARTINETTI, D., ADAMO, L., BUCCHERI, S., GIUFFRIDA, R., PARRINELLO, N., LOMBARDO, L., ANASTASI, G., AMATO, G., CAVALLI, M., CHIARENZA, A., DE MARIA, R., GIUSTOLISI, R., GULISANO, M. & DI RAIMONDO, F. 2012. Disulfiram, an old drug with new potential therapeutic uses for human hematological malignancies. *Int J Cancer*, 131, 2197-203.
- CVEK, B. 2011. Targeting malignancies with disulfiram (Antabuse): multidrug resistance, angiogenesis, and proteasome. *Curr Cancer Drug Targets*, 11, 332-7.
- DAI, L. E. I., LU, C., YU, X. I., DAI, L.-J. & ZHOU, J. X. 2015. Construction of orthotopic xenograft mouse models for human pancreatic cancer. *Experimental and Therapeutic Medicine*, 10, 1033-1038.
- DALLA POZZA, E., DONADELLI, M., COSTANZO, C., ZANIBONI, T., DANDO, I., FRANCHINI, M., ARPICCO, S., SCARPA, A. & PALMIERI, M. 2011. Gemcitabine response in pancreatic adenocarcinoma cells is synergistically enhanced by dithiocarbamate derivatives. *Free Radic Biol Med*, 50, 926-33.
- DANHIER, F., FERON, O. & PRÉAT, V. 2010. To exploit the tumor microenvironment: Passive and active tumor targeting of nanocarriers for anti-cancer drug delivery. *Journal of Controlled Release*, 148, 135-146.
- DAS, D. & LIN, S. 2005. Double-coated poly (butylcyanoacrylate) nanoparticulate delivery systems for brain targeting of dalargin via oral administration. *J Pharm Sci*, 94, 1343-53.
- DE JONG, W. H. & BORM, P. J. 2008. Drug delivery and nanoparticles: applications and hazards. *Int J Nanomedicine*, 3, 133-49.
- DENIZOT, F. & LANG, R. 1986. Rapid colorimetric assay for cell growth and survival. Modifications to the tetrazolium dye procedure giving improved sensitivity and reliability. *J Immunol Methods*, 89, 271-7.
- DERENDORF, H. & MEIBOHM, B. 1999. Modeling of Pharmacokinetic/Pharmacodynamic (PK/PD) Relationships: Concepts and Perspectives. *Pharmaceutical Research*, 16, 176-185.
- DING, Y., CRAVERO, J. D., ADRIAN, K. & GRIPPO, P. 2010. Modeling pancreatic cancer in vivo: from xenograft and carcinogen-induced systems to genetically engineered mice. *Pancreas*, 39, 283-92.
- DINNEN, R. D., MAO, Y., QIU, W., CASSAI, N., SLAVKOVICH, V. N., NICHOLS, G., SU, G. H., BRANDT-RAUF, P. & FINE, R. L. 2013. Redirecting Apoptosis to Aponecrosis Induces Selective Cytotoxicity to Pancreatic Cancer Cells through Increased ROS, Decline in ATP Levels, and VDAC. *American Association for Cancer Research*, 12, 2792-2803.
- DIXON, J. B. 2010. Lymphatic lipid transport: sewer or subway? *Trends in Endocrinology & Metabolism*, 21, 480-487.
- DUAN, X., XIAO, J., YIN, Q., ZHANG, Z., YU, H., MAO, S. & LI, Y. 2013. Smart pH-sensitive and temporal-controlled polymeric micelles for effective combination therapy of doxorubicin and disulfiram. *ACS Nano*, 7, 5858-69.
- DUFOUR, P., LANG, J. M., GIRON, C., DUCLOS, B., HAEHNEL, P., JAECK, D., JUNG, J. M. & OBERLING, F. 1993. Sodium dithiocarb as adjuvant immunotherapy for high risk breast cancer: a randomized study. *Biotherapy*, 6, 9-12.
- DUNCAN, R. & GASPARD, R. 2011. Nanomedicine(s) under the Microscope. *Molecular Pharmaceutics*, 8, 2101-2141.
- DWYER, C., VIEBKE, C. & MEADOWS, J. 2005. Propofol induced micelle formation in aqueous block copolymer solutions. *Colloids and Surfaces A: Physicochemical and Engineering Aspects*, 254, 23-30.
- ECCLESTON, G. M. 2013. Emulsions and creams. In: AULTON, M. E. & TAYLOR, K. M. G. (eds.) *Aulton's Pharmaceutics; The Design and Manufacture of Medicines*. Fourth ed.: Churchill Livingstone
- ELLERHORST, J. A., BEDIKIAN, A., RING, S., BUZAID, A. C., ETON, O. & LEGHA, S. S. 1999. Phase II trial of doxil for patients with metastatic melanoma refractory to frontline therapy. *Oncol Rep*, 6, 1097-9.
- ENEANYA, D. I., BIANCHINE, J. R., DURAN, D. O. & ANDRESEN, B. D. 1981. The actions of metabolic fate of disulfiram. *Annu Rev Pharmacol Toxicol*, 21, 575-96.

- ENSIGN, L. M., CONE, R. & HANES, J. 2012. Oral drug delivery with polymeric nanoparticles: The gastrointestinal mucus barriers. *Advanced Drug Delivery Reviews*, 64, 557-570.
- EVANS, R. G., ENGEL, C., WHEATLEY, C. & NIELSEN, J. 1982. Modification of the sensitivity and repair of potentially lethal damage by diethyldithiocarbamate during and following exposure of plateau-phase cultures of mammalian cells to radiation and cis-diamminedichloroplatinum(II). *Cancer Res*, 42, 3074-8.
- FAIMAN, M. D., ARTMAN, L. & HAYA, K. 1980. Disulfiram distribution and elimination in the rat after oral and intraperitoneal administration. *Alcohol Clin Exp Res*, 4, 412-9.
- FAIMAN, M. D., ARTMAN, L. & MAZIASZ, T. 1983. Diethyldithiocarbamic acid-methyl ester distribution, elimination, and LD50 in the rat after intraperitoneal administration. *Alcohol Clin Exp Res*, 7, 307-11.
- FAIMAN, M. D., DODD, D. E. & HANZLIK, R. E. 1978. Distribution of S35 disulfiram and metabolites in mice, and metabolism of S35 disulfiram in the dog. *Res Commun Chem Pathol Pharmacol*, 21, 543-67.
- FAIMAN, M. D., JENSEN, J. C. & LACOURSIERE, R. B. 1984. Elimination kinetics of disulfiram in alcoholics after single and repeated doses. *Clin Pharmacol Ther*, 36, 520-6.
- FAIMAN, M. D., KAUL, S., LATIF, S. A., WILLIAMS, T. D. & LUNTE, C. E. 2013. S-(N, N-diethylcarbamoyl)glutathione (carbamathione), a disulfiram metabolite and its effect on nucleus accumbens and prefrontal cortex dopamine, GABA, and glutamate: a microdialysis study. *Neuropharmacology*, 75, 95-105.
- FAROKHZAD, O. C. & LANGER, R. 2009. Impact of Nanotechnology on Drug Delivery. *ACS Nano*, 3, 16-20.
- FASEHEE, H., ZARRINRAD, G., TAVANGAR, S. M., GHAFFARI, S. H. & FAGHIHI, S. 2016a. The inhibitory effect of disulfiram encapsulated PLGA NPs on tumor growth: Different administration routes. *Materials Science and Engineering: C*, 63, 587-595.
- FASEHEE, H., ZARRINRAD, G., TAVANGAR, S. M., GHAFFARI, S. H. & FAGHIHI, S. 2016b. The inhibitory effect of disulfiram encapsulated PLGA NPs on tumor growth: Different administration routes. *Mater Sci Eng C Mater Biol Appl*, 63, 587-95.
- FASSAS, A. & ANAGNOSTOPOULOS, A. 2005. The use of liposomal daunorubicin (DaunoXome) in acute myeloid leukemia. *Leuk Lymphoma*, 46, 795-802.
- FDA. 2015. *Select Committee on GRAS Substances (SCOGS) Opinion: Copper (cupric) gluconate, Copper (cupric) sulfate, Cuprous iodide* [Online]. Available: <http://www.fda.gov/food/ingredientspackaginglabeling/gras/scogs/ucm261260.htm>.
- FERRARI, M. 2005. Cancer nanotechnology: opportunities and challenges. *Nat Rev Cancer*, 5, 161-71.
- FIALKOW, P. J. 1990. Stem cell origin of human myeloid blood cell neoplasms. *Verh Dtsch Ges Pathol*, 74, 43-7.
- FIDLER, I. J. 1986. Rationale and methods for the use of nude mice to study the biology and therapy of human cancer metastasis. *Cancer and Metastasis Reviews*, 5, 29-49.
- FOOD AND DRUG ADMINISTRATION 2001. Guidance for Industry: Bioanalytical Method Validation. *US Department of Health and Human Services, Food and Drug Administration, Center for Drug Evaluation and Research*. Rockville, MD.
- FORMAN, D. & FERLAY, J. 2014. The global and regional burden of cancer. In: STEWART, B. W. & WILD, C. P. (eds.) *World Cancer Report 2014*. Lyon, France: International Agency for Research on Cancer.
- FUGUET, E., RÀFOLS, C., ROSÉS, M. & BOSCH, E. 2005. Critical micelle concentration of surfactants in aqueous buffered and unbuffered systems. *Analytica Chimica Acta*, 548, 95-100.
- GALKIN, A., KULAKOVA, L., LIM, K., CHEN, C. Z., ZHENG, W., TURKO, I. V. & HERZBERG, O. 2014. Structural basis for inactivation of Giardia lamblia carbamate kinase by disulfiram. *J Biol Chem*, 289, 10502-9.
- GANTA, S. & AMIJI, M. 2009. Coadministration of Paclitaxel and Curcumin in Nanoemulsion Formulations To Overcome Multidrug Resistance in Tumor Cells. *Molecular Pharmaceutics*, 6, 928-939.
- GARRETT, N. L., LALATSA, A., UCHEGBU, I., SCHÄTZLEIN, A. & MOGER, J. 2012. Exploring uptake mechanisms of oral nanomedicines using multimodal nonlinear optical microscopy. *Journal of Biophotonics*, 5, 458-468.

- GINESTIER, C., HUR, M. H., CHARAFE-JAUFFRET, E., MONVILLE, F., DUTCHER, J., BROWN, M., JACQUEMIER, J., VIENS, P., KLEER, C. G., LIU, S., SCHOTT, A., HAYES, D., BIRNBAUM, D., WICHA, M. S. & DONTU, G. 2007. ALDH1 is a marker of normal and malignant human mammary stem cells and a predictor of poor clinical outcome. *Cell Stem Cell*, 1, 555-67.
- GOTHWAL, A., KHAN, I. & GUPTA, U. 2016. Polymeric Micelles: Recent Advancements in the Delivery of Anticancer Drugs. *Pharmaceutical Research*, 33, 18-39.
- GOULET, O., ANTEBI, H., WOLF, C., TALBOTEC, C., ALCINDOR, L. G., CORRIOL, O., LAMOR, M. & COLOMB-JUNG, V. 2010. A new intravenous fat emulsion containing soybean oil, medium-chain triglycerides, olive oil, and fish oil: a single-center, double-blind randomized study on efficacy and safety in pediatric patients receiving home parenteral nutrition. *JPEN J Parenter Enteral Nutr*, 34, 485-95.
- GRAMATTE, T., EL DESOKY, E. & KLOTZ, U. 1994. Site-dependent small intestinal absorption of ranitidine. *Eur J Clin Pharmacol*, 46, 253-9.
- GREEN, M. R., MANIKHAS, G. M., ORLOV, S., AFANASYEV, B., MAKHSON, A. M., BHAR, P. & HAWKINS, M. J. 2006. Abraxane, a novel Cremophor-free, albumin-bound particle form of paclitaxel for the treatment of advanced non-small-cell lung cancer. *Ann Oncol*, 17, 1263-8.
- GREGORIADIS, G. & FLORENCE, A. T. 1993. Recent advances in drug targeting. *Trends in Biotechnology*, 11, 440-442.
- GUERRA, C. & BARBACID, M. 2013. Genetically engineered mouse models of pancreatic adenocarcinoma. *Molecular Oncology*, 7, 232-247.
- GUILLAUMIN, J. M., LEPAPE, A. & RENOUX, G. 1986. Fate and distribution of radioactive sodium diethyldithiocarbamate (Imuthiol) in the mouse. *Int J Immunopharmacol*, 8, 859-65.
- GUO, X., XU, B., PANDEY, S., GOESSL, E., BROWN, J., ARMESILLA, A. L., DARLING, J. L. & WANG, W. 2010. Disulfiram/copper complex inhibiting NFkappaB activity and potentiating cytotoxic effect of gemcitabine on colon and breast cancer cell lines. *Cancer Lett*, 290, 104-13.
- GUPTE, A. & MUMPER, R. J. 2009. Elevated copper and oxidative stress in cancer cells as a target for cancer treatment. *Cancer Treatment Reviews*, 35, 32-46.
- HALL, J. B., DOBROVOLSKAIA, M. A., PATRI, A. K. & MCNEIL, S. E. 2007. Characterization of nanoparticles for therapeutics. *Nanomedicine (Lond)*, 2, 789-803.
- HALMA, C., DAHA, M. R. & VAN ES, L. A. 1992. In vivo clearance by the mononuclear phagocyte system in humans: an overview of methods and their interpretation. *Clinical and Experimental Immunology*, 89, 1-7.
- HAN, J., LIU, L., YUE, X., CHANG, J., SHI, W. & HUA, Y. 2013. A binuclear complex constituted by diethyldithiocarbamate and copper(I) functions as a proteasome activity inhibitor in pancreatic cancer cultures and xenografts. *Toxicol Appl Pharmacol*, 273, 477-83.
- HANSCH, C., LEO, A. & HOEKMAN, D. H. 1995. Exploring QSAR, Hydrophobic, Electronic and Steric Constants. *American Chemical Society, Washington, DC, USA*, pg 80.
- HART, B. W. & FAIMAN, M. D. 1992. In vitro and in vivo inhibition of rat liver aldehyde dehydrogenase by S-methyl N,N-diethylthiolcarbamate sulfoxide, a new metabolite of disulfiram. *Biochem Pharmacol*, 43, 403-6.
- HART, B. W. & FAIMAN, M. D. 1994. In vivo pharmacodynamic studies of the disulfiram metabolite S-methyl N,N-diethylthiolcarbamate sulfoxide: inhibition of liver aldehyde dehydrogenase. *Alcohol Clin Exp Res*, 18, 340-5.
- HERMANN, P. C., HUBER, S. L., HERRLER, T., AICHER, A., ELLWART, J. W., GUBA, M., BRUNS, C. J. & HEESCHEN, C. 2007. Distinct populations of cancer stem cells determine tumor growth and metastatic activity in human pancreatic cancer. *Cell Stem Cell*, 1, 313-23.
- HIDALGO, M. 2010. Pancreatic Cancer. *New England Journal of Medicine*, 362, 1605-1617.
- HOCHREITER, J., MCCANCE-KATZ, E. F., LAPHAM, J., MA, Q. & MORSE, G. D. 2012. Disulfiram metabolite S-methyl-N,N-diethylthiocarbamate quantitation in human plasma with reverse phase ultra performance liquid chromatography and mass spectrometry. *J Chromatogr B Analyt Technol Biomed Life Sci*, 897, 80-4.

- HODA, M., PAJANIRADJE, S., SHAKYA, G., MOHANKUMAR, K. & RAJAGOPALAN, R. 2016. Anti-proliferative and apoptosis-triggering potential of disulfiram and disulfiram-loaded polysorbate 80-stabilized PLGA nanoparticles on hepatocellular carcinoma Hep3B cell line. *Nanomedicine*, 12, 1641-50.
- HODA, M., SUFI, S. A., SHAKYA, G., KUMAR, K. M. & RAJAGOPALAN, R. 2015. Influence of stabilizers on the production of disulfiram-loaded poly(lactic-co-glycolic acid) nanoparticles and their anticancer potential. *Therapeutic Delivery*, 6, 17-25.
- HOTHI, P., MARTINS, T. J., CHEN, L., DELEYROLLE, L., YOON, J. G., REYNOLDS, B. & FOLTZ, G. 2012. High-throughput chemical screens identify disulfiram as an inhibitor of human glioblastoma stem cells. *Oncotarget*, 3, 1124-36.
- HUANG, H., CAO, K., MALIK, S., ZHANG, Q., LI, D., CHANG, R., WANG, H., LIN, W., VAN DOREN, J., ZHANG, K., DU, Z. & ZHENG, X. 2015. Combination of 12-O-tetradecanoylphorbol-13-acetate with diethyldithiocarbamate markedly inhibits pancreatic cancer cell growth in 3D culture and in immunodeficient mice. *Int J Mol Med*, 35, 1617-24.
- HUYNH, A. S., ABRAHAMS, D. F., TORRES, M. S., BALDWIN, M. K., GILLIES, R. J. & MORSE, D. L. 2011. Development of an orthotopic human pancreatic cancer xenograft model using ultrasound guided injection of cells. *PLoS One*, 6, e20330.
- ILLUM, L., DAVIS, S. S., WILSON, C. G., THOMAS, N. W., FRIER, M. & HARDY, J. G. 1982. Blood clearance and organ deposition of intravenously administered colloidal particles. The effects of particle size, nature and shape. *Int J Pharm*, 12, 135-146.
- ITO, Y., CAI, H., KOIZUMI, Y., NAKAO, M. & TERAOKA, M. 1999. Correlation between prevention of cataract development by disulfiram and fates of selenium in selenite-treated rats. *Curr Eye Res*, 18, 292-9.
- JAIN, R. K. 1987. Transport of molecules in the tumor interstitium: a review. *Cancer Res*, 47, 3039-51.
- JAIN, R. K. 1997. Delivery of molecular and cellular medicine to solid tumors. *Adv Drug Deliv Rev*, 46, 149-68.
- JAMES, T. L. 1998. Chapter 1, Fundamentals of NMR. 1-31.
- JENSEN, J. C. & FAIMAN, M. D. 1980. Determination of disulfiram and metabolites from biological fluids by high-performance liquid chromatography. *J Chromatogr*, 181, 407-16.
- JIANG, F., QIU, Q., KHANNA, A., TODD, N. W., DEEPAK, J., XING, L., WANG, H., LIU, Z., SU, Y., STASS, S. A. & KATZ, R. L. 2009. Aldehyde dehydrogenase 1 is a tumor stem cell-associated marker in lung cancer. *Mol Cancer Res*, 7, 330-8.
- JIMENO, A., FELDMANN, G., SUAREZ-GAUTHIER, A., RASHEED, Z., SOLOMON, A., ZOU, G. M., RUBIO-VIQUEIRA, B., GARCIA-GARCIA, E., LOPEZ-RIOS, F., MATSUI, W., MAITRA, A. & HIDALGO, M. 2009. A direct pancreatic cancer xenograft model as a platform for cancer stem cell therapeutic development. *Mol Cancer Ther*, 8, 310-4.
- JOHANSSON, B. 1988. Stabilization and quantitative determination of disulfiram in human plasma samples. *Clin Chim Acta*, 177, 55-63.
- JOHANSSON, B. 1992. A review of the pharmacokinetics and pharmacodynamics of disulfiram and its metabolites. *Acta Psychiatr Scand Suppl*, 369, 15-26.
- JOHANSSON, B. & STANKIEWICZ, Z. 1985. Bis-(diethyldithiocarbamate) copper complex: a new metabolite of disulfiram? *Biochem Pharmacol*, 34, 2989-91.
- JONES, C. & MULLOY, B. 1993. Introduction to Nuclear Magnetic Resonance. In: JONES, C., MULLOY, B. & THOMAS, A. H. (eds.) *Spectroscopic Methods and Analyses: NMR, Mass Spectrometry, and Metalloprotein Techniques*. Totowa, NJ: Humana Press.
- JONES, M.-C. & LEROUX, J.-C. 1999. Polymeric micelles – a new generation of colloidal drug carriers. *European Journal of Pharmaceutics and Biopharmaceutics*, 48, 101-111.
- KANG, J.-S. 2012. *Principles and Applications of LC-MS/MS for the Quantitative Bioanalysis of Analytes in Various Biological Samples*, InTech.
- KAPLAN, C. S., PETERSEN, E. A., YOCUM, D. & HERSH, E. M. 1989. A randomized, controlled dose response study of intravenous sodium diethyldithiocarbamate in patients with advanced human immunodeficiency virus infection. *Life Sci*, 45, iii-ix.

- KIM, J. Y., CHO, Y., OH, E., LEE, N., AN, H., SUNG, D., CHO, T.-M. & SEO, J. H. 2016. Disulfiram targets cancer stem-like properties and the HER2/Akt signaling pathway in HER2-positive breast cancer. *Cancer Letters*, 379, 39-48.
- KIM, M. P., EVANS, D. B., WANG, H., ABBRUZZESE, J. L., FLEMING, J. B. & GALLICK, G. E. 2009. Generation of orthotopic and heterotopic human pancreatic cancer xenografts in immunodeficient mice. *Nat. Protocols*, 4, 1670-1680.
- KIM, S. K., KIM, H., LEE, D. H., KIM, T. S., KIM, T., CHUNG, C., KOH, G. Y. & LIM, D. S. 2013. Reversing the intractable nature of pancreatic cancer by selectively targeting ALDH-high, therapy-resistant cancer cells. *PLoS One*, 8, e78130.
- KITSON, T. M. 1976. The effect of some analogues of disulfiram on the aldehyde dehydrogenases of sheep liver. *Biochem J*, 155, 445-8.
- KUMAR, M. N. V. R., MUZZARELLI, R. A. A., MUZZARELLI, C., SASHIWA, H. & DOMB, A. J. 2004. Chitosan Chemistry and Pharmaceutical Perspectives. *Chemical Reviews*, 104, 6017-6084.
- LALATSA, A., GARRETT, N. L., FERRARELLI, T., MOGER, J., SCHATZLEIN, A. G. & UCHEGBU, I. F. 2012a. Delivery of peptides to the blood and brain after oral uptake of quaternary ammonium palmitoyl glycol chitosan nanoparticles. *Mol Pharm*, 9, 1764-74.
- LALATSA, A., LEE, V., MALKINSON, J. P., ZLOH, M., SCHATZLEIN, A. G. & UCHEGBU, I. F. 2012b. A prodrug nanoparticle approach for the oral delivery of a hydrophilic peptide, leucine(5)-enkephalin, to the brain. *Mol Pharm*, 9, 1665-80.
- LALATSA, A., SCHATZLEIN, A. G., MAZZA, M., LE, T. B. & UCHEGBU, I. F. 2012c. Amphiphilic poly(L-amino acids) - new materials for drug delivery. *J Control Release*, 161, 523-36.
- LAPIDOT, T., SIRARD, C., VORMOOR, J., MURDOCH, B., HOANG, T., CACERES-CORTES, J., MINDEN, M., PATERSON, B., CALIGIURI, M. A. & DICK, J. E. 1994. A cell initiating human acute myeloid leukaemia after transplantation into SCID mice. *Nature*, 367, 645-648.
- LASSER, A. 1983. The mononuclear phagocytic system: A review. *Human Pathology*, 14, 108-126.
- LEHR, C.-M., BOUWSTRA, J. A., SCHACHT, E. H. & JUNGINGER, H. E. 1992. In vitro evaluation of mucoadhesive properties of chitosan and some other natural polymers. *International Journal of Pharmaceutics*, 78, 43-48.
- LEWISON, E. F. 1977. Spontaneous regression of breast cancer. *Prog Clin Biol Res*, 12, 47-53.
- LI, T., SU, Y., MEI, Y., LENG, Q., LENG, B., LIU, Z., STASS, S. A. & JIANG, F. 2010. ALDH1A1 is a marker for malignant prostate stem cells and predictor of prostate cancer patients' outcome. *Lab Invest*, 90, 234-44.
- LIKAVČAN, L., KOŠÍK, M., BÍLIK, J. & MARTINKOVIČ, M. 2014. Determination of Apparent Viscosity as Function of Shear Rate and Fibres Fraction in Polypropylene.
- LIN, J., HAFFNER, M. C., ZHANG, Y., LEE, B. H., BRENNEN, W. N., BRITTON, J., KACHHAP, S. K., SHIM, J. S., LIU, J. O., NELSON, W. G., YEGNASUBRAMANIAN, S. & CARDUCCI, M. A. 2011. Disulfiram is a DNA demethylating agent and inhibits prostate cancer cell growth. *Prostate*, 71, 333-43.
- LIN, P. S., KWOCK, L. & BUTTERFIELD, C. E. 1979. Diethyldithiocarbamate enhancement of radiation and hyperthermic effects on Chinese hamster cells in vitro. *Radiat Res*, 77, 501-11.
- LINDAHL, A., UNGELL, A. L., KNUTSON, L. & LENNERNÅS, H. (1997) Characterization of fluids from the stomach and proximal jejunum in men and women. *Pharmaceutical Research*, 14, 497-502.
- LIU, J., SHIGENAGA, M. K., YAN, L. J., MORI, A. & AMES, B. N. 1996. Antioxidant activity of diethyldithiocarbamate. *Free Radic Res*, 24, 461-72.
- LIU, P., BROWN, S., GOKTUG, T., CHANNATHODIYIL, P., KANNAPPAN, V., HUGNOT, J. P., GUICHET, P. O., BIAN, X., ARMESILLA, A. L., DARLING, J. L. & WANG, W. 2012. Cytotoxic effect of disulfiram/copper on human glioblastoma cell lines and ALDH-positive cancer-stem-like cells. *Br J Cancer*, 107, 1488-97.
- LIU, P., KUMAR, I. S., BROWN, S., KANNAPPAN, V., TAWARI, P. E., TANG, J. Z., JIANG, W., ARMESILLA, A. L., DARLING, J. L. & WANG, W. 2013. Disulfiram targets cancer

- stem-like cells and reverses resistance and cross-resistance in acquired paclitaxel-resistant triple-negative breast cancer cells. *Br J Cancer*, 109, 1876-85.
- LIU, P., WANG, Z., BROWN, S., KANNAPPAN, V., TAWARI, P. E., JIANG, W., IRACHE, J. M., TANG, J. Z., ARMESILLA, A. L., DARLING, J. L., TANG, X. & WANG, W. 2014. Liposome encapsulated Disulfiram inhibits NFkappaB pathway and targets breast cancer stem cells in vitro and in vivo. *Oncotarget*, 5, 7471-85.
- LÖBLER, M., ROHM, H. W., SCHMITZ, K.-P., JOHNSTON, A. H., NEWMAN, T. A., RANJAN, S., SOOD, R. & KINNUNEN, P. K. J. 2009. Drug delivery by nanoparticles — facing the obstacles. In: VANDER SLOTEN, J., VERDONCK, P., NYSSSEN, M. & HAUEISEN, J. (eds.) *4th European Conference of the International Federation for Medical and Biological Engineering: ECIFMBE 2008 23–27 November 2008 Antwerp, Belgium*. Berlin, Heidelberg: Springer Berlin Heidelberg.
- LOBO, N. A., SHIMONO, Y., QIAN, D. & CLARKE, M. F. 2007. The biology of cancer stem cells. *Annu Rev Cell Dev Biol*, 23, 675-99.
- LOO, T. W., BARTLETT, M. C. & CLARKE, D. M. 2004. Disulfiram metabolites permanently inactivate the human multidrug resistance P-glycoprotein. *Mol Pharm*, 1, 426-33.
- LOO, T. W. & CLARKE, D. M. 2000. Blockage of drug resistance in vitro by disulfiram, a drug used to treat alcoholism. *J Natl Cancer Inst*, 92, 898-902.
- LÓPEZ-DÁVILA, V., MAGDELDIN, T., WELCH, H., DWEK, M. V., UCHEGBU, I. & LOIZIDOU, M. 2016. Efficacy of DOPE/DC-cholesterol liposomes and GCPQ micelles as AZD6244 nanocarriers in a 3D colorectal cancer in vitro model. *Nanomedicine*, 11, 331-344.
- LOVELYN, C. & ATTAMA, A. A. 2011. Current state of nanoemulsions in drug delivery. *Journal of Biomaterials and Nanobiotechnology*, 2, 626-639.
- LUN, X., WELLS, J. C., GRINSHTEIN, N., KING, J. C., HAO, X., DANG, N. H., WANG, X., AMAN, A., UEHLING, D., DATTI, A., WRANA, J. L., EASAW, J. C., LUCHMAN, A., WEISS, S., CAIRNCROSS, J. G., KAPLAN, D. R., ROBBINS, S. M. & SENGER, D. L. 2016. Disulfiram when Combined with Copper Enhances the Therapeutic Effects of Temozolomide for the Treatment of Glioblastoma. *Clin Cancer Res*, 22, 3860-75.
- MA, S., CHAN, K. W., LEE, T. K., TANG, K. H., WO, J. Y., ZHENG, B. J. & GUAN, X. Y. 2008. Aldehyde dehydrogenase discriminates the CD133 liver cancer stem cell populations. *Mol Cancer Res*, 6, 1146-53.
- MADDAMS, J., UTLEY, M. & MØLLER, H. 2012. Projections of cancer prevalence in the United Kingdom, 2010–2040. *British Journal of Cancer*, 107, 1195-1202.
- MADEIRA, P. J. A. & FLORÊNCIO, M. H. 2012. *Applications of Tandem Mass Spectrometry: From Structural Analysis to Fundamental Studies*, InTech.
- MAEDA, H. 1992. The tumor blood vessel as an ideal target for macromolecular anticancer agents. *Journal of Controlled Release*, 19, 315-324.
- MALKA, F., DAIROU, J., RAGUNATHAN, N., DUPRET, J. M. & RODRIGUES-LIMA, F. 2009. Mechanisms and kinetics of human arylamine N-acetyltransferase 1 inhibition by disulfiram. *FEBS J*, 276, 4900-8.
- MARCATO, P., DEAN, C. A., GIACOMANTONIO, C. A. & LEE, P. W. 2011. Aldehyde dehydrogenase: its role as a cancer stem cell marker comes down to the specific isoform. *Cell Cycle*, 10, 1378-84.
- MARIKOVSKY, M., NEVO, N., VADAI, E. & HARRIS-CERRUTI, C. 2002. Cu/Zn superoxide dismutase plays a role in angiogenesis. *Int J Cancer*, 97, 34-41.
- MARQUES, M. R., LOEBENBERG, R. & ALMUKAINZI, M. 2011. Simulated biological fluids with possible application in dissolution testing. *Dissolution Technol*, 18, 15-28.
- MARTIN, L., WILSON, C. G., KOOSHA, F., TETLEY, L., GRAY, A. I., SENEL, S. & UCHEGBU, I. F. 2002. The release of model macromolecules may be controlled by the hydrophobicity of palmitoyl glycol chitosan hydrogels. *J Control Release*, 80, 87-100.
- MCCLEMENTS, D. J. 2012. Nanoemulsions versus microemulsions: terminology, differences, and similarities. *Soft Matter*, 8, 1719-1729.
- MEIBOHM, B. & DERENDORF, H. 1997. Basic concepts of pharmacokinetic/pharmacodynamic (PK/PD) modelling. *Int J Clin Pharmacol Ther*, 35, 401-13.

- MENNINI, N., FURLANETTO, S., BRAGAGNI, M., GHELARDINI, C., DI CESARE MANNELLI, L. & MURA, P. 2014. Development of a chitosan-derivative micellar formulation to improve celecoxib solubility and bioavailability. *Drug Dev Ind Pharm*, 40, 1494-502.
- MEYER, V. R. 2006. Introduction. *Practical High-Performance Liquid Chromatography*. John Wiley & Sons, Ltd.
- MISRA, R., ACHARYA, S. & SAHOO, S. K. 2010. Cancer nanotechnology: application of nanotechnology in cancer therapy. *Drug Discov Today*, 15, 842-50.
- MIYATA, K., CHRISTIE, R. J. & KATAOKA, K. 2011. Polymeric micelles for nano-scale drug delivery. *Reactive and Functional Polymers*, 71, 227-234.
- MOGHIMI, S. M., HUNTER, A. C. & MURRAY, J. C. 2001. Long-Circulating and Target-Specific Nanoparticles: Theory to Practice. *Pharmacological Reviews*, 53, 283-318.
- MOGHIMI, S. M., HUNTER, A. C. & MURRAY, J. C. 2005. Nanomedicine: current status and future prospects. *FASEB J*, 19, 311-30.
- MOHAN, P. & RAPOPORT, N. 2010. Doxorubicin as a Molecular Nanotheranostic Agent: Effect of Doxorubicin Encapsulation in Micelles or Nanoemulsions on the Ultrasound-Mediated Intracellular Delivery and Nuclear Trafficking. *Molecular Pharmaceutics*, 7, 1959-1973.
- MONOPOLI, M. P., WALCZYK, D., CAMPBELL, A., ELIA, G., LYNCH, I., BOMBELLI, F. B. & DAWSON, K. A. 2011. Physical-chemical aspects of protein corona: relevance to in vitro and in vivo biological impacts of nanoparticles. *J Am Chem Soc*, 133, 2525-34.
- MOORE, J. C. 1964. Gel permeation chromatography. I. A new method for molecular weight distribution of high polymers. *Journal of Polymer Science Part A: General Papers*, 2, 835-843.
- MOSMANN, T. 1983. Rapid colorimetric assay for cellular growth and survival: Application to proliferation and cytotoxicity assays. *Journal of Immunological Methods*, 65, 55-63.
- MUZIO, G., MAGGIORA, M., PAIUZZI, E., ORALDI, M. & CANUTO, R. A. 2012. Aldehyde dehydrogenases and cell proliferation. *Free Radic Biol Med*, 52, 735-46.
- NAGENDRA, S. N., FAIMAN, M. D., DAVIS, K., WU, J. Y., NEWBY, X. & SCHLOSS, J. V. 1997. Carbamylation of brain glutamate receptors by a disulfiram metabolite. *J Biol Chem*, 272, 24247-51.
- NAIR, L. S. & LAURENCIN, C. T. 2007. Biodegradable polymers as biomaterials. *Progress in Polymer Science*, 32, 762-798.
- NGAN, C. L., BASRI, M., TRIPATHY, M., ABEDI KARJIBAN, R. & ABDUL-MALEK, E. 2014. Physicochemical Characterization and Thermodynamic Studies of Nanoemulsion-Based Transdermal Delivery System for Fullerene. *The Scientific World Journal*, 2014, 12.
- NIE, S. 2010. Understanding and overcoming major barriers in cancer nanomedicine. *Nanomedicine (London, England)*, 5, 523-528.
- NING, Y. C. 2005. An Introduction to Nuclear Magnetic Resonance. *Structural identification of organic compounds with spectroscopic techniques*. Wiley-VCH.
- NOBEL, C. S., BURGESS, D. H., ZHIVOTOVSKY, B., BURKITT, M. J., ORRENIUS, S. & SLATER, A. F. 1997. Mechanism of dithiocarbamate inhibition of apoptosis: thiol oxidation by dithiocarbamate disulfides directly inhibits processing of the caspase-3 proenzyme. *Chem Res Toxicol*, 10, 636-43.
- OBERLE, R. L. & AMIDON, G. L. 1987. The influence of variable gastric emptying and intestinal transit rates on the plasma level curve of cimetidine; an explanation for the double peak phenomenon. *J Pharmacokinet Biopharm*, 15, 529-44.
- OKADA, M. 2002. Chemical syntheses of biodegradable polymers. *Progress in Polymer Science*, 27, 87-133.
- OWENS, D. E. & PEPPAS, N. A. 2006. Opsonization, biodistribution, and pharmacokinetics of polymeric nanoparticles. *Int J Pharm*, 307, 93-102.
- PAL, R. 1999. Yield stress and viscoelastic properties of high internal phase ratio emulsions. *Colloid and Polymer Science*, 277, 583-588.
- PANG, H., CHEN, D., CUI, Q. C. & DOU, Q. P. 2007. Sodium diethyldithiocarbamate, an AIDS progression inhibitor and a copper-binding compound, has proteasome-inhibitory and apoptosis-inducing activities in cancer cells. *Int J Mol Med*, 19, 809-16.

- PATHAK, Y. 2009. Recent Developments in Nanoparticulate Drug Delivery Systems. *Drug Delivery Nanoparticles Formulation and Characterization*. New York: Informa Healthcare.
- PETROS, R. A. & DESIMONE, J. M. 2010. Strategies in the design of nanoparticles for therapeutic applications. *Nat Rev Drug Discov*, 9, 615-627.
- PISKIN, E. 1995. Biodegradable polymers as biomaterials. *Journal of Biomaterials Science, Polymer Edition*, 6, 775-795.
- QU, X., KHUTORYANSKIY, V. V., STEWART, A., RAHMAN, S., PAPAHAADJOPOULOS-STERNBERG, B., DUFES, C., MCCARTHY, D., WILSON, C. G., LYONS, R., CARTER, K. C., SCHATZLEIN, A. & UCHEGBU, I. F. 2006. Carbohydrate-based micelle clusters which enhance hydrophobic drug bioavailability by up to 1 order of magnitude. *Biomacromolecules*, 7, 3452-9.
- RAHMAN, M., LAURENT, S., TAWIL, N., YAHIA, L. H. & MAHMOUDI, M. 2013. Nanoparticle and Protein Corona. *Protein-Nanoparticle Interactions: The Bio-Nano Interface*. Berlin, Heidelberg: Springer Berlin Heidelberg.
- RAPOPORT, N. 2007. Physical stimuli-responsive polymeric micelles for anti-cancer drug delivery. *Progress in Polymer Science*, 32, 962-990.
- RASHEED, Z. A., YANG, J., WANG, Q., KOWALSKI, J., FREED, I., MURTER, C., HONG, S. M., KOORSTRA, J. B., RAJESHKUMAR, N. V., HE, X., GOGGINS, M., IACOBUZIO-DONAHUE, C., BERMAN, D. M., LAHERU, D., JIMENO, A., HIDALGO, M., MAITRA, A. & MATSUI, W. 2010. Prognostic significance of tumorigenic cells with mesenchymal features in pancreatic adenocarcinoma. *J Natl Cancer Inst*, 102, 340-51.
- RASPER, M., SCHAFER, A., PIONTEK, G., TEUFEL, J., BROCKHOFF, G., RINGEL, F., HEINDL, S., ZIMMER, C. & SCHLEGEL, J. 2010. Aldehyde dehydrogenase 1 positive glioblastoma cells show brain tumor stem cell capacity. *Neuro Oncol*, 12, 1024-33.
- REYA, T., MORRISON, S. J., CLARKE, M. F. & WEISSMAN, I. L. 2001. Stem cells, cancer, and cancer stem cells. *Nature*, 414, 105-11.
- REZK, Y. A., YANG, K., BAI, S., MCLEAN, K., JOHNSTON, C., REYNOLDS, R. K. & BUCKANOVICH, R. J. 2015. Disulfiram's Antineoplastic Effects on Ovarian Cancer. *Journal of Cancer Therapy*, Vol.06No.14, 10.
- RINAUDO, M. 2006. Chitin and chitosan: Properties and applications. *Progress in Polymer Science*, 31, 603-632.
- ROBERTS, M. S., MAGNUSSON, B. M., BURCZYNSKI, F. J. & WEISS, M. 2002. Enterohepatic Circulation. *Clinical Pharmacokinetics*, 41, 751-790.
- ROBINSON, T., PAI, M., LIU, J., VIZEACOUMAR, F., SUN, T., EGAN, S., DATTI, A., HUANG, J. & ZACKSENHAUS, E. 2013. High-throughput screen identifies disulfiram as a potential therapeutic for triple-negative breast cancer cells: Interaction with IQ motif-containing factors. *Cell Cycle*, 12, 3013-3024.
- ROSER, M., FISCHER, D. & KISSEL, T. 1998. Surface-modified biodegradable albumin nano- and microspheres. II: effect of surface charges on in vitro phagocytosis and biodistribution in rats. *Eur J Pharm Biopharm*, 46, 255-63.
- ROVIRA, M., SCOTT, S. G., LISS, A. S., JENSEN, J., THAYER, S. P. & LEACH, S. D. 2010. Isolation and characterization of centroacinar/terminal ductal progenitor cells in adult mouse pancreas. *Proc Natl Acad Sci U S A*, 107, 75-80.
- ROWE, R. C., SHESKEY, P. J. & OWEN, S. C. 2006. *Handbook of pharmaceutical excipients*, London, Pharmaceutical Press.
- SAHOO, S. K. & LABHASETWAR, V. 2003. Nanotech approaches to drug delivery and imaging. *Drug Discovery Today*, 8, 1112-1120.
- SAHOO, S. K., PARVEEN, S. & PANDA, J. J. 2007. The present and future of nanotechnology in human health care. *Nanomedicine: Nanotechnology, Biology and Medicine*, 3, 20-31.
- SAINZ, V., CONNIOT, J., MATOS, A. I., PERES, C., ZUPANÓIO, E., MOURA, L., SILVA, L. C., FLORINDO, H. F. & GASPAR, R. S. 2015. Regulatory aspects on nanomedicines. *Biochemical and Biophysical Research Communications*, 468, 504-510.
- SAVJANI, K. T., GAJJAR, A. K. & SAVJANI, J. K. 2012. Drug solubility: importance and enhancement techniques. *ISRN Pharm*, 2012, 195727.

- SCAPPATICCI, B., SOUBEYRAND, J., ROUSSEAU-TSANGARIS, M., DESAGE, M., BRAZIER, J. L. & COQUET, B. 1990. Determination of sodium diethyldithiocarbamate (Imuthiol) and its S-methyl metabolite by gas chromatography-mass spectrometry. Use of deuteromethyl iodide derivatization. *J Chromatogr*, 534, 57-66.
- SCHRAMM, L. L. 2006. Colloid Stability. *Emulsions, Foams, and Suspensions*. Wiley-VCH Verlag GmbH & Co. KGaA.
- SCHRECK, R., MEIER, B., MANNEL, D. N., DROGE, W. & BAEUERLE, P. A. 1992. Dithiocarbamates as potent inhibitors of nuclear factor kappa B activation in intact cells. *J Exp Med*, 175, 1181-94.
- SERRANO, D. R., LALATSA, A., DEA-AYUELA, M. A., BILBAO-RAMOS, P. E., GARRETT, N. L., MOGER, J., GUARRO, J., CAPILLA, J., BALLESTEROS, M. P., SCHÄTZLEIN, A. G., BOLÁS, F., TORRADO, J. J. & UCHEGBU, I. F. 2015. Oral Particle Uptake and Organ Targeting Drives the Activity of Amphotericin B Nanoparticles. *Mol Pharm*, 12, 420-431.
- SHAH, D. T., WALKER, E. M., JR., JONES, M. M., SINGH, P. K. & LARSEN, B. 1997. Inhibitory effects of seven organosulphur compounds on clinical isolates of *Candida* species in vitro. *Ann Clin Lab Sci*, 27, 282-6.
- SHAH, P., BHALODIA, D. & SHELAT, P. 2010. Nanoemulsion: A pharmaceutical review. *Sys Rev Pharm*, 1, 24-32.
- SHEN, M. L., JOHNSON, K. L., MAYS, D. C., LIPSKY, J. J. & NAYLOR, S. 2001. Determination of in vivo adducts of disulfiram with mitochondrial aldehyde dehydrogenase. *Biochem Pharmacol*, 61, 537-45.
- SHIAN, S. G., KAO, Y. R., WU, F. Y. & WU, C. W. 2003. Inhibition of invasion and angiogenesis by zinc-chelating agent disulfiram. *Mol Pharmacol*, 64, 1076-84.
- SIEW, A., LE, H., THIOVOLET, M., GELLERT, P., SCHATZLEIN, A. & UCHEGBU, I. 2012. Enhanced oral absorption of hydrophobic and hydrophilic drugs using quaternary ammonium palmitoyl glycol chitosan nanoparticles. *Mol Pharm*, 9, 14-28.
- SLATER, T. F., SAWYER, B. & STRÄULI, U. 1963. Studies on succinate-tetrazolium reductase systems. *Biochimica et Biophysica Acta*, 77, 383-393.
- SNYDER, L. R., KIRKLAND, J. J. & DOLAN, J. W. 2010a. Basic Concepts and the Control of Separation. *Introduction to Modern Liquid Chromatography*. John Wiley & Sons, Inc.
- SNYDER, L. R., KIRKLAND, J. J. & DOLAN, J. W. 2010b. Introduction. *Introduction to Modern Liquid Chromatography*. John Wiley & Sons, Inc.
- SOLANS, C., IZQUIERDO, P., NOLLA, J., AZEMAR, N. & GARCIA-CELMA, M. J. 2005. Nano-emulsions. *Current Opinion in Colloid & Interface Science*, 10, 102-110.
- SONG, W., TANG, Z., LEI, T., WEN, X., WANG, G., ZHANG, D., DENG, M., TANG, X. & CHEN, X. 2016a. Stable loading and delivery of disulfiram with mPEG-PLGA/PCL mixed nanoparticles for tumor therapy. *Nanomedicine*, 12, 377-86.
- SONG, W., TANG, Z., SHEN, N., YU, H., JIA, Y., ZHANG, D., JIANG, J., HE, C., TIAN, H. & CHEN, X. 2016b. Combining disulfiram and poly(l-glutamic acid)-cisplatin conjugates for combating cisplatin resistance. *Journal of Controlled Release*, 231, 94-102.
- SONIA, T. A. & SHARMA, C. 2011. Chitosan and Its Derivatives for Drug Delivery Perspective. In: JAYAKUMAR, R., PRABAHARAN, M. & MUZZARELLI, R. A. A. (eds.) *Chitosan for Biomaterials I*. Springer Berlin Heidelberg.
- SOO CHOI, H., LIU, W., MISRA, P., TANAKA, E., ZIMMER, J. P., ITTY IPE, B., BAWENDI, M. G. & FRANGIONI, J. V. 2007. Renal clearance of quantum dots. *Nat Biotech*, 25, 1165-1170.
- SPIVAK, A. M., ANDRADE, A., EISELE, E., HOH, R., BACCHETTI, P., BUMPUS, N. N., EMAD, F., BUCKHEIT, R., MCCANCE-KATZ, E. F., LAI, J., KENNEDY, M., CHANDER, G., SILICIANO, R. F., SILICIANO, J. D. & DEEKS, S. G. 2014. A Pilot Study Assessing the Safety and Latency-Reversing Activity of Disulfiram in HIV-1-Infected Adults on Antiretroviral Therapy. *Clinical Infectious Diseases*, 58, 883-890.
- STOCKERT, J. C., BLAZQUEZ-CASTRO, A., CANETE, M., HOROBIN, R. W. & VILLANUEVA, A. 2012. MTT assay for cell viability: Intracellular localization of the formazan product is in lipid droplets. *Acta Histochem*, 114, 785-96.

- STORMS, R. W., TRUJILLO, A. P., SPRINGER, J. B., SHAH, L., COLVIN, O. M., LUDEMAN, S. M. & SMITH, C. 1999. Isolation of primitive human hematopoietic progenitors on the basis of aldehyde dehydrogenase activity. *Proc Natl Acad Sci U S A*, 96, 9118-23.
- STRICKLEY, R. G. 2004. Solubilizing excipients in oral and injectable formulations. *Pharm Res*, 21, 201-30.
- STROBEL, O., DOR, Y., ALSINA, J., STIRMAN, A., LAUWERS, G., TRAINOR, A., CASTILLO, C. F., WARSHAW, A. L. & THAYER, S. P. 2007. In vivo lineage tracing defines the role of acinar-to-ductal transdifferentiation in inflammatory ductal metaplasia. *Gastroenterology*, 133, 1999-2009.
- SUZUKI, Y., FUJII, S., TOMINAGA, T., YOSHIMOTO, T., YOSHIMURA, T. & KAMADA, H. 1997. The origin of an EPR signal observed in dithiocarbamate-loaded tissues. Copper(II)-dithiocarbamate complexes account for the narrow hyperfine lines. *Biochim Biophys Acta*, 1335, 242-5.
- TADROS, T., IZQUIERDO, P., ESQUENA, J. & SOLANS, C. 2004. Formation and stability of nano-emulsions. *Adv Colloid Interface Sci*, 108-109, 303-18.
- TANFORD, C. 1978. The hydrophobic effect and the organization of living matter. *Science*, 200, 1012-1018.
- TIWARI, G. & TIWARI, R. 2010. Bioanalytical method validation: An updated review. *Pharm Methods*, 1, 25-38.
- TIWARI, S. B. & AMIJI, M. M. 2006. Improved oral delivery of paclitaxel following administration in nanoemulsion formulations. *J Nanosci Nanotechnol*, 6, 3215-21.
- TOMLINSON, A. J., JOHNSON, K. L., LAM-HOLT, J., MAYS, D. C., LIPSKY, J. J. & NAYLOR, S. 1997. Inhibition of human mitochondrial aldehyde dehydrogenase by the disulfiram metabolite S-methyl-N,N-diethylthiocarbamoyl sulfoxide: structural characterization of the enzyme adduct by HPLC-tandem mass spectrometry. *Biochem Pharmacol*, 54, 1253-60.
- TRATHNIGG, B. 1995. Determination of MWD and chemical composition of polymers by chromatographic techniques. *Progress in Polymer Science*, 20, 615-650.
- TREVASKIS, N. L., KAMINSKAS, L. M. & PORTER, C. J. H. 2015. From sewer to saviour [mdash] targeting the lymphatic system to promote drug exposure and activity. *Nat Rev Drug Discov*, 14, 781-803.
- TRISCOTT, J., LEE, C., HU, K., FOTOVATI, A., BERNS, R., PAMBID, M., LUK, M., KAST, R. E., KONG, E., TOYOTA, E., YIP, S., TOYOTA, B. & DUNN, S. E. 2012. Disulfiram, a drug widely used to control alcoholism, suppresses the self-renewal of glioblastoma and over-rides resistance to temozolomide. *Oncotarget*, 3, 1112-23.
- TSUJI, K., YANG, M., JIANG, P., MAITRA, A., KAUSHAL, S., YAMAUCHI, K., KATZ, M. H., MOOSSA, A. R., HOFFMAN, R. M. & BOUVET, M. 2006. Common bile duct injection as a novel method for establishing red fluorescent protein (RFP)-expressing human pancreatic cancer in nude mice. *JOP*, 7, 193-9.
- UCHEGBU, I. F., SADIQ, L., ARASTOO, M., GRAY, A. I., WANG, W., WAIGH, R. D. & SCHATZLEIN, A. G. 2001. Quaternary ammonium palmitoyl glycol chitosan--a new polysoap for drug delivery. *Int J Pharm*, 224, 185-99.
- UCHEGBU, I. F., SADIQ, L., PARDAKHTY, A., EL-HAMMADI, M., GRAY, A. I., TETLEY, L., WANG, W., ZINSELMAYER, B. H. & SCHÄTZLEIN, A. G. 2004. Gene Transfer with Three Amphiphilic Glycol Chitosans—the Degree of Polymerisation is the Main Controller of Transfection Efficiency. *Journal of Drug Targeting*, 12, 527-539.
- URSO, R., BLARDI, P. & GIORGI, G. 2002. A short introduction to pharmacokinetics. *European review for medical and pharmacological sciences*, 6, 33-44.
- VALERIOTE, F. & GRATES, H. E. 1989. Potentiation of nitrogen mustard cytotoxicity by disulfiram, diethyldithiocarbamic acid, and diethylamine in mice. *Cancer Res*, 49, 6658-61.
- VAN MEERLOO, J., KASPERS, G. J. & CLOOS, J. 2011. Cell sensitivity assays: the MTT assay. *Methods Mol Biol*, 731, 237-45.
- VERTZONI, M., DRESSMAN, J., BUTLER, J., HEMPENSTALL, J. & REPPAS, C. 2005. Simulation of fasting gastric conditions and its importance for the in vivo dissolution of lipophilic compounds. *Eur J Pharm Biopharm*, 60, 413-7.

- VINCENT, A., HERMAN, J., SCHULICK, R., HRUBAN, R. H. & GOGGINS, M. 2011. Pancreatic cancer. *Lancet*, 378, 607-20.
- VOGEL, A. I. 1989. *Vogel's Textbook of Quantitative Chemical Analysis*, Thames Polytechnic, London, Longman Scientific & Technical.
- VOLL, R. E., MIKULOWSKA, A., KALDEN, J. R. & HOLMDAHL, R. 1999. Amelioration of type II collagen induced arthritis in rats by treatment with sodium diethyldithiocarbamate. *J Rheumatol*, 26, 1352-8.
- VROMAN, L., ADAMS, A. L., FISCHER, G. C. & MUNOZ, P. C. 1980. Interaction of high molecular weight kininogen, factor XII, and fibrinogen in plasma at interfaces. *Blood*, 55, 156-9.
- WANG, J., MONGAYT, D. & TORCHILIN, V. P. 2005. Polymeric micelles for delivery of poorly soluble drugs: preparation and anticancer activity in vitro of paclitaxel incorporated into mixed micelles based on poly(ethylene glycol)-lipid conjugate and positively charged lipids. *J Drug Target*, 13, 73-80.
- WANG, W., MCLEOD, H. L. & CASSIDY, J. 2003. Disulfiram-mediated inhibition of NF-kappaB activity enhances cytotoxicity of 5-fluorouracil in human colorectal cancer cell lines. *Int J Cancer*, 104, 504-11.
- WANG, Y., ROY, A., SUN, L. & LAU, C. E. 1999. A Double-Peak Phenomenon in the Pharmacokinetics of Alprazolam after Oral Administration. *Drug Metabolism and Disposition*, 27, 855-859.
- WANG, Z., TAN, J., MCCONVILLE, C., KANNAPPAN, V., TAWARI, P. E., BROWN, J., DING, J., ARMESILLA, A. L., IRACHE, J. M., MEI, Q. B., TAN, Y., LIU, Y., JIANG, W., BIAN, X. & WANG, W. 2016. Poly lactic-co-glycolic acid controlled delivery of disulfiram to target liver cancer stem-like cells. *Nanomedicine*.
- WATSON, J. T. & SPARKMAN, O. D. 2008. Mass Spectrometry/Mass Spectrometry. *Introduction to Mass Spectrometry: Instrumentation, Applications, and Strategies for Data Interpretation*. 4th ed.: John Wiley & Sons, Ltd.
- WEITSCHIES, W., BERNSDORF, A., GIESSMANN, T., ZSCHIESCHE, M., MODESS, C., HARTMANN, V., MRAZEK, C., WEGNER, D., NAGEL, S. & SIEGMUND, W. 2005. The talinolol double-peak phenomenon is likely caused by presystemic processing after uptake from gut lumen. *Pharm Res*, 22, 728-35.
- WILLIAMS, D. H. & FLEMING, I. 1995. *Spectroscopic Methods in Organic Chemistry*, McGraw-Hill Education.
- WRIGHT, C. & MOORE, R. D. 1990. Disulfiram treatment of alcoholism. *The American Journal of Medicine*, 88, 647-655.
- XU, W., LING, P. & ZHANG, T. 2013. Polymeric Micelles, a Promising Drug Delivery System to Enhance Bioavailability of Poorly Water-Soluble Drugs. *Journal of Drug Delivery*, 2013, 15.
- YALKOWSKY, S. & HE, Y. 2003. Solubility Data. *Handbook of Aqueous Solubility Data, Second Edition*. CRC Press.
- YÁÑEZ, J. A., BROCKS, D. R., FORREST, L. M. & DAVIES, N. M. 2011. Pharmacokinetic behaviors of orally administered drugs. *Oral bioavailability: Basic principles, advanced concepts, and applications*, 183-219.
- YIP, N. C., FOMBON, I. S., LIU, P., BROWN, S., KANNAPPAN, V., ARMESILLA, A. L., XU, B., CASSIDY, J., DARLING, J. L. & WANG, W. 2011. Disulfiram modulated ROS-MAPK and NFkappaB pathways and targeted breast cancer cells with cancer stem cell-like properties. *Br J Cancer*, 104, 1564-74.
- YOKOYAMA, M., MIYAUCHI, M., YAMADA, N., OKANO, T., SAKURAI, Y., KATAOKA, K. & INOUE, S. 1990. Characterization and Anticancer Activity of the Micelle-forming Polymeric Anticancer Drug Adriamycin-conjugated Poly(ethylene glycol)-Poly(aspartic acid) Block Copolymer. *Cancer Research*, 50, 1693-1700.
- YOO, H. S. & PARK, T. G. 2001. Biodegradable polymeric micelles composed of doxorubicin conjugated PLGA-PEG block copolymer. *Journal of Controlled Release*, 70, 63-70.
- YUAN, F., DELLIAN, M., FUKUMURA, D., LEUNIG, M., BERK, D. A., TORCHILIN, V. P. & JAIN, R. K. 1995. Vascular permeability in a human tumor xenograft: molecular size dependence and cutoff size. *Cancer Res*, 55, 3752-6.

- ZAMBITO, Y. 2013. *Nanoparticles Based on Chitosan Derivatives*, INTECH Open Access Publisher.
- ZEMAITIS, M. A. & GREENE, F. E. 1976. Impairment of hepatic microsomal drug metabolism in the rat during daily disulfiram administration. *Biochemical Pharmacology*, 25, 1355-1360.
- ZEMBKO, I., AHMED, I., FAROOQ, A., DAIL, J., TAWARI, P., WANG, W. & MCCONVILLE, C. 2015. Development of Disulfiram-Loaded Poly(Lactic-co-Glycolic Acid) Wafers for the Localised Treatment of Glioblastoma Multiforme: A Comparison of Manufacturing Techniques. *Journal of Pharmaceutical Sciences*, 104, 1076-1086.
- ZHANG, L., JIANG, Y., JING, G., TANG, Y., CHEN, X., YANG, D., ZHANG, Y. & TANG, X. 2013. A novel UPLC-ESI-MS/MS method for the quantitation of disulfiram, its role in stabilized plasma and its application. *J Chromatogr B Analyt Technol Biomed Life Sci*, 937, 54-9.
- ZHANG, L., TIAN, B., LI, Y., LEI, T., MENG, J., YANG, L., ZHANG, Y., CHEN, F., ZHANG, H., XU, H. & TANG, X. 2015. A Copper-Mediated Disulfiram-Loaded pH-Triggered PEG-Shedding TAT Peptide-Modified Lipid Nanocapsules for Use in Tumor Therapy. *ACS Appl Mater Interfaces*, 7, 25147-61.
- ZHANG, T., CHEN, J., ZHANG, Y., SHEN, Q. & PAN, W. 2011. Characterization and evaluation of nanostructured lipid carrier as a vehicle for oral delivery of etoposide. *European Journal of Pharmaceutical Sciences*, 43, 174-179.
- ZHANG, Y., HUO, M., ZHOU, J. & XIE, S. 2010. PKSolver: An add-in program for pharmacokinetic and pharmacodynamic data analysis in Microsoft Excel. *Computer Methods and Programs in Biomedicine*, 99, 306-314.